

Defining a microRNA-mRNA targetome for calcineurin
inhibitor induced nephrotoxicity

A thesis submitted by
Christopher J. Benway
In partial fulfillment of the requirements
for the degree of

PhD

in

Genetics

Tufts University

Sackler School of Graduate Biomedical Sciences

August 2017

Adviser: John Iacomini, Ph.D.

Abstract

The use of calcineurin inhibitors has revolutionized solid organ transplantation increasing survival rates dramatically. However, calcineurin inhibitor induced nephrotoxicity severely limits the use of this class of drugs in transplantation and other diseases. Here we set out to define a microRNA (miRNA)-messenger RNA (mRNA) interaction map to identify the role of miRNAs in cyclosporine-induced nephrotoxicity and the gene pathways they regulate. By integrating miRNA and mRNA expression profiling with photoactivatable ribonucleoside-enhanced crosslinking and immunoprecipitation (PAR-CLIP) against endogenous Argonaute 2 (AGO2) protein in human proximal tubule cells, we identified miRNAs and mRNAs undergoing active targeting in cyclosporine A (CsA) treated-cells and vehicle-treated controls. First, expression profiling of miRNAs and mRNAs in CsA-treated versus vehicle-treated cells identified the key canonical pathways and cellular processes which are dysregulated in proximal tubule epithelial cells (PTECs) by CsA. Our data support a model whereby CsA induces an epithelial-to-mesenchymal-like (EMT-like) re-programming of PTECs by down-regulation of key apical surface, cell junction, and adherens junction genes as well as up-regulation of major pro-EMT cell signaling pathways such as PI3K/AKT, ERK, and TGF- β . Our data indicate that CsA causes specific changes in miRNAs and mRNAs associated with the RNA-Induced Silencing Complex (RISC) complex. Pathway enrichment analysis identified canonical pathways specifically under regulation by miRNAs following CsA treatment. Analysis of active miRNA-mRNA targeting interactions revealed that CsA suppresses an upstream regulator of JNK and p38 MAPKs by inducing targeting of MAP3K1 by miR-101-3p

thereby uncovering a previously undefined mechanism by which CsA affects calcineurin-independent molecular pathways. These insights into the molecular pathways governing expression of genes involved in cyclosporine-induced nephrotoxicity may provide novel therapeutic approaches to preventing chronic renal injury in transplant recipients.

Dedicated to the memory of
Dr. Nabil El Tayar (1957-2001) and *James Bowlby* (1983-2008).

Acknowledgements

First and foremost, I must thank my adviser, Dr. John Iacomini, for his mentorship and friendship throughout the course of my research and studies at Tufts. I am extremely grateful for the many opportunities and freedom to pursue the research and skills I desired. He has been a terrific mentor to me. I am thankful for the responsibilities entrusted to me, the academic and scientific guidance, and the in-depth Boston sports discussions.

I would like to thank my thesis committee, Drs. Rajendra Kumar-Singh, Gavin Schnitzler, Karl Munger, and F. Rob Jackson for their support, guidance, and enthusiasm for my project as well as career advice. I also would like to thank my outside examiner, Dr. Carl Novina, for accepting my invitation to evaluate my dissertation.

I must also thank the members of the Iacomini lab for their support and friendship these last few years: Dr. Jessamyn Bagley, for her scientific expertise and helpful discussions; Dr. Jin Yuan, who is both a tremendously talented scientist and medical doctor, for his guidance, mentorship, and setting the groundwork for me to pursue this project; Suraiya Begum, for her laboratory support, kindness, and home-cooked meals; Michael Hyde and Linus Williams, who both have terrific scientific careers ahead of them, for their support and friendship.

I would also like to thank the fellow students who help make the best of this challenging experience. A big thanks to Michael Sweeney and Gabrielle McDonald, my fellow Genetics classmates with whom I shared most of this journey with. We've had a lot of fun and laughs through the ups and downs of graduate school and I am thankful for their friendship. I would like to also thank two Tufts Genetics Program alumnae, Drs. Benjamin

Hardwood and Crystal Bryan, whose advice was so important to me throughout my time at Tufts. Lastly, a big thanks to all the students who participate in a certain Tuesday evening journal club, with whom it has been a pleasure to commiserate, celebrate, and libate.

Throughout my scientific career thus far, I have felt tremendously fortunate to work with and learn from some amazing scientists. If I have accomplished anything of merit, it has been by “standing on the shoulders of giants.” I am forever indebted to the many scientists who taught, advised, and inspired me over the years: Barbara Plonski, Dr. Alan Michelson, Dr. Brian Busser, Dr. Beatriz Estrada, Dr. Sam Kunes, Dr. Tehyen Chu, Anna Gorska, Dr. Andrew Berry, Dr. Laurie Glimcher, Dr. Ann-Hwee Lee, Dr. Fabio Martinon, Dr. Vanja Lazarevic, Dr. Tracy Staton, Dr. Richard Mulligan, Dr. Michael Volles, and Dr. Dan Stoleru.

Most importantly, I thank my family for their eternal support and love. I thank my parents, Frank and Maureen, for providing me the encouragement and opportunity to pursue my dreams as well as the strength and conviction to achieve them. I also thank my amazing Swiss family and mother-in-law, Marie-Christine, for the love, encouragement, inspiration, and chocolate. Above all, I thank my wife, Nadia, for her unwavering love, support, and patience throughout this roller coaster ride. I truly could not have accomplished this without her.

Table of Contents

Abstract.....	ii
Dedication	iv
Acknowledgements	v
Table of Contents.....	vii
List of Tables	ix
List of Figures	x
List of Copyrighted Materials	xii
List of Abbreviations	xiii
Chapter 1: Introduction	1
1.1. Calcineurin Inhibitor Nephrotoxicity: a Rate Limiting Step in Kidney Transplantation Outcomes	1
1.2. Normal Kidney Structure and Function.....	2
1.3. Structure and Cellular Composition of the Proximal Convolute Tubule.....	4
1.4. Acute Kidney Injury	5
1.5. Calcineurin Inhibitors	10
1.6. Cyclosporine-induced Nephrotoxicity (Calcineurin Inhibitor Nephrotoxicity).....	15
1.7. Molecular Re-programming in Calcineurin Inhibitor Nephrotoxicity Induces Epithelial-to-Mesenchymal Transition.....	18
1.8. Epithelial-to-Mesenchymal Transition	26
1.9. Post-transcriptional regulation of gene expression by microRNAs	27
1.10. CLIP and PAR-CLIP experiments	33
1.11. Role of microRNAs in CIN.....	39
Chapter 2: Materials and Methods.....	41
2.1. Cell culture	41
2.2. Animal model of CsA-induced nephrotoxicity	42
2.3. Deep sequencing of miRNAs.....	43
2.4. Deep sequencing of mRNAs.....	45
2.5. Differential Expression Analysis of miRNA-seq and mRNA-seq Data.....	46
2.6. Photoactivatable Ribonucleotide-enhanced Crosslinking and Immunoprecipitation (PAR-CLIP)	47
2.7. Bioinformatic Analysis of PAR-CLIP Data.....	49
2.8. Gene Set Enrichment Analysis.....	50
2.9. Ingenuity Pathway Analysis.....	51
2.10. Construction of miRNA-expression vectors and target site luciferase reporter vectors.....	51
2.11. Transfection of cultured cells	52
2.12. Luciferase Assay	52
2.13. Quantitative RT-PCR.....	53
2.13. Western Blot Analysis	55
2.14. Data Access	56
Chapter 3: Cyclosporine A causes aberrant miRNA and mRNA gene expression program in proximal tubule epithelial cells.....	57
3.1. Differential microRNA expression in HK-2 cells treated with CsA	57

3.2. In-silico target prediction and pathway analysis of differentially expressed miRNAs in CsA-treated HK-2 cells	76
3.3. Differential mRNA expression in HK-2 cells treated with CsA.....	79
3.4. GSEA identifies enriched pathways and biological processes in HK-2 cells treated with CsA.....	85
3.5. Expression of EMT genes is dysregulated by CsA treatment in HK-2 cells	98
3.6. Conclusions	105
Chapter 4: PAR-CLIP defines functional miRNA-mRNA targetome in proximal tubule epithelial cell model of calcineurin inhibitor nephrotoxicity	108
4.1. PAN-AGO-PAR-CLIP defines a functional miRNA-mRNA targetome in HK-2 cells.....	108
4.2. AGO2-PAR-CLIP defines miRNAs associated with the RISC complex in human proximal tubule cells treated with CsA	119
4.3. Defining mRNA-binding events in the RISC complex of human proximal tubule cells treated with CsA.....	126
4.4. mRNAs in the AGO2 complex contain seed sequences of miRNAs identified by PAR-CLIP	129
4.5. Comparing PAR-CLIP and RNA-seq reveals that a relatively small number of miRNAs and mRNAs are involved in active targeting	133
4.6. Gene pathways regulated by miRNAs following CsA treatment	136
4.7. miR-101-3p targets MAP3K1 expression in vitro	142
4.8 Conclusions	147
Chapter 5: Discussion.....	149
Chapter 6: Bibliography.....	162

List of Tables

Chapter 1	1
Table 1-1. Genes up-regulated more than two fold in response to treatment with 4.2 μmol/L CsA for 48 hours	23
Table 1-2. Genes down-regulated more than two fold in response to treatment with 4.2 μmol/L CsA for 48 hours	25
Table 1-3. Summary of AGO-CLIP experiments	38
Chapter 2	41
Table 2-1. Illumina index PCR primer sequences used	44
Table 2-2. NEBNext Small RNA Library adaptor and primer sequences used	45
Table 2-3. NEBNext mRNA Library adapter and primer sequences	46
Table 2-4. PAR-CLIP oligonucleotides and adapters.....	49
Table 2-5. Human oligonucleotide primers used for qRT-PCR.....	54
Table 2-6. Mouse oligonucleotide primers used for qRT-PCR.....	54
Chapter 3	57
Table 3-1. Summary of miRNA-seq de-multiplexing and quality scores.....	59
Table 3-2. miRNAs up-regulated by CsA in HK-2 cells	70
Table 3-3. miRNAs down-regulated by CsA in HK-2 cells.....	71
Table 3-4. GSEA of differentially expressed mRNAs after CsA treatment in HK-2 cells (Hallmark Pathways).....	87
Table 3-5. GSEA of differentially expressed mRNAs after CsA treatment in HK-2 cells (Reactome Pathways).....	97
Chapter 4	108
Table 4-1. Top PAN-AGO-PAR-CLIP 3'UTR target genes.....	116
Table 4-2. Summary of AGO2-PAR-CLIP Illumina sequencing and alignment.....	121
Table 4-3. Differential expression of top mature miRNAs increased and decreased in RISC complex after CsA treatment	124
Table 4-4. Top CsA-specific miRNAs detected by AGO2-PAR-CLIP.....	125
Table 4-5. Top vehicle-specific miRNAs detected by AGO2-PAR-CLIP	125
Table 4-6. Top miRNA seed matches in 3'UTR	132

List of Figures

Chapter 1	1
Figure 1-1. Acute ischemic kidney injury pathogenesis and pathophysiology in proximal tubular cells	9
Figure 1-2. Pharmacodynamics of calcineurin inhibitor pathway	14
Figure 1-3. Pathogenesis of cyclosporine-induced nephropathy	16
Figure 1-4. Summary of MiRBase v21 microRNA database	28
Figure 1-5. Overview of miRNA biogenesis pathway	31
Figure 1-6. Canonical and non-canonical miRNA target site types.....	32
Figure 1-7. Protein-RNA crosslinking and immunoprecipitation (CLIP) methods.....	37
Chapter 3	57
Figure 3-1. Construction of cDNA libraries derived from small RNAs	61
Figure 3-2. Prediction of the miRNA-seq experiment's statistical power using 'Scotty.'	62
Figure 3-3. Quality control and DESeq2 analysis of miRNA-seq data.....	63
Figure 3-4. Heatmap for differentially expressed miRNAs in CsA-treated HK-2 cells compared to vehicle control.....	72
Figure 3-5. Volcano plot of differentially expressed miRNAs in CsA-treated HK-2 cells	73
Figure 3-6. Total mean miRNA abundance across all HK-2 samples	74
Figure 3-7. Hsa-miR-7974 is widely expressed in human tissues and cell lines.....	75
Figure 3-8. Functional characterization of differentially expressed miRNAs in CsA-treated HK-2 cells	78
Figure 3-9. Agarose gel size fractionation of mRNA cDNA libraries for sequencing ..	81
Figure 3-10. Quality control analysis of mRNA-seq data by DESeq2	82
Figure 3-11. Volcano plot of differentially expressed mRNAs in CsA-treated HK-2 cells.....	83
Figure 3-12. Kidney expression of <i>ANGPTL4</i> and <i>MMP7</i> in a mouse model of CsA-induced nephrotoxicity	84
Figure 3-13. Expression of DUSPs are up-regulated in HK-2 cells treated with CsA ..	88
Figure 3-14. Apical membrane surface genes are down-regulated by CsA-treatment in HK-2 cells	90
Figure 3-15. CsA causes aberrant expression of solute carrier family (SLC) transporters in HK-2 proximal tubule cells.....	93
Figure 3-16. Enrichment plots for top four Veh-enriched Hallmark gene sets by GSEA	96
Figure 3-17. GSEA enrichment plot for Hallmark EMT gene set	101
Figure 3-18. Expression of cadherins and claudins is down-regulated in HK-2 cells treated with CsA.....	102
Figure 3-19. Down-regulation of cadherins by CsA is dose-dependent	103
Figure 3-20. Expression of conventional EMT markers in HK-2 cells treated with CsA	104
Chapter 4	108

Figure 4-1. PAN-AGO-PAR-CLIP of HK-2 cells	112
Figure 4-2. PAN-AGO-PAR-CLIP cDNA library PCR optimization	113
Figure 4-3. Mutational frequencies in PAN-AGO-PAR-CLIP sequencing	114
Figure 4-4. PAN-AGO-PAR-CLIP clusters are enriched in the transcript regions of the genome.....	115
Figure 4-5. PAN-AGO-PAR-CLIP identified 3'UTR DDAH1 target sequence is repressed in vitro	117
Figure 4-6. Mutation of putative miRNA seed target sites in PAN-AGO-PAR-CLIP clusters de-repressed luciferase activity	118
Figure 4-7. Preparation of the AGO2-PAR-CLIP cDNA libraries	120
Figure 4-8. Analysis of RISC-bound RNAs and miRNAs obtained by AGO2-PAR-CLIP	122
Figure 4-9. Alignment of PAR-CLIP reads to miR-1290	123
Figure 4-10. AGO2-PAR-CLIP target sites are enriched in transcripts.....	127
Figure 4-11. AGO2-PAR-CLIP identifies CsA-induced miRNA target sites.....	128
Figure 4-12. Differential miRNA targetome induced by CsA treatment of HK-2 cells	131
Figure 4-13. miRNAs and mRNAs detected by AGO2-PAR-CLIP represent a small proportion of the total RNA pool in HK-2 cells	135
Figure 4-14. Canonical pathways regulated by miRNAs in CsA-treated HK-2 cells..	139
Figure 4-15. Canonical pathways regulated by mRNAs in CsA-treated versus vehicle-treated HK-2 cells.....	140
Figure 4-16. Glucocorticoid receptor signaling pathway genes specifically regulated by miRNAs in CsA-treated HK-2 cells	141
Figure 4-17. miR-101-3p targets MAP3K1 expression in HK-2 cells.....	145
Figure 4-18. miR-101-3p overexpression is not sufficient to affect downstream p38/JNK MAPK transcriptional targets	146

List of Copyrighted Materials

Sharfuddin, Asif A., and Bruce A. Molitoris. 2011. “Pathophysiology of ischemic acute kidney injury” *Nature Reviews Nephrology* 7 (4): 189-200. doi:10.1038/nrneph.2011.16.

Figures 1 and 2 were reprinted for Figure 1-1.

Reprinted by permission from Macmillan Publishers Ltd: *Nature Reviews Cancer* (Sharfuddin and Molitoris 2011), copyright 2011.

Barbarino JM, Staatz CE, Venkataraman R, Klein TE, Altman RB. 2013.

“PharmGKB summary: cyclosporine and tacrolimus pathways.” *Pharmacogenet Genomics* 23: 563–585. <http://www.ncbi.nlm.nih.gov/pmc/articles/PMC4119065/>. <http://www.pharmgkb.org/pathway/PA165985892>.

Figure 2 was reprinted for Figure 1-2.

Reprinted with permission from PharmGKB and Stanford University (Barbarino et al. 2013), copyright 2013..

Liptak P, Ivanyi B. 2006. “Primer: Histopathology of calcineurin-inhibitor toxicity in renal allografts.” *Nat Clin Pract Nephrol* 2: 398–404.

<http://www.ncbi.nlm.nih.gov/pubmed/16932468>.

Figures 1 and 5 were reprinted for Figure 1-3.

Reprinted with permission from Macmillan Publishers Ltd: *Nature Reviews Nephrology* (Liptak and Ivanyi 2006), copyright 2006.

Lin, Shuabin, and Richard I Gregory. 2015. “MicroRNA Biogenesis Pathways in Cancer.” *Nature Review Cancer* 15 (6): 321–33. doi:10.1038/nrc3932.

Figure 1 was reprinted for Figure 1-5.

Reprinted by permission from Macmillan Publishers Ltd: *Nature Reviews Cancer* (Lin and Gregory 2015), copyright 2015

Gruber AR, Martin G, Keller W, Zavolan M. 2014. “Means to an end: mechanisms of alternative polyadenylation of messenger RNA precursors.” *Wiley Interdiscip Rev RNA* 5: 183–196.

Figure 4 was reprinted for Figure 1-7

Reprinted under Creative Commons license (Gruber et al. 2014).

Slattery, Craig, Eric Campbell, Tara McMorrow, and Michael P Ryan. 2005.

“Cyclosporine A-Induced Renal Fibrosis: A Role for Epithelial-Mesenchymal Transition.” *The American Journal of Pathology* 167 (2): 395–407.

Table 1 and 2 were reprinted for Tables 1-1 and 1-2.

Reprinted with permission from Elsevier (Slattery et al. 2005).

List of Abbreviations

4-SU: 4 thiouridine

α -SMA: α -smooth muscle actin

AGO/Ago: argonaute

AKI: acute kidney injury

ANCA: antineutrophil cytoplasm antibodies

ATCC: American Type Culture Collection

ATN: acute tubular necrosis

ATP: adenosine triphosphate

β -gal: β -galactosidase

BAM: binary alignment format

BMDM: bone marrow-derived macrophage

BED: browser extensible data

BPE: bovine pituitary extract

BUN: blood urea nitrogen

CASAVA: consensus assessment of sequence and variation

cDNA: complementary DNA

CD: cluster of differentiation

CDS: coding sequence

ChIP-seq: chromatin immunoprecipitation and sequencing

CIN: calcineurin inhibitor nephrotoxicity

CKD: chronic kidney disease

CLASH: crosslinking, ligation, and sequencing of miRNA-RNA hybrids

CLIP: crosslinking and immunoprecipitation

CsA: cycloporine A

DMEM: Dulbecco's Modified Eagle's Medium

DNA: deoxyribonucleic acid

E-cadherin: epithelial cadherin

ECM: extracellular matrix

EGF: epidermal growth factor

ERK: extracellular regulated kinase

ESRD: end-stage renal disease

DGCR8: DiGeorge Syndrome Critical Region Gene 8

ESRD: end stage renal disease

FBS: fetal bovine serum

FDR: false discovery rate

FKBP: FK506 binding protein

FSGS: focal segmental glomerulosclerosis

GSK3(α/β): glycogen synthase kinase 3 α/β

GFF: general feature format

GFR: glomerular filtration rate

HEK293: human embryonic kidney 293

hESC: human embryonic stem cell

HITS-CLIP: high-throughput sequencing of RNA isolated by crosslinking
immunoprecipitation

HIV: human immunodeficiency virus

HK-2: human kidney 2

HOMER: hypergeometric optimization of motif enrichment

IACUC: Institutional Animal Care and Use Committee

iCLIP: individual-nucleotide resolution crosslinking and immunoprecipitation

IFN- γ : interferon gamma

IL: interleukin

IgA: immunoglobulin A

ILK: integrin linked kinase

IP: immunoprecipitation

JNK: c-Jun N-terminal kinases

K-cadherin: kidney cadherin

KSP-cadherin: kidney specific cadherin

KSHV: Kaposi's sarcoma-associated herpesvirus

MAP3K1: mitogen-activated protein kinase kinase kinase 1

MAPK: mitogen-activated protein kinase

MEKK1: MAPK/ERK kinase kinase 1

miR/miRNA: microRNA

MMF: mycophenolate mofetil

MMP: Matrix metalloprotease

MOPS: 3-(N-morpholino)propanesulfonic acid

mRNA: messenger RNA

mTOR: mechanistic target of rapamycin

N-cadherin: neural cadherin

NFAT: nuclear factor of activated T-cells

NF-κB: nuclear factor kappa-light-chain-enhancer of activated B cells

nm: nanometer(s)

NP40: Tergitol-type NP-40, nonyl phenoxy polyethoxylethanol

NSAID: Nonsteroidal anti-inflammatory drug

nt: nucleotide(s)

OAT: organic ion transporter

ORF: open reading frame

PAR-CLIP: photoactivatable ribonucleoside-enhanced crosslinking and immunoprecipitation

PBMC: peripheral blood mononuclear cell

P-cadherin: placental cadherin

PCR: polymerase chain reaction

PCT: proximal convoluted tubule

PEL: primary effusion lymphoma

PKC: protein kinase C

PNK: polynucleotide kinase

PTB: polypyrimidine tract-binding protein

PTEC: proximal tubule epithelial cell

PTEN: phosphatase and tension homolog

PTLD: post-transplant lymphoproliferative disorder

Pol II/III: RNA polymerase II/III

qPCR: quantitative polymerase chain reaction

rApp: adenylation-5'

RBP: RNA-binding protein

RBM9: RNA binding motif protein 9

RISC: RNA-induced silencing complex

RNA: ribonucleic acid

RPF: renal plasma flow

RQN: RNA quality number

RRT: renal replacement therapy

RT-PCR: reverse transcription polymerase chain reaction

SAPK: stress-activated protein kinase

SDS-PAGE: sodium dodecyl sulfate polyacrylamide gel electrophoresis

SGLT: sodium-glucose linked transporter

SLC: solute carrier

snRNA: small nuclear RNA

SRSF1: serine/arginine-rich splicing factor 1

SRTR/OPTN: Scientific Registry of Transplant Recipients/Organ Procurement and
Transplantation Network

TCR: T-cell receptor

TGF- β : transforming growth factor beta

TRBP: transactivation-responsive RNA-binding protein

tRNA: transfer RNA

UTR: untranslated region

UV: ultraviolet

VE-cadherin: vascular endothelial cadherin

VEGF: vascular endothelial growth factor

XPO5: exportin 5

ZO: zonula occulens

Chapter 1: Introduction

1.1. Calcineurin Inhibitor Nephrotoxicity: a Rate Limiting Step in Kidney Transplantation Outcomes

In the United States, nearly 100,000 patients with renal failure or end-stage renal disease (ESRD) are on the waitlist for renal replacement therapy (Hart et al. 2017). Wait times vary, but as many as 15.7% of patients on the waitlist have exceeded 5 years. The fundamental challenge facing the kidney replacement waitlist is insufficient supply. Further, as of the 2015 SRTR/OPTN Annual Data Report, only modest positive trends are observed in unadjusted graft and patient survival compared to a decade ago. Graft survival is severely limited by a host of factors, meaning that many transplant recipients (13.1% in 2015) will require re-transplantation. One major factor contributing to limited graft survival is, ironically, the necessary use of immunosuppressant drugs which have essentially made modern transplantation possible (Naesens, Kuypers, and Sarwal 2009).

Calcineurin inhibitors cyclosporine and tacrolimus are remarkably effective at inhibiting T cell activation via competitive binding of immunophilin-drug complexes to calcineurin and subsequent prevention of NFAT-dependent activation of IL-2. However, since its first use in human transplantation it was observed that cyclosporine administration was associated with nephrotoxicity (Calne et al. 1978; Calne et al. 1979). Tacrolimus, a much more potent calcineurin inhibitor which binds to a separate immunophilin, has mostly supplanted cyclosporine as the primary immunosuppressant agent in solid organ transplantation in the U.S. Still, tacrolimus administration suffers many of the same pitfalls as cyclosporine since similar incidences of nephrotoxicity have

been reported (The U.S. Multicenter FK506 Liver Study Group 1994; Canzanello et al. 1998).

Recently, a novel T cell co-stimulation blocker, belatacept, was shown to reduce some of the adverse outcomes in renal transplantation immunosuppression regimens (Vincenti et al. 2010). However, belatacept administration presents its own risks, for instance, an increased risk of post-transplant lymphoproliferative disorder (PTLD) (Masson et al. 2014). Further, belatacept treatment remains three times more expensive than tacrolimus and requires patients to undergo a monthly infusion (Heher and Markmann 2016).

Incidence of ESRD has grown exponentially in the last three decades (Bastani 2015). This accelerated prevalence of ESRD may be at least in part attributable to the steady rise of ESRD-causative conditions such as diabetes mellitus and hypertension. As these conditions reach epidemic levels, it is almost certain that the kidney supply gap will continue to grow. In the absence of sufficient alternative immunosuppressants, understanding the mechanisms of calcineurin inhibitor nephrotoxicity has become paramount in order develop novel clinical interventions and extend long-term graft survival.

1.2. Normal Kidney Structure and Function

As a critical component of the urinary system, the kidney's primary function is excretion: removal and elimination of metabolic waste, such as urea, from the blood. In addition to filtering blood, the kidney regulates the osmolarity of body fluids, regulates blood

volume, contributes to hormonal regulation of blood pressure, secretes the hormone erythropoietin, synthesizes calcitrol (vitamin D), regulates acid-base balance of body fluids, and detoxifies free radicals and drugs from the blood supply. Further, in starvation conditions, the kidney may perform gluconeogenesis, the conversion of amino acids to glucose (Saladin 2008).

These many functions are accomplished by a network of circulatory structures and tubules which interface as a functional unit called the nephron. Blood, about 21% of cardiac output, enters the kidney through a system of branching arteries and travels through afferent arterioles which supply individual nephrons. Each human kidney contains approximately 1.2 million nephrons which span the cortex and medulla. At the first step of filtration by the nephron, blood enters a mass of capillaries within the Bowman's capsule which interact with a specialized visceral layer of podocytes. Here, water and some solutes in the blood plasma are able to exit the capillaries into the capsular space.

This glomerular filtrate flows onward to the renal tubule, which consists of four distinct regions: the proximal convoluted tubule, the nephron loop, the distal convoluted tubule, and the collecting duct. The distinct architecture, cellular composition, and physiological properties of these structures allow the nephron to achieve efficient resorption of water and solutes and further removal of waste products from the blood. In particular, the proximal convoluted tubule is responsible for the bulk of tubular resorption of important solutes including glucose, amino acids, proteins, vitamins, lactate, sodium, potassium, calcium, chloride, bicarbonate, and phosphate.

1.3. Structure and Cellular Composition of the Proximal Convoluted Tubule

The cells that make up the proximal convoluted tubule (PCT) form a simple cuboidal epithelium with numerous microvilli, referred to as a “brush border.” The increased surface area of the apical, lumen-facing, brush border facilitates the PCT’s primary role of reabsorption. Throughout this apical membrane, expression of integral protein transporters promotes reabsorption of solutes, especially sodium. The reabsorption of sodium is critical to creating an osmotic and electrical gradient which drives water reabsorption. There are several types of sodium transporters expressed on the apical membrane, including glucose-symporters SGLT1 (*SLC5A1*) and SGLT2 (*SLC5A2*), sodium-hydrogen antiporters, and sodium-phosphate co-transporters (Balen et al. 2008; Vallon et al. 2011; Bobulescu and Moe 2009; Murer et al. 2003). Na⁺/K⁺ pumps located on the basolateral membranes utilize ATP to continually pump sodium out of the cell and into the extracellular fluid (Tsuchiya et al. 1992; Salyer et al. 2013; Bertorello and Aperia 1989). A comparative transcriptomic study of the various compartments of the kidney with all other organs identified 120 proteins which were ‘kidney elevated’ and localized to the proximal tubule (Habuka et al. 2014). These included 32 members of the solute carrier family (SLC) proteins. Microdissection of 14 nephron segments in rat kidneys followed by deep sequencing revealed even more specific expression patterns within the kidney compartments (J. W. Lee, Chou, and Knepper 2015). In the proximal tubule (segments S1, S2, and S3), the specific expression of *Aqp1*, *Slc22a6* (OAT1), and *Slc34a1* (NaPi-IIa) was demonstrated. In addition to water and solute transporters, the proximal tubule expressed specific G protein-coupled receptor *Pth1r*, protein kinases (*Map3k7*, *Pink*, *Pim3*), and secreted proteins *Sepp1* and

Kap (J. W. Lee, Chou, and Knepper 2015). Thus, the proximal tubule is a highly differentiated and specialized segment of the nephron. The expression of a specific repertoire of proteins in proximal tubule epithelial cells confers the specialized structure and function of the proximal convoluted tubule, namely water and solute reabsorption.

1.4. Acute Kidney Injury

Acute kidney injury (AKI) is defined as the rapid loss of the kidney's excretory function. The syndrome is typically diagnosed by the accumulation of urea and creatinine, end products of nitrogen metabolism, which indicates a decrease in glomerular filtration rate (GFR). Decreased urine output may also indicate acute kidney injury (Bellomo, Kellum, and Ronco 2012). The consensus definition of the criteria for diagnosing the severity of the acute kidney injury is termed 'RIFLE' for risk, injury failure, loss, and stage (Bellomo et al. 2004). Increasing serum creatinine and decreasing urine output define the criteria for risk, injury, and failure. Renal loss is characterized by a complete loss of kidney function for greater than 4 weeks, requiring renal replacement therapy (RRT) such as dialysis. Complete loss of kidney function for greater than three months indicates end stage renal disease and requires permanent RRT such as dialysis or transplantation.

Acute kidney injury can occur for several reasons. Typically, the causes of AKI are categorized based on the compartment of the kidney most affected. For instance, injuries caused by decreased blood flow to the kidneys are classified as 'prerenal.' Prerenal disease, i.e. renal ischemia, can be caused by hypotension, hypovolemic shock due to excessive blood or water loss, heart attack (and other conditions leading to decreased heart function), organ failure, afferent arteriole vasoconstriction due to use of

NSAIDs, severe allergic reactions, burns, and major surgery. AKI caused by obstruction of the urinary tract is classified as ‘postrenal.’ Obstruction can occur for a number of reasons and in any location within the urinary tract. Bladder, prostate, cervical cancers (as well as metastatic cancers) are common causes of postrenal disease in patients that do not have underlying chronic kidney disease (CKD). An enlarged prostate, neurogenic bladder, kidneys stones, and blood clots in the urinary tract may also lead to postrenal disease. Obstructive nephropathy may leads to irreversible tubulointerstitial fibrosis, and intrinsic renal disease, if left untreated (Coroneos et al. 1997). ‘Intrinsic renal’ AKI refers to direct damage to the kidney, i.e pathology of the vessels, glomeruli, or tubules-interstitium. These are typically classified by compartment. Intrinsic renal vascular diseases such as microangiopathic hemolytic anemia and scleroderma affect the blood vessels of the kidney. Intrinsic glomerular diseases such as focal segmental glomerulosclerosis (FSGS) which is characterized by scarring of the glomerulus may arise from genetic abnormalities, drug treatments, or diseases such as diabetes and HIV infection. Tubular and interstitial diseases are much more common intrinsic causes of AKI. Acute interstitial nephritis and acute tubular necrosis (ATN) are often caused by inflammation due to infection or toxins. For instance, a common cause of ATN is contrast nephropathy, which occurs after the use of radiocontrast media for medical imaging.

In ischemic and nephrotoxic AKI, it is generally thought that the proximal tubule is the primary site of injury (Basile, Anderson, and Sutton 2012). This is evidenced in biopsy data of patients (Bohle et al. 1976; López-Gómez and Rivera 2008; Solez, Morel-Maroger, and Sraer 1979). In biopsies of patients with ATN, it was observed that necrosis of individual tubular epithelial cells and loss of brush border occurred in the proximal

tubules (Solez, Morel-Maroger, and Sraer 1979). Further detachment of epithelial cells from the basement membrane and sloughing off of cells into the tubular lumen contributes to the formation of tubular casts. It was noted also that in patients recovering from ATN, there was evidence of re-epithelialization, suggesting that the process is reversible (Basile, Anderson, and Sutton 2012; Solez, Morel-Maroger, and Sraer 1979).

Figure 1-1 illustrates the key pathophysiological features of ischemic AKI. .

Contrary to AKI, chronic kidney disease (CKD) refers to a condition in which kidney damage is detected by albumin production or reduced kidney function is observed for over three months. Diabetes mellitus and hypertension are the prevalent risk factors for this condition, as well as age, obesity, and cardiovascular disease. It is thought that glomerulosclerosis and hypertensive nephrosclerosis drive the pathophysiology of CKD (Levey and Coresh 2012). Once the disease has progressed and symptoms progress to extremely low GFR, considered renal failure, the only course of action is renal replacement therapy, i.e. dialysis or transplantation. Long-term survival of patients undergoing dialysis is much lower than transplant recipients (Levey and Coresh 2012). However, the high cost of transplantation and low supply of kidney donors remains a significant challenge. Further, although 10-year graft survival in renal transplantations has improved compared to a decade prior, chronic renal allograft nephropathy and rejection remain a challenge and a burden. Over 20 percent of kidney transplants performed in the US go to patients who have previously failed a graft. Immunologic factors as well as non-immunologic factors such as hypertension are critical risk factors. One major risk factor, that is largely unavoidable, is the use of calcineurin inhibitors as part of the immunosuppression regime necessary to prevent acute rejection. Thus, the

drugs that have made short-term graft survival not only possible, but extremely effective, ultimately limit the long-term survival of both graft and host.

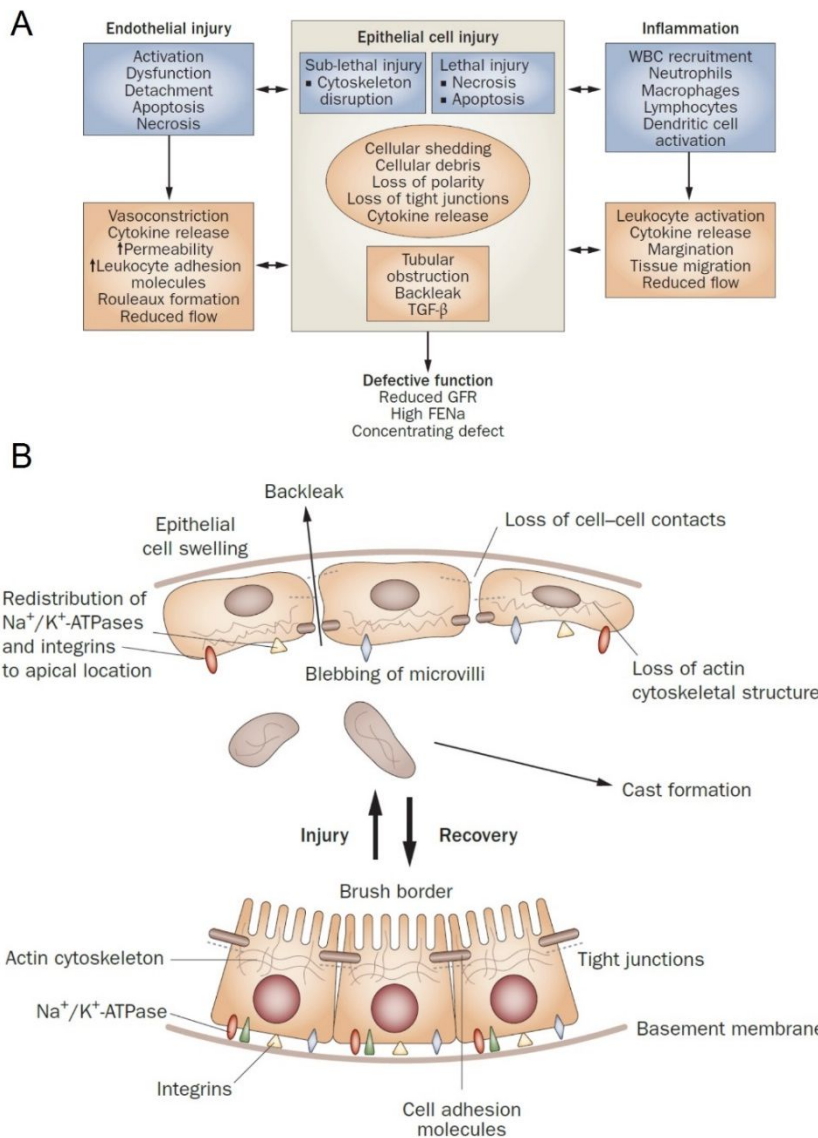


Figure 1-1. Acute ischemic kidney injury pathogenesis and pathophysiology in proximal tubular cells. Acute ischemic kidney injury may occur as a result of intravascular volume depletion, reduced cardiac input, systemic vasodilation, and renal vasoconstriction. (A) Sub-lethal and lethal injury to the vascular and tubular cells is largely a result of ATP depletion and results in cytoskeletal changes, necrosis, and apoptosis of affected cells. Inflammatory cells play a role in the injury response and respond to signals released by injured epithelial cells. Dissolution of the tubule epithelium results in tubular obstruction, backleaking, cytokine release and ultimately defective function. (B) Diagram of the proximal tubular epithelium depicts the gross cytoskeletal, structural, and morphological changes after sub-lethal injury. This process is largely reversible and can lead to re-epithelialization. Reprinted by permission from (Sharfuddin and Molitoris 2011).

1.5. Calcineurin Inhibitors

Calcineurin inhibitors cyclosporine and tacrolimus are powerful immunosuppressant drugs primarily administered for prophylaxis of organ rejection in kidney, liver, and heart transplants. As part of an immunosuppression regimen to prevent graft rejection, calcineurin inhibitors are most often administered in combination with other immunosuppressant agents that differ by mechanism of action, for instance glucocorticoids (such as prednisone), antimetabolites azathioprine (inhibits DNA replication and blocks purine synthesis) or mycophenolate mofetil (MMF, inhibits *de novo* guanosine nucleotide synthesis), mTOR inhibitors everolimus or sirolimus (rapamycin), and T-cell costimulation blocker belatacept. Approved uses for systemic cyclosporine administration in the U.S. include treatment of severe cases of rheumatoid arthritis and psoriasis.

Both drugs, cyclosporine and tacrolimus, were first isolated from soil samples. Cyclosporine is a lipophilic cyclic peptide of 11 amino acids, derived from the fungus *Trichoderma polysporum* (Dreyfuss et al. 1976). Tacrolimus is a 23-member macrolide lactone isolated from cultures of *Streptomyces tsukubaensis* (Kino et al. 1987). Despite their different chemical properties, both drugs act on a similar class of molecules in immune cells, called immunophilins (Schreiber and Crabtree 1992; Wiederrecht et al. 1993; Matsuda et al. 2000). Cyclosporine binds to the immunophilin cyclophilin A (*PPIA*) whereas tacrolimus binds with high affinity to the FK-binding protein FKBP12 (Jun Liu et al. 1991). The drug-receptor complexes exhibit increased binding to calcineurin, thus inhibiting its phosphatase activity.

Calcineurin is a calmodulin-dependent phosphatase which is expressed in virtually all cell types and at especially high levels in the brain (Rusnak and Mertz 2000). In T lymphocytes, calcineurin phosphatase activity is increased after immune stimulation in a calcium and calmodulin dependent manner (Rusnak and Mertz 2000; Yamashita et al. 2000). The primary target of calcineurin is cytoplasmic NFATc1 (Nuclear factor of activated T-cells, cytoplasmic 1), which it dephosphorylates (Smith-Garvin et al. 2009; Macian 2005; K. T. Shaw et al. 1995; Rao, Luo, and Hogan 1997). Dephosphorylation of NFATc1 by calcineurin causes its translocation into the nucleus where it acts as a transcription factor (Rao, Luo, and Hogan 1997; Wesselborg et al. 1996; Ruff and Leach 1995; Shibasaki et al. 1996). Other NFAT family members, NFAT1-4, have also been shown to be regulated by calcium in a similar fashion (Macian 2005; Rao, Luo, and Hogan 1997). In the nucleus, NFAT family members are involved in the transcriptional activation of genes encoding many cytokines and co-stimulatory molecules, including IL-2 and IL-4, and CD40 ligand, which are required for activation of T cells (Peng et al. 2001; Hermann-Kleiter and Baier 2010). Because IL-2 stimulates the growth and differentiation of T cells, this is perhaps the most studied role of NFAT in relation to immunosuppression by calcineurin inhibitors (J. P. Shaw et al. 1988; Wiederrecht et al. 1993; Boyman and Sprent 2012).

Calcineurin has also been shown to indirectly regulate the activation of nuclear factor kappa-light-chain-enhancer of activated B cells (NF- κ B) by causing the degradation of I κ B, a negative regulator of NF κ B (Palkowitsch et al. 2011; Frantz et al. 1994). Like NFAT, NF κ B can induce transcription of IL-2 (Hoyos et al. 1989; Jain, Loh, and Rao 1995). NF κ B is integral in innate and adaptive immune responses as well as T

cell development (Gerondakis et al. 2014). Thus, inhibition of NFkB by calcineurin inhibitors further blocks the induction of gene expression programs critical for a complete immune response.

Alternatively, in the immortalized Jurkat T cell line, it has been shown that both calcineurin inhibitors cyclosporine and tacrolimus could block activation of p38 and JNK mitogen-activated protein kinase (MAPK) pathways. MAPK families are classically divided into three main arms that are well-defined: extracellular signal-regulated kinase (ERK), Jun kinase (JNK/SAPK), and p38 MAPK. These signaling cascades play a key role in signaling transduction, receiving extracellular cues (growth factors, cytokines, cell stress) and promoting cellular responses such as proliferation (W. Zhang, Liu, and Tu LIU 2002). For instance, throughout early thymocyte development p38-MAPK activity is crucial to the expansion and stepwise differentiation of CD44+/CD25- to CD44+/CD25+ to CD44-/CD25+ thymocytes (Crompton, Gilmour, and Owen 1996). It was further shown that ERK signaling was required for differentiation of immature CD25+/CD44- thymocytes and that anti-CD3 monoclonal antibody activated ERK (Crompton, Gilmour, and Owen 1996). Thus, ERK acts a signal transducer of the pre-TCR complex. MAP-kinases are also essential for CD4+ and CD8+ T cell activation and effector function. ERK signaling is required for generating CD4+ Th2 effector cells whereas JNK1 is a negative regulator of Th2 differentiation (Yamashita et al. 1999). JNK2 and p38 MAP-kinases promote IFN- γ production and CD4+ Th1 differentiation (B Li et al. 2000). In CD8+ cells, p38 MAP-kinase was shown to regulate the production of IFN- γ and CD8+ effector molecules but also induce apoptosis in CD8+ T cells (Merritt et al. 2000; J. Zhang et al. 2000). Further, TCR and CD28 co-stimulation activates JNK and p38 via

MAPK signaling, promoting the nuclear regulation of AP-1 family members which promote the transcription of essential immune cytokines such as IL-2 (Matsuda et al. 1998; Aplin et al. 2002). CsA inhibition of JNK and p38 activation prevents this co-stimulation-dependent activation of IL-2 expression (Matsuda et al. 1998). In experiments performed in Jurkat cells, it was shown that the inhibitory effect of CsA on p38 and JNK activation by chemical stimuli was mediated through inhibition of MEKK1 (*MAP3K1*), an upstream member of the signaling cascade, and that this pathway was calcineurin-independent (Matsuda et al. 2000).

Transforming growth factor beta (TGF- β 1), a secreted cytokine and master regulator of cell growth, cell proliferation, cell differentiation and apoptosis, is known to elicit an inhibitory effect on a variety of immune cells, including T cells (Chantry et al. 1989; M. O. Li et al. 2006; Moses, Yang, and Pietenpol 1990; S. S. Huang and Huang 2005; Laiho et al. 1990). *In vitro* both calcineurin inhibitors CsA and tacrolimus were shown to induce expression of *TGFB1* mRNA (A Khanna, Cairns, and Hosenpud 1999). Further, in kidney transplant patients pre-conditioned with CsA, *TGFB1* mRNA was increased in sera and PBMCs (Shin et al. 1998). Though the effects of *TGFB1* on immune cells are well understood, the effect of CsA on *TGFB1* remains a controversial issue. At therapeutic CsA doses, high enough to inhibit IL-2, it has been suggested that CsA may not induce *de novo* *TGFB1* expression (Goppelt-Struebe, Esslinger, and Kunzendorf 2003; Minguillon et al. 2005). Thus, the role for TGF- β 1 in mediating therapeutic immunosuppressive effects by calcineurin inhibitors remains unclear.

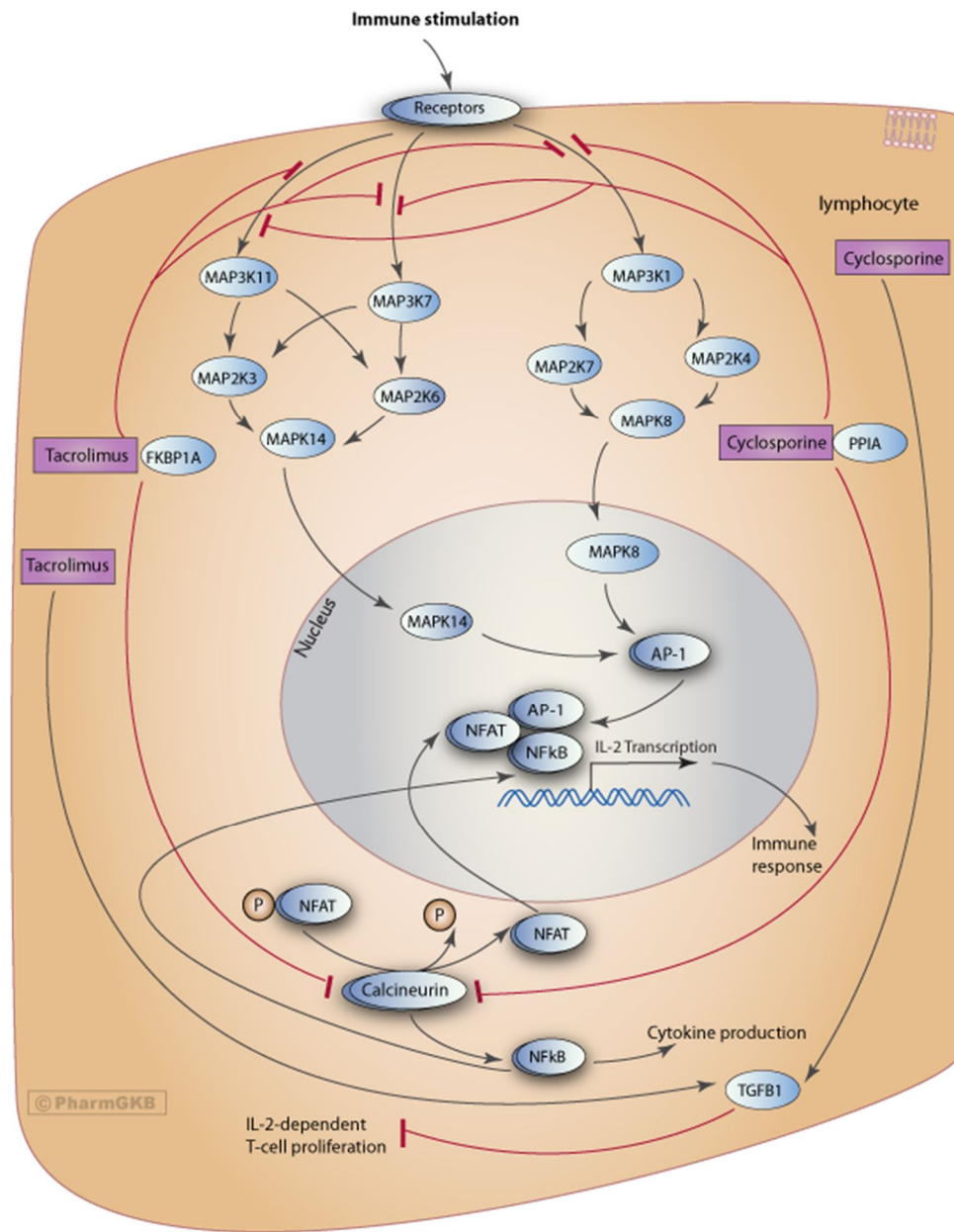


Figure 1-2. Pharmacodynamics of calcineurin inhibitor pathway. Stylized depiction of the mechanism of action of tacrolimus and cyclosporine in lymphocytes, as well as the candidate genes believed to interact with the two drugs. The primary mechanism by which calcineurin inhibitors cause immunosuppression is by binding immunophilins thereby inhibiting calcineurin which prevents activation of NFAT in T cells. Other mechanisms contributing to immunosuppressive effects of these drugs include inhibition of c-Jun N-terminal kinase (JNK) and p38 MAPK pathways and the induction of transforming growth factor β 1 (TGF- β 1). The exact mechanisms of these alternative immunosuppressive pathways is unknown. Reprinted with permission from (Barbarino et al. 2013).

1.6. Cyclosporine-induced Nephrotoxicity (Calcineurin Inhibitor Nephrotoxicity)

Since its first use in clinical renal transplantation, cyclosporine therapy has been associated with acute renal dysfunction. The nephrotoxic effects of cyclosporine, and alternate calcineurin inhibitor tacrolimus, are not limited to transplanted kidneys. Deleterious effects to native kidneys have been observed in a host of other cyclosporine therapies including various non-kidney transplantations, polyarthritis, and inflammatory ophthalmic disease. Since both drugs cyclosporine and tacrolimus primarily act to inhibit calcineurin-dependent activation of immune cells and the administration of both drugs results in similar deleterious effects on kidney structure and function, this condition is referred to as calcineurin inhibitor nephrotoxicity (CIN). CIN is manifested in two distinct subtypes: acute nephrotoxicity and chronic nephrotoxicity. Acute nephrotoxicity is often reversible by withdrawal of the drug or dose reduction whereas the chronic progressive form of the disease is usually irreversible. Acute nephrotoxicity is largely characterized by acute azotemia, an elevation of blood urea nitrogen (BUN) and serum creatinine levels, indicating a decline in glomerular filtration rate (GFR). Further, urine concentration ability and sodium retention are impaired. Acute CIN is distinguished from acute rejection histologically by the absence of inflammatory infiltrate. (Hall et al. 1985). An early study comparing cyclosporine to previous immunosuppression regimens in cadaver renal transplant recipients demonstrated that prolonged ischemia is a confounding factor and increases the risk of acute nephrotoxicity and nonfunction (Novick et al. 1986).

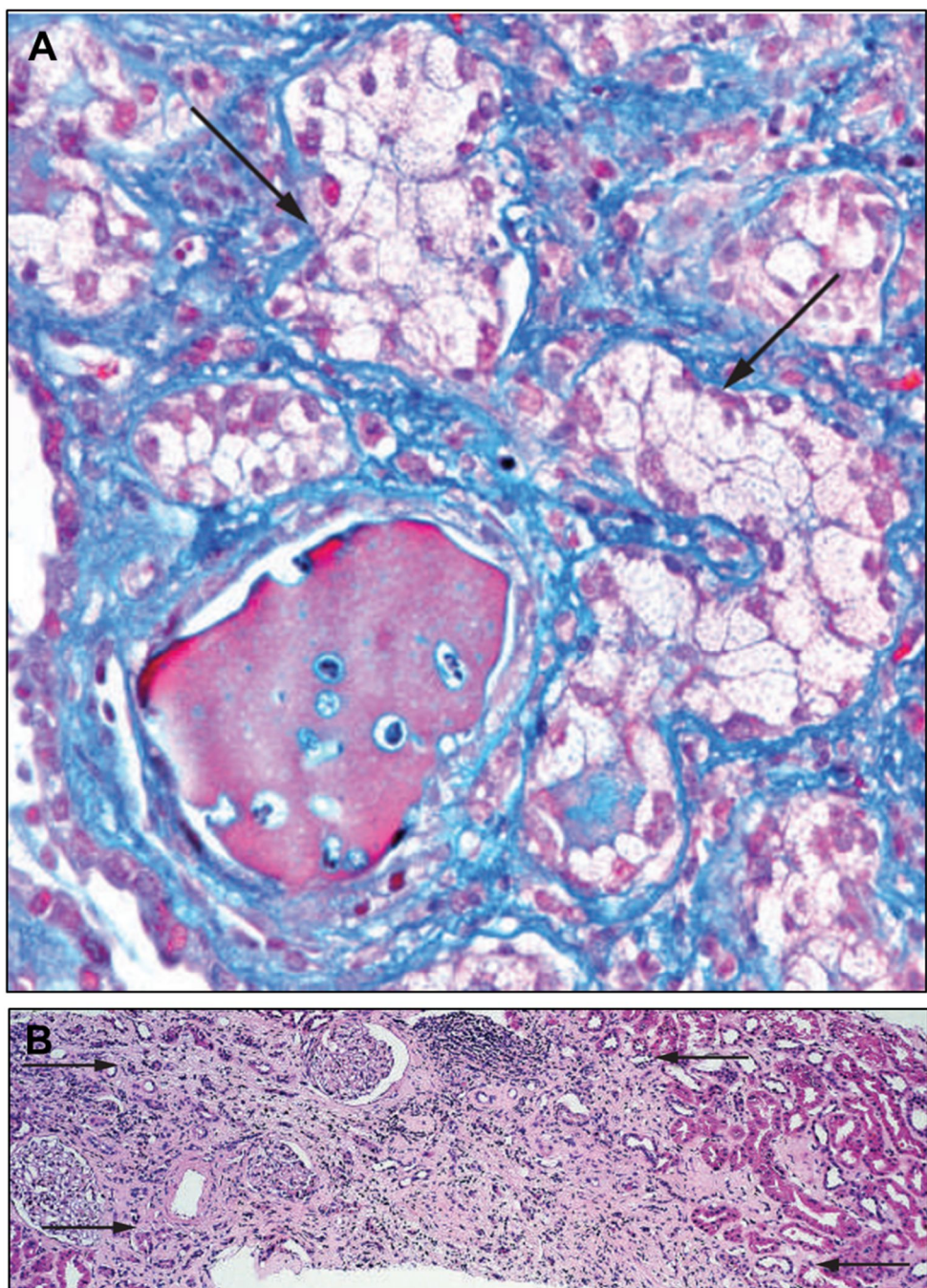


Figure 1-3. Pathogenesis of cyclosporine-induced nephropathy. (A) Fine vacuolization of the proximal tubule is associated with CIN and distinguishes pathogenesis from other conditions such as ischemia. Trichrome, 200X. (B) Example of interstitial fibrosis presenting as “striped” fibrosis. The fibrotic tubules also exhibit atrophy (area between arrows). Hematoxylin–eosin, 100X. Reprinted with permission from (Liptak and Ivanyi 2006).

It is believed that the primary physiological explanation for acute nephrotoxicity due to cyclosporine therapy is that cyclosporine induces vasoconstriction of the afferent and efferent glomerular arterioles and subsequently reduces renal blood flow, impairing GFR (Lane and Conger 1993). Mechanistically, it has been shown that cyclosporine impairs endothelial cell function, decreasing vasodilators such as nitric oxide and prostaglandins while also increasing vasoconstrictors such as endothelin, thromboxane, and the renin-angiotensin system. Renal vasoconstriction may be prevented by treatment with a calcium channel blocker, as administration of the drug lacidipine in kidney transplant recipients prevented cyclosporine-induced decline of renal plasma flow (RPF) and GFR (Ruggenenti et al. 1993). However, treatment with calcium channel inhibitors does not prevent a rise in endothelin excretion and thus may not prevent long-term vascular disease (W. M. Bennett 2014).

In early trials, at high concentrations, cyclosporine was shown to be directly toxic to the proximal tubule. This toxicity manifests as morphological changes such as isometric vacuolization (shown in **Figure 1-3A**), microcalcification, and the presence of inclusion bodies (nuclear and cytosolic aggregates) due to the presence of giant mitochondria (Kopp and Klotman 1990; Chapman 2011; Naesens, Kuypers, and Sarwal 2009). It has been noted that therapeutic levels of cyclosporine do not depress proximal tubule function and that the incidence of acute nephrotoxicity with morphologic evidence of tubular injury has fallen since the early years of the drug's use (Kopp and Klotman 1990). Chronic nephrotoxicity due to calcineurin inhibitors manifest as irreversible deterioration of renal function as a result of interstitial fibrosis, tubular atrophy, arteriolar hyalinosis, glomerulosclerosis (Kemper and Kniska 2014). Histologically, this often

appears a pattern of “striped” fibrosis and tubular atrophy, shown in **Figure 1-3B** (Liptak and Ivanyi 2006). This deterioration is thought to be caused in part by the acute vascular damage which creates local hypoxia/ischemia, free radical formation and activation of the renin angiotensin system (Kemper and Kniska 2014).

A key growth factor which has widely been reported to drive pathogenesis, fibrosis in particular, is transforming growth factor beta 1 (TGF- β 1). Up-regulation of *TGFB1* directly in proximal tubular cells by calcineurin inhibitors has been observed to be profibrogenic (Islam et al. 2001; Ashwani Khanna et al. 2002; Prashar et al. 1995). *TGFB1*, fibronectin, and collagen were also elevated in patients exhibiting CIN (Ashwani Khanna et al. 2002). The fibrogenic properties of TGF- β 1 are well known: it can induce renal fibrosis via activation of both canonical (Smad-based) and non-canonical (non-Smad-based) signaling pathways. This results in activation of myofibroblasts, excessive production of extracellular matrix (ECM) and inhibition of ECM degradation (Meng, Nikolic-Paterson, and Lan 2016). TGF- β 1 is also known as key regulator of epithelial-to-mesenchymal transition, in which cells lose their epithelial characteristics, such as apical-basal polarity and specialized cell-cell contacts, and acquire a more motile and migratory phenotype (J. Xu, Lamouille, and Deryck 2009).

1.7. Molecular Re-programming in Calcineurin Inhibitor Nephrotoxicity Induces Epithelial-to-Mesenchymal Transition

A major characteristic of chronic cyclosporine-induced nephrotoxicity leading to progressive and irreversible renal failure is extensive tubule-interstitial fibrosis (Myers et al. 1984). Specifically, tubulo-interstitial fibrosis manifests as tubular atrophy, ECM

accumulation, and thickening of the basement membrane ultimately resulting in loss of tubular function (Slattery et al. 2005). These pathological features of the chronic condition have led investigators to conclude that the proximal tubule epithelial cells are a primary target for chronic cyclosporine-induced nephrotoxicity (McMorrow et al. 2005). In the progression of tubule-interstitial fibrosis, it was first observed in other renal diseases such as diabetic nephropathy and IgA glomerulonephritis that interstitial myofibroblast activation plays a key role in pathogenesis (Hewitson and Becker 1995; Essawy et al. 1997).

To determine the source of activated myofibroblasts in the progression of renal diseases, Rastaldi et al. analyzed by immunohistochemistry and *in situ* hybridization 133 human renal biopsies accounting for nine different histological diagnoses, including minimal change disease, membranous nephropathy, IgA glomerulonephritis, primary focal segmental glomerulosclerosis, membranoproliferative glomerulonephritis, systemic lupus erythematosus, diabetic glomerulosclerosis, ANCA-positive renal vasculitis, and nephroangiosclerosis (Rastaldi et al. 2002). In these renal disease samples, it was found that tubular epithelial cells could become collagen-producing cells, expressing markers of proliferation and a mesenchymal phenotype (vimentin and alpha-smooth muscle actin) accompanied by loss of expression of epithelial markers (Rastaldi et al. 2002). This phenomenon of epithelial-to-mesenchymal transition (EMT) has been implicated in numerous developmental processes and diseases, with a particular focus on its role in the development of metastasis of tumors originating from epithelial tissues. Outside the context of normal development or neoplasia, it has widely been observed that EMT plays

a significant role in the process of wound healing, fibrotic remodeling, and the inflammatory response (Stone et al. 2016).

In order to define the key molecular events during EMT of tubular epithelial cells to myofibroblasts, Yang and Liu treated a tubular epithelial cell line (HCK-8) with TGF-beta, inducing *de novo* expression of a-SMA, loss of E-cadherin, transformation of myofibroblastic morphology, and production of ECM. Further, they observed increased expression of matrix-metalloproteinase-2 (MMP2) which specifically degrades the tubular basement membrane, leading to increased motility, migration and invasiveness.

Slattery et al. therefore hypothesized that cyclosporine treatment, which leads to irreversible renal failure characterized by tubulointerstitial fibrosis, may induce EMT in the HK-2 human proximal tubule cell line. Indeed, the authors demonstrated that CsA induced morphological changes (cell elongation, detachment, cytoskeletal rearrangement, and junctional disruption) consistent with phenotypical EMT. Further, they demonstrated that CsA induced *de novo* expression of a-SMA in HK-2 cells, a phenotypic marker of myofibroblast cells. Conversely, CsA reduced expression and membrane localization of the junctional structure proteins ZO-1, B-catenin, and E-cadherin. In addition to examining these conventional EMT markers, the authors performed a large-scale gene expression analysis of CsA-treated HK-2 cells compared to controls cells. This experiment was conducted using Affymetrix GeneChip microarray technology. Probing a total of 7070 genes, 128 genes were significantly differentially regulated after 48 h exposure to CsA (93 up more than two-fold; 35 down more than two-fold, **Tables 1-1 and 1-2**).

Slattery et al. observed that many of the up-regulated genes were known to be pro-fibrotic, including *TGFB1*, which encodes the multifunctional cytokine and growth factor TGF- β 1. Expression of *TGFB1* was confirmed by immunoblot and TGF- β 1-specific ELISA. The authors also confirmed by RT-PCR the increased expression of *FUS*, *PRKCB*, *PAX8*, *TCF3*, *COL14A1*, and *ACTA2*. Collectively, these genes may contribute to the pro-fibrotic phenotype. *FUS* is an RNA-binding oncogene which, when fused and translocated with DNA-binding transcription factors, is involved in the pathogenesis of liposarcomas. Evidence suggests that normal *FUS* expression is involved in the transactivation of NF-kB (Uranishi et al. 2001). *PRKCB* encodes protein kinase C beta (PKC-B), a Ca²⁺-dependent signal transducer which stimulates the Na⁺/H⁺ exchanger NHE3 (encoded by *SLC9A3*) and basolateral Na⁺/K⁺ ATPase, which both promote Na⁺ reabsorption (Wiederkehr, Zhao, and Moe 1999; Boron and Boulpaep 2017). PKC-dependent Na⁺-ATPase activity in the renal proximal tubule is stimulated by angiotensin II (Rangel et al. 2002). Further, in response to high-glucose, PKC activity has been shown to inhibit proximal tubule cell proliferation and increase secretion of TGF-B1 (S. H. Park et al. 2001). *PAX8* plays a critical role in kidney development, specifically nephron differentiation and branching morphogenesis of the metanephros (Narlis et al. 2007). Using immunohistochemistry, *PAX8* protein was detected in 85% of metastatic renal tumors, suggesting that this gene may be a useful marker to study renal cell carcinoma (Barr et al. 2015; Tong et al. 2009).

TCF3 encodes the transcription factor 3 protein, also known as E2A immunoglobulin enhancer-binding factors E12/E47. Increased expression of the E2A proteins has been confirmed in CsA-treated HK-2 cells (Slattery, McMorrow, and Ryan

2006). Overexpression of the E2A isoforms resulted in altered proximal tubule cell morphology, F-actin cytoskeletal rearrangement, decreased E-cadherin expression, and increased *ACTA2* expression, thus inducing EMT in HK-2 cells (Slattery, McMorrow, and Ryan 2006). *COL14A1* encodes the alpha chain of type XIV collagen, a member of the FACIT (fibril-associated collagens with interrupted triple helices) collagen family which has been implicated in pulmonary and hepatic fibroses (Bracht et al. 2015; Tzortzaki et al. 2003; Bolarin and Azinge 2007). *ACTA2* encodes alpha-smooth muscle actin, an actin-isoform typical of smooth muscle differentiation and prototypical marker of EMT used to define myofibroblasts (Nagamoto, Eguchi, and Beebe 2000). Thus, in proximal tubule cells, CsA induced a large-scale reprogramming of gene expression. This expression program suggests that the proximal tubule cells undergo EMT in response to CsA treatment and the evidence suggests that PKC- β and TGF- β 1 activation may drive this phenomenon.

Table 1-1. Genes up-regulated more than two fold in response to treatment with 4.2 $\mu\text{mol/L}$ CsA for 48 hours

Type	Gene	FC
Enzymes - membrane associated	Serine protease hepsin	8.24
	Liver dipeptidyl peptidase IV	4.56
	Autotaxin	3.21
	Prostaglandin D2 synthase	2.46
	Receptor tyrosine kinase (DTK)	2.31
	Receptor tyrosine kinase DDR	2.04
Enzymes - cytosolic	Protein kinase C (PKC) type β	4.79
	Long-chain acyl-CoA synthetase	3.15
	Catechol estrogen UDP-glucuronosyl- transferase	2.87
	Transketolase	2.80
	Cysteinyl-tRNA synthetase	2.76
	Long-chain acyl-coenzyme A synthetase	2.48
	Sulfotransferase, Phenol-Preferring	2.44
	Mitochondrial isocitrate dehydrogenase	2.44
	p33/HEH epoxide hydrolase	2.38
	Hydroxymethylglutaryl-CoA lyase	2.34
	Argininosuccinate synthetase	2.25
	Neuron specific (gamma) enolase	2.23
	P1MT isozyme I	2.11
	Red cell-type low MW acid phosphatase	2.06
	Arg protein tyrosine kinase-binding protein	2.04
Enzymes - extracellular	Plasma (extracellular) glutathione peroxidase	2.53
Cytokines and secreted proteins	Extracellular proteinase inhibitor homologue	6.31
	Transforming growth factor-beta 1*	2.91
	Pre-B cell enhancing factor (PBEF)	2.32
	Transcobalamin II	2.30
	Epithelin 1 and 2	2.28
	TGF-beta superfamily protein	2.03
Membrane Associated - cell membrane	Epithelial mucin 1*	4.58
	Cardiac gap junction protein	3.81
	Natriuretic peptide receptor (ANP-A receptor)	3.51
	Lutheran blood group glycoprotein	3.50
	C5a anaphylatoxin receptor	3.27
	NMB	3.13
	Glucose transporter-like protein-III	2.86

	Human B61	2.55
	Heparan sulfate proteoglycan	3.55
	Glycophorin C*	2.41
	Membrane cofactor protein	2.36
	Pancreatic mucin	2.29
	APXL	2.23
	Amyloid A4 precursor	2.27
	Amyloid β (A4) Precursor	2.17
	Na,K-ATPase gamma subunit	2.04
	Ryudocan core protein	2.01
Membrane associated - extracellular barriers	Laminin-related protein	3.28
	Collagen XIV	2.93
	Laminin B1 chain	2.71
	Collagen IV	2.12
	Apolipoprotein AI regulatory protein	3.40
Nuclear - transcription factors	Nuclear Factor Nf-IL6	2.69
	Transcription elongation factor S-II, hS-II-T1	2.39
	Class I homeoprotein	2.31
	Id1	2.17

Reprinted with permission from (Slattery et al. 2005).

Table 1-2. Genes down-regulated more than two fold in response to treatment with 4.2 μ mol/L CsA for 48 hours

Type	Gene	FC
Enzymes	Cytosolic acetoacetyl-coenzyme A thiolase	4.90
	Tissue plasminogen activator (PLAT)	3.52
	Squalene epoxidase	2.33
	Ornithine decarboxylase	2.30
	Glutamine PRPP amidotransferase	2.12
	ADE2H1 homology to SAICAR synthetase	2.10
	Dual-specificity protein phosphatase	2.07
	Deoxyguanosine kinase	2.05
	DNA topoisomerase 1	2.00
Cytokines and secreted proteins	Heparin-binding EGF-like growth factor	2.18
Membrane associated	[Alpha]tubulin	3.72
	Transferrin receptor	3.61
	Neurofilament-66	2.17
	Annexin II	2.09
	Myosin light chain 2	2.06
Nuclear - TFs/co-factors	HMGI-C protein	3.58
	Nuclear localization sequence receptor	2.63
	Acid finger protein	2.11
	Hepatocyte nuclear factor-3/fork head homolog 11A	2.05
	Centromere protein-A	2.05
	Human C2f	2.04
Intracellular - cell cycle	Cyclin B	2.77
	p55CDC	2.75
	Cyclin F	2.45
	Cyclin A2	2.35
Other	S100A2 gene	4.10
	Cyr61 gene	3.01
	H105e3	2.73
	[Mu]crystallin	2.54
	Pre-mRNA splicing factor	2.44
	Heterogeneous Nuclear Ribonucleoprotein	2.36
	Nucleolar protein p40	2.32
	Nm23 gene	2.21
	Ubiquitin fusion-degradation protein	2.03
Undefined	mRNA for KIAA0095	2.2

Reprinted with permission from (Slattery et al. 2005)

1.8. Epithelial-to-Mesenchymal Transition

Epithelial-mesenchymal transition is a critical process in development and wound healing (Zeisberg and Kalluri 2004; Larue and Bellacosa 2005; Stone et al. 2016). It also plays a major role in conferring ‘stemness’ to pluripotent cell types (Radisky and LaBarge 2008). However, EMT is plays a major role in the pathogenesis of cancer and fibrosis (Rastaldi 2006; Horowitz and Thannickal 2006; Kalluri and Weinberg 2009; Voulgari and Pintzas 2009). The molecular mechanisms of EMT have largely been deciphered in the context of cancer invasiveness and metastasis. In cells undergoing EMT, genes which express epithelial proteins such as E-cadherin are downregulated, whereas gene programs promoting migration, motility, cytoskeletal changes and modification of the extracellular matrix are upregulated. EMT progression may result from several contributing signaling pathways including ILK, TGF- β 1, SMAD, PI3K/AKT, ERK MAPK, p38 MAPK, and JNK (Lamouille, Xu, and Derynck 2014).

EMT has become an accepted model for interpreting the events that lead to tubulo-interstitial fibrosis in CIN (Slattery et al. 2005; Rastaldi 2006; Fragiadaki and Mason 2011; Zeisberg and Kalluri 2004; McMorrow et al. 2005). For instance, in cell-based models of CIN, our lab and other have investigated the molecular mechanisms leading to EMT phenotypical changes which contribute to CIN pathology. In kidney proximal tubule cell lines, such as human kidney 2 (HK-2) cells, CsA induces loss of epithelial characteristics and gain of more mesenchymal morphology, migratory properties, and gene expression program. For example, treatment of HK-2 cells induces expression of alpha-smooth muscle actin (α -SMA) and fibroblast specific protein-1 (FSP-1) and decreases expression of epithelial-specific e-cadherin (Yuan et al. 2015). Since

miRNAs have been shown to play a major role in EMT and renal diseases (Abba et al. 2016; Godwin et al. 2010; Aguado-Fraile et al. 2013; Carew, Wang, and Kantharidis 2012), our lab sought to determine the role of microRNAs in CIN and cyclosporine-induced EMT. We found that miR-494, which was elevated in the kidneys of mice exhibiting CIN, targets *PTEN* expression in proximal tubule cells, thereby promoting an EMT phenotype (Yuan et al. 2015). CsA induction of EMT markers and morphological changes could be abrogated by blocking miR-494 activity. In a similar fashion, miR-21 was found by another lab to repress *PTEN* expression after CsA treatment, activating Akt signaling and contributing to EMT and CIN pathology (J. Chen et al. 2015). Thus, microRNAs (miRNAs), which are known to play a significant role in EMT progression in a variety of cellular contexts may also play a significant role in CIN and EMT in proximal tubule cells.

1.9. Post-transcriptional regulation of gene expression by microRNAs

MicroRNAs (miRNAs) are small non-coding RNAs, usually 20-24 nucleotides in length (**Figure 1-4A**). Mature microRNAs are single-stranded oligonucleotides derived from the endogenous cleavage of hairpin stem-loop precursor-miRNAs (pre-miRNAs). The first microRNA gene was discovered in *C. elegans* following the observation that the gene *lin-4*, responsible for controlling normal temporal control of larval development, was not a protein-coding gene but encoded two small transcripts of 61 and 22 nucleotides (Rosalind C. Lee, Feinbaum, and Ambros 1993). It was determined that the small RNA transcripts produced by *lin-4* contained sequences complementary to a repeated sequence element in

the 3'UTR of *lin-14* mRNA, a gene which controls the temporal sequence of developmental events in the *C. elegans* postembryonic cell lineage. The authors demonstrated that antisense RNA-RNA interactions between *lin-4* RNA and *lin-14* mRNA resulted in reduced translation of LIN-14 protein, leading to developmental transitions (Wightman, Ha, and Ruvkun 1993). Not until years later did the discovery of *let-7* in *C. elegans*, a 22-nucleotide regulatory RNA necessary to promote late larval-stage cells into adult-stage cells, awaken the field to the possibility of conserved and widespread regulation by small non-coding RNAs (Reinhart et al. 2000; Slack et al. 2000). *Let-7* and *let-7* homologs were discovered in human, fly, and several other animal genomes soon thereafter (Pasquinelli et al. 2000). The most recent release of MiRBase (v21), the miRNA registry and database of published miRNA sequences and annotation, contains a total of 1,881 precursor and 2,588 mature human miRNAs (Griffiths-Jones et al. 2006; Kozomara and Griffiths-Jones 2014; Griffiths-Jones et al. 2008; Kozomara and Griffiths-Jones 2011). Since its inception, the repository has grown at an exponential rate (**Figure 1-4B**), resulting in 28,645 total precursor and 35,828 mature miRNA entries across 223 species.

MiRNA genes are located primarily in intergenic regions, making up dedicated miRNA gene loci with independent transcription units (M Lagos-Quintana et al. 2001; R. C. Lee and Ambros 2001). As much as 30% of miRNA genes are located in intronic regions of annotated genes and most miRNAs are transcribed by RNA polymerase II (Pol II) in the nucleus (Y. Lee et al. 2004). RNA polymerase III (Pol III), which transcribes most small RNAs such as tRNAs and U6 snRNA, may also transcribe some human miRNAs, especially those residing within repetitive elements such as Alu repeats

(Borchert, Lanier, and Davidson 2006). The resulting transcripts, called primary miRNAs (pri-miRNAs), are capped, spliced and polyadenylated. Some primary miRNA transcripts may contain clusters of multiple miRNA stem loops (M Lagos-Quintana et al. 2001; Y. Lee et al. 2002). Within the nucleus, RNase-III type endonuclease DROSHA and co-factor DGCR8/PASHA (collectively known as ‘Microprocessor’) cleave the pri-miRNA transcripts into ~70 nt long stem-loop precursor miRNAs called pre-miRNAs (Denli et al. 2004; Gregory et al. 2004; Y. Lee et al. 2003). Export of the pre-miRNA from the nucleus to the cytoplasm is facilitated by exportin 5 (XPO5) (Yi et al. 2003; Lund et al. 2004; Bohnsack, Czaplinski, and Gorlich 2004). In the cytoplasm, the RNAase III endonuclease Dicer (encoded by *DICER1*) processes the pre-miRNA hairpin by cleavage at a measured distance from the 5' and 3' ends (J.-E. Park et al. 2011; Haidi Zhang et al. 2002). Asymmetric cleavage produces the mature miRNA duplex, usually 20-24 nucleotides, containing a characteristic 2 nucleotide 3'-overhang (Bernstein et al. 2001). These events are summarized in **Figure 1-5**.

This duplex contains one “guide” strand, the mature single-stranded miRNA, and one “passenger” strand which is degraded. Transactivation-responsive RNA-binding protein (TRBP) associates with DICER1 to promote cleavage and influences guide-strand selection (H. Y. Lee and Doudna 2012). Further, TRBP recruits the Dicer complex to Argonaute proteins (AGO1-4) and is required for assembly the miRNA-induced silencing complex (miRISC), also referred to as RISC (Chendrimada et al. 2005). The AGO-miRNA complex forms the basis for targeted repression of mRNAs. Nucleotides 2-7 of the miRNA are particularly exposed when complexed with AGO proteins, allowing for complementary Watson-Crick base pairing to mRNAs (Wee et al. 2012; Doench and

Sharp 2004). A summary of canonical seed pairing is illustrated in **Figure 1-6**. Recruitment of GW182 family proteins induces post-transcriptional gene silencing by translational repression and degradation of mRNAs (Eulalio, Huntzinger, and Izaurralde 2008; Braun et al. 2011; Zekri et al. 2009; Eulalio, Tritschler, and Izaurralde 2009). Within the cytoplasm, the specific foci where RISC proteins, RNA substrates and proteins such as de-capping enzymes and RNA helicases localize to promote gene silencing are called processing bodies, or P-bodies (J Liu et al. 2005).

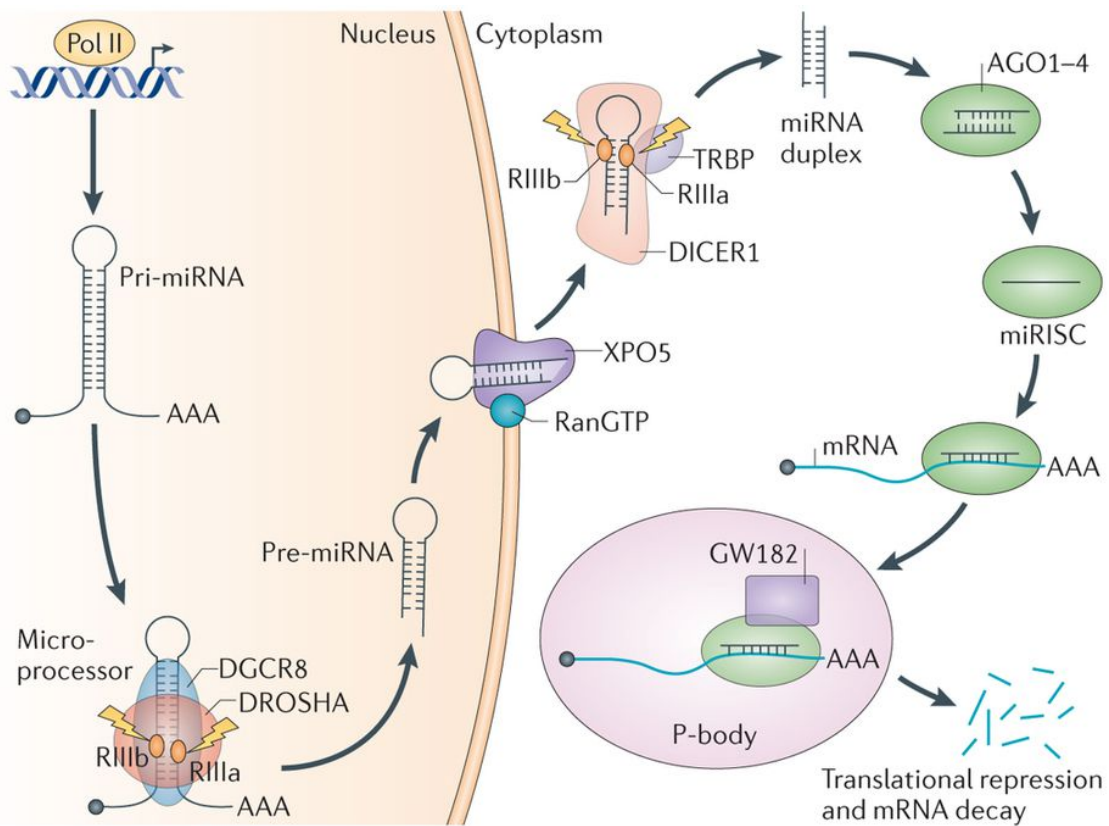
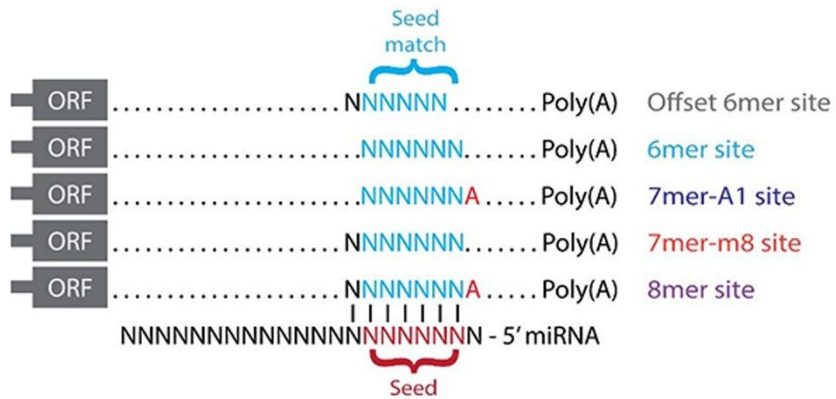


Figure 1-5. Overview of miRNA biogenesis pathway. MicroRNA (miRNA) genes are transcribed as primary miRNAs (pri-miRNAs) by RNA polymerase II (Pol II) in the nucleus. The long pri-miRNAs are cleaved by Microprocessor, which includes DROSHA and DiGeorge syndrome critical region 8 (DGCR8), to produce the 60–70-nucleotide precursor miRNAs (pre-miRNAs). The pre-miRNAs are then exported from the nucleus to the cytoplasm by exportin 5 (XPO5) and further processed by DICER1, a ribonuclease III (RIII) enzyme that produces the mature miRNAs. One strand of the mature miRNA (the guide strand) is loaded into the miRNA-induced silencing complex (miRISC), which contains DICER1 and Argonaute (AGO) proteins, directs the miRISC to target mRNAs by sequence complementary binding and mediates gene suppression by targeted mRNA degradation and translational repression in processing bodies (P-bodies). TRBP, transactivation-responsive RNA-binding protein. Reprinted with permission from (Lin and Gregory 2015).

A Canonical site types



B Non-canonical site types

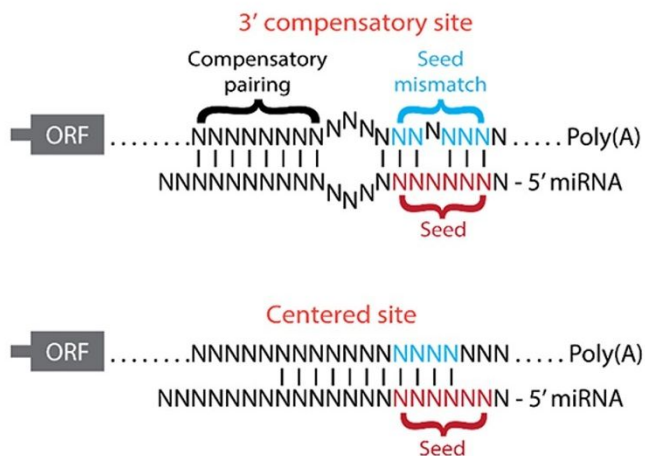


Figure 1-6. Canonical and non-canonical miRNA target site types. (A) Diagram of the five canonical miRNA binding site types aligned to the 3'UTR of a transcript. An 8mer site contains an exact match to positions 2-8 of the mature miRNA (the seed + position 8) followed by an 'A.' There are two types of 7mer sites: 7mer-m8, an exact match to positions 2-8 of the mature miRNA (the seed + position 8); 7mer-A1, an exact match to positions 2-7 of the mature miRNA (the seed) followed by an 'A.' A 6mer site is an exact match to positions 2-7 of the mature miRNA (the seed). An offset 6mer site is an exact match to positions 3-8 of the mature miRNA. 6mer sites are considered 'poorly conserved.' (B) Diagram of the two types of non-canonical miRNA binding sites aligned to the 3'UTR of a transcript. Non-canonical sites do not involve canonical pairing in the seed region (positions 2-7) of the mature miRNA. A 3' compensatory site contains an imperfect seed match that is compensated by strong 3' pairing. A centered site also lacks perfect seed pairing and 3' compensatory pairing but instead has 11-12 contiguous Watson-Crick pairs to miRNA positions 4-15.

1.10. CLIP and PAR-CLIP experiments

There are currently several technologies available to investigate the roles of RNA-binding proteins on target RNAs and mRNAs. Much in the way ChIP-seq (chromatin immunoprecipitation combined with massive parallel DNA sequencing) was designed to analyze protein interactions with DNA, crosslinking and immunoprecipitation (CLIP) methods have been developed for analyzing protein interactions with RNAs. Licatalosi et al. developed the first such method for genome-wide mapping of protein-RNA binding sites *in vivo*, termed HITS-CLIP (high-throughput sequencing of RNA isolated by crosslinking immunoprecipitation) (Licatalosi et al. 2008). The HITS-CLIP method (also referred to as CLIP-seq) is an improved version of an earlier CLIP method employed by the same laboratory in which isolated RNAs were cloned and sequenced by Sanger sequencing (Ule et al. 2003; Ule et al. 2005). In the HITS-CLIP study, the authors constructed and analyzed a genome-wide map of *in vivo* RNA binding sites for the neuron-specific splicing factor Nova2 in mouse brain tissue (Licatalosi et al. 2008). This was accomplished by using UV-irradiation of neocortex tissue to induce covalent crosslinks between protein-RNA complexes *in situ*, followed by immunoprecipitation of the Nova2 protein, purification of isolated RNAs and high-throughput pyrosequencing. Analysis of the Nova2-bound RNAs confirmed a mechanism by which the position of Nova binding in transcripts determined the outcome of alternative splicing. Further, a novel role for Nova in regulating alternative polyadenylation was discovered based on binding of Nova to the 3'UTR of transcripts.

Subsequently, HITS-CLIP has been used to define the RNA-binding maps attributed to the splicing repressor polypyrimidine tract-binding protein (PTB) in HeLa

cells, cell type-specific splicing regulator FOX2/RBM9 in human embryonic stem cells, splicing factor SFRS1 in human embryonic kidney cells (Y. Xue et al. 2009; Yeo et al. 2009; Sanford et al. 2009). In a study of heterogeneous nuclear ribonucleoprotein C (hnRBPC), Konig et al. developed individual-nucleotide resolution UV-cross-linking and immunoprecipitation (iCLIP). Based on HITS-CLIP/Clip-seq, iCLIP takes advantage of the observation that in the conventional CLIP protocol the vast majority of cDNAs prematurely truncate immediately before the ‘cross-link nucleotide.’ The authors captured these truncation sites by introduction of a second barcoded adapter after reverse transcription via self-circularization. Subsequent Solexa sequencing reveals the identity and quantity of truncation, and thus crosslinking, sites.

To address the inherent challenges of miRNA target prediction, HITS-CLIP of the RNA binding protein Ago was conducted on mouse brain tissue to covalently crosslink native Ago protein-RNA complexes revealing both Ago-miRNA and Ago-mRNA binding sites (Chi et al. 2009). Bioinformatic analysis of the combined datasets identified interaction maps for the 20 most abundant miRNAs present in the P13 mouse brain (Chi et al. 2009). Subsequently, Ago-HITS-CLIP was also used to decode miRNA-mRNA interaction maps in *C. elegans* and KSHV-infected primary effusion lymphoma (PEL) cell lines (Zisoulis et al. 2010; Haecker et al. 2012).

PAR-CLIP was designed to improve upon HITS-CLIP technology by increasing crosslinking efficiency and resolution of detected RNA binding-protein (RBP) crosslinking sites (Hafner et al. 2010). This is accomplished by pre-treating cells with a uridine analog, 4-thiouridine (4-SU), which gets incorporated into nascent RNAs. RNAs that have incorporated 4-SU can be crosslinked to RBPs at 365 nm UV light rather than

265 nm light which increases specificity. This crosslinking is also more efficient than conventional crosslinking (Hafner et al. 2010). Also, crosslinking of 4-SU to aromatic side chains of peptides is distinct from endogenous ribonucleosides. Because the crosslinking is irreversible, amino acids bound to 4-SU in isolated RNAs cause errors to occur in reverse transcription leading to mutations in the resulting cDNAs. These mutations can be used in bioinformatic analysis of the sequencing data to define high-resolution binding sites. Many software tools have been developed to analyze these data using a variety of models to handle the mutations including PARalyzer (Corcoran et al. 2011), CLIPZ (Khorshid, Rodak, and Zavolan 2011), wavClusteR (Comoglio, Sievers, and Paro 2015), and PIPE-CLIP (B. Chen et al. 2014). Several PAR-CLIP studies have been used to identify miRNA-mRNA interactions in specific cell types including embryonic stem cells, prostate cancer cells, bone derived macrophages, and colorectal carcinoma cells (Lu et al. 2014; Hamilton et al. 2016; Lipchina et al. 2011; Farazi et al. 2014; Krell et al. 2016).

Some caveats and limitations remain in these CLIP methods. For instance, in both HITS-CLIP and PAR-CLIP large amounts of covalently crosslinked background binding to RNAs (such as ribosomal RNA) is common (Friedersdorf and Keene 2014). miRNA-mRNA interactions must be imputed based on expression of miRNAs or miRNA binding to the RISC complex and seed complementarity matching to mRNA binding sites. To identify miRNA-mRNA interactions more directly, the CLASH (crosslinking, ligation and sequencing of hybrids) was developed (Helwak et al. 2013). In this method, crosslinked miRNAs and mRNAs that are bound to the RISC complex are ligated to form chimeras which are then sequenced by deep sequencing. The resulting interactions

revealed that non-canonical seed sequences were identified far more frequently than expected. They also reported a high proportion of the mRNA target sites were located in the coding sequence of transcripts whereas PAR-CLIP experiments typically produce high proportion of 3'UTR target sites. Still, due to the technical nature of the CLASH protocol the method has very low efficiency. It has been suggested that this method is also likely to be biased towards longer miRNA/mRNA fragments due to steric hindrance of RISC (Cloonan 2015).

For the reasons and advantages described above, we determined that the PAR-CLIP method was best suited to map the miRNA-mRNA interactions in our cell model of CIN. PAR-CLIP offers efficiency and specificity advantages over traditional HITS-CLIP and the T>C mutations introduced offer superior resolution when determining binding sites by bioinformatic methods. CLASH is a more technically challenging and has not yet been demonstrated in a more physiological setting using endogenous levels of target protein. Our goal was to identify the most physiologically relevant miRNA-mRNA interactions in PTECs before and after treatment with CsA using an established cell model without perturbing the miRNA/RISC stoichiometry. There are many examples of successful PAR-CLIP experiments in a variety of cell types (summarized in **Table 1-3**). Further, numerous bioinformatic software packages and algorithms have been developed for the analysis of PAR-CLIP data since Hafner et al first described the method: notably PARalyzer, PIPE-CLIP, CLIPZ, and wavClusteR (Corcoran et al. 2011; B. Chen et al. 2014; Khorshid, Rodak, and Zavolan 2011; Sievers et al. 2012). These tools seek to address the various technical obstacles and allow for stringent quality control of the data.

Previous example datasets may also serve as benchmarks for comparison throughout the analysis pipeline.

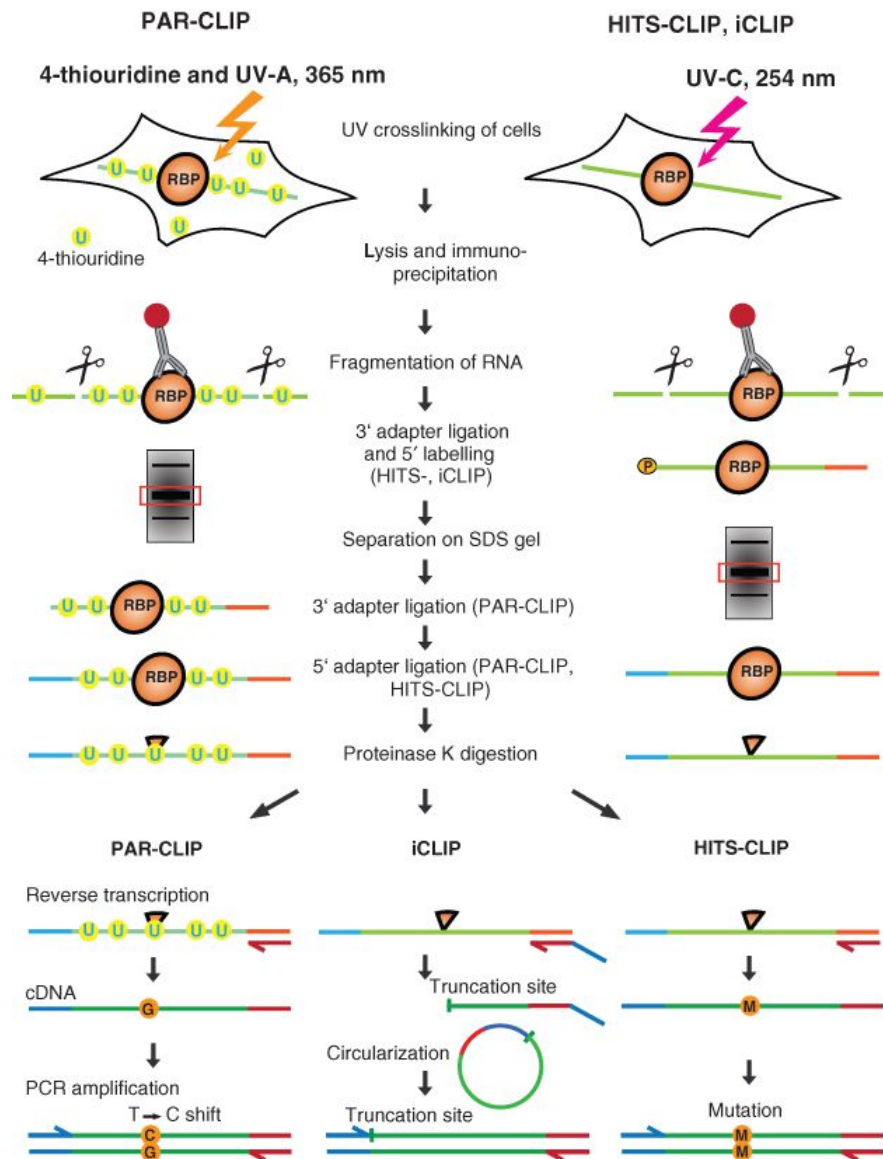


Figure 1-7. Protein-RNA crosslinking and immunoprecipitation (CLIP) methods.
Reproduced under Creative Commons License (Gruber et al. 2014)

Table 1-3. Summary of AGO-CLIP experiments

Author	Year	Type	Antibody	Source
Chi et al.	2009	HITS-CLIP	Anti-Ago1-4 (2A8) mAb	Mouse brain tissue
Hafner et al.	2010	PAR-CLIP	Anti-FLAG M2 mAb	FLAG/HA-AGO1-4-HEK293 cells
Lipchina et al.	2011	PAR-CLIP	Anti-AGO2 (9E8.2) mAb	hESCs
Kishore et al.	2011	PAR-CLIP	Anti-AGO2 (11A9) mAb	HEK293 cells
Leung et al.	2011	PAR-CLIP	Anti-Ago2 mAb	mESCs
Gottwein et al.	2011	PAR-CLIP	Not specified	BC-1/BC-3 cells
Skalsky et al.	2012	PAR-CLIP	Anti-FLAG M2 mAb/ Anti-AGO2 (9E8.2) mAb	BC-1/BC-3 cells
Helwak et al.	2013	CLASH	IgG-Dynabeads	Flp-In T-REx 293-PTH-AGO1 cells
Lu et al.	2014	PAR-CLIP	Anti-Ago2 (2D4)	BMDM cells
Hamilton et al.	2016	PAR-CLIP	Anti-AGO2 (11A9) mAb	LNCaP, 22Rv1, LAPC4, DU145, and PC3 cell lines
Krell et al.	2016	PAR-CLIP	Anti-AGO2 (11A9) mAb	HCT116 TP53 ^{+/+} cells; HCT116 TP53 ^{-/-} cells
Schwentner et al.	2016	PAR-CLIP	Anti-AGO2 (11A9) mAb	A673/TR/shEF cells

1.11. Role of microRNAs in CIN

To date, few studies have examined the specific role of miRNAs in CIN. Our lab demonstrated that miR-494 expression was aberrant in kidneys of mice treated with CsA and presenting with renal injury (Yuan et al. 2015). In HK-2 cells, CsA treatment induced miR-494 expression in a time and dose dependent manner which corresponded to increased alpha-smooth muscle actin and decreased e-cadherin. It was shown that *PTEN* was a target of miR-494 and that treatment with a miR-494 inhibitor could prevent CsA-induced EMT. Chen et al. profiled miRNA expression in PTECs treated with CsA for 6 hours and found that miR-21 was highly up-regulated (J. Chen et al. 2015). The authors found that miR-21 was also capable of targeting *PTEN* in PTECs and that this targeting resulted in increased AKT signaling which promoted EMT/fibrotic genes. Treatment of cells with anti-miR-21 reduced CsA-induced AKT activation and EMT gene expression.

Gooch et al. performed an *in vivo* miRNA profile experiment of CIN in mice, identifying 76 differentially expressed miRNAs in whole kidneys, including up-regulation of miR-21 (Gooch et al. 2017). Paired with mRNA expression data and using the computational tool Diana-miRPath, the authors determined that the major molecular pathways predicted to be regulated by these miRNAs were MAPK, PI3K-Akt signaling, Wnt, Erb, insulin signaling, TGF- β , mTOR, and VEGF signaling.

Thus, it is evident that miRNAs play a significant role in CIN pathogenesis in proximal tubule cells. To date, however, a complete and integrative analysis of miRNA-mRNA targeting in this model has not been achieved. The majority of studies performed rely on profiling conducted with outdated microarray technologies and prediction algorithms which may not take into account experimentally validated data. Thus our

understanding of physiologically relevant targeting relationships remains limited. Further, our understanding of gene expression reprogramming in CIN of the proximal tubule is restricted to similarly outdated and limited array data. Thus, in order to better elucidate the physiological roles of miRNAs in the pathogenesis of CIN, we conducted an integrative analysis of miRNA and mRNA expression profiling paired with AGO-PAR-CLIP in HK-2 proximal tubule cells treated with CsA.

Chapter 2: Materials and Methods

2.1. Cell culture

HK-2 cells and 293T cells were obtained from ATCC (American Type Culture Collection, Manassas, VA, USA). HK-2 cells are an immortalized cell line derived from a primary proximal tubule cell culture from normal adult human renal cortex (Ryan et al. 1994). This cell line was established by transduction with human papilloma virus (HPV 16) E6/E7 genes and cultured cells were subsequently evaluated for phenotypical characteristics of well-differentiated PTECs, including positive markers alkaline phosphatase and cytokeratin and functional transporter characteristics (Ryan et al. 1994). The HK-2 cell line has since been utilized as an experimental model of proximal tubule epithelium physiology and function in a variety of contexts including high glucose response, toxicology screens, EGF and TGF- β 1 signaling response and epithelial-to-mesenchymal transition (Panchapakesan, Pollock, and Chen 2004; Wu et al. 2009; Yan et al. 2009; Lv et al. 2011; B. C. Liu et al. 2006; McMorrow et al. 2005; Slattery et al. 2005).

As per ATCC's recommendation, HK-2 cells were cultured in serum-free keratinocyte medium supplemented with 0.05 mg/mL bovine pituitary extract (BPE), 5 ng/mL human recombinant epidermal growth factor 1-53 (EGF 1-53), and 100 units/mL Penicillin-Streptomycin antibiotic mix. 293T cells were cultured in Dulbecco's Modified Eagle's Medium (DMEM) supplemented with 10% heat-inactivated fetal bovine serum (FBS), 2 mM L-glutamine and 100 units/mL Penicillin-Streptomycin antibiotic mix. All components were obtained from Thermo Fisher Scientific, Waltham, MA. All cells were

maintained at 37°C in a humidified atmosphere containing 5% CO₂. Routine sub-culturing of HK-2 cells was performed using TrypLE™ Express Enzyme (Thermo Fisher Scientific) when cells became ~80% confluent. A standard subcultivation ratio of 1:4 was used and media was replaced as necessary every 2-3 days. Special care was taken to not allow HK-2 cells to reach confluence. Routine sub-culturing of 293T cells was achieved in a similar manner, except that a subcultivation ratio of 1:10 was used. For experimental treatment of HK-2 cells with CsA, CsA (Sigma-Aldrich, St. Louis, MO) was prepared as a stock solution (5 ug/uL) in 100% ethanol. 80% confluent HK-2 cells were treated with CsA at predetermined concentrations or ethanol (0.1%, as vehicle control) for indicated durations.

2.2. Animal model of CsA-induced nephrotoxicity

Ten to twelve-week-old male C57BL/6J mice were purchased from The Jackson Laboratory (Bar Harbor, ME) and housed under microisolator conditions. All experiments were performed in accordance with the humane use and care policies of our Institution and were approved by the standing IACUC. CsA nephrotoxicity was induced as in (Andoh et al. 1997; Yang et al. 2002; Yuan et al. 2015). Briefly, mice were placed on a low sodium diet (0.01% sodium, TD.90228, Harlan laboratories, USA) and received a daily subcutaneous injection of CsA (30 mg/kg) diluted in olive oil (MP Biomedicals, Solon, OH). Control mice (vehicle) received a daily subcutaneous injection of olive oil only. Kidneys were harvested at 1, 2, and 3 weeks and flash-frozen. Each group included 4–5 animals.

2.3. Deep sequencing of miRNAs

Small RNAs were isolated from CsA-treated and vehicle control treated HK-2 cells 48 hours post-treatment. Total RNA, including small RNAs from 18 nucleotides upwards, was isolated using the miRNeasy Mini Kit (Qiagen, Valencia, CA). A protocol for preparation of miRNA-enriched fractions separate from larger RNAs (>200 nt) was performed. Briefly, larger RNAs were precipitated in 70% ethanol, filtered in silica-membrane columns and retained for mRNA analysis. The miRNA-enriched fraction was then precipitated with 100% ethanol, bound to columns, washed and eluted in RNase-free water.

The miRNA-enriched fractions were subsequently used for construction of small RNA cDNA libraries for Illumina sequencing. Construction of multiplexed small RNA cDNA libraries was accomplished using the NEBNext Multiplex Small RNA Library Prep Set for Illumina (Set 1) Kit (New England Biolabs, Ipswich, MA). The sequences of adaptor and primers used are listed in **Table 2-1**. Following adaptor ligation and reverse transcription, sample-specific barcodes were introduced in the final PCR amplification step (**Table 2-2**). Samples were amplified for 15 cycles and then fractionated by agarose gel electrophoresis to perform size selection prior to Illumina sequencing. The desired size of correctly ligated adapter-miRNA molecules is ~147 nucleotides.

The gel purified miRNA libraries were sequenced in one flowcell lane to produce single end, 50 base pair reads in high output mode on an Illumina HiSeq 2500 at the Tufts University Core Facility Genomics Core. Demultiplexing of reads was completed using Illumina's Consensus Assessment of Sequence and Variation (CASAVA) pipeline.

Table 2-1. NEBNext Small RNA Library adaptor and primer sequences used

Adaptor/primer	Sequence
NEBNext 3' SR Adaptor for Illumina	5'-rAppAGATCGGAAGAGAGCACACGTCT-NH ₂ -3'
NEBNext 5' SR Adaptor for Illumina	5'-rGrUrUrCrArGrArGrUrUrCrUrArCrArGrUrCrCrGrArCrG-rArUrC-3'
NEBNext SR RT Primer for Illumina	5'-AGACGTGTGCTCTTCCGATCT-3'
NEBNext SR Primer for Illumina	5'-AATGATA CGGC ACCACCGAGATCTACACGTT CAG-AGTTCTACAGTCCG-s-A-3'
NEBNext Index [X] Primer for Illumina	5'-CAAGCAGAACGGCATACGAGAT-[INDEX]-GTGA-CTGGAGTT CAGACGTGTGCTCTTCCGATC-s-T-3'

Table 2-2. Illumina index PCR primer sequences used

Sample	Illumina Index
HK2-E2	CGATGT
HK2-E3	TTAGGC
HK2-E4	TGACCA
HK2-E5	ACAGTG
HK2-C1	GCCAAT
HK2-C3	ACTTGA
HK2-C4	GATCAG
HK2-C5	TAGCTT

2.4. Deep sequencing of mRNAs

Large RNA fractions isolated from CsA-treated and vehicle-treated HK-2 cells that were separated from small RNAs (<200 nucleotides) were analyzed by Fragment Analyzer (Advanced Analytical Technologies, Inc., Ankeny, IA) to assess quality as determined by RNA Quality Number (RQN). This method computes the area under the peak for 18S and 28S RNA as a ratio of total RNA as well as the relative height of the 18S and 28S peaks to determine RNA quality (Schroeder et al. 2006). To enrich for mRNAs, intact poly(A)+ RNA was isolated from the samples using The NEBNext Poly(A) mRNA Magnetic Isolation Module (New England Biolabs, Ipswich, MA). In this procedure, magnetic oligo-d(T)₂₅-coupled beads are used to bind and isolate poly-A- RNA. The eluted mRNA samples were then converted into cDNA libraries using the NEBNext mRNA Library Prep Reagent Set for Illumina and NEBNext Multiplex Oligos for Illumina (Index Primers Set 1, New England Biolabs, Ipswich, MA). Prior to adaptor ligation and amplification, mRNA samples were subjected to a fragmentation protocol at 94°C for 5 minutes to generate 200 nucleotide RNA fragments. The resulting mRNA fragments were reverse transcribed and ligated to the adaptors listed in **Table 2-3**.

Barcodes for multiplexing were introduced by PCR amplification using Index Primers as in the miRNA-seq samples. PCR products were purified using MinElute PCR Purification Kit (Qiagen) and eluted in water. Size selection of the adaptor-ligated cDNA libraries was performed using a 2% agarose gel. Excised gel products were purified by QIAquick Gel Extraction Kit (Qiagen) and eluted in water.

Concentrations of the final library samples were determined by Quantifluor RNA System (Promega, Madison, WI), a fluorescent RNA-binding dye-based assay. The gel purified mRNA libraries were sequenced in one flowcell lane to produce single end, 50 base pair reads in high output mode on an Illumina HiSeq 2500 at the Tufts University Core Facility Genomics Core. Demultiplexing of reads was completed using Illumina's CASAVA pipeline

Table 2-3. NEBNext mRNA Library adapter and primer sequences

Adaptor/primer	Sequence
NEBNext Adaptor for Illumina	5'-/5Phos/GATCGGAAGAGCACACGTCTGAAGTCAGT-C/ideoxyU/ACACTCTTCCCTACACGACGCTCTTCCGAT-C*T-3'
NEBNext Universal PCR Primer for Illumina	5'-AATGATACGGCGACCACCGAGATCTACACTCTTC-CCTACACGACGCTCTTCCGATC*T-3'
NEBNext Index [X] Primer for Illumina	5'-CAAGCAGAAGACGGCATACGAGAT-[INDEX]-GTGAC-CTGGAGTTAGACGTGTGCTCTCCGATC-s-T-3'

2.5. Differential Expression Analysis of miRNA-seq and mRNA-seq Data

Small RNA reads were adapter-trimmed and filtered by size (greater than 16 nucleotides) using ‘Fastx_clipper’ (HannonLab 2014). Trimmed reads were aligned to the ‘hg19canon’ reference genome using Bowtie [-l 17 -n 0 -k 1 -m 100 -best -strata]

(Langmead et al. 2009). Counts of reads mapped to mature miRNAs (miRBase v21) were then computed using the count feature of HTSeq (Anders, Pyl, and Huber 2015). Count matrices were used to detect differentially expressed genes using the R package ‘DESeq2’ (Michael I Love, Huber, and Anders 2014). A similar workflow was utilized for mRNA differential expression analysis, except that TopHat (Trapnell et al. 2012) was utilized for alignment and a GFF reference containing the hg19 coordinates for all gene exons was used to compute count matrices.

To perform differential expression analysis using count data, the DESeq2 method tests for differential expression by use of negative binomial generalized linear models (M. I. Love, Anders, and Huber 2014). Estimates of dispersion and logarithmic fold changes incorporate data-driven prior distributions. To perform data quality assessment sample-to-sample Euclidean distances were computed and plotted to observe similarities an dissimilarities between samples. Similarly, principle component analysis was performed and the first 2 principle components were plotted to visualize the overall effect of experimental covariates and batch effects.

2.6. Photoactivatable Ribonucleotide-enhanced Crosslinking and Immunoprecipitation (PAR-CLIP)

PAR-CLIP was performed as previously described (Spitzer et al. 2014; Hafner et al. 2010; Hafner et al. 2012). Briefly, sub-confluent HK-2 cells were cultured overnight in medium supplemented with 100 uM 4-SU. Experimental cultures were treated with CsA (5 µg/mL) for 24 hours prior to crosslinking. Live cells were irradiated with 365 nm UV

light in a Stratalinker 2400 at 0.15 J/cm² and lysed in NP40 lysis buffer.

Immunoprecipitation of endogenous Argonaute protein was performed in NP40 lysis buffer with either monoclonal anti-pan-AGO1-4 antibody (2A8, Sigma-Aldrich) or monoclonal anti-AGO2 antibody (C34C6, Cell Signaling Technology, Danvers, MA) using Dynabeads Protein G (Thermo Fisher). Ago-RNA complexes radiolabeled by T4 PNK with [γ -32P]-ATP were fractionated by SDS-PAGE under reducing conditions using Novex NuPAGE 4-12% gels and Novex NuPAGE MOPS buffer (Thermo Scientific) and transferred onto 0.45 μ M nitrocellulose membranes (Bio-Rad) using Novex NuPAGE Transfer Buffer (Thermo Scientific). The radiolabeled RNA-protein complexes were visualized using a Typhoon FLA 7000 Phosphorimager (GE Healthcare). cDNA libraries were constructed from recovered RNAs using a pre-adenylated 3'-RNA-linker and truncated T4 DNA Ligase 2 K227Q (New England Biolabs), followed by 5'-linker ligation. After reverse transcription, a pilot PCR was used to determine the optimal number of cycles for cDNA amplification. Subsequently, a large-scale, 22 cycle PCR was performed and PCR product of the appropriate size was gel fractionated, excised, isolated, and submitted for Illumina sequencing at the Tufts University Core Facility. Sequences of adapters, size markers, and PCR primers used for PAR-CLIP library construction are listed in **Table 2-4**.

Table 2-4. PAR-CLIP oligonucleotides and adapters

Adaptor/primer	Sequence
3' adapter (DNA, 5'rApp)	5'-rAppAGATCGGAAGAGAGCACACGTCT-NH ₂ -3' 5'rApp)
5' adapter (RNA)	5' GUUCAGAGUUCUACAGUCCGACGAUC-3'
3' PCR primer (DNA)	5' CAAGCAGAAGACGGCATACGA-3'
5' PCR primer (DNA)	5' -AATGATA CGGCGACCACCGACAGGTT CAGAGTTCT ACAGTCCGA-3'
19-nt size marker (RNA)	5' CGUACGC GGGUUUAAACGA-3'
35-nt size marker (RNA)	5'CUCAUCU UGGUCGUAC GCGGAAUAGUUU AACUGU -3'

2.7. Bioinformatic Analysis of PAR-CLIP Data

Raw reads were pre-processed by adapter clipping (FASTX, Hannon Lab) and low quality reads were filtered out (less than average 20 Phred score). For identifying mRNA targets, the resulting reads with length of at least 13 nucleotides were mapped to the hg19 genome index using Bowtie, allowing for 2 mismatches. Mutational frequencies were calculated for mapped reads using the program ‘rnaseqmut’ (<https://github.com/davidliwei/rnaseqmut>).

To identify Ago crosslinking sites, the PIPE-CLIP analysis pipeline was used to identify enriched clusters of reads overlapping by at least one nucleotide containing statistically enriched and reliable T>C mutations. Annotation of clusters to genomic

features (intron, CDS, 5UTR, 3UTR, etc.) was achieved with the annotation package HOMER (Heinz et al. 2010).

To identify miRNAs bound to the RISC complex, pre-processed reads were filtered by size (19-24 nt) and mapped using the same parameters to a reference index of all mature miRNA sequences obtained from miRBase (Release 21, 06/2014) (Griffiths-Jones 2004; Griffiths-Jones et al. 2006; Griffiths-Jones et al. 2008; Kozomara and Griffiths-Jones 2011; Kozomara and Griffiths-Jones 2014). Read counts were normalized to total sample reads and log transformed.

2.8. Gene Set Enrichment Analysis

We acknowledge our use of the gene set enrichment analysis (GSEA), GSEA software, and Molecular Signature Database (MSigDB) (Subramanian et al. 2005). This analysis was performed using the latest release of the GSEA software (obtained from <http://software.broadinstitute.org/gsea/downloads.jsp>). To conduct the analysis and identify the enriched *a priori* defined gene sets in each condition, all genes identified by differential expression analysis exhibiting a statistically significant adjusted p-value (less than 0.05) were used as input. The genes are then ordered in a ranked list, according to their differential expression between the conditions. The GSEA software and algorithm then determines, given an *a priori* defined set of genes such as a gene ontology category, whether the members of the set are randomly distributed throughout the ranked list or primarily found at the top or bottom. An enrichment score (ES) reflects the degree to which a set is overrepresented at the extremes (top or bottom) of the entire ranked list. Analysis was conducted using the curated gene lists from the MSigDB ‘Hallmark,’ ‘Kegg

canonical pathways,’ and ‘Reactome canonical pathways’ collections (Liberzon et al. 2015; Ogata et al. 1999; Fabregat et al. 2016).

2.9. Ingenuity Pathway Analysis.

Genes of transcripts containing AGO2 crosslinking sites were used as input for Ingenuity Pathway Analysis (IPA, Qiagen). To identify canonical pathways under regulation by miRNAs in CsA-treated HK-2 cells, IPA core analysis was performed on genes for which CsA-specific AGO2 crosslinking sites were identified in the transcript (5'UTR, CDS, and 3'UTR). IPA Core Analysis calculates whether the proportion of sample genes mapping to a curated gene set or pathway is similar to the proportion of all measurable genes (reference set) that map to the pathway (Fisher’s exact test). Specific analysis of the genes in which AGO2 crosslinking sites were found in the 3'UTR was also performed. To determine which pathways were most negatively regulated by miRNAs we further restricted analysis to those genes that were down regulated after CsA treatment as determined by RNA-seq. To determine the function of the most active miRNAs targeting high confidence binding sites, we analyzed the transcripts that were matched to the most frequently targeting miRNA seeds in the 3'UTR region.

2.10. Construction of miRNA-expression vectors and target site luciferase reporter vectors

Overlapping oligos corresponding to pre-miRNA sequences (obtained from miRbase) plus cloning sites were designed using DNAWorks (Hoover and Lubkowski 2002). PCR assembled and amplified inserts were cut with restriction enzymes and cloned into the lentiviral backbone expression vector pLL3.7-Lentilox (Rubinson et al. 2003). Target

sequences from PAR-CLIP and corresponding mutant sequences were similarly prepared by overlapping oligos. Inserts were cloned into the multiple cloning site of pMIR-REPORT luciferase reporter plasmid (Thermo Fisher) by directional cloning.

2.11. Transfection of cultured cells

For luciferase assays, 293T cells were plated overnight at 2×10^4 cells per well. Transfections were performed in duplicate or triplicate with FuGene HD transfection reagent (Promega) according to manufacturer's protocol. For HK-2 cell in 6-well plates, 1.5×10^5 cells were plated per well. Transfections were performed in duplicate or triplicate with FuGene HD. A ratio of 2.5 ug DNA to 1 uL FuGene HD reagent was used.

2.12. Luciferase Assay

Cells were plated and transfected as previously described in 96-wll plates with pMIR-REPORT. A control vector was transfected in equal amounts, pMIR-REPORT β -gal Control Plasmid. 48 hours after transfection media was removed and cells were lysed in Glo-Lysis Buffer (Promega). To conduct the assay equal parts lysate and Steady-Glo Luciferase Assay System reagent (Promega) were mixed and incubated for 30 minutes at room temperature in white-bottom assay plates. To perform the normalization control reaction, equal parts lysate and Beta-Glo Assay reagent (Promega) and incubated for 30 minutes at room temperature. Luminescence of both assays was measured using a GloMax-Multi Detection System (Promega).

2.13. Quantitative RT-PCR

Total RNA from cultured cells or frozen kidney tissue samples were extracted using the RNAeasy Mini Kit (Qiagen). For the extraction of total RNA containing small RNAs such as microRNAs, the MiRNAeasy Mini Kit was used (Qiagen). Both kits combine phenol/guanidine-based lysis of samples in Qiazol (Qiagen) with silica-membrane-based purification of total RNA. RNA concentration and quality was measured by A260 absorbance and A260/A280 absorbance ratios on a NanoVue Plus Spectrophotometer (GE Healthcare). cDNA was prepared from RNA samples using the High Capacity cDNA Reverse Transcription Kit (Applied Biosystems, Foster City, CA). qPCR of mRNA targets was conducted using PerfeCTa SYBR Green SuperMix (Quanta Bio, Beverly, MA) or SsoFast EvaGreen Supermix (Bio-Rad, Hercules, CA). All data were acquired using a Bio-Rad CFX96 real time PCR system and analyzed using CFX Manager Software v3.1 (Bio-Rad). Normalized relative quantification was calculated using the $\Delta\Delta CT$ method using housekeeping genes such as *TBP* and *ACTB* as internal controls. DNA oligonucleotide primers were ordered from and synthesized by Sigma-Aldrich with standard de-salting purification. The human and mouse primers used in this study are listed in **Tables 2-5 and 2-6**. All primers were designed to have melting temperatures around 60°C, to produce amplicons 95 to 140 bp long, and to cover exon junctions.

Table 2-5. Human oligonucleotide primers used for qRT-PCR

Gene	Forward	Reverse
<i>ACTA2</i>	CTATGCCTCTGGACGCACAAC	CAGATCCAGACGCATGATGGCA
<i>ACTB</i>	CACCATTGGCAATGAGCGGTTC	AGGTCTTGCGGATGTCCACGT
<i>ADRB1</i>	TTCCTGCCCATCCTCATGCACT	GTTAGAAGGAGACTACGGACGAG
<i>ANGPTL4</i>	GATGGCTCAGTGGACTTCAACC	TGCTATGCACCTCTCCAGACC
<i>CDH1</i>	GCCTCCTGAAAAGAGAGTGGAAAG	TGGCAGTGTCTCTCAAATCCG
<i>CDH16</i>	AGCCTATCCACCTGGCAGAGAA	TCTGGTCACGTAGAGGTTCCC
<i>CDH6</i>	AGATGCTGCCAGGAATCCTGTC	CCATAGCAGTGTCTCGGTCAA
<i>DDAHI1</i>	ATGCAGTCTCCACAGTGCCAGT	TTGTCGTAGCGGTGGTCACTCA
<i>ECT2</i>	GCAGTCAGCAAGGTGGCAAGTT	CTCTGGTGCAAGGATAGGTCCA
<i>EEF2</i>	CCTCTACCTGAAGCCAATCCAG	CCGTCTTCACCAGGAACGGTC
<i>GSK3A</i>	GCAGATCATGCGTAAGCTGGAC	GGTACACTGTCTCGGGCACATA
<i>GSK3B</i>	CCGACTAACACCAGTGGAAAGCT	AGGATGGTAGCCAGAGGTGGAT
<i>ILK</i>	GGACATGACTGCCCGAATTAGC	GCGTCTGTTGTGTCTTCAGGC
<i>IRS2</i>	CCTGCCCTGCCAACACCT	TGTGACATCCTGGTATAAAGCC
<i>MAP3K1</i>	CCAGACCAAGTATCTCAGGAGATG	CCGCTAAACTGTGGCAAGGAGT
<i>RHOQ</i>	TGAGCTATGCCAACGACGCCCT	GCCGTGTCATAGAGTCCTAGGA
<i>SNAI1</i>	TGCCCTCAAGATGCACATCCGA	GGGACAGGAGAAGGGCTCTC
<i>SNAI2</i>	ATCTGCGGCAAGGCCTTCCA	GAGCCCTCAGATTGACCTGTC
<i>TBP</i>	TGTATCCACAGTGAATCTGGTTG	GTTCGTGGCTCTCTTATCCTC
<i>TGFB1</i>	TACCTGAACCCGTGTTGCTCTC	GTTGCTGAGGTATGCCAGGAA

Table 2-6. Mouse oligonucleotide primers used for qRT-PCR

Gene	Forward	Reverse
<i>Angptl4</i>	CTGGACAGTGATTGAGAGACGC	GATGCTGTGCATCTTCCAGGC
<i>Cdh1</i>	GGTCATCAGTGTGCTCACCTCT	GCTGGTGTGCTCAAGCCTTCAC
<i>Gsk3a</i>	TGTGTACCGTGACATCAAGCC	GAGTTCTGGAGCACGGTAGTAC
<i>Ilk</i>	GTGCTGAAGGTCGTGACTGGA	TCCAGTGTGATGAGGGTTGG
<i>Irs2</i>	CCAGTAAACGGAGGTGGCTACA	CCATAGACAGCTGGAGGCCACA
<i>Map3k1</i>	TACACTCCTGCCACAGTCTGG	CCTTGCAGAGTCCAGCACTGT
<i>Mmp7</i>	AGGTGTGGAGTGCCAGATGTTG	CCACTACGATCCGAGGTAAGTC
<i>Pten</i>	TGAGTTCCTCAGCCATTGCT	GAGGTTCCCTGGTCTGGTA
<i>Tgfb2</i>	TTGTTGCCCTCCTACAGACTGG	GTAAAGAGGGCGAAGGCAGCAA

2.13. Western Blot Analysis

Cultured cells were rinsed with DPBS (Thermo Fisher Scientific) and lysed directly on culture dishes in ice-cold RIPA buffer (G-Bioscience, St. Louis, MO) supplemented with phosphatase and protease inhibitors (Cell Signaling Technology). After 10 minutes, cell lysate was removed with a cell scraper and transferred to micro-centrifuge tubes on ice. Lysates were sonicated for 10 seconds and then cleared of cellular debris by centrifugation at 13,000 RPM for 10 minutes. Concentration of protein in lysates was determined by BCA assay using the Pierce BCA Protein Assay Kit (Thermo Fisher Scientific). Absorbance of assay plates was measured on a GloMax-Multi+ Microplate Multimode Reader (Promega). SDS-PAGE was performed using 4-12% Novex NuPAGE Bis-Tris gels in MOPS buffer under reducing conditions (Thermo Fisher Scientific). Protein transfer onto Immobilon-P 0.45 µm PVDF Membrane was conducted by wet-transfer using NuPAGE Transfer Buffer and a Mini Blot Module (Thermo Fisher Scientific). Membranes were incubated with primary antibodies diluted in 5% bovine serum albumin in TBS-T overnight at 4°C with rocking. Incubation with HRP-conjugated secondary antibodies was done for 1 hour at room temperature. Secondary antibodies used were either anti-mouse IgG, HRP-linked antibody or anti-rabbit IgG, HRP-linked antibody (Cell Signaling Technology). Monoclonal primary antibodies used for immunodetection were anti-MAP3K1/MEKK1 (Clone 2F6, Novus Biologicals, Littleton, CO) and anti-GAPDH (Clone 71.1, Sigma-Aldrich).

2.14. Data Access

All raw and processed RNA sequencing data reported here have been deposited in the NCBI Gene Expression Omnibus database under accession number GSE98670.

Chapter 3: Cyclosporine A causes aberrant miRNA and mRNA gene expression program in proximal tubule epithelial cells

3.1. Differential microRNA expression in HK-2 cells treated with CsA

Previous experiments have profiled the expression of miRNAs in the context of CsA-induced nephrotoxicity. Chen et al. screened the PT2 human proximal tubular cell line for changes in miRNA expression after 6 hours CsA treatment (6 uM) compared to vehicle control using a TaqMan human miRNA array, which quantifies 377 human miRNAs. This assay identified 46 significantly altered microRNAs, only 2 of which (hsa-miR-21 and hsa-miR-124) were up-regulated (J. Chen et al. 2015). Gooch et al. identified 76 differentially expressed miRNAs in kidneys of mice treated with CsA for six weeks compared to control mice. This experiment was also conducted using microarray technology, probing 1900 mouse miRNAs, and used RNA isolated from whole kidney tissue.

To better define the differential expression of miRNAs in CsA-induced nephrotoxicity and specifically define the expression of miRNAs in kidney proximal tubular cell before and after CsA treatment, we performed miRNA-seq on the HK-2 human proximal tubular cell line treated with CsA (5 ug/mL = 4.2 uM) or vehicle control (0.1% ethanol) for 48 hours. HK-2 cells were chosen as a model for CsA-induced nephrotoxicity based on the established literature. These cells have widely been used to study the cellular and molecular mechanisms of kidney injury and fibrosis arising from hypoxia, diabetes, and drug-induced nephrotoxicity as well as normal proximal tubule function (Wu et al. 2009; Yan et al. 2009; Q. Wang et al. 2006; H. Li et al. 2005; L. Yang

et al. 2010; B. Du et al. 2010). Further, HK-2 cells were derived from normal adult kidney, whereas PT-2 cells were cloned from centrifuged urine obtained from a transplant recipient undergoing acute rejection (Ryan et al. 1994; S. Wang et al. 2011).

The limitations of profiling RNA expression, especially miRNAs, by hybridization-based methods have previously been discussed and debated (Willenbrock et al. 2009; 't Hoen et al. 2008; Chugh and Dittmer 2012; Koshiol et al. 2010; Git et al. 2010; Pritchard, Cheng, and Tewari 2012). As is exemplified by the Chen et al. study, microarray or PCR-array platforms are limited by the size of the miRNA library studied; in that case only 377 mature miRNAs out of the possible 2588 described in the latest version of miRbase (v21) were analyzed. Further, these platforms exclude the possibility of detecting novel miRNAs. Both microarray and PCR-array platforms rely on hybridization to probes or primers. MiRNAs may exhibit preferential binding or hybridization resulting in biases when using universal conditions such as melting temperature (Chugh and Dittmer 2012). Issues pertaining to hybridization are especially pertinent when considering the degree of similarity found in many families of mature miRNAs (Pritchard, Cheng, and Tewari 2012). For instance, the *let-7* family of miRs often differ by only a single nucleotide (Roush and Slack 2008). The availability of next-generation sequencing miRNA data highlights another issue with hybridization-based platforms: the variable length of miRNA molecules produced due to extensive 3' processing (Newman, Mani, and Hammond 2011).

Thus, to accurately quantify the differential expression of miRNAs in CsA-treated human proximal tubule cells and avoid the pitfalls of microarray technology we utilized small RNA sequencing by Illumina. We prepared five replicate cDNA libraries from

small RNA enriched fractions isolated from HK-2 cell cultures treated with either CsA or vehicle control for 48 hours. Library construction consisted of sequential adapter ligation steps followed by reverse transcription and cDNA amplification with multiplexed primers. Resulting libraries were size fractionated to isolate only miRNA-containing molecules (**Figure 3-1**). Due to technical error, one sample from the control group ('E1') and one sample from the CsA group ('C2') were lost or insufficient to proceed with Illumina sequencing. The remaining eight barcoded libraries were sequenced on one lane of a flowcell. Illumina single-end 50 bp sequencing on a HiSeq 2500 produced a total of 167,839,633 raw clusters, of which 158,698,244 passed Illumina QC filters (94.55 %). Total yield was 8,094 MBases. **Table 3-1** summarizes the results of de-multiplexing, including total cluster yield and mean quality scores of the reads.

Table 3-1. Summary of miRNA-seq de-multiplexing and quality scores

Sample	Barcode	PF Clusters	Yield (Mb)	% PF	MQS
HK2-C1	GCCAAT	19,059,292	972	96.29	36.70
HK2-C3	ACTTGA	15,146,084	772	96.57	36.69
HK2-C4	GATCAG	17,689,587	902	96.28	36.67
HK2-C5	TAGCTT	13,608,132	694	96.60	36.68
HK2-E2	CGATGT	19,292,983	984	96.14	36.65
HK2-E3	TTAGGC	16,724,676	853	96.26	36.69
HK2-E4	TGACCA	17,476,463	891	96.25	36.68
HK2-E5	ACAGTG	16,785,596	856	96.42	36.67
UND	<i>unknown</i>	22,915,431	1,169	85.21	35.83

MQS: mean quality score, PF: passing filters, UND: undetermined,

Reads were then adapter trimmed, filtered by size (< 16 nt removed), and aligned to the hg19 reference genome. Reads that aligned to mature miRNA sequences were tabulated and the resulting count matrix of miRNAs and samples was used to calculate the differential expression using DESeq2.

In order to assess the quality and power of the experiment we performed several preliminary analyses of the data. First, using the web application ‘Scotty,’ we performed power analysis on the count data (Busby et al. 2013). With an average of 11.7 million mapped reads per sample and 4 replicates in each group, we determined that our experiment was powerful enough to detect 70% of genes with a fold change of 1.5 at p-value 0.05 (**Figure 3-2**). For a 2-fold change, greater than 95% of genes at p-value 0.05 can be detected. Within our DESeq2 analysis, we assessed the overall similarity between samples. Principal component analysis (PCA) projects the samples into 2D space representing the two directions that explain most of the variance. Although we observed considerable variance between samples in the y-axis ('PC2'), the differences are not stronger than those due to CsA treatment (**Figure 3-3A**). We also compared the Euclidean distances between samples. CsA-treated ('treated') samples clustered together and vehicle control samples ('untreated') separately clustered with one another (**Figure 3-3B**). In order for DESeq2 to statistically infer differential expression of genes from read counts, an accurate estimation of the dispersion (variance) parameter for each gene is required. Shown in **Figure 3-3C**, a dispersion estimate plot illustrates the ‘fitting’ of each miRNA gene’s dispersion to a curve that is constructed based on the assumption that genes of similar average expression strength have similar dispersion. In order to control the multiple-testing false discovery rate used to determine differential expression, independent filtering of genes which have little or no chance being detected is conducted. This is accomplished by omitting genes with low mean normalized counts. Shown in **Figure 3-3D**, independent filtering of low-count genes removes more genes that have

high nominal p-values (shown in yellow), thus improving the subsequent multiple-testing analysis.

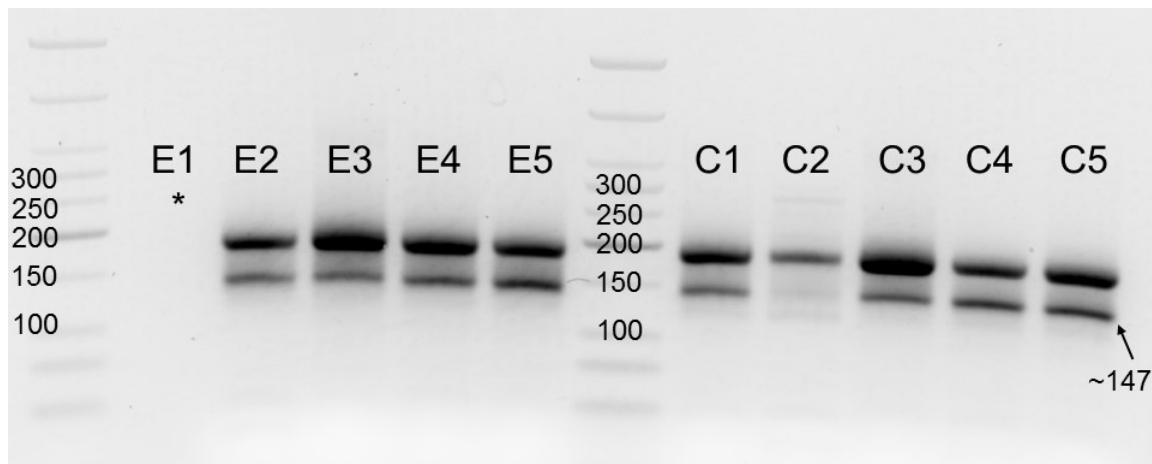


Figure 3-1. Construction of cDNA libraries derived from small RNAs. Small RNA enriched fractions were isolated from HK-2 cells treated with CsA or vehicle control. After sequential ligation steps, the cDNA products were PCR amplified prior to Illumina sequencing to increase the concentration of the libraries and introduce multiplex sequences. Shown, a 2.0 % agarose gel containing the amplified libraries. After adapter ligation and amplification the desired product size of miRNA-containing library molecules is ~147 bp. The higher molecular weight band may contain pre-miRNAs, snoRNAs, or tRNAs.

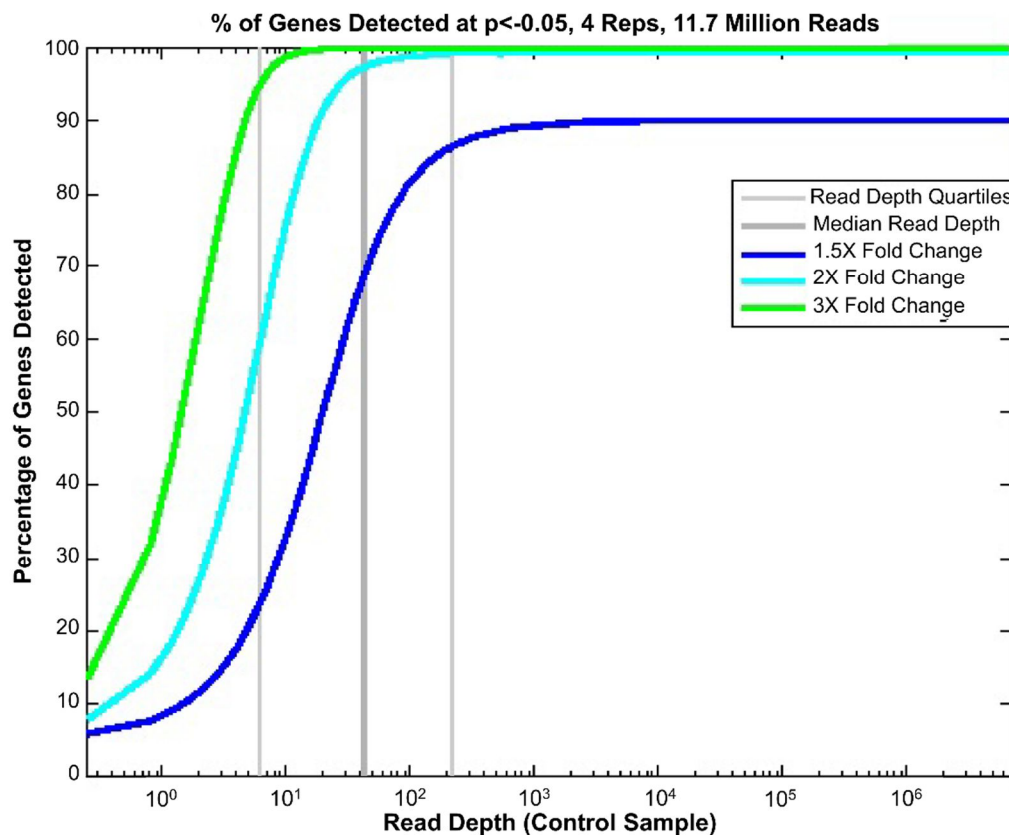


Figure 3-2. Prediction of the miRNA-seq experiment’s statistical power using ‘Scotty.’ The plot displays the results of the Scotty power calculations, showing the statistical power to identify 3X, 2X, and a 1.5X change in expression at the read depth and p-value indicated. Genes are divided into quartiles of read depth (vertical gray lines). Thus, in our experimental configuration, power to detect differential gene expression in genes that are measured with counts greater than ~50, the median, is high.

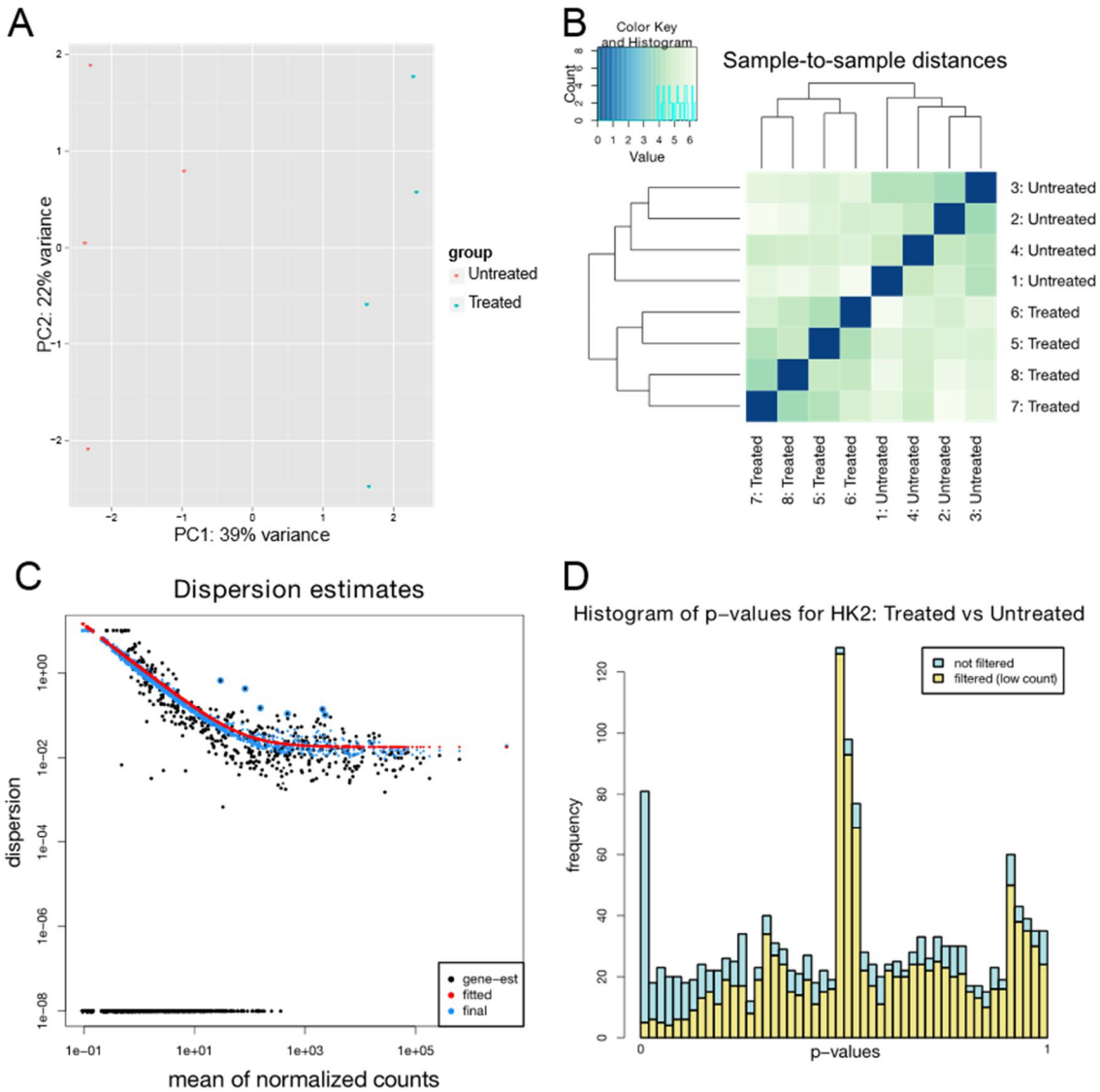


Figure 3-3. Quality control and DESeq2 analysis of miRNA-seq data. (A) Principal component analysis of the treated (CsA) and untreated (Vehicle) miRNA-seq libraries. (B) Euclidean sample-to-sample distances of regularized log transformed gene data are plotted in a heatmap. (C) Dispersion plot shows how the dispersion (variance) estimates are shrunk from the gene wise values (black dots) toward the fitted estimates. Values in blue are the final values used in testing. (D) Histogram depicts the results of independent filtering by mean of normalized counts on frequency of p-values. Genes with very low counts, yellow, are filtered from analysis to improve multiple testing. Most genes filtered for low read counts have high p-values and only a small fraction of low p-value genes are filtered by this step.

Overall, 1575 mature miRNAs were detected at any level across the eight samples. Using a Benjamini-Hochberg adjusted p-value cutoff of 0.1, representing a false discovery rate of 10%, we identified 72 differentially expressed miRNAs in HK-2 cells after CsA treatment (**Figure 3-4**). Among these 72 miRNAs, 35 were up-regulated (log₂ fold change 0.285 to 0.986, **Table 3-2**) and 37 were down-regulated (log₂ fold change -0.288 to -1.601, **Table 3-3**). No miRNAs were up-regulated more than two-fold, whereas four were down-regulated more than two-fold (**Figure 3-5**). Contrary to prior reports of miRNA expression in proximal tubule cells, we did not observe a statistically significant increase in miR-21 or miR-124. In fact, there were no detected reads aligning to miR-124 at all. However, miR-21-5p was the most abundant miRNA detected in all samples, making up almost 60% of all mapped reads sequenced (**Figure 3-6**). This phenomenon has been previously reported in miRNA-seq studies. Lu et al. reported that murine miR-21a accounted for almost 50% of miRNA abundance in mouse bone marrow derived macrophages (Lu et al. 2014). Further, miRmine, a database of human miRNA expression profiles consisting of 304 tissue and cell line samples, has reported that miR-21-5p is the top expressed human miRNA in the public data (Panwar, Omenn, and Guan 2017).

The top five up-regulated miRNAs by adjusted p-value were hsa-miR-222-5p (log₂FC = 0.986), hsa-miR-148a-5p (log₂FC = 0.868), hsa-miR-22-5p (log₂FC = 0.554), hsa-miR-155-5p (log₂FC = 0.476), and hsa-miR-148a-3p (log₂FC = 0.626). The roles of most of these miRNAs have been defined in a variety of cellular contexts. miR-222-5p is the star/passenger strand of pre-miR-222. Little is known about the function of miR-222-5p (miR-222 ‘star’ strand), though its expression is frequently correlated with the more

abundant miR-222-3p. The large increase in miR-222-5p may reflect up-regulation of the pre-miRNA, since miR-222-3p is also significantly up-regulated ($\log_{2}FC = +0.297$, $\text{adjPvalue} = 9.15 \times 10^{-2}$). MiR-222 expression has been implicated in the pathogenesis of a variety of cancers by promoting cancer cell proliferation: prostate cancer, adenoid cystic carcinoma, gastric cancer, breast cancer, melanoma, glioma, colorectal cancer, renal cell carcinoma, and thyroid cancer (Zhou et al. 2017; Noormohammad et al. 2016; Iman et al. 2016; Shen et al. 2017; L. Xue et al. 2017; Aherne et al. 2016; Bailong Li et al. 2016; Felicetti et al. 2016; Galardi et al. 2007; le Sage et al. 2007; Osanto et al. 2012). Further, by targeting p27(Kip1) and p57(Kip2), miR-222 has been shown to promote vascular smooth muscle cell (VSMC) proliferation (X. Liu et al. 2009). Along with miR-221, miR-222 has been associated with liver fibrosis progression and hepatic stellate cell activation (Ogawa et al. 2012). Both miR-148a-5p and corresponding star strand miR-148a-3p are implicated in cancer mechanisms by impacting proliferation and apoptosis pathways. (S. L. Guo et al. 2011; Xia et al. 2014; H Zhang et al. 2011). Also in the context of cancer cells, miR-148a has been shown to suppress EMT and metastasis by targeting ROCK1 and Met/Snail signaling (Zheng et al. 2011; J.-P. Zhang et al. 2014; S. H. Wang et al. 2013). miR-22 has been shown to exhibit both tumor suppressor properties (D. Xu et al. 2011; Patel et al. 2011; Jun Li et al. 2010), inducing cellular senescence and repressing metastatic invasion and cell migration, and oncogenic properties (Song et al. 2013), promoting hematopoietic stem cell self-renewal. miR-155 is best known for its role in hematopoiesis and immune regulation, as it is critical for T and B cell activation and dendritic cell development (Faraoni et al. 2009). Further, we observed that hsa-miR-4443 had the second highest up-regulation effect size ($\log_{2}FC =$

+0.872, adjusted p-value = 6.86×10^{-3}). MiR-4443 was found to be up-regulated in BRCA2-associated breast adenocarcinomas compared to normal tissue of BRCA2 germ-line mutation carriers (Vos et al. 2015). Further, it was observed that miR-4443 was also up-regulated in drug-resistant (epirubicin) breast cancer metastasis cell line cultures (S. Zhong et al. 2016). It was suggested by *in silico* target analysis that miR-4443 may contribute to acquired drug resistance in these cells by targeting the p53, Wnt, MAPK, and ErbB signaling pathways. Subsequently, investigators determined that miR-4443 was sufficient to induce drug-resistance in these cells, whereas inhibition of miR-4443 restored drug sensitivity (X. Chen et al. 2016). It was also found that miR-4443 suppressed expression of *TIMP2*, an endogenous metalloproteinase 2 (*MMP2*) inhibitor, and induced migration in breast cancer cells (X. Chen et al. 2016). Conversely, miR-4443 has also been associated with decreased invasiveness of colon cancer cells, acting in a tumor-suppressive manner via targeting of *TRAF4* and *NCOA1* downstream of MEK-C/EBP-mediated leptin and insulin signaling (Meerson and Yehuda 2016). In the context of breast cancer, *TRAF4* is considered a major driver of metastasis, promoting TGF- β receptor signaling (Long Zhang et al. 2013). Zhang et al. also determined that *TRAF4* was necessary for efficient TGF- β -induced EMT, migration, and invasion of breast cancer cell lines.

Two miRNAs that were notably up-regulated were hsa-miR-1-3p (+0.346 log2 fold change, 9.15×10^{-2}) and hsa-miR-133a-3p (+0.490 log2 fold change, 6.86×10^{-3}). In a study characterizing the expression of 345 miRNAs in 40 normal human tissues it was found that miR-1 and miR-133a/b were most highly expressed in different parts of heart and skeletal muscle (Liang et al. 2007). The authors also reported that expression of these

miRNAs may also be associated with smooth muscle tissues. The lowest expression of miR-1 and miR-133a/b was observed in kidney, liver, lung, spleen, and PBMCs. MiR-1 had previously been characterized as a heart tissue-specific miRNA in mice (Mariana Lagos-Quintana et al. 2002). Further, a recent analysis of 199 miRNAs in 61 human tissue biopsies revealed that miR-1-3p was the overall most tissue-specific miRNA, expressed highly in myocardium and muscle tissue (Ludwig et al. 2016). The authors of this study also confirmed that miR-133a/b was specific to heart and muscle tissues. Thus, CsA-induced up-regulation of miR-1-3p and hsa-miR-133a-3p indicates the induction of a highly cardiac and muscle specific miRNA signature in HK-2 proximal tubule cells.

The most down-regulated miRNAs in HK-2 cells treated with CsA were hsa-miR-7974 ($\log_{2}FC = -1.240$), hsa-miR-7-5p ($\log_{2}FC = -0.962$), hsa-miR-4485-3p ($\log_{2}FC = -1.230$), hsa-miR-4485-5p ($\log_{2}FC = -1.601$), hsa-miR-3687 ($\log_{2}FC = -0.884$), hsa-miR-3917 ($\log_{2}FC = -1.268$), hsa-miR-4461 ($\log_{2}FC = -1.096$). Few studies have examined the functions of miRs -7974, -4485-3p, -4485-5p, -3687, -3917, and -4461. miR-7974 was first described in experiments profiling miRNAs in human granulosa cells (Velthut-Meikas et al. 2013). The authors analyzed the putative targets of miR-7974 by DIANA microT v3.0, a web-based target prediction algorithm and gene ontology database, suggesting that miR-7974 may regulate transcripts related to cell morphogenesis as well as inhibit translation of several transcription activators (Velthut-Meikas et al. 2013; Vlachos et al. 2015). Interestingly, a study re-examining the roles of *DROSHA*, *XPO5*, and *DICER* in miRNA biogenesis reported that miR-7974 expression was not affected substantially by knockout of each of the three major biogenesis enzymes (Y.-K. Kim, Kim, and Kim 2016). This led the authors to conclude that miR-7974 was not a bona fide

miRNA. They also noted that miR-7974 was poorly conserved and exhibited unstable *in silico* hairpin structure. However, Dicer-independent biogenesis of miRNAs has been reported previously (J.-S. Yang et al. 2010). Further, as reported by miRmine, miR-7974 expression is detected in a wide variety of human tissues and cell lines, with highest expression in brain and breast tissue (Panwar, Omenn, and Guan 2017). The relative expression of miR-7974 across these tissues and cell lines is shown in **Figure 3-7**. Hsa-miR-4485 may act as a tumor suppressor in breast cancer cells via negatively regulating mitochondrial RNA processing and mitochondrial functions (Sripada et al. 2017). miR-7 has been shown to suppress brain metastasis by cancer stem-like cells (CSCs) derived from metastatic breast cancer cell lines (Okuda et al. 2013). Highly metastatic CSC cell lines expressed low levels of miR-7 and the miR-7 could suppress brain metastasis *in vivo* in mice. This anti-metastatic effect was found to act through inhibition of *KLF4*, a well-known inducer of pluripotency and one of the four original Yamanaka factors (G. Guo et al. 2009; Takahashi and Yamanaka 2006).

Thus, analysis of the documented roles of the miRNAs dysregulated in CsA-treated HK-2 proximal tubule cells provides insight into their possible functional roles which may contribute to the pathophysiology of CIN. We identified several miRNAs which were up-regulated by CsA treatment in HK-2 cells which have known roles in promoting EMT, fibrosis, and various tumorigenic processes including metastasis. Two key pathways that were implicated were PTEN/Akt signaling and TGF- β signaling. Based on the literature, not all miRNAs that were up-regulated appear to contribute to pathogenicity and may indeed act in a more protective role. Further, we observed CsA-induced expression of two highly tissue-specific cardiac and skeletal muscle miRNAs

(hsa-miR-1-3p and hsa-miR-133a/b). Expression of these miRNAs may reflect the characteristic CsA-induced EMT response in proximal tubule cells. It is yet unknown whether expression of these tissue-specific markers are sufficient to drive the observed EMT phenotype in HK-2 cells or if increased expression is a consequence of EMT-associated signaling pathways. Work in the context of cancer metastasis indicates that miR-1 acts to inhibit or restrain key EMT pathway members. In colorectal cancer cells, expression of miR-1 suppressed cell proliferation migration and reversed EMT through modulation of the expression of genes involved in the MAPK and PI3K/AKT pathways, ultimately inhibiting phosphorylation of ERK and AKT (L. Xu et al. 2014). Through direct regulation of *SLUG*, miR-1 has also been shown in adenocarcinoma cells to prevent EMT (Y.-N. Liu et al. 2013). Although the miRNAs down-regulated after CsA treatment in HK-2 cells were characterized less in the literature, it appears that at least two are major tumor and metastasis suppressors (miR-7 and miR-4485).

Table 3-2. miRNAs up-regulated by CsA in HK-2 cells

miRNA	baseMean	log2FC	pvalue	adjpvalue
hsa-miR-222-5p	99.388	0.986	4.87E-08	3.52E-06
hsa-miR-148a-5p	102.193	0.868	2.77E-06	1.50E-04
hsa-miR-22-5p	446.699	0.554	3.24E-06	1.56E-04
hsa-miR-155-5p	58985.762	0.476	1.14E-05	4.13E-04
hsa-miR-148a-3p	14308.708	0.626	1.63E-05	5.44E-04
hsa-miR-29a-3p	41623.793	0.436	3.43E-05	9.31E-04
hsa-miR-19a-3p	1332.472	0.474	7.95E-05	1.77E-03
hsa-miR-139-5p	447.266	0.501	1.66E-04	3.13E-03
hsa-miR-193a-3p	84.184	0.656	2.67E-04	4.45E-03
hsa-miR-27a-3p	18737.959	0.384	4.30E-04	6.66E-03
hsa-miR-29b-3p	860.561	0.434	4.82E-04	6.86E-03
hsa-miR-133a-3p	411.932	0.490	4.92E-04	6.86E-03
hsa-miR-212-5p	112.300	0.578	5.21E-04	6.86E-03
hsa-miR-4443	15.070	0.872	5.15E-04	6.86E-03
hsa-miR-92a-1-5p	116.670	0.584	6.77E-04	8.16E-03
hsa-miR-26a-2-3p	32.787	0.738	7.64E-04	8.73E-03
hsa-miR-132-3p	433.025	0.477	1.27E-03	1.28E-02
hsa-miR-3929	257.488	0.442	1.26E-03	1.28E-02
hsa-miR-27a-5p	551.547	0.536	1.51E-03	1.49E-02
hsa-miR-23a-3p	2571.210	0.432	2.41E-03	2.27E-02
hsa-miR-221-5p	2838.453	0.368	3.26E-03	2.95E-02
hsa-miR-22-3p	39151.517	0.300	4.42E-03	3.76E-02
hsa-miR-98-5p	5913.127	0.346	5.69E-03	4.38E-02
hsa-miR-186-5p	3928.770	0.353	5.71E-03	4.38E-02
hsa-miR-424-5p	912.137	0.363	5.69E-03	4.38E-02
hsa-miR-133a-5p	15.187	0.678	6.62E-03	4.96E-02
hsa-miR-584-5p	2487.728	0.285	7.65E-03	5.54E-02
hsa-miR-19b-3p	2048.954	0.335	8.44E-03	5.91E-02
hsa-miR-331-5p	245.549	0.377	9.58E-03	6.60E-02
hsa-miR-561-5p	207.134	0.363	1.15E-02	7.71E-02
hsa-miR-125b-2-3p	106.039	0.415	1.28E-02	8.43E-02
hsa-miR-222-3p	73162.723	0.297	1.47E-02	9.15E-02
hsa-miR-1-3p	3482.797	0.346	1.42E-02	9.15E-02
hsa-miR-4677-3p	130.425	0.380	1.48E-02	9.15E-02

baseMean: average of normalized count values divided by size factors, log2FC: log2 fold change/effect size estimate, adjpvalue: Benjamini-Hochberg adjusted p-value.

Table 3-3. miRNAs down-regulated by CsA in HK-2 cells

miRNA	baseMean	log2FC	pvalue	adjpvalue
hsa-miR-7974	559.258	-1.240	4.28E-20	1.86E-17
hsa-miR-7-5p	29097.220	-0.962	1.62E-17	3.51E-15
hsa-miR-4485-3p	110.709	-1.230	3.21E-12	4.64E-10
hsa-miR-4485-5p	26.845	-1.601	2.63E-11	2.85E-09
hsa-miR-3687	223.769	-0.884	1.15E-09	1.00E-07
hsa-miR-3917	22.627	-1.268	2.26E-07	1.40E-05
hsa-miR-4461	17.121	-1.096	8.53E-06	3.70E-04
hsa-miR-573	45.603	-0.907	1.04E-05	4.12E-04
hsa-miR-449c-5p	114.325	-0.664	1.76E-05	5.46E-04
hsa-miR-4521	622.701	-0.646	1.92E-05	5.56E-04
hsa-miR-10a-5p	122729.560	-0.444	6.04E-05	1.54E-03
hsa-miR-99b-3p	2156.543	-0.432	8.15E-05	1.77E-03
hsa-miR-335-3p	91.174	-0.664	7.42E-05	1.77E-03
hsa-miR-5091	50.803	-0.863	1.25E-04	2.59E-03
hsa-miR-425-3p	371.693	-0.484	1.32E-04	2.61E-03
hsa-miR-1248	315.037	-0.718	1.83E-04	3.32E-03
hsa-miR-130b-5p	630.134	-0.526	1.97E-04	3.42E-03
hsa-miR-577	60.955	-0.666	3.62E-04	5.83E-03
hsa-miR-181a-2-3p	3029.757	-0.443	4.80E-04	6.86E-03
hsa-miR-425-5p	1897.492	-0.495	6.00E-04	7.53E-03
hsa-miR-769-5p	1411.083	-0.369	6.07E-04	7.53E-03
hsa-miR-10b-5p	8517.196	-0.361	7.38E-04	8.65E-03
hsa-miR-345-5p	861.898	-0.388	7.98E-04	8.89E-03
hsa-miR-135b-3p	141.840	-0.498	8.99E-04	9.73E-03
hsa-miR-27b-5p	103.490	-0.549	9.19E-04	9.73E-03
hsa-miR-99b-5p	17445.199	-0.369	2.23E-03	2.15E-02
hsa-miR-135b-5p	3610.407	-0.335	3.09E-03	2.85E-02
hsa-miR-30d-5p	87679.872	-0.307	3.85E-03	3.41E-02
hsa-miR-28-3p	8807.020	-0.312	4.32E-03	3.75E-02
hsa-miR-191-5p	11551.048	-0.354	4.57E-03	3.81E-02
hsa-miR-585-3p	20.918	-0.658	5.32E-03	4.36E-02
hsa-miR-143-3p	285.457	-0.384	5.75E-03	4.38E-02
hsa-miR-3662	91.401	-0.534	7.43E-03	5.47E-02
hsa-miR-301a-5p	194.448	-0.416	7.94E-03	5.65E-02
hsa-let-7b-5p	10998.816	-0.296	1.13E-02	7.67E-02
hsa-let-7i-5p	271226.552	-0.288	1.47E-02	9.15E-02
hsa-miR-671-5p	536.089	-0.301	1.50E-02	9.15E-02

baseMean: average of normalized count values divided by size factors, log2FC: log2 fold change/effect size estimate, adjpvalue: Benjamini-Hochberg adjusted p-value.

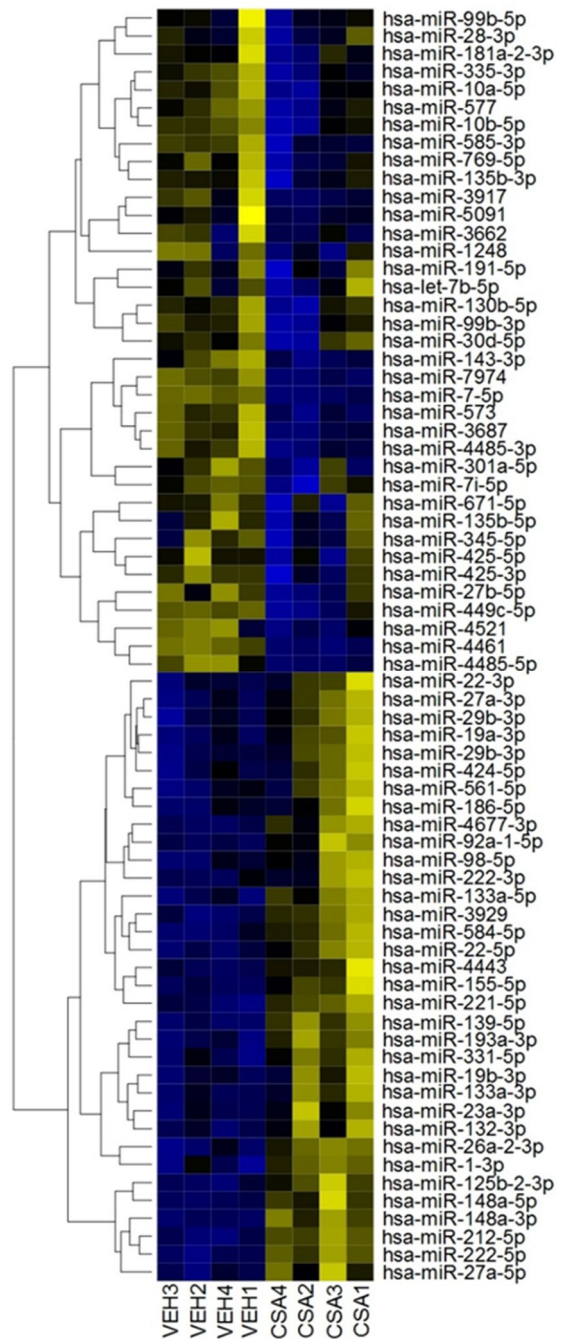


Figure 3-4. Heatmap for differentially expressed miRNAs in CsA-treated HK-2 cells compared to vehicle control. Of the 1575 miRNAs detected by miRNA-seq, 72 were differentially expressed (Benjamini-Hochberg adjusted p-value < 0.1). In the above heatmap, values are normalized by sample (column) and row (miRNA). Dendograms of miRNAs were constructed by unsupervised hierarchical clustering using the complete linkage method. Yellow shading indicates higher expression whereas blue shading indicates lower expression.

CsA/Veh miRNA expression

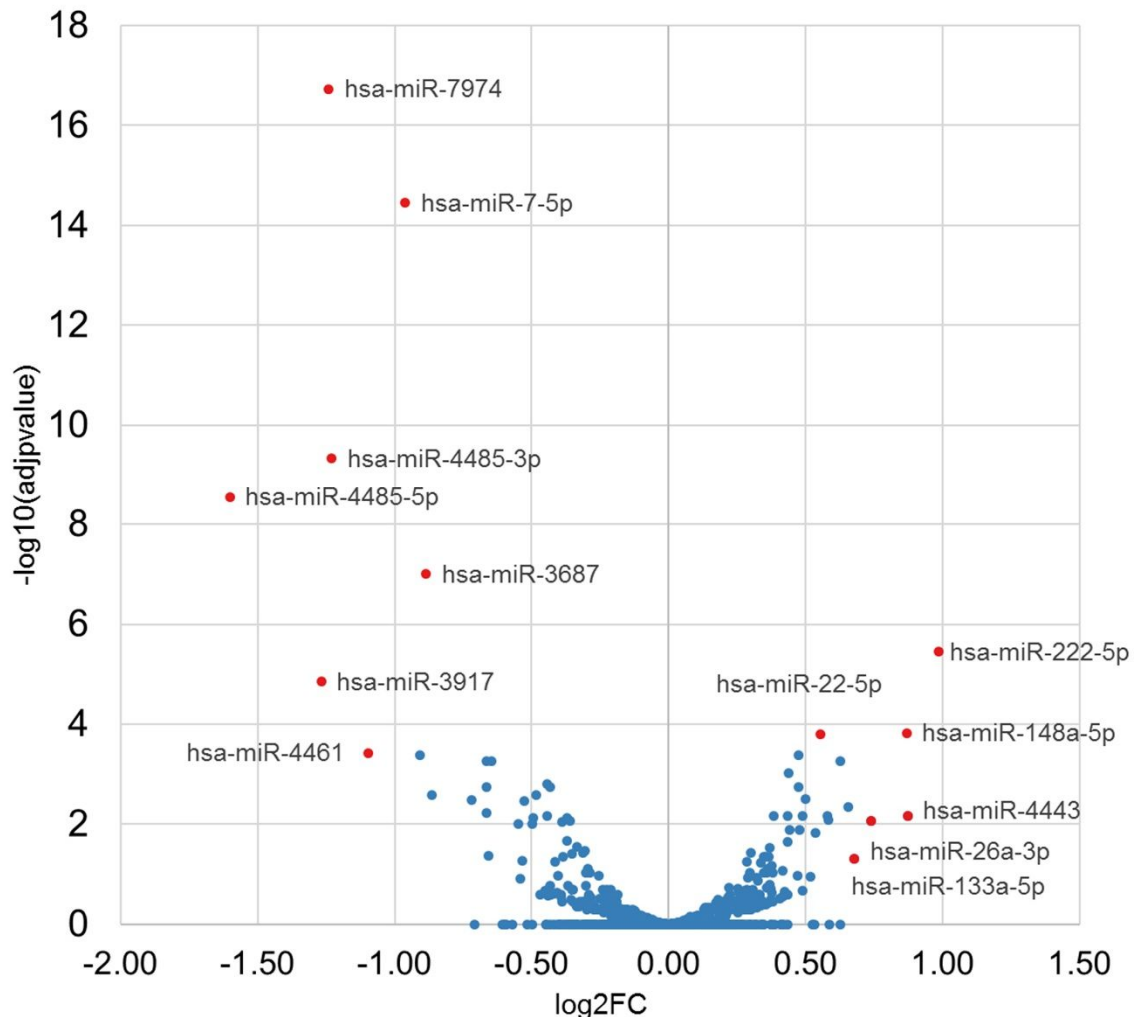


Figure 3-5. Volcano plot of differentially expressed miRNAs in CsA-treated HK-2 cells. Volcano plot depicts the log₂ fold change of miRNAs in HK-2 cells after CsA-treatment plotted against the -log₁₀ adjusted p-value (Benjamini-Hochberg method). Selected miRNAs, including the top 10 miRNAs differentially expressed, ranked by -log₁₀(adjPvalue) are indicated in red and labeled.

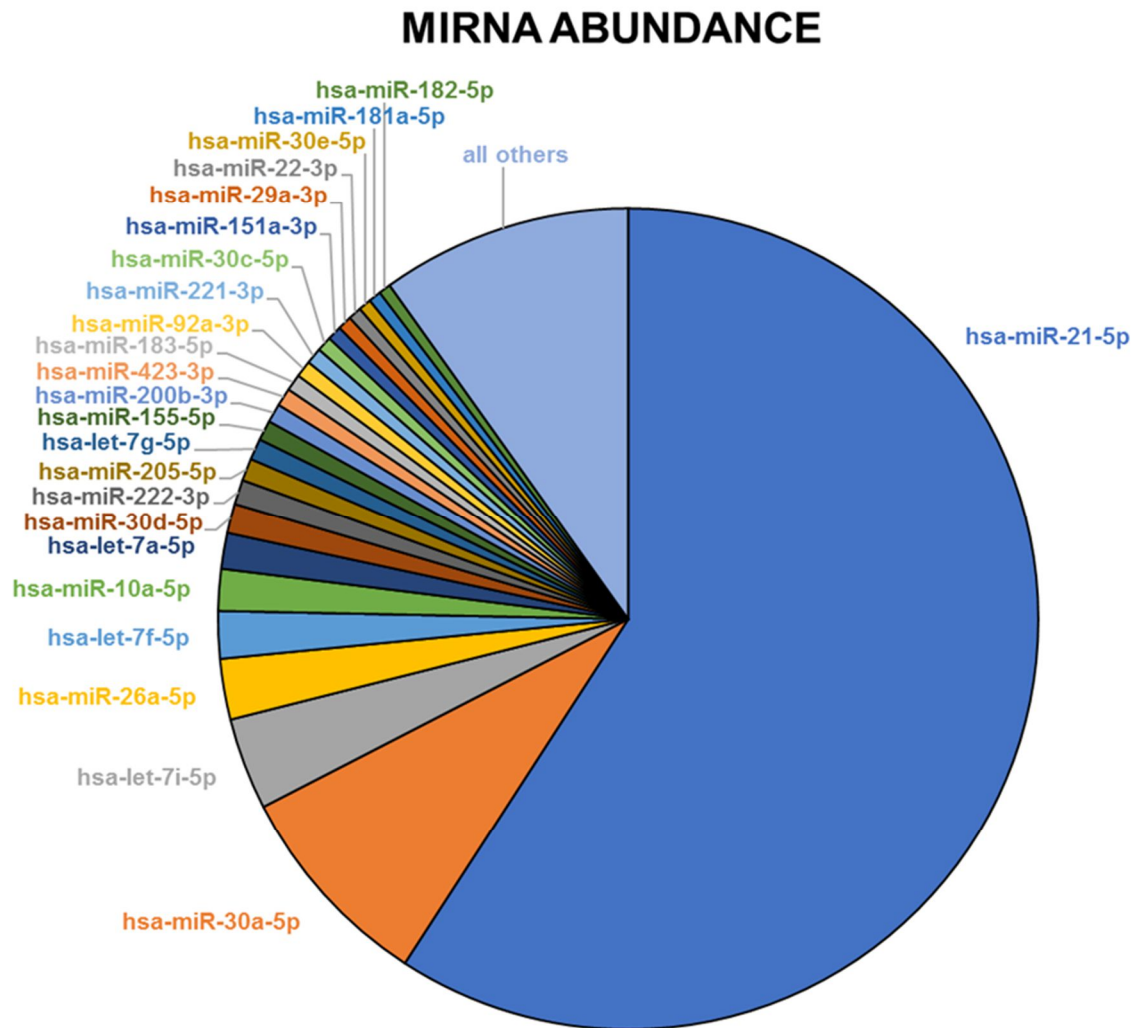


Figure 3-6. Total mean miRNA abundance across all HK-2 samples. Pie chart shows the relative abundance of miRNAs detected by miRNA-seq. The base mean of normalized count for all samples was calculated by DESeq2. Across all samples, hsa-miR-21 accounted for almost 60% of reads detected. The top 25 miRNAs accounted for nearly 90% of total miRNA reads.

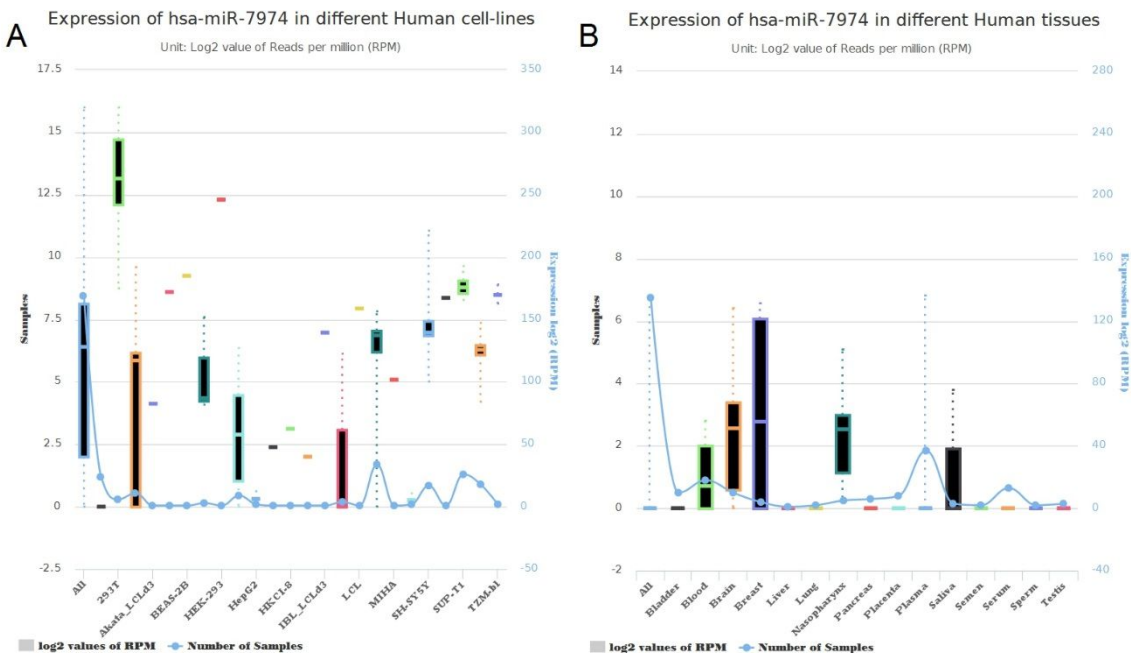


Figure 3-7. Hsa-miR-7974 is widely expressed in human tissues and cell lines. The online miRNA expression database miRmine was accessed to report the expression of hsa-miR-7974 across human cell lines and tissues. (A) In human cell lines, expression hsa-miR-7974 in 169 samples was reported. The box and whiskers plot in the leftmost column indicates the expression in all samples with a median expression of 6.42 log₂ reads per million (RPM). The number of samples reported in each group varies. Thin line plots represent one samples. In the remaining cell lines, the number of samples considered varied from 2 to 34. The highest expression of hsa-miR-7974 was detected in 293T cells, median log₂ value of RPM: 13.155; n = 6. (B) Similarly, the expression of hsa-miR-7974 in human tissue samples is reported. In 135 samples, the majority exhibited no expression of hsa-miR-7974. Breast, brain, and nasopharynx tissues exhibited the highest expression: 2.765, 2.555, and 2.54 median log₂ value of RPM, respectively; n = 4, 10, 5 respectively.

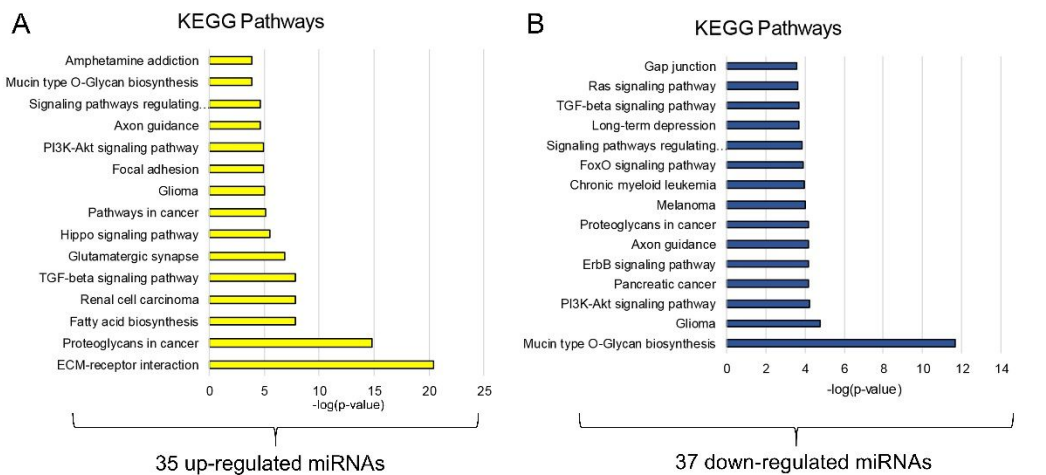
3.2. In-silico target prediction and pathway analysis of differentially expressed miRNAs in CsA-treated HK-2 cells

We hypothesized that these 72 differentially expressed miRNAs play roles in CIN. We utilized the DIANA-mirPATH v3.0 software (Vlachos et al. 2015) to identify KEGG molecular pathways enriched with predicted gene targets of the up or down-regulated miRNAs (Ogata et al. 1999). Target predictions were based on the DIANA-microT-CDS and TargetScan algorithms (Paraskevopoulou et al. 2013; Reczko et al. 2012; Agarwal et al. 2015). DIANA-microT-CDS is a database derived from computational analysis of existing mammalian high-throughput immunoprecipitation and sequencing data which predicts miRNA-mRNA targeting using a combined CDS/3'UTR model (Paraskevopoulou et al. 2013; Reczko et al. 2012). Targetscan is a quantitative model of canonical 3'UTR targeting which considers site type among 14 other features to predict targeting (Agarwal et al. 2015).

Using miRNAs that were down-regulated as input, we found that among the significantly targeted pathways were ‘Mucin type O-Glycan biosynthesis’, ‘Glioma’, and PI3K-Akt signaling pathway’ (**Figure 3-8A**). Conversely, the miRNAs that were up-regulated after CsA treatment are predicted to target members of the ‘ECM-Receptor interaction,’ ‘Proteoglycans in cancer,’ and ‘Fatty Acid Biosynthesis’ pathways (**Figure 3-8B**). Dysregulation of these pathways by aberrant miRNA expression may contribute the cellular phenotypes observed in CIN. Indeed, it is known that mucin type O-glycan biosynthesis is crucial in development for mediating cell interactions, signaling, and adhesion (Tran and Ten Hagen 2013; Liping Zhang, Tran, and Ten Hagen 2010). Further, in many models of cancer, proteoglycans have been implicated in progression, invasion,

and metastasis by modulating the tumor microenvironment via interactions with the extracellular matrix (Iozzo and Sanderson 2011; Yanagishita 1993). Dissolution of cell-cell contacts and the ability to alter the cell's interaction with the ECM are essential to the initiation and progression of EMT (Lamouille, Xu, and Derynck 2014). It is therefore plausible that these changes are at least in part governed by miRNA-guided targeting of transcripts. It is interesting to note that many pathways are enriched in both targets of up- and down-regulated miRNAs. These pathways ('Glioma,' 'TGF- β signaling,' 'PI3K-Akt signaling pathway,' 'Focal adhesion,' 'Axon guidance,' and 'Mucin type O-glycan biosynthesis') consist of many genes already implicated in the molecular mechanisms of EMT such as *PTEN*, *ROCK1*, *EGFR*, *ITGB1*, *GSK3B* and *GALNT7* (Gaziel-Sovran et al. 2011; Shan et al. 2013; Kalaji et al. 2012; Jipeng Li et al. 2013; Daley et al. 2012; Kang et al. 2012; Holz et al. 2011; Chia, Goh, and Bard 2016; Kao et al. 2014; Mulholland et al. 2012; J. Yang et al. 2016). Thus, differential expression of miRNAs induced by CsA treatment in proximal tubule cells is predicted to contribute to CIN by dysregulation of molecular pathways which contribute to hallmark EMT signaling events.

DIANA-miRPath v3.0 – microT-CDS



DIANA-miRPath v3.0 – TargetScan v6.2

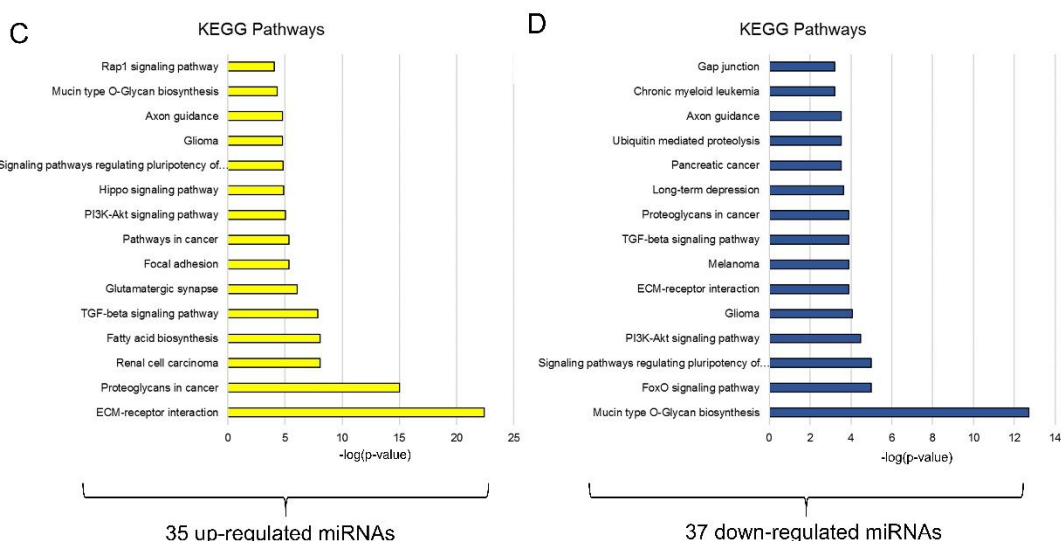


Figure 3-8. Functional characterization of differentially expressed miRNAs in CsA-treated HK-2 cells. Differentially expressed miRNAs after CsA-treatment were analyzed by the online software suite DIANA-miRPath v3.0 which assesses miRNA regulatory roles and identifies miRNA-controlled pathways by functional annotation based on predicted target genes. (A) KEGG pathways regulated by down-regulated miRNAs as predicted by DIANA-microT-CDS computational analysis. (B) KEGG Pathways regulated by up-regulated miRNAs as predicted by DIANA-microT-CDS computational analysis. (C) KEGG pathways regulated by down-regulated miRNAs as predicted by DIANA-TargetScan computational analysis. (D) KEGG Pathways regulated by up-regulated miRNAs as predicted by DIANA-TargetScan computational analysis

3.3. Differential mRNA expression in HK-2 cells treated with CsA

To determine differential gene expression in proximal tubule kidney cells after CsA treatment we performed RNA-seq on the large RNA fractions of HK-2 cell samples treated as previously described. Polyadenylated mRNAs were isolated and converted into multiplexed cDNA libraries for Illumina sequencing (**Figure 3-9**). Quality control analyses were performed as part of the DESeq2 workflow, as in the miRNAseq experiment. PCA and calculation of Euclidean sample-to-sample distances demonstrated the similarity of replicate samples in each group and the segregation of CsA-treated samples from vehicle-treated samples (**Figure 3-10A,B**). Differences between CsA and vehicle-treated samples accounted for 98% of variance (**Figure 3-10A**).

Differential expression analysis identified 7,688 total genes which were differentially expressed with an FDR-adjusted p-value less than 0.05 (Benjamini-Hochberg method). Of these differentially expressed genes, 1,625 exhibited an absolute log₂ fold-change greater than 1, 160 exhibited an absolute log₂ fold-change greater than 2, and 35 exhibited an absolute log₂ fold-change greater than 3 (**Figure 3-11**).

Notably, the gene up-regulated the most (+4.64 log₂ fold change, adjusted p-value < 2.22 x 10⁻³⁰⁸) after CsA-treatment was *ANGPTL4* (angiopoietin-like 4), a PPAR target hormone which is induced under hypoxic conditions and has been implicated in the metastatic potential of cancers due to effects on cell motility and invasiveness (Padua et al. 2008; S.-H. Kim et al. 2011). *ANGPTL4* expression is also associated with clear cell renal-cell carcinoma (Verine et al. 2010) and had been shown to mediate proteinuria in glucocorticoid-sensitive nephrotic syndrome (Clement et al. 2011). Surprisingly, the most down-regulated gene (-5.34 log₂ fold change, adjusted p-value < 2.22 x 10⁻³⁰⁸) was

MMP7 (matrix metalloprotease 7), an enzyme often implicated in tumor malignancy and metastasis (F. Q. Wang et al. 2005; Koskensalo et al. 2011). In the kidney, MMP-7 is considered not only a marker but also a driver of renal fibrosis, via cleavage of ECM substrates and non-ECM proteins such as E-cadherin and Fas ligand (Ke et al. 2017).

We evaluated whether these findings could be validated *in vivo*. In a mouse model of CsA-induced nephrotoxicity we examined the relative expression of *ANGPTL4* and *MMP7* mRNA from whole kidney after 1, 2, and 3 weeks of treatment with CsA or vehicle control. In this model, proximal tubule cells in CsA-treated mice exhibit progressive increases of EMT markers α -SMA and FSP-1 between 1 and 4 weeks compared to control mice (Yuan et al. 2015). We observed that *ANGPTL4* mRNA expression was significantly increased at 1, 2 and 3 weeks (**Figure 3-12A**). Despite the large decrease in expression detected in HK-2 cells, *MMP7* was only moderately down-regulated after 1 week and showed no change in expression at 2 and 3 week time points (**Figure 3-12B**).

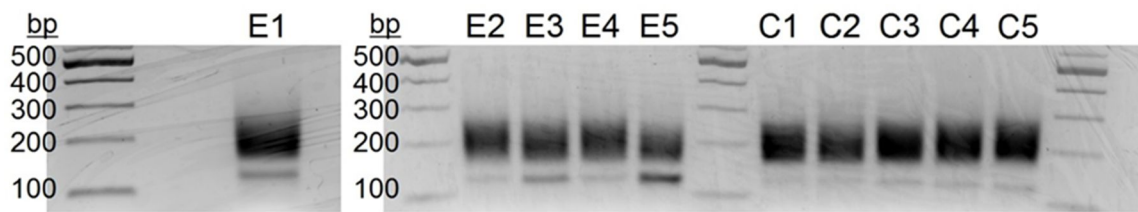


Figure 3-9. Agarose gel size fractionation of mRNA cDNA libraries for sequencing.
Isolated mRNAs were converted into cDNA libraries from CsA-treated ('C1-5') and ethanol-treated ('E1-5') HK-2 cells. Libraries were PCR amplified for 12 cycles and separated by electrophoresis on a 2.0% agarose gel. Bands corresponding to the smear of mRNA fragments (~150 bp to ~250 bp) were excised and purified.

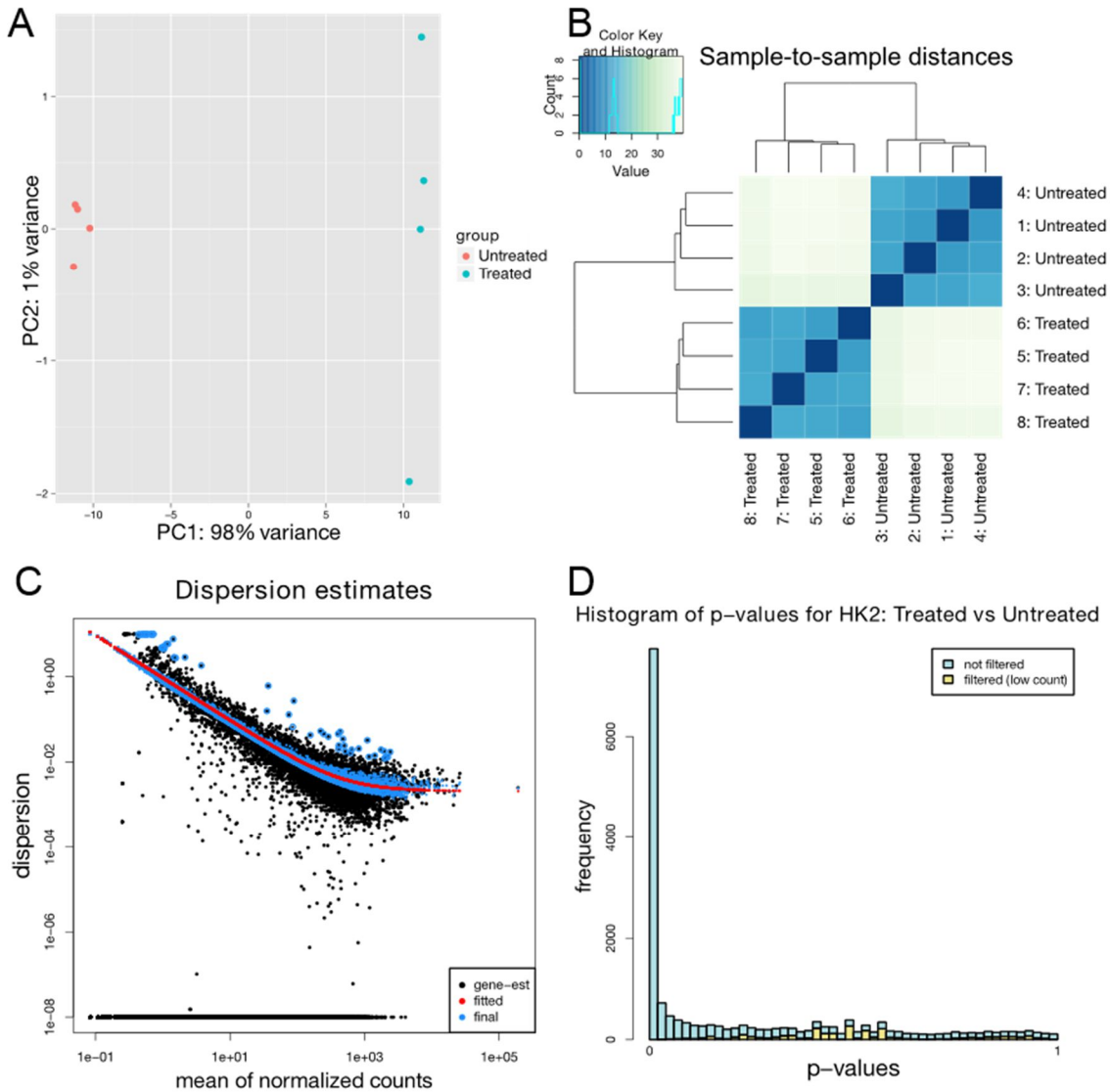


Figure 3-10. Quality control analysis of mRNA-seq data by DESeq2. (A) Principal component plot of the samples. The 2D plot indicates the samples spanned by their first two principal components (B) Heatmap and dendrogram showing the Euclidean distances between the samples as calculated from the regularized log transformation. (C) The dispersion estimate plot shows the gene-wise estimates (black), the fitted values (red), and the final maximum *a posteriori* estimates used in testing (blue). (D) Histogram of p-values shows that after filtering for low-count genes, the frequency of low p-values (close to zero) is high compared to a uniform distribution of null p-values.

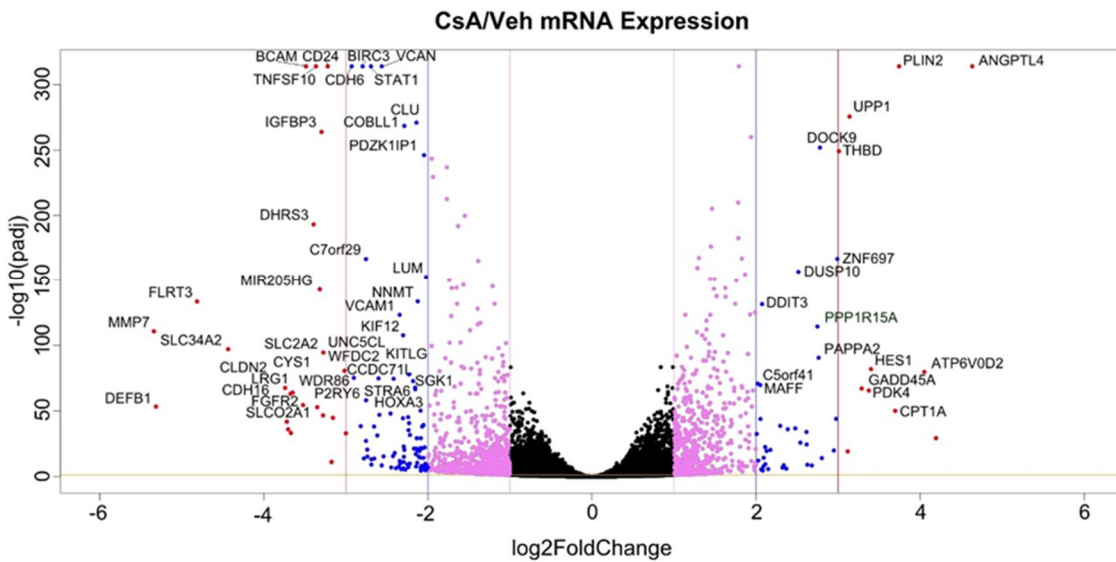


Figure 3-11. Volcano plot of differentially expressed mRNAs in CsA-treated HK-2 cells. Poly-A enriched RNA-seq was performed on HK-2 cells treated with CsA (5 ug/mL in ethanol) or vehicle control (0.01% ethanol final concentration). Volcano plot shows differential expression of all genes (7688 total) after cyclosporine treatment. Adjusted p-value of 0.05 is indicated by horizontal orange line. Coloring of dots depict log2FC > [1] (pink), > [2] (blue), and > [3] (red). Gene symbols are displayed on genes for which log2FC > [2] and $-\log_{10}(\text{padj}) > 50$.

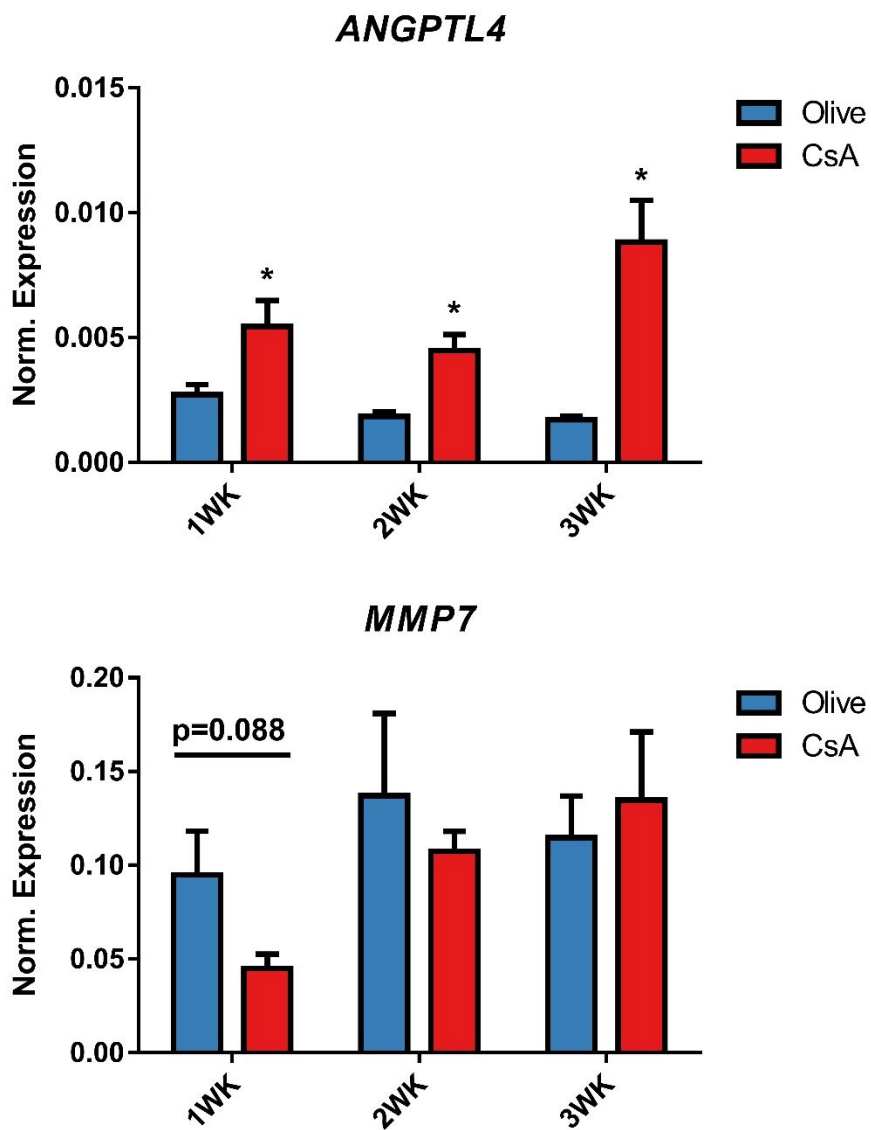


Figure 3-12. Kidney expression of *ANGPTL4* and *MMP7* in a mouse model of CsA-induced nephrotoxicity. qPCR analysis of RNA extracted from mice injected with CsA [30 mg/kg] or olive oil control for 1, 2, and 3 weeks. Four mice were examined in each group at each time point to determine the relative normalized expression of (A) *ANGPTL4* and (B) *MMP7* mRNAs. * p < 0.05 by unpaired t-test.

3.4. GSEA identifies enriched pathways and biological processes in HK-2 cells treated with CsA

To identify pathways dysregulated in proximal tubule cells after exposure to CsA, we performed gene set enrichment analysis (GSEA) using the RNA-seq expression data and the MSigDB genes sets containing hallmark gene sets (H), curated canonical gene sets (C2), and gene ontology gene sets (C5). GSEA is “a computational method that determines whether an *a priori* defined set of genes shows statistically significant, concordant differences between two biological states” (Subramanian et al. 2005). GSEA identified 11 enriched ‘hallmark’ gene sets in CsA treated cells and 10 enriched ‘hallmark’ gene sets in vehicle control cells with FDR < 25% (**Table 3-4**).

This analysis indicates that genes involved in TNF- α signaling, the unfolded protein response, and KRAS signaling are most enriched in CsA treated HK-2 cells. The TNF- α signaling gene set contains genes regulated by NF- κ B in response to TNF. This is a somewhat peculiar result, as CsA has long been known to inhibit NF- κ B (Meyer, Kohler, and Joly 1997; S. Du et al. 2009). Notably, this gene set reflects increases in pro-inflammatory cytokine subunit *IL23A*, the pluripotency-inducing *KLF4*, and a number of dual-specificity protein phosphatases (*DUSP5*, *DUSP2*, *DUSP4*, and *DUSP1*). DUSPs dephosphorylate both the threonine and tyrosine sites in the Thr-X-Tyr activation motif in mitogen-activated protein kinases (MAPKs) leading to inactivation (Jeffrey et al. 2007). Upon closer examination, we identified six total DUSP transcripts that were significantly up-regulated by CsA treatment (**Figure 3-13**). DUSPs function largely as negative regulators of mitogen-activated protein kinases (MAPKs) via dephosphorylation of threonine and tyrosine residues controlling MAPK signal intensity and duration

(Jeffrey et al. 2007). As MAPKs are critical regulators of fundamental immune cell processes such as proliferation and differentiation, modulation of DUSP expression and activity in genetic mouse models have been shown to affect immune function as well as contribute to a variety of malignancies (Dong, Davis, and Flavell 2002; Rincón 2001; Jeffrey et al. 2007). One key property of the DUSPs observed in *in vitro* studies is that most exhibit different degrees of substrate specificity. For instance, DUSP1 has been shown to target all three canonical MAPK pathways (p38, JNK, and ERK) *in vitro*, although *in vivo* work found that *Dusp1* -/- macrophages exhibited elevated p38 and JNK activity but no change in ERK (Chu et al. 1996; Zhao et al. 2006). It was demonstrated that DUSP5 specifically targets ERK MAPK (Mandl, Slack, and Keyse 2005). A complete summary of DUSP substrate specificity is reviewed in Jeffrey et al, 2007. Thus, increased expression of several DUSP genes by cyclosporine may contribute to the previously observed inactivation of p38 and JNK MAPKs. Indeed, expression of the p38/JNK-specific DUSP, *DUSP10*, was induced over 5.5-fold. However, the up-regulation of ERK-specific phosphatases *DUSP4* and *DUSP5* does not correlate with observations that p38 and JNK MAPK are inhibited by cyclosporine but not ERK in Jurkat cells (Matsuda et al. 2000). Further, ERK activation induced by cyclosporine has been observed in HK-2 cells (J. Chen et al. 2015). It is important to note, that in HK-2 cells, the reported ERK activation was induced at a peak level in early time points (15 minutes) and then was reduced to a lower level plateauing in subsequent time points. It is therefore possible that DUSP activation participates in regulating and controlling the duration and degree of ERK signaling in these cells.

Table 3-4. GSEA of differentially expressed mRNAs after CsA treatment in HK-2 cells (Hallmark Pathways)

Hallmark Pathway	ES	NES	FDR
HALLMARK_APICAL_SURFACE	0.50	1.46	0.08
HALLMARK_IL6_JAK_STAT3_SIGNALING	0.45	1.42	0.08
HALLMARK_E2F_TARGETS	0.45	1.56	0.06
HALLMARK_KRAS_SIGNALING_DN	0.44	1.42	0.10
HALLMARK_INTERFERON_ALPHA_RESPONSE	0.43	1.34	0.15
HALLMARK_G2M_CHECKPOINT	0.42	1.48	0.10
HALLMARK_PEROXISOME	0.40	1.29	0.18
HALLMARK_MYOGENESIS	0.39	1.32	0.14
HALLMARK_ESTROGEN_RESPONSE_LATE	0.39	1.33	0.14
HALLMARK_INTERFERON_GAMMA_RESPONSE	0.38	1.26	0.21
HALLMARK_IL2_STAT5_SIGNALING	-0.23	-1.33	0.12
HALLMARK_INFLAMMATORY_RESPONSE	-0.23	-1.29	0.14
HALLMARK_UV_RESPONSE_DN	-0.23	-1.20	0.24
HALLMARK_HYPOXIA	-0.26	-1.52	0.05
HALLMARK_MTORC1_SIGNALING	-0.26	-1.52	0.06
HALLMARK_COMPLEMENT	-0.27	-1.49	0.06
HALLMARK_TGF_BETA_SIGNALING	-0.31	-1.45	0.07
HALLMARK_KRAS_SIGNALING_UP	-0.33	-1.85	0.02
HALLMARK_TNFA_SIGNALING_VIA_NFKB	-0.36	-2.41	0.00
HALLMARK_UNFOLDED_PROTEIN_RESPONSE	-0.37	-2.06	0.00
HALLMARK_REACTIVE_OXIGEN_SPECIES_PATHWAY	-0.39	-1.71	0.02

ES: enrichment score, NES: normalized enrichment score, FDR: false discovery rate.
Positive ES/NES indicates enrichment of gene set in vehicle-treated samples, negative values indicates enrichment in CsA-treated samples.

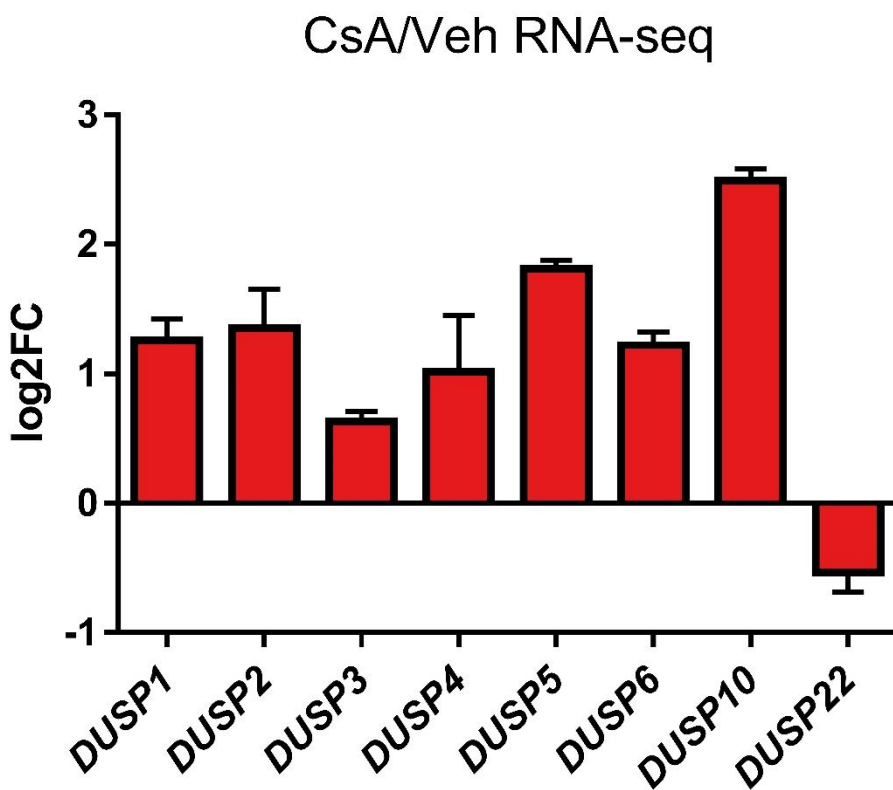


Figure 3-13. Expression of DUSPs are up-regulated in HK-2 cells treated with CsA.
 Seven DUSP genes were differentially expressed in HK-2 proximal tubule cells after treatment with CsA as detected by RNA-seq. All genes depicted exhibited an adjusted p-value less than 0.05. Six DUSPs (*DUSP1*, *DUSP2*, *DUSP3*, *DUSP4*, *DUSP5*, *DUSP6*, *DUSP10*) were significantly up-regulated and one (*DUSP22*) was down-regulated. DUSPs function primarily as negative regulators of mitogen-activated protein kinases (MAPKs) via dephosphorylation of threonine and tyrosine residues.

Further, GSEA analysis supports previous findings that reactive oxygen species, hypoxia, and TGF- β signaling pathways contribute to the injury response in proximal tubule cells (Slattery et al. 2005; McMorrow et al. 2005; Z. Zhong et al. 1998; Neria et al. 2009; Justo et al. 2003). Gene sets that are enriched in the vehicle control samples may be thought of as inversely correlated to CsA treatment. Thus, genes of the ‘Apical Surface’ are down-regulated after treatment, underscoring the loss of apical-basal polarity that is phenotypical of EMT (**Figure 3-14**). A total of 23 out of 44 genes encoding proteins over-represented on the apical surface of epithelial cells (important for cell polarity) were down-regulated. Notably, down-regulated genes in this set include *BRCA1*, *MAL*, *NTNG1*, *RTN4RL1*, *EFNA5*, *AIM1*, *ATP6V0A4*, *PKHD1*, *GASI*, *APP*, and *NCOA6*. *MAL* (Mal, T-Cell Differentiation Protein) has identified roles in T-cell signal transduction, myelin biogenesis and function in cells of the nervous system, and down-regulation has been associated with several human epithelial malignancies. *NTNG1* (Netrin G1) guides axonal growth during development (Laurén et al. 2003; Hunt, Coffin, and Anderson 2002). *RTN4RL1* (Reticulon 4 Receptor Like 1) may regulate axonal regeneration and plasticity in the adult central nervous system (O’Neill 2002; Buffart et al. 2008; Kurashige et al. 2013; Kalmár et al. 2015). *EFNA5* encodes Ephrin-A5, a member of the family of ligands for Eph receptors, which regulate the processes of migration, repulsion and adhesion during nervous system development (as well as vascular and epithelial development) (O’Leary and Wilkinson 1999; Wilkinson DG 2001). The Eph receptor has also been found to play a critical regulatory role in breast cancer initiation and metastatic progression (Vaught, Brantley-Sieders, and Chen 2008). *AIM1* (Absent in

Melanoma 1) by regulating mitosis, acts as a tumor suppressor, controlling tumorigenicity in human malignant melanoma (Ray et al. 1997).

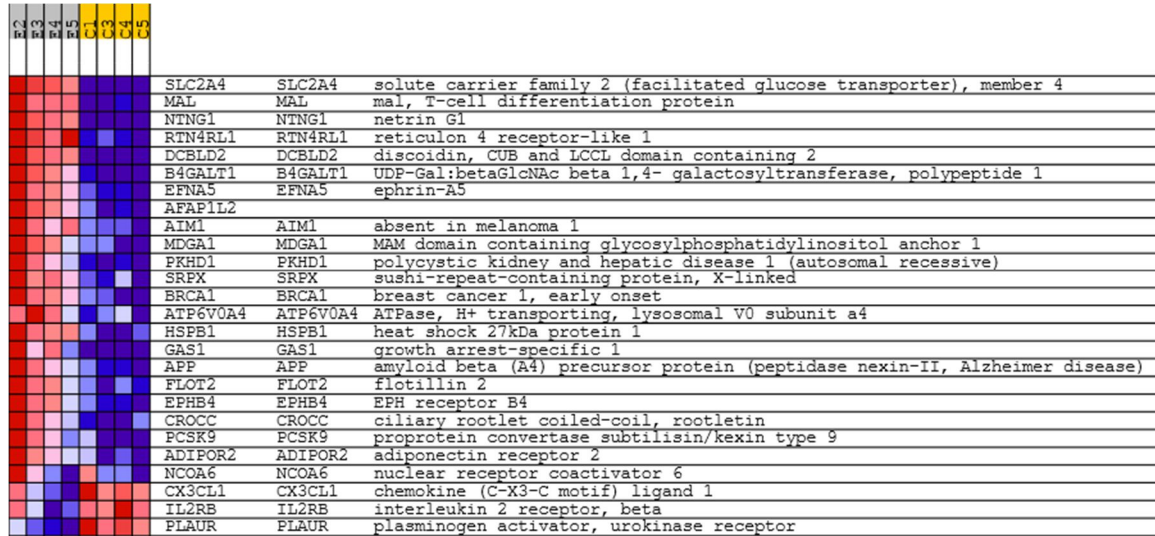


Figure 3-14. Apical membrane surface genes are down-regulated by CsA-treatment in HK-2 cells. GSEA analysis identified Hallmark Apical Surface as the highest enriched gene set (by ES score) in vehicle-treated HK-2 cells compared to CsA-treated cells. This set contains genes encoding proteins over-represented on the apical surface of epithelial cells, e.g., important for cell polarity (apical area). The heatmap shows the genes contained in this gene set which were differentially expressed after 48 hour CsA treatment in HK-2 cells (Benjamini-Hochberg adjusted p-value < 0.05). Samples indicated by 'E' represent vehicle (ethanol) control; 'C' samples indicate CsA-treated samples. Red indicates high expression whereas blue indicates low expression. A total of 23 genes encoding proteins over-represented on the apical surface of epithelial cells (important for cell polarity) were down-regulated after CsA treatment.

GAS1 (Growth arrest-specific 1) is also a putative tumor suppresser as its known molecular function is to block entry to S phase and prevent cycling of normal and transformed cells. *ATP6V0A4* encodes a component of vacuolar ATPase, which controls acidification of intracellular compartments of eukaryotic cells such as those in the kidney tubule. Defects in this gene are known to lead to renal tubular acidosis (Smith et al. 2000). Mutations to the transmembrane protein encoded by *PKHD1* cause autosomal recessive polycystic kidney disease (Bastos and Onuchic 2011). *APP* (Amyloid Beta Precursor Protein) is best known for its role in Alzheimer Disease. This gene encodes a cell surface receptor on the surface of neurons critical for growth, adhesion, and axonogenesis (H. C. Huang and Jiang 2011). *NCOA6* encodes a nuclear receptor coactivator which stimulates transcription in response to signaling from hormones such as steroids, retinoids, vitamin D3, and prostanoids (Mahajan and Samuels 2008). *BRCA1* is a tumor suppressor gene best known for its role in breast cancer risk (Fackenthal and Olopade 2007). The protein encoded by *BRCA1* functions primarily as part of a complex that repairs double-strand breaks in DNA (Roy, Chun, and Powell 2011). Mutations in the gene which lead to defective genome surveillance contribute to tumorigenesis. Not only mutation, but loss of *BRCA1* expression is attributed to breast and ovarian cancers (Wilson et al. 1999). We observed that *BRCA2*, a similar cancer susceptibility gene, is also down-regulated by CsA treatment in HK-2 cells (-0.797 log 2 fold change, adj p-value = 1.44×10^{-5}). Thus, down-regulation of both *BRCA1* and *BRCA2* by CsA in HK-2 proximal tubule cells may impede DNA repair mechanisms which are known prevent tumorigenesis in certain tissues. It is unknown whether CsA-induced down-regulation of *BRCA1* and *BRCA2* (or down-regulation of the other cancer related genes mentioned

here) may contribute to transformation of proximal tubule epithelial cells of the kidney or other tissues.

We can conclude that, as a result of CsA treatment, expression of transcripts encoding apical genes are down-regulated significantly. The genes identified by this analysis exhibit a wide breadth of functions in other tissues and disease contexts. Together, the literature suggests that this almost uniform down-regulation of apical genes contributes to proliferation, migration, motility, and morphogenic phenotypes observed in CsA treated HK-2 cells. A number of genes affected by CsA treatment have previously been associated with neuronal development and function as well as a variety of malignancies, especially breast cancer metastasis. These intriguing findings may provide insight into the pharmacological effects of CsA treatment in other organs and the potential molecular mechanisms which drive comorbidities.

We also observed that the ‘Apical Surface’ gene set also included *SLC2A4*, encoding the GLUT4 facilitated glucose transporter, which was greatly down-regulated (-2.099 log₂ fold change, adj p-value = 2.70 x 10⁻²⁴). As we observed that other members of the solute carrier family (SLC) were amongst the most greatly reduced transcripts (*SLC34A2*, *SLC2A2*, and *SLCO2A1*, **Figure 3-11**), we sought to examine the effect of CsA on this class of proteins in proximal tubule cells. Examination of transcript levels of all the solute carrier family transporters revealed widespread aberrant expression. 151 SLC members were up- or down-regulated after CsA treatment. 100/151 (66.2%) were down-regulated and 51/151 (33.8%) were up-regulated (**Figure 3-15**).

Notably, several genes encoding sodium-dependent phosphate transporters were dysregulated in HK-2 cells after CsA-treatment. Expression of type II sodium/phosphate

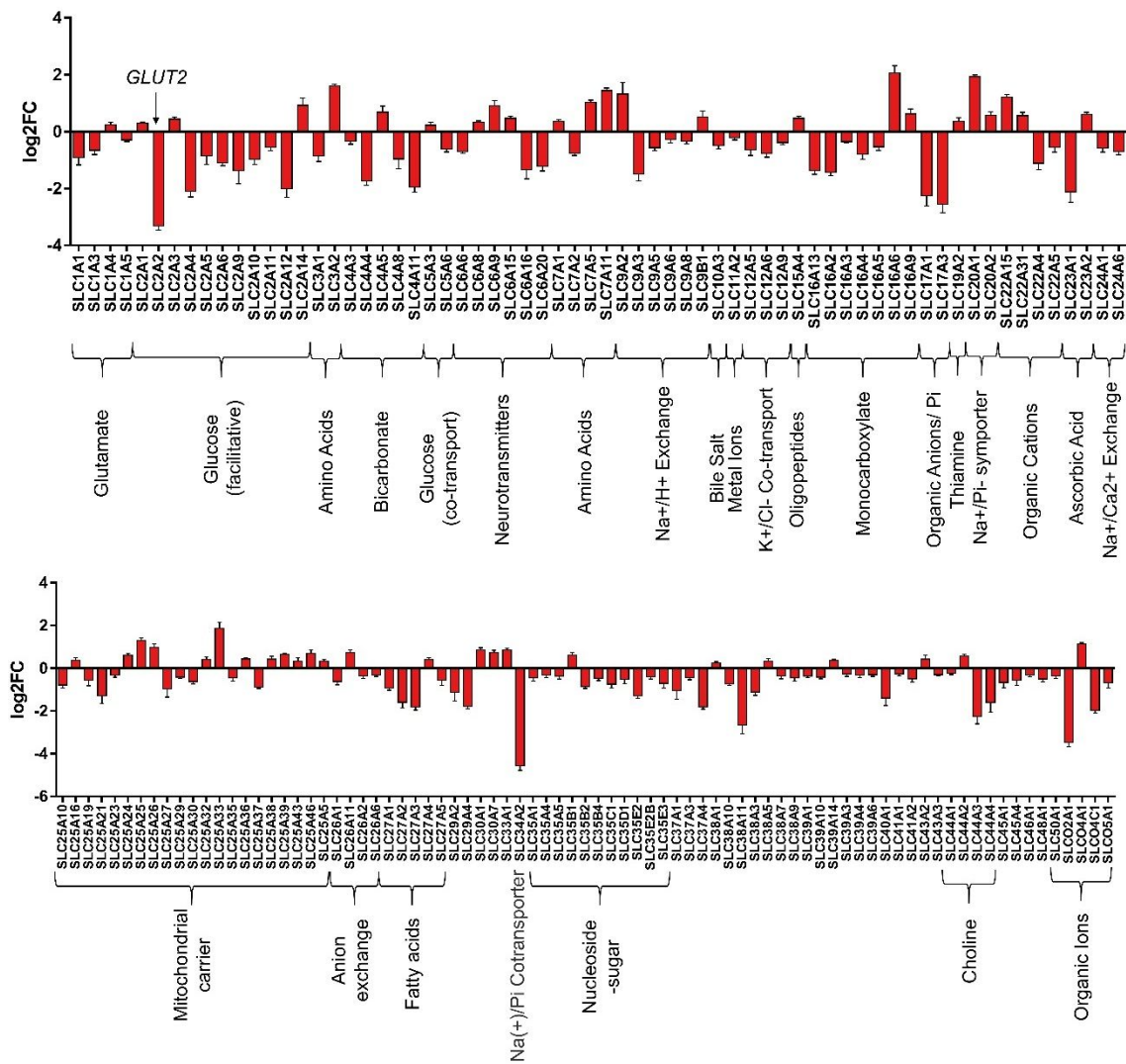


Figure 3-15. CsA causes aberrant expression of solute carrier family (SLC) transporters in HK-2 proximal tubule cells. Bar graph depicts the calculated effect size (log₂ fold change) of CsA treatment on mRNA expression of 151 SLC transporter genes in HK-2 cells as determined by RNA-seq. Error bars represent standard error. All genes depicted exhibited significant differential expression (adjusted p-value < 0.05)

cotransporter transcripts *SLC34A1* and *SLC34A2* were both down-regulated by CsA (-0.922 log₂ fold change, p-value = 0.08; -4.579 log₂ fold change, adjusted p-value = 4.59 x 10⁻¹⁰⁶, respectively). Type I sodium/phosphate cotransporters *SLC17A1* and *SLC17A3* was also down-regulated (-2.258 log₂ fold change, adjusted p-value = 7.98 x 10⁻¹⁰; -2.548 log₂ fold change, adjusted p-value = 1.40 x 10⁻¹⁶). *SLC20A1*, a type III sodium/phosphate cotransporter, however, was highly up-regulated after CsA treatment (+1.936 log₂ fold change, adjusted P-value = 9.84 x 10⁻²⁵⁹). *SLC20A1* encodes a transmembrane high-affinity Na⁺-phosphate (Pi) cotransporter, which is critical in osteoblast differentiation and contributes to vascular smooth muscle cell calcification (Nielsen et al. 2001; Li et al. 2006b). This protein was originally identified for its role in retroviral entry susceptibility (Miller and Miller 1994). In the proximal tubule, sodium-dependent phosphate cotransporters function to facilitate the reabsorption of sodium and phosphate from the glomerular filtrate. It has reported that impaired phosphate handling and hypophosphatemia due to urinary phosphate wasting is common in renal allograft patients due to proximal tubule dysfunction and that cyclosporine inhibits phosphate transport in brush border cells (Falkiewicz et al. 2006; Demeule and Beliveau 1991). Thus, the direct CsA-induced dysregulation of sodium-dependent phosphate cotransporter mRNA expression (especially down-regulation of the type I cotransporters) in the proximal tubule epithelium may contribute the clinical manifestation of hypophosphatemia in calcineurin inhibitor nephrotoxicity.

IL6/JAK/STAT3, E2F, and G2M checkpoint signaling are all down-regulated by CsA (**Figure 3-16**). Further analysis of the enriched ‘Reactome’ gene sets confer that gene programs pertaining to cell-cell junction organization, collagen formation, and

extracellular matrix organization are actively repressed upon CsA treatment (**Table 3-5**). Several signaling pathways (NFKB, B-cell Receptor Signaling, PERK, PPARA, WNT, NOTCH, and PI3K/AKT) were enriched in CsA treated cells. Results indicate that EGFR signaling was down-regulated.

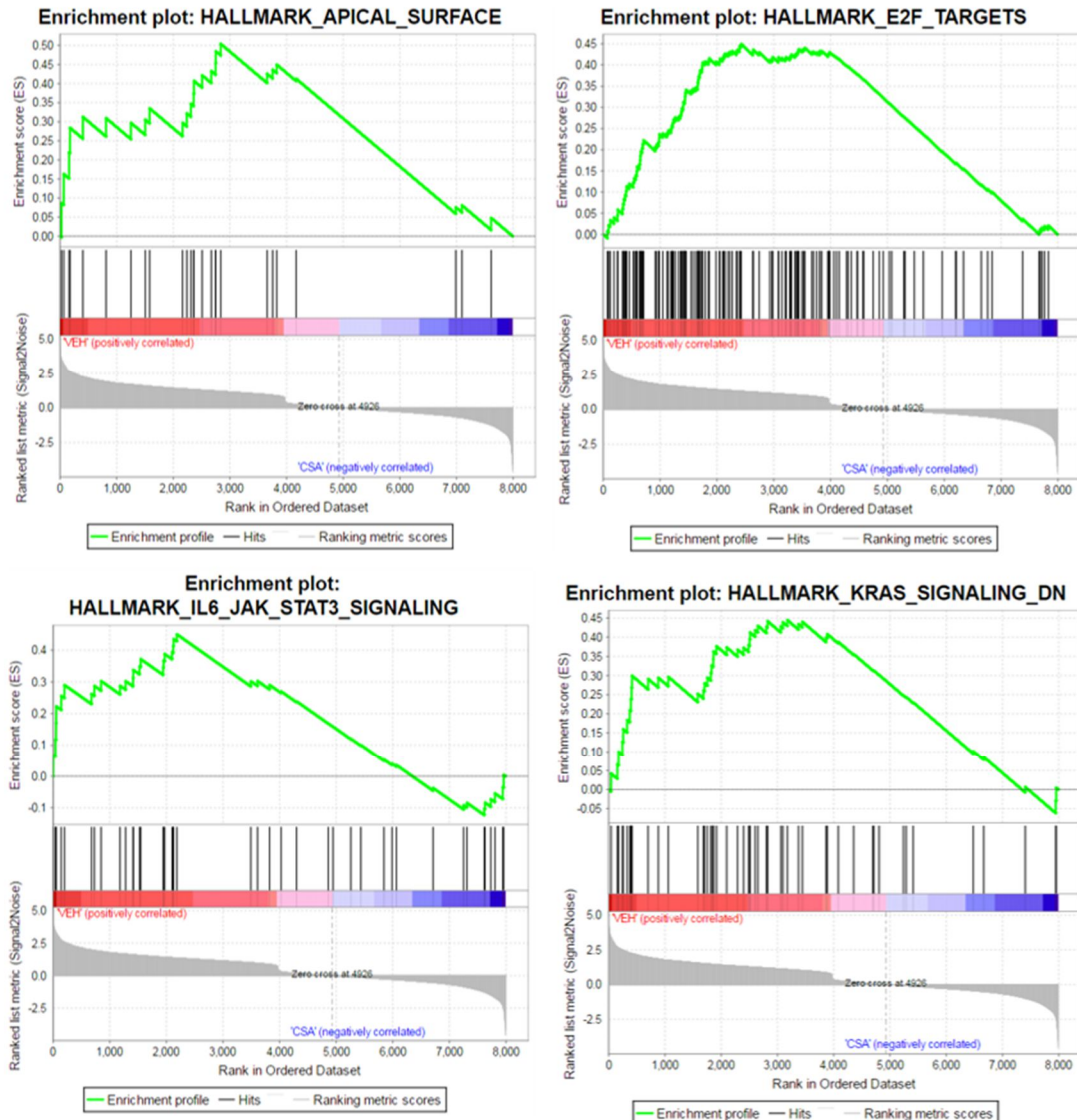


Figure 3-16. Enrichment plots for top four Veh-enriched Hallmark gene sets by GSEA. Gene set enrichment analysis (GSEA) identified ‘HALLMARK APICAL SURFACE,’ ‘HALLMARK E2F TARGETS,’ ‘HALLMARK IL6 JAK STAT3 SIGNALING,’ and ‘HALLMARK KRAS SIGNALING DN’ as the top four ‘Hallmark’ (Molecular Signatures Database, MSigDB) gene sets enriched in vehicle-treated HK-2 cells compared to CsA-treated cells. The green line on the plot shows the running enrichment score (ES) for the gene set as the analysis walks down the ranked list of differentially expressed genes. The score at the peak of the plot (the score furthest from 0.0) is the ES for the gene set. Location of the gene set members are indicated by black lines in the center of the plot. The gray plot at the bottom represents the ranked list of all differentially expressed genes. Genes which are more highly expressed in the vehicle-treated cells (VEH) are in red whereas genes more highly expressed in CsA-treated cells (CSA) are blue. Thus, in these four gene sets, we infer that the majority of genes are down-regulated by CsA treatment.

Table 3-5. GSEA of differentially expressed mRNAs after CsA treatment in HK-2 cells (Reactome Pathways)

Reactome Pathway	ES	NES	FDR
CELL CELL JUNCTION ORGANIZATION	0.605	1.684	0.045
COLLAGEN FORMATION	0.506	1.512	0.200
EXTRACELLULAR MATRIX ORGANIZATION	0.486	1.502	0.202
CELL JUNCTION ORGANIZATION	0.488	1.456	0.245
ACTIVATION OF NF KAPPAB IN B CELLS	-0.499	-2.390	0.000
DOWNSTREAM SIGNALING EVENTS OF B			
CELL RECEPTOR BCR	-0.434	-2.248	0.002
EGFR DOWNREGULATION	-0.604	-2.174	0.003
PERK REGULATED GENE EXPRESSION	-0.557	-1.974	0.009
PPARA ACTIVATES GENE EXPRESSION	-0.405	-1.963	0.009
SIGNALING BY WNT	-0.345	-1.658	0.041
PI3K AKT ACTIVATION	-0.402	-1.643	0.044
SIGNALING BY NOTCH1	-0.317	-1.385	0.119

ES: enrichment score, NES: normalized enrichment score, FDR: false discovery rate.
Positive ES/NES indicates enrichment of gene set in vehicle-treated samples, negative values indicates enrichment in CsA-treated samples.

3.5. Expression of EMT genes is dysregulated by CsA treatment in HK-2 cells

We used GSEA analysis to evaluate the extent to which EMT genes were differentially expressed in HK-2 cells after CsA treatment, as has been previously reported (Slattery et al. 2005). A total of 128 genes (of the 200 which comprise the gene set) were significantly up- or down-regulated. GSEA analysis (**Figure 3-17**) of the EMT gene set (within the MSigDB ‘Hallmark’ database) resulted in an enrichment score (ES) of +0.34, indicating higher enrichment in the vehicle control (FDR q-val = 0.417). This indicates that a large proportion of the genes in the set are down-regulated by CsA treatment. This does not mean to suggest that the EMT process is down-regulated, as the genes comprising the EMT are not unidirectional. For instance, the set contains both genes that are conventionally up-regulated in EMT such as *SNAII* and genes which are conventionally down-regulated in EMT such as *CDH1*. We noted that several cadherin, collagen, and claudin genes within the gene set were down-regulated. Closer inspection of these gene families revealed that several genes within the cadherin and claudin family are down-regulated after treatment with CsA. This is consistent with previous findings that *CDH1* is down-regulated by CsA. *CDH1* encodes E-cadherin which is routinely used as a marker for differentiated epithelial cells. We found that CsA treatment also resulted in down-regulation of *CDH2* (N-cadherin), *CDH3* (P-cadherin), *CDH5* (VE-cadherin), *CDH6* (K-cadherin), *CDH16* (KSP-cadherin), *CDH24*, and *CDH26* (**Figure 3-18A**). Therefore the inhibitory effects of CsA are not specific to E-cadherin and at this time point and drug concentration. N-cadherin (which is often thought to be activated in EMT) is also repressed (Gravdal et al. 2007). We confirmed the down-regulation of *CDH1*, *CDH6*, and *CDH16* by CsA treatment in HK-2 cells by qPCR and observed that down-

regulation was dose-dependent (**Figure 3-19**). We observed that the effect of CsA on kidney-specific cadherins (*CDH6* and *CDH16*) was greater and that expression more sensitive to treatment compared to the epithelial specific *CDH1*.

A second family of genes which were observed to be down-regulated by CsA are the claudins, proteins essential to the formation of tight junctions between epithelial cells. *CLDN1*, *CLDN2*, *CLDN3*, *CLDN11*, *CLDN12*, *CLDN16*, and *CLDN23* were all significantly down-regulated by CsA treatment in HK-2 cells (**Figure 3-18B**).

Dissolution of tight junctions is a key step in the progression of canonical EMT and a key feature in the pathophysiology of acute kidney injury (Lamouille, Xu, and Derynck 2014; Sharfuddin and Molitoris 2011). *CLDN2* was down-regulated the greatest (-3.860 log₂ fold change, adjusted p-value = 8.57×10^{-110}). *CLDN2* is typically very highly expressed in the tight junctions of renal proximal tubules and helps create a selectively leaky epithelium to support salt transport by forming paracellular water channels (Kiuchi-Saishin et al. 2002; Muto, Furuse, and Kusano 2012; Rosenthal et al. 2010). In *Cldn2*^{-/-} mice it was shown that deletion of claudin-2 caused a loss of cation (Na⁺) selectivity and therefore relative anion (Cl⁻) selectivity in the proximal tubule paracellular pathway leading to increased NaCl loss when challenged (Muto et al. 2010). Thus, CsA-induced down-regulation of *CLDN2* in proximal tubules may lead to defective tight junction barrier function and dysregulation Na⁺ and Cl⁻ paracellular transport.

Also contained within the Hallmark EMT gene set are other canonical markers of the phenomenon such as *TGFB1* (TGF-β1), *ACTA2* (α-SMA), and *VIM* (vimentin). In HK-2 cells, CsA has been reported to induce expression of *TGFB1* protein and mRNA (Slattery et al. 2005; McMorrow et al. 2005). *ACTA2*, *S100A4*, and *VIM* are all routinely

used as markers of CsA-induced EMT in HK-2 cells. Although *VIM* expression was up-regulated by CsA treatment, *ACTA2* and *S100A4* transcript abundances were actually down-regulated (**Figure 3-20**). We observed up-regulation of both *SNAI1* (Snail) and *SNAI2* (Slug), both critical EMT transcription factors. Unexpectedly, we observed that *TGFB1* expression was slightly, but significantly, down-regulated (**Figure 3-20**). This is contrary to many reports indicating that *TGFB1* is induced by CsA in proximal tubule cells (J. Bennett et al. 2016; McMorrow et al. 2005; Slattery et al. 2005). It is important to note that not all investigators have observed *TGFB1* induction by CsA (Goppelt-Struebe, Esslinger, and Kunzendorf 2003). Further, both *TGFB2* and TGF- β receptor *TGFBR2* were significantly down-regulated. Also, notably, the cell adhesion inhibiting and collagen interacting *TGFB1* (Transforming growth factor, beta-induced) was down-regulated by CsA treatment. Thus, at the transcript level we observed no evidence of *de novo* synthesis of *TGFB1* mRNA. We were also unable to detect any CsA-dependent *TGFB1* induction by qPCR (data not shown). We did not, however, determine by immunoblot or ELISA the relative amounts of TGF- β 1 protein.

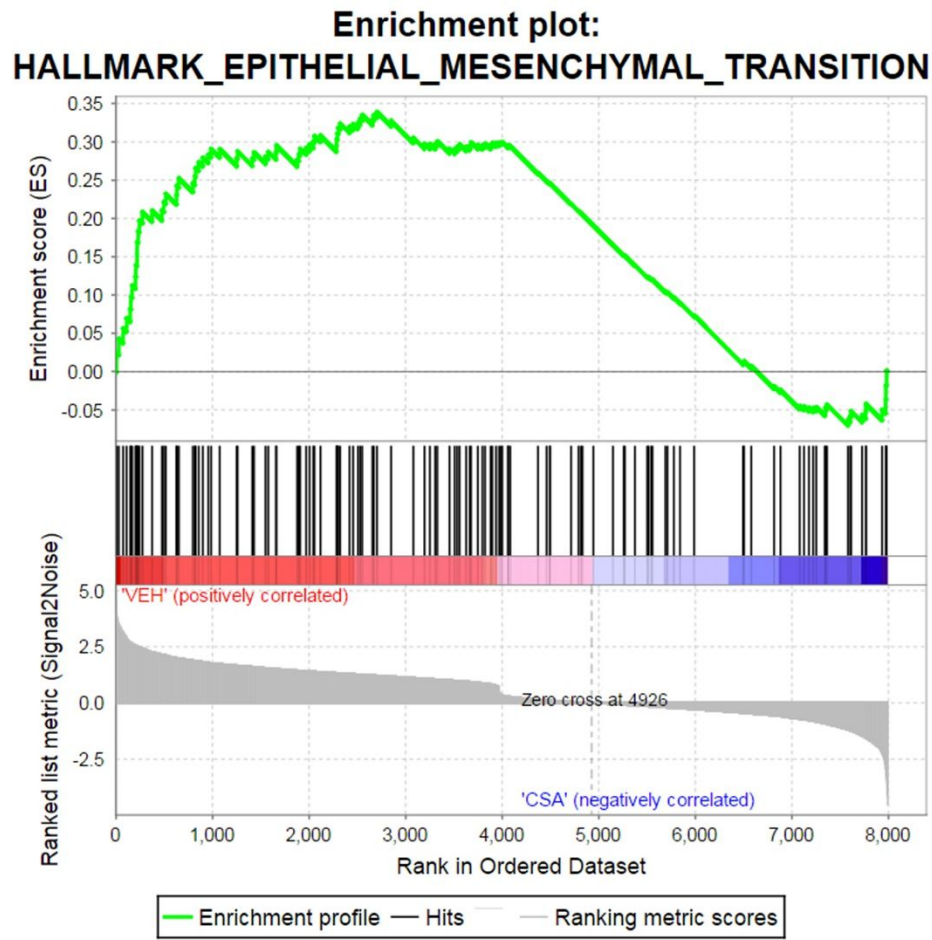


Figure 3-17. GSEA enrichment plot for Hallmark EMT gene set. The profile of the running ES score (green) and positions of gene set members on the rank ordered list (black lines) are indicated. Genes which are more highly expressed in the vehicle-treated cells (VEH) are in red whereas genes more highly expressed in CsA-treated cells (CSA) are blue. A total of 128 genes out of 200 in the set are differentially expressed (adjusted p-values < 0.05).

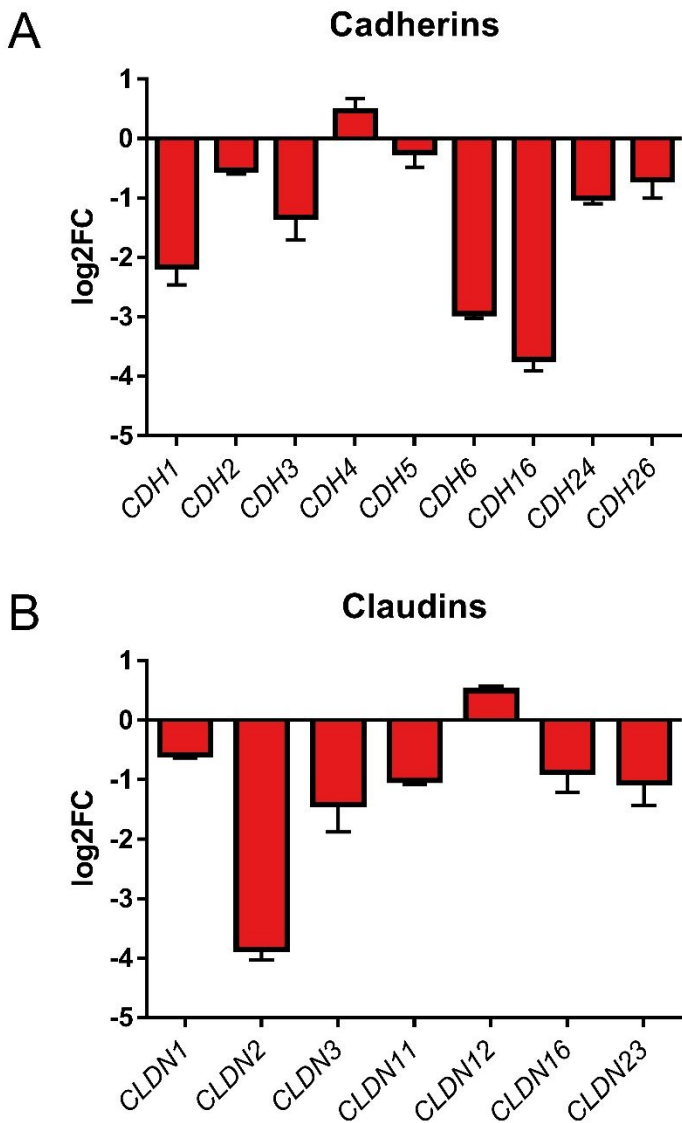


Figure 3-18. Expression of cadherins and claudins is down-regulated in HK-2 cells treated with CsA. Two families of genes essential for forming adherens junctions (A, cadherins) and tight junctions (B, claudins) are down-regulated by CsA treatment in the HK-2 proximal tubule cell line, consistent with EMT progression phenotype. The results depicted represent the effect size and standard error observed in RNA-seq of 4 replicate libraries in each condition as calculated by DESeq2 analysis. All genes depicted exhibited an adjusted p-value less than 0.05.

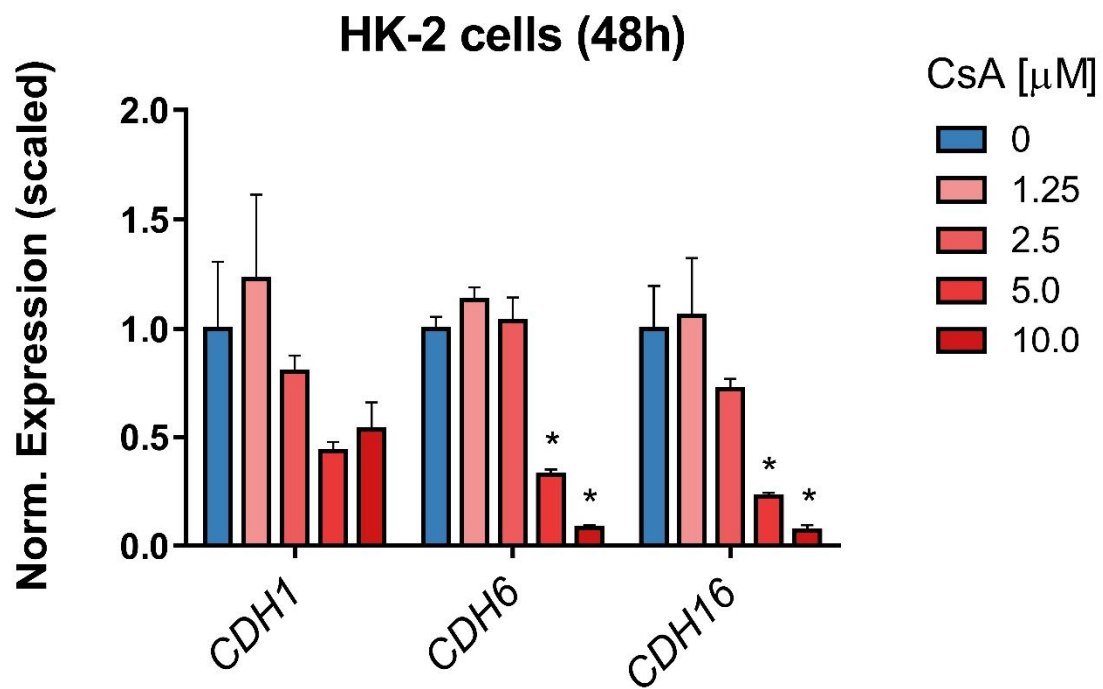


Figure 3-19. Down-regulation of cadherins by CsA is dose-dependent. Expression of *CDH1*, *CDH6*, and *CDH16* mRNA in HK-2 cells treated with increasing doses of CsA was analyzed. Mean expression was compared to vehicle-treated control by unpaired t-test, * $p < 0.05$, $n = 4$ for each condition.

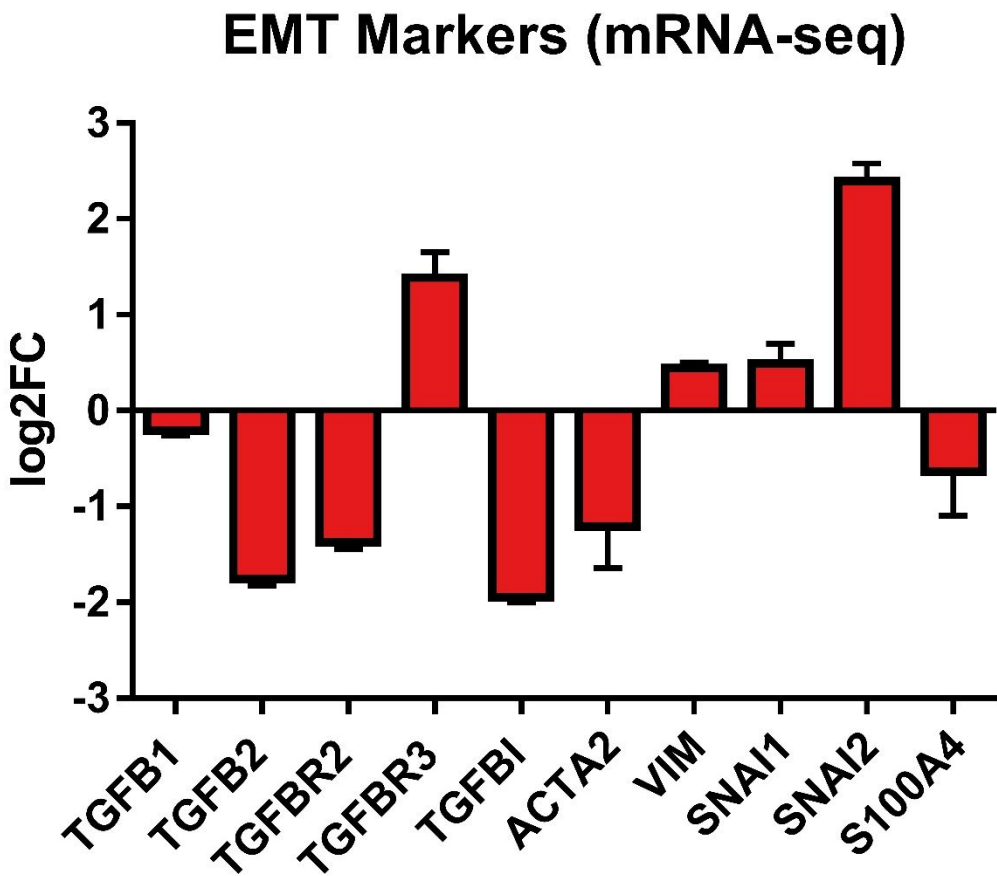


Figure 3-20. Expression of conventional EMT markers in HK-2 cells treated with CsA. Differential expression of conventional EMT markers as determined by mRNA-seq of HK-2 cells treated with CsA compared to vehicle control. The results depicted represent the effect size and standard error observed in RNA-seq of 4 replicate libraries in each condition as calculated by DESeq2 analysis. All genes depicted exhibited an adjusted p-value less than 0.05. TGFB: transforming growth factor beta, TGFBR: transforming growth factor beta receptor, TGFB1I: transforming growth factor beta induced, ACTA2: smooth muscle actin alpha 2, VIM: vimentin, SNAI1: snail, SNAI2: slug, S100A4: fibroblast-specific protein 1.

3.6. Conclusions

In this section we report the results of miRNA and mRNA expression profiling experiments in a proximal tubule cell line model of calcineurin inhibitor nephrotoxicity. We identified a CsA-specific miRNA expression profile in HK-2 proximal tubule epithelial cells by small RNA sequencing. 72 total miRNAs were differentially expressed (35 up-regulated, 37 down-regulated). Profiling of miRNAs differentially expressed after CsA treatment revealed differential expression of several miRNAs with well-characterized functions in different tissues and disease contexts. Analysis of the literature suggests that the top up-regulated miRNAs contribute to both pathogenic and protective roles. For instance, miR-22, miR-26a, miR-222, and miR-4433 may promote fibrosis and ECM accumulation by targeting TIMP proteins and indirectly activating TGF- β 1 and Akt signaling pathways. miR-133a and miR-143 up-regulation, on the other hand, may target key EMT genes. Of the down-regulated miRNAs, miR-4485 and miR-7 have been shown to act as tumor suppressor miRNAs. It is unknown whether over-expression or knockout of these miRNAs is sufficient to drive and/or inhibit CsA-induced EMT in HK-2 cells. Further, the functional targets mRNAs of these miRNAs in the context of CIN is not determined.

Using in silico prediction software (DIANA-miRPath v3.0) which predicts miRNA targeting to the CDS and 3'UTR of transcripts, we determined the pathways and cellular functions most likely regulated by the differentially expressed miRNAs. Results indicate that CsA-induced miRNAs regulate ECM-Receptor Interaction and CsA-repressed miRNAs regulate Mucin type O-glycan biosynthesis. Interactions between cells and the ECM lead to direct or indirect control of cellular activities such as adhesion, migration,

differentiation, proliferation, and apoptosis, all of which are key processes in current models of CsA-induced EMT of proximal tubule cells. The role of Mucin-type O-glycosylation in CIN is unknown, however irregularities in O-glycosylation are implicated in many diseases such as cancer and under normal conditions this pathway may be important to apical trafficking of proteins (Tran and Ten Hagen 2013; Weisz and Rodriguez-Boulan 2009).

Profiling of these miRNAs in the proximal tubule may serve as valuable biomarkers for CIN. In addition to the better characterized miRNAs, several miRNAs detected were virtually unannotated. Further work to profile the specificity of these miRNAs to this cell type and tissue as well as CIN may provide a useful means to distinguish kidney pathologies. CsA-induced miRNA profiling in PTECs may also translate to other tissues and disease contexts (i.e. fibrosis, cancer). The deleterious effects of CsA are not limited to the kidney and the roles of CsA-induced miRNA expression must be explored in other compartments.

Likewise, we profiled gene expression changes transcriptome-wide in proximal tubule epithelial cells. Our analysis identified 7,688 total genes which were up or down-regulated by CsA treatment, underscoring the vast cellular reprogramming that occurs in exposed proximal tubule cells. Using GSEA, we identified canonical cellular pathways and biological functions that were affected. Our results are largely consistent with previous efforts in the field to determine the molecular pathology of CIN. We found that apical surface, cell junction, adherens junction, ECM, collagen, and cell adhesion genes were down-regulated in CsA-treated cells. Further, we identified several critical cellular pathways that were activated by CsA treatment: NFKB, P-ERK, PPAR- α , WNT,

PI3K/AKT, NOTCH1, MTORC1, TGF- β 1, KRAS, UPR, Reactive Oxygen species and Hypoxia pathways. In addition to the structural, morphological, and cell signaling gene sets affected, we observed widespread dysregulation of solute carrier genes which may have critical consequences to the functionality of proximal tubule cells exposed to CsA. In examining the role of EMT genes in CIN, we observed that some previously identified markers for EMT (*TGFB1* and *ACTA2*) were not induced as previously reported. Together, our data and analysis increases the depth and understanding of gene reprogramming occurring in the proximal tubule in CIN.

Chapter 4: PAR-CLIP defines functional miRNA-mRNA targetome in proximal tubule epithelial cell model of calcineurin inhibitor nephrotoxicity

4.1. PAN-AGO-PAR-CLIP defines a functional miRNA-mRNA targetome in HK-2 cells

As we have illustrated, the use of paired miRNA and mRNA expression data can be useful to identify putative targets and construct broad mechanisms of gene expression regulation. However, there are many factors which limit the usefulness of this approach and may even impair the pursuit of determining the physiological role of miRNAs in normal and disease contexts. Thus, in order to determine miRNA-mRNA targeting relationships in proximal tubule cells directly, we employed PAR-CLIP (Photoactivatable-Ribonucleoside-Enhanced Crosslinking and Immunoprecipitation). In this method, the incorporation of a 4-thiouracil (4-SU), a uridine analog, into nascent RNAs allows for more efficient crosslinking to RNA binding proteins and high resolution identification of binding sites due to experimentally introduced crosslinking mutations.

PAR-CLIP was conducted as previously described (Hafner et al. 2010). Briefly, HK-2 cells were cultured overnight in medium supplemented with 100 uM 4-SU. The cells were then exposed to UV light (365 nm) to crosslink RNAs to associated RNA binding proteins. AGO-associated RNAs were then isolated by immunoprecipitation using the anti-PAN-AGO monoclonal antibody 2A8 which binds all four AGO isoforms (**Figure 4-1A**). AGO-associated RNAs were then purified, reverse transcribed, prepared

into cDNA libraries and sequenced by Illumina sequencing (**Figure 4-1B and C, Figure 4-2A-C**).

The incorporation of 4-SU into nascent RNAs allows for efficient crosslinking to RBPs following exposure to UV light at 365nm and results in T to C transitions in subsequent reverse transcribed cDNAs at the crosslinking sites. To confirm the incorporation of 4-SU into RNAs and crosslinking to AGO proteins, we analyzed the crosslinking mutation frequencies of all possible nucleotide transitions induced by incorporation of 4-SU and crosslinking. These frequencies were tabulated for each chromosome to examine whether any biases in the data existed. It has previously been reported that high background mutation rates in rRNA were observed in the Y chromosome (Hafner et al. 2012). We observed that genome-wide T>C and the reverse complement A>G mutations were the most abundant base substitutions (**Figure 4-3**).

PIPE-CLIP analysis (minimum sequence length of 20 and stringent FDR cutoff of 0.001) of the PAN-AGO-PAR-CLIP library identified 8,059 total crosslinking sites, supported by 9,102 reliable T>C mutations. A large proportion of sites were located in intergenic and intronic regions (4,001 and 3,418, respectively). As previously reported in AGO-PAR-CLIP studies, crosslinking clusters were enriched within the 3'UTR as well as coding exons (**Figure 4-4**). Although PIPE-CLIP clusters were identified throughout genomic and transcriptomic features, based on the canonical mechanisms of regulation (Bartel 2009) and the observation by Hafner et al that CDS localized binding sites only marginally reduce mRNA stability (Hafner et al. 2010), we chose to focus on clusters which mapped to the 3'UTRs of mRNAs for downstream functional validation.

From the list of target sequences generated by PIPE-CLIP, we examined the targets which mapped to the 3'UTRs of genes. Seventy-five total genes contained PIPE-CLIP crosslinking sites in the 3'UTR region. The ten genes with the highest number of reads, referred to as ‘Peak’ score, are summarized in **Table 4-1**. To assign putative miRNA regulator to these genes, we matched the target sequences to miRNAs which were also identified by PAN-AGO-PAR-CLIP via seed sequence complementarity. The assigned miRNAs for the top ten mRNA targets are listed in **Table 4-1**.

To test the functional validity of these PAR-CLIP-derived targeting interactions, we utilized a luciferase reporter plasmid system designed to examine 3'UTR function *in vitro*. We cloned the target sequences, which represent small fragments of the 3'UTR, of the top two ranked genes *ECT2* and *DDAH1* into the multiple cloning site (MCS) of pMIR-REPORT, which is located downstream of the luciferase coding sequence. Shown in **Figure 4-5A** is a schematic of the DDAH1 target sequence cloned into pMIR-REPORT. The DDAH1 target sequence contains a 6mer complementary to the seed of miR-21-5p. To evaluate if this sequence was sufficient to confer miR-21-5p targeting to the construct, we transfected it into 293T cells, which express miR-21-5p at a high level. As controls we transfected the empty pMIR-REPORT vector and four positive control constructs containing short sequences in the MCS that contain the canonical seed sequence target sites for miR-21-5p (6mer, 7merA1, 7mer8, and 8mer). Compared to the empty vector the DDAH1 target sequence caused significant repression of the luciferase activity (**Figure 4-5B**). All four canonical miR-21-5p sites were also repressed, confirming activity of miR-21-5p in the cells. To confirm that the miR-21-5p seed site was responsible for the reduction in luciferase activity, we mutated the seed sequence by

flipping it. Compared to the original DDAH1 target sequence, transfection of the mutant plasmid resulted in luciferase activity significantly higher than the target construct and back to the level of vector control (**Figure 4-6A**). Using a similar strategy, we engineered a reporter construct for the *ECT2* 3'UTR sequence, to which we assigned two putative miRNA regulators (hsa-miR-27a/b and hsa-miR-33). To assess the function of these miRNAs in regulating the *ECT2* sequence we made three mutant vectors, two single site mutants ('ECT2-MUT27' and 'ECT2-MUT33') and a double site mutant ('ECT2-MUT27+33'). As a positive control we constructed an hsa-miR-27a/b reporter construct. In 293T cells, transfection of these plasmids demonstrated that neither single site mutation was sufficient to de-repress luciferase activity (**Figure 4-6B**). Only mutation of both sites increased expression of the reporter gene. Thus, in the *ECT2* 3'UTR target sequence we have shown that either hsa-miR-27a/b or hsa-miR-33a can regulate the transcript.

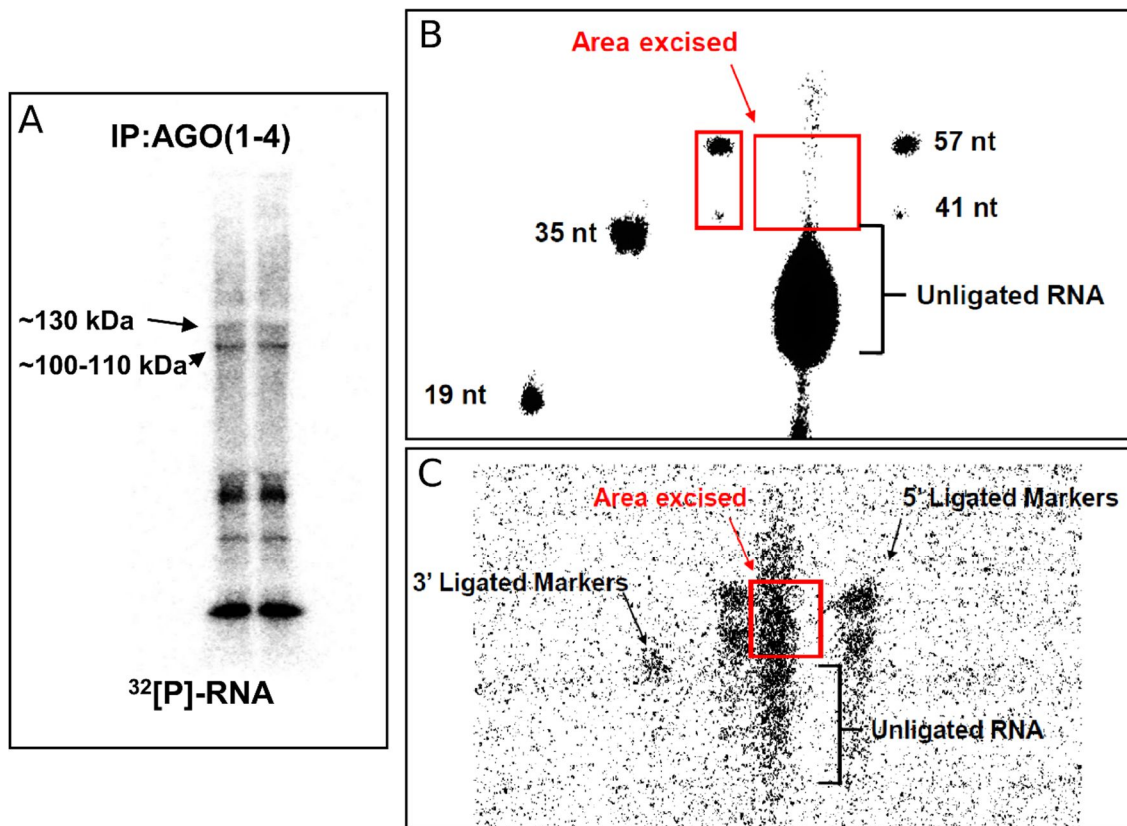


Figure 4-1. PAN-AGO-PAR-CLIP of HK-2 cells. (A) SDS-PAGE fractionation of crosslinked and immunoprecipitated AGO(1-4)-RNA complexes. Bound RNA was 5' radiolabeled. 100-110 kDa and 130 kDa bands correspond to Argonaute bound to small, i.e. miRNAs, and large RNA species. Non-specific RNA binding to the IgG light chain runs much lower. Exposure to phosphorimaging scan was 2 hours. One sample was split across the two lanes shown. (B) 5% denaturing 8-M urea PAGE gel to isolate products of 3' pre-adenylated adapter ligation to isolated RNAs recovered from the SDS-PAGE gel. Ligation is monitored by parallel ligation of size markers. (C) 12% denaturing 8-M urea PAGE gel containing 5' adapter ligated RNA library.

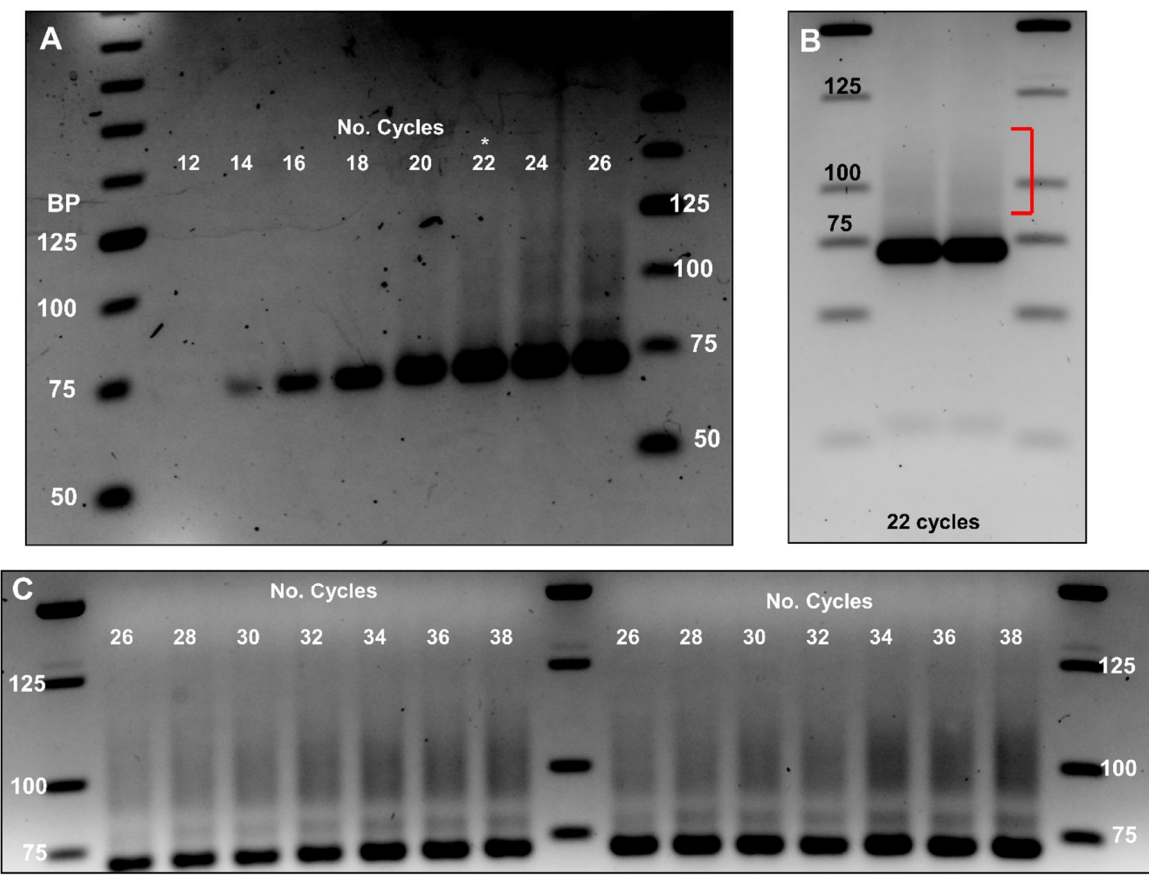


Figure 4-2. PAN-AGO-PAR-CLIP cDNA library PCR optimization. (A) A preliminary PCR of the reverse transcribed PAR-CLIP library was run, removing 10 uL every two cycles to determine the optimal number of cycles for preparatory PCR prior to Illumina sequencing. * indicates the optimal number of cycles, in the log phase of amplification. Bands migrating at ~75 represent unwanted adapter-adapter products. (B) 2.5% agarose gel for preparatory PCR. The area excised for gel purification is indicated. (C) 2.5% agarose gel demonstrates the saturation of the cDNA library amplicons after 24 cycles.

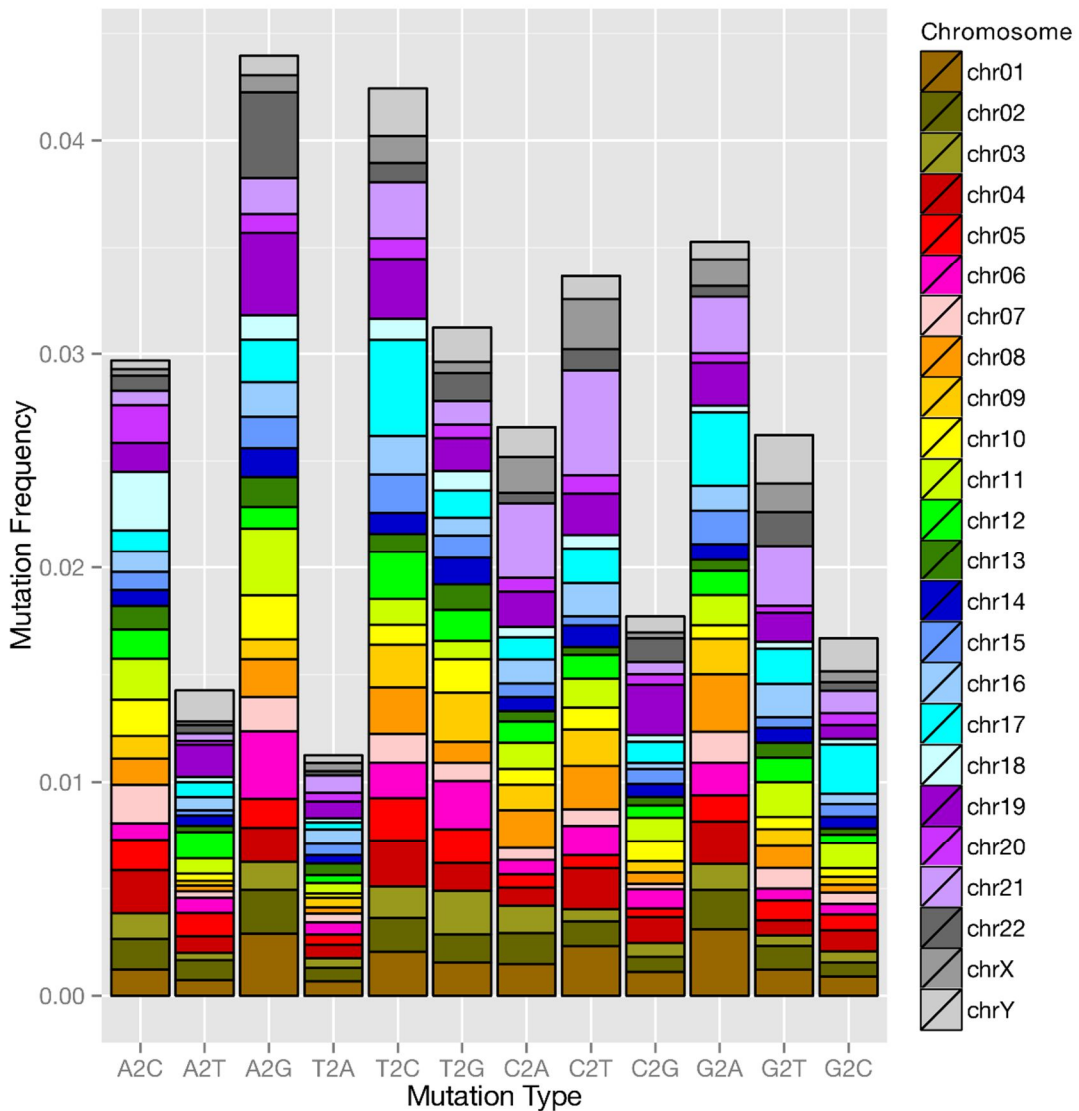


Figure 4-3. Mutational frequencies in PAN-AGO-PAR-CLIP sequencing. All 12 possible base substitutions were tabulated in the sequenced AGO-PAR-CLIP reads. T2C and reverse complement A2G were the most frequent substitutions, providing evidence of crosslinking.

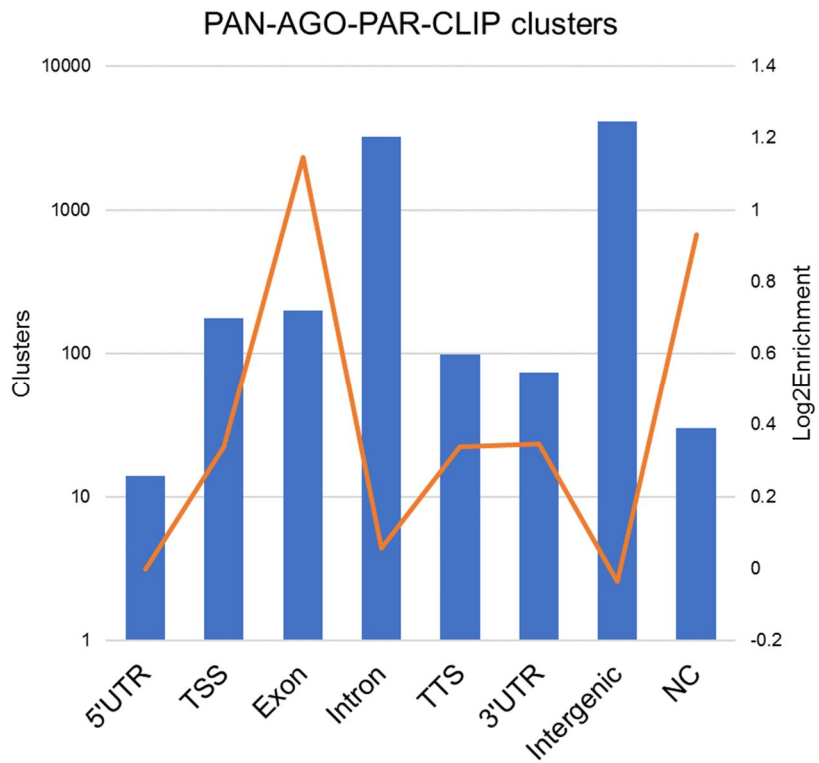


Figure 4-4. PAN-AGO-PAR-CLIP clusters are enriched in the transcript regions of the genome. The bar chart represents the number of PIPE-CLIP clusters identified and assigned to each genomic region by HOMER. The orange line indicates log₂ enrichment of the clusters in each region when relative size of each region is considered. UTR: untranslated region, TSS: transcriptional start site, TTS: transcription termination site, NC: non-coding.

Table 4-1. Top PAN-AGO-PAR-CLIP 3'UTR target genes

Gene	Strand	Peak	TranscriptID	6mer seed (2-7)	5mer seed (2-8)
ECT2	+	2119	NM_018098	hsa-miR-33a-5p	hsa-miR-33a-5p
				hsa-miR-27b-3p	hsa-miR-23b-3p
				hsa-miR-27a-3p	hsa-miR-27b-3p
DDAH1	-	1697	NM_001134445	hsa-miR-21-5p	hsa-miR-21-5p
ADRB1	+	938	NM_000684	hsa-miR-4746-5p	hsa-miR-4497
					hsa-miR-3605-3p
					hsa-miR-5100
SLC25A36	+	915	NM_001104647	none	hsa-miR-4746-5p
					hsa-miR-146a-5p
					hsa-miR-1910-5p
PARK2	+	549	NM_013988	hsa-miR-449a	hsa-miR-1910-5p
					hsa-miR-3190-5p
					hsa-miR-449a
DPY19L4	-	369	NM_181787	hsa-miR-27b-3p hsa-miR-27a-3p	hsa-miR-1910-5p
					hsa-miR-23b-3p
					hsa-miR-27b-3p
CMBL	-	309	NM_138809	hsa-miR-4485-5p	hsa-miR-27a-3p
					hsa-miR-451a
					hsa-miR-4485-5p
C2orf72	+	270	NM_001144994	hsa-miR-29a-3p hsa-miR-4530 hsa-miR-29c-3p hsa-miR-383-3p	hsa-miR-29a-3p
					hsa-miR-4530
					hsa-miR-29c-3p
POLR3K	+	195	NM_016310	hsa-miR-449a	hsa-miR-4738-5p
					hsa-miR-449a
					hsa-miR-383-3p
PAQR9	-	187	NM_198504	none	hsa-miR-1911-3p
					hsa-miR-22-3p
					hsa-miR-138-5p
PAQR9	-	187	NM_198504	none	hsa-miR-3190-5p
					hsa-miR-449a
					hsa-miR-320b
PAQR9	-	187	NM_198504	none	hsa-miR-320a
					hsa-miR-320b
					hsa-miR-320d

'Peak' values reflect the number of reads aligning to the identified PIPE-CLIP cluster.

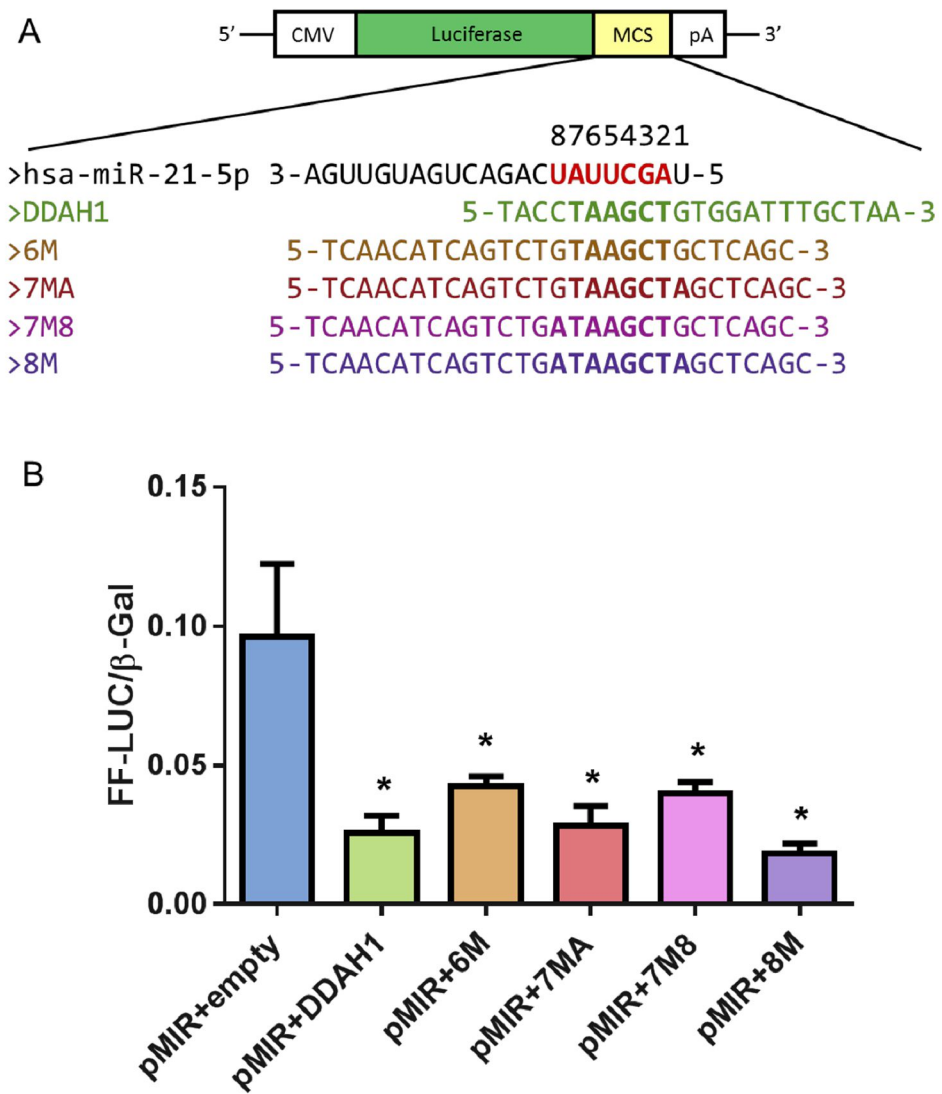


Figure 4-5. PAN-AGO-PAR-CLIP identified 3'UTR DDAH1 target sequence is repressed in vitro. (A) Schematic of inserts cloned into the MCS of pMIR-REPORT 3'UTR luciferase reporter construct. The DDAH1 3'UTR sequence was identified by PAN-AGO-PAR-CLIP in HK-2 cells. The putative regulatory miRNA, miR-21-5p is aligned to illustrate predicted binding at a complementary 6mer seed sequence in the DDAH1 fragment. Constructs containing four possible canonical seed target sites for miR-21-5p were constructed as positive controls (6M: 6mer, 7MA: 7mer-A1, 7M8: 7mer, 8M: 8mer). (B) Luciferase activity after transfection of the reporter constructs in 293T cells. Luciferase activity is normalized to a co-transfected Beta-galactosidase reporter construct. . * p = < 0.05 Mann-Whitney test, unpaired.

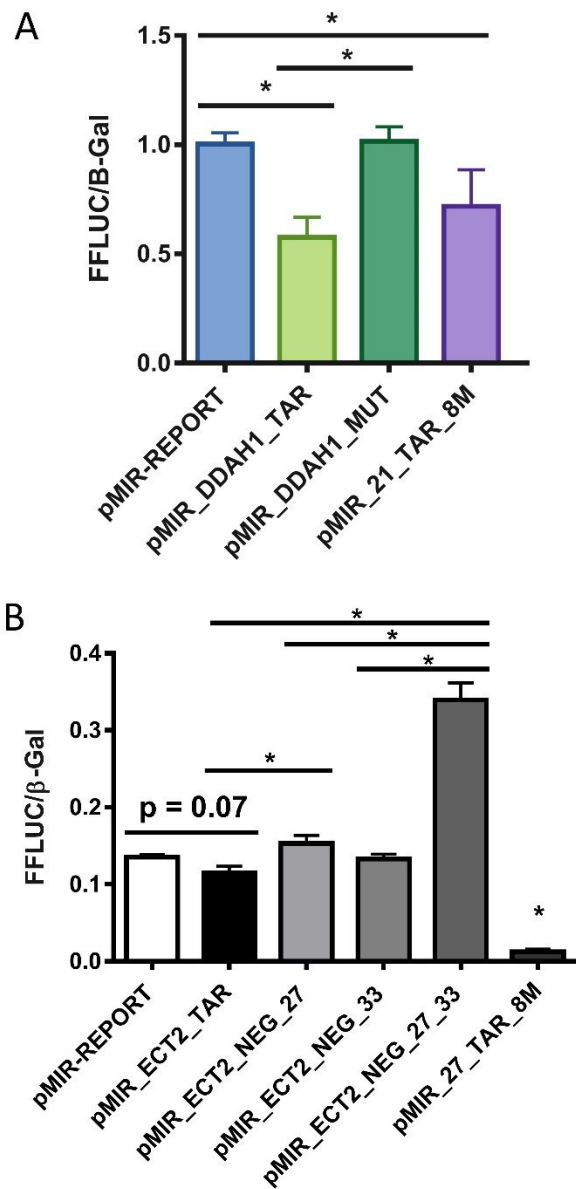


Figure 4-6. Mutation of putative miRNA seed target sites in PAN-AGO-PAR-CLIP clusters de-repressed luciferase activity. (A) pMIR-DDAH1-MUT contains a mutant version of the *DDAH1* target sequence where the 6mer seed site for miR-21-5p has been flipped (TAAAGCT to TCGAAT). * $< p = 0.05$, Mann-Whitney test, unpaired. (B) Luciferase activity of target sequence identified in the 3'UTR of *ECT2*. The target site contains 6mer matches to two miRNAs (hsa-miR-33a and hsa-miR-27a/b). ‘MUT27’ and ‘MUT33’ contain single mutations for each miRNA target site. ‘MUT27+33’ contains an insert with both sites flipped. ‘27-TAR-8M’ contains a canonical 8mer site complementary to miR-27a/b. * $p = < 0.05$ unpaired t-test.

4.2. AGO2-PAR-CLIP defines miRNAs associated with the RISC complex in human proximal tubule cells treated with CsA

To define a miRNA-mRNA targetome of CIN, we performed AGO2-PAR-CLIP and deep sequencing on the human kidney proximal tubule cell line HK-2 (ATCC CRL-2190) treated with CsA or vehicle control. This model has previously been shown to result in characteristic morphologic and gene expression alterations consistent with CIN pathology (Esposito et al. 2000; Jennings et al. 2007; Papachristou et al. 2009; Puigmule et al. 2009; Yuan et al. 2015). PAR-CLIP was conducted as previously described (Hafner et al. 2010). Briefly, HK-2 cells were cultured overnight in medium supplemented with 100 uM 4-thiouracil (4-SU) and then treated with CsA (5ug/mL) for 24 hours. The cells were then exposed to UV light (365 nm) to crosslink RNAs to associated RNA binding proteins. AGO2-associated RNAs were then isolated by immunoprecipitation using the anti-AGO2 monoclonal antibody C34C6 (**Figure 4-7A,B**). AGO2-associated RNAs were then purified, reverse transcribed, prepared into cDNA libraries and sequenced (**Figure 4-7C**). PAR-CLIP was performed in duplicate for each experimental condition and the resulting Illumina sequencing reads were pooled for maximal read depth (**Table 4-2**).

Sequencing produced a total of 191,329,924 and 209,471,643 trimmed and quality-filtered reads for vehicle and CsA-treated samples, respectively. Alignment of these sequences to the hg19 reference genome resulted in 63,264,816 and 72,901,293 mapped reads in the respective samples. Low overall mapping efficiency in PAR-CLIP experiments is common due to the technical nature of recovering RNA and the high rate of mutations introduced (Hafner et al. 2012).

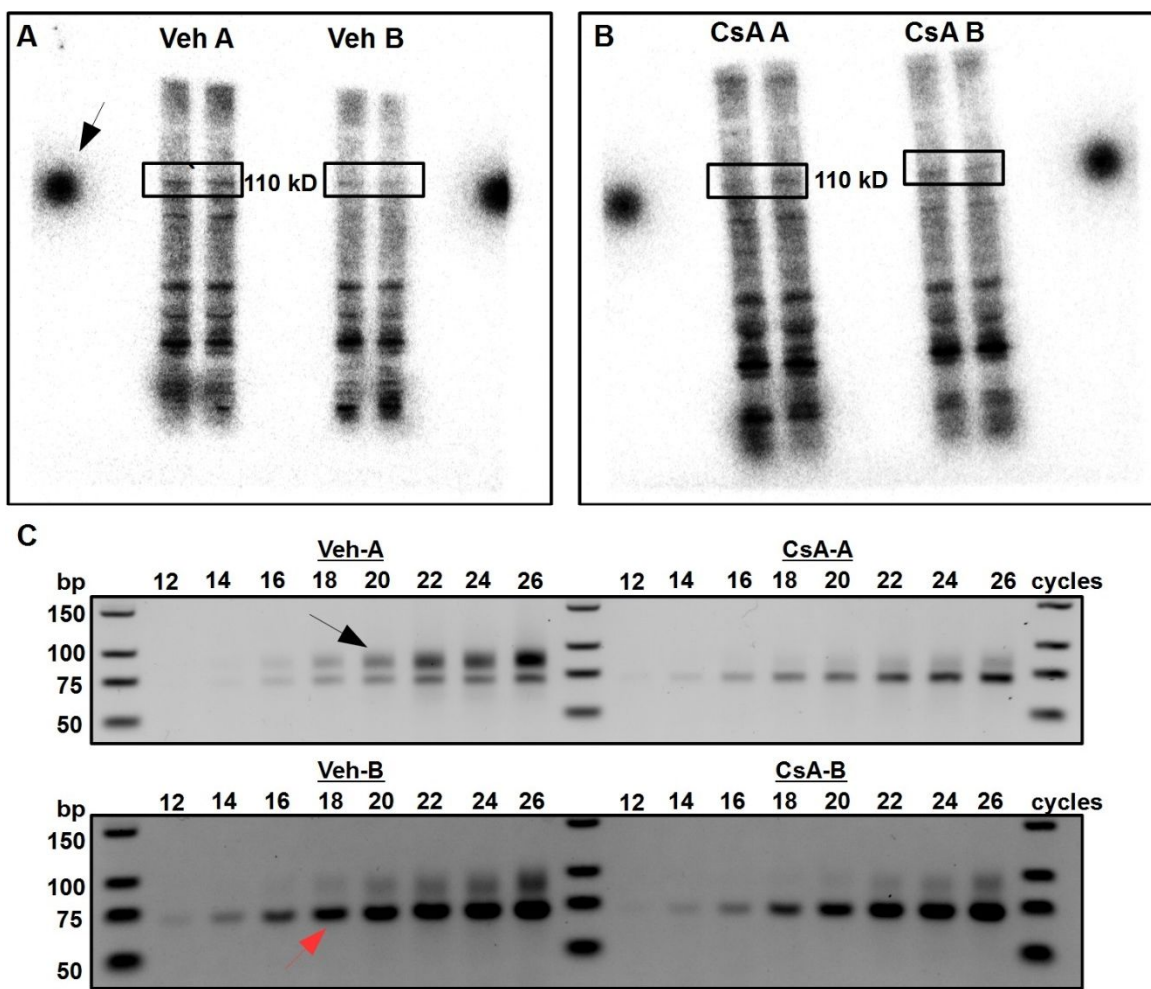


Figure 4-7. Preparation of the AGO2-PAR-CLIP cDNA libraries. After treatment with 4-SU and UV crosslinking, HK-2 cells treated with (A) vehicle control or (B) CsA [5 ug/mL] were lysed and AGO2 was immunoprecipitated. Shown in (A) and (B) are the 5'-radiolabeled RNA-protein complex immunoprecipitates after SDS-PAGE. Bands corresponding to the size of AGO2-RNA complexes (~110 kDa) were excised for RNA isolation. The arrow indicates radioactive mark made on 110 kDa band. (C) Agarose gels after preliminary PCR to determine optimal number of cycles for pre-sequencing amplification. The black arrow indicates the band (~95-100 bp) corresponding to the desired ligation product containing 19-35 nt inserts. The red arrow indicates insert-less adapter-adapter products. To avoid overduplication of abundant targets, a cycle number is selected prior to signal saturation. For this experiment and the larger preparatory PCR, 20 cycles was chosen.

Table 4-2. Summary of AGO2-PAR-CLIP Illumina sequencing and alignment.

Sample	Clusters(PF)	Trimmed Reads	Mapped Reads
HK2-AGO2-Veh	448,555,404	191,329,924 (42.65%)	63,264,816 (14.10%)
HK2-AGO2-CSA	464,858,433	209,471,643 (45.06%)	72,901,293 (15.68%)

The percentage of reads containing T>C or A>G crosslinking mutations was higher than all other mutations (**Figure 4-8A**), suggesting that the AGO2-associated RNAs isolated were enriched for those actively targeted in the RNA-AGO2 protein complex.

To characterize miRNAs in the AGO2 protein complex, we mapped the AGO2-associated RNA sequence reads we obtained through PAR-CLIP to the miRbase v21 reference pre-miRNA hairpin sequences. Mapping and subsequent quantification was performed with miRDeep2, allowing for one mutation (Friedlander et al. 2012). Initial results revealed an abundance of three mature miRNAs (hsa-miR-1246, hsa-miR-1290, and hsa-miR-7641) accounting for nearly 70% of all normalized expression in both samples (**Figure 4-8B, Table 4-2**). However, evidence suggests that reads mapping to hsa-miR-1246 and hsa-miR-1290 may in fact represent non-coding RNAs that correspond to the U2 small nuclear RNA, *RNU2* (Mazieres et al. 2013). Indeed, closer inspection of the PAR-CLIP reads which aligned to the hsa-miR-1290 hairpin reference reveals that nearly all contained a mismatch and that these sequences match the U2 small nuclear RNA perfectly (**Figure 4-9**). Further, hsa-miR-7641 has been identified as a derivative of rRNA repeats within 5S ribosomal pseudogene 387 (Matylla-Kulinska et al. 2014). We therefore excluded these miRNAs from downstream analysis. Of the remaining mature miRNAs, hsa-miR-4792 and hsa-miR-21-5p were the most abundant. By comparing normalized read counts of the CsA-treated and vehicle-treated samples we

defined AGO2-associated miRNAs that are either up or down-regulated relative to control samples following CsA treatment (**Table 4-3**). Hsa-miR-10a-5p exhibited the greatest increase in RISC binding after CsA treatment, whereas hsa-miR-4516 was decreased most. miRNAs ($n = 118$) were also identified that were present only in vehicle or CsA samples. The top miRNAs (greater than 150 normalized reads) specific to either CsA or vehicle-treated samples are listed in **Tables 4-4 and 4-5**.

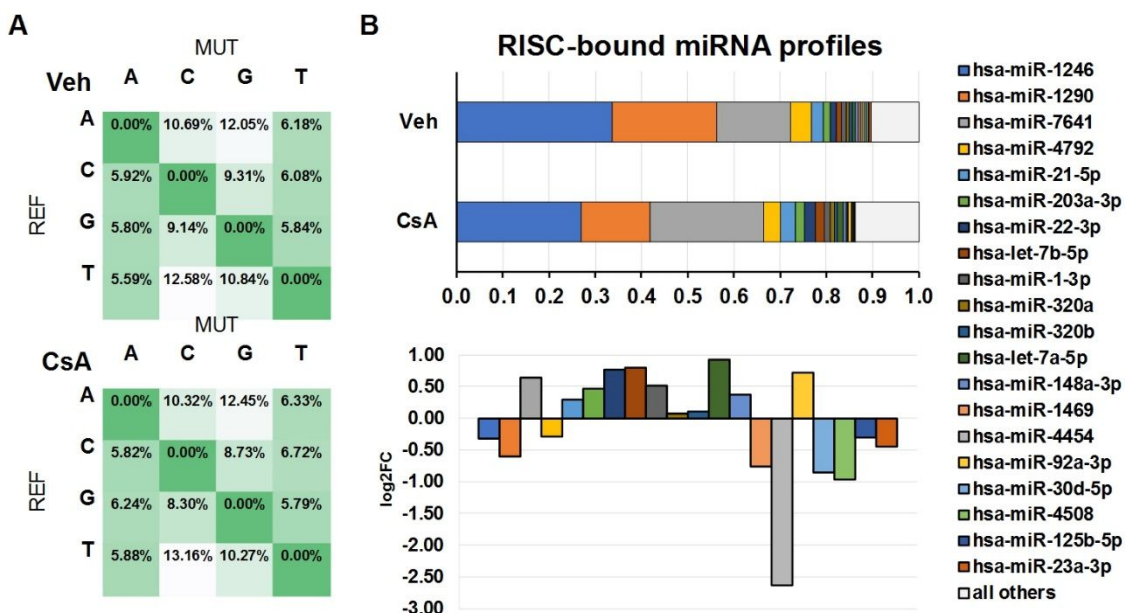


Figure 4-8. Analysis of RISC-bound RNAs and miRs obtained by AGO2-PAR-CLIP. (A) Mutational frequencies of all possible transitions in Ago2-PAR-CLIP sequences derived from vehicle (Veh) and CsA-treated HK-2 cells. (B) Proportions of the top 20 miRs that were detected in Ago-PAR-CLIP libraries by alignment to miRbase v21 reference database. Below, log₂ fold change of top 20 miRs detected in RISC complex after treatment with CsA.

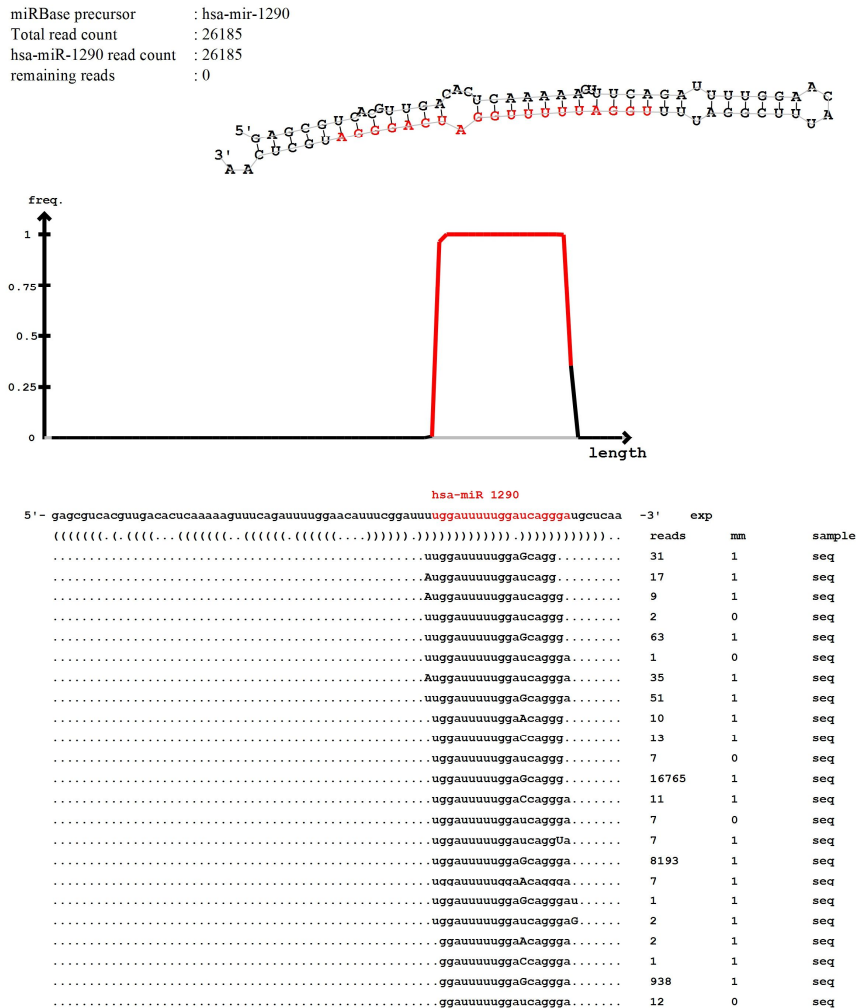


Figure 4-9. Alignment of PAR-CLIP reads to miR-1290. AGO2-PAR-CLIP reads obtained from vehicle-treated HK-2 cells were aligned to the miRbase v21 reference hairpin sequences using miRdeep2 software. Top, diagram illustrates the hairpin-loop structure of hsa-miR-1290. Red letters indicate the mature miRNA sequence. Middle, the graph indicates the abundance of reads mapping to the hsa-miR-1290 hairpin sequence. Bottom, the sequences of the reads mapping to the miR-1290 hairpin sequence are tabulated. Because miRdeep2 allows for one mismatch in the alignment, a large majority of reads (>99%) aligning to this hairpin contain a mismatch, whereas very few reads align perfectly. The sequences which make up the largest proportion of this alignment match perfectly to a U2 small nuclear RNA which is produced by alternative processing (Mazières et al. 2013). The full U2 snRNA sequence is 5'-AUCGUUCUCGGCCUUU GGCUAAGAUCAAGUGUAGUAUCUGUUCUUAUCAGUUUAUAUCUGAUACG UCCUCUAUCCGAGGAACAAUAUAAAAUGGAUUUUUGGAGCAGGGAGAUGG AAUAGGAGCUUGCUCCGUCCACUCCACGCAUCGACCUGGUAUUGCAGUACC UCCAGGAACGGUGCACCC-3'

Table 4-3. Differential read counts of top mature miRNAs increased and decreased in RISC complex after CsA treatment

miRNA	Veh_seq(norm)	CsA_seq(norm)	FoldChange	Log2FC
hsa-miR-10a-5p	7	2801	396.71	8.63
hsa-miR-98-5p	14	451	31.91	5.00
hsa-miR-424-5p	35	630	17.83	4.16
hsa-miR-574-3p	57	776	13.74	3.78
hsa-miR-378a-3p	438	4581	10.46	3.39
hsa-miR-184	85	863	10.18	3.35
hsa-miR-5684	71	673	9.53	3.25
hsa-miR-744-5p	71	668	9.45	3.24
hsa-miR-7975	57	527	9.32	3.22
hsa-miR-103a-3p	71	646	9.15	3.19
hsa-miR-107	71	646	9.15	3.19
hsa-miR-17-5p	71	592	8.38	3.07
hsa-miR-101-3p	325	2481	7.64	2.93
hsa-miR-27a-5p	169	1162	6.85	2.78
hsa-miR-99a-5p	304	1992	6.56	2.71
hsa-let-7c-5p	388	2133	5.49	2.46
hsa-miR-3687	78	413	5.31	2.41
hsa-miR-499a-5p	120	630	5.24	2.39
hsa-miR-486-5p	169	885	5.22	2.38
hsa-miR-34a-5p	120	613	5.11	2.35
hsa-miR-4508	3100	1466	0.47	-1.08
hsa-miR-199a-5p	600	282	0.47	-1.09
hsa-miR-199a-3p	1335	597	0.45	-1.16
hsa-miR-199b-3p	1335	597	0.45	-1.16
hsa-let-7d-5p	14	5	0.38	-1.38
hsa-miR-542-5p	14	5	0.38	-1.38
hsa-miR-7847-3p	14	5	0.38	-1.38
hsa-miR-130a-3p	1766	586	0.33	-1.59
hsa-miR-30c-5p	1843	608	0.33	-1.60
hsa-miR-200c-3p	2232	581	0.26	-1.94
hsa-miR-6802-5p	21	5	0.26	-1.96
hsa-miR-4485-3p	1194	261	0.22	-2.20
hsa-miR-3168	247	49	0.2	-2.34
hsa-miR-4454	3686	548	0.15	-2.75
hsa-miR-22-5p	42	5	0.13	-2.96
hsa-let-7e-5p	148	16	0.11	-3.19
hsa-miR-5100	78	5	0.07	-3.84
hsa-miR-6773-5p	367	22	0.06	-4.08
hsa-miR-4787-5p	318	16	0.05	-4.29
hsa-miR-4516	996	11	0.01	-6.52

Table 4-4. Top CsA-specific miRNAs detected by AGO2-PAR-CLIP

miRNA	NT_reads(norm)	CsA_reads(norm)
hsa-miR-106a-5p	0	771
hsa-miR-25-3p	0	749
hsa-miR-212-5p	0	537
hsa-miR-92b-3p	0	527
hsa-miR-153-3p	0	494
hsa-miR-3622a-5p	0	489
hsa-miR-23a-5p	0	440
hsa-miR-1307-3p	0	407
hsa-miR-4539	0	337
hsa-miR-8062	0	299

Table 4-5. Top vehicle-specific miRNAs detected by AGO2-PAR-CLIP

miRNA	NT_reads(norm)	CsA_reads(norm)
hsa-miR-133a-5p	1455	0
hsa-miR-619-5p	1201	0
hsa-miR-151a-3p	1151	0
hsa-miR-378a-5p	1010	0
hsa-miR-484	939	0
hsa-miR-941	890	0
hsa-miR-196a-5p	826	0
hsa-miR-18a-5p	770	0
hsa-miR-210-3p	664	0
hsa-miR-3154	664	0
hsa-miR-1273e	600	0
hsa-miR-1248	593	0
hsa-miR-125a-5p	579	0
hsa-miR-5096	516	0
hsa-miR-4466	438	0
hsa-miR-15a-5p	346	0
hsa-miR-142-3p	332	0
hsa-miR-4448	325	0
hsa-miR-186-5p	254	0
hsa-miR-1260b	219	0
hsa-miR-26b-5p	191	0
hsa-miR-33a-5p	169	0
hsa-miR-3529-5p	169	0
hsa-miR-17-3p	155	0

4.3. Defining mRNA-binding events in the RISC complex of human proximal tubule cells treated with CsA

To determine direct genome-wide targets of miRNAs in CsA-treated human proximal tubule cells we analyzed the sequence data obtained by PAR-CLIP using the bioinformatic pipeline PIPE-CLIP (Chen et al. 2014). PIPE-CLIP identifies enriched clusters of overlapping sequences by computing read counts of sequences overlapping by at least one nucleotide and then determines reliable binding sites by crosslinking-induced T>C mutations. This makes it possible to estimate the degree to which sequences throughout the genome are undergoing active targeting in the AGO2 complex. Candidate crosslinking sites are defined as those enriched clusters of sequences that contain crosslinking induced mutation sites passing a false discovery rate (FDR) that we set at 0.05. We identified 56,985 and 36,812 significant crosslinking sites in sequence clusters from vehicle and CsA-treated libraries respectively. Within these clusters, we observed 65,263 and 42,069 reliable T>C mutations. Annotation of the sequences in each cluster revealed that a large proportion map to intergenic and intronic regions of the genome (**Figure 4-10A**). However, normalization to the relative sizes of the genomic regions revealed enrichment for crosslinking sites in 3'UTR, exon, and 5'UTR transcript regions as well as promoter and transcription termination sites (**Figure 4-10B**).

We next compared the crosslinking mutations discovered in sequence clusters using PIPE-CLIP between CsA and vehicle control libraries. We identified 45,575 mutations unique to vehicle control samples, 19,689 present in both vehicle controls and CsA treated samples and 22,381 unique to CsA treated samples (**Figure 4-11A**). These

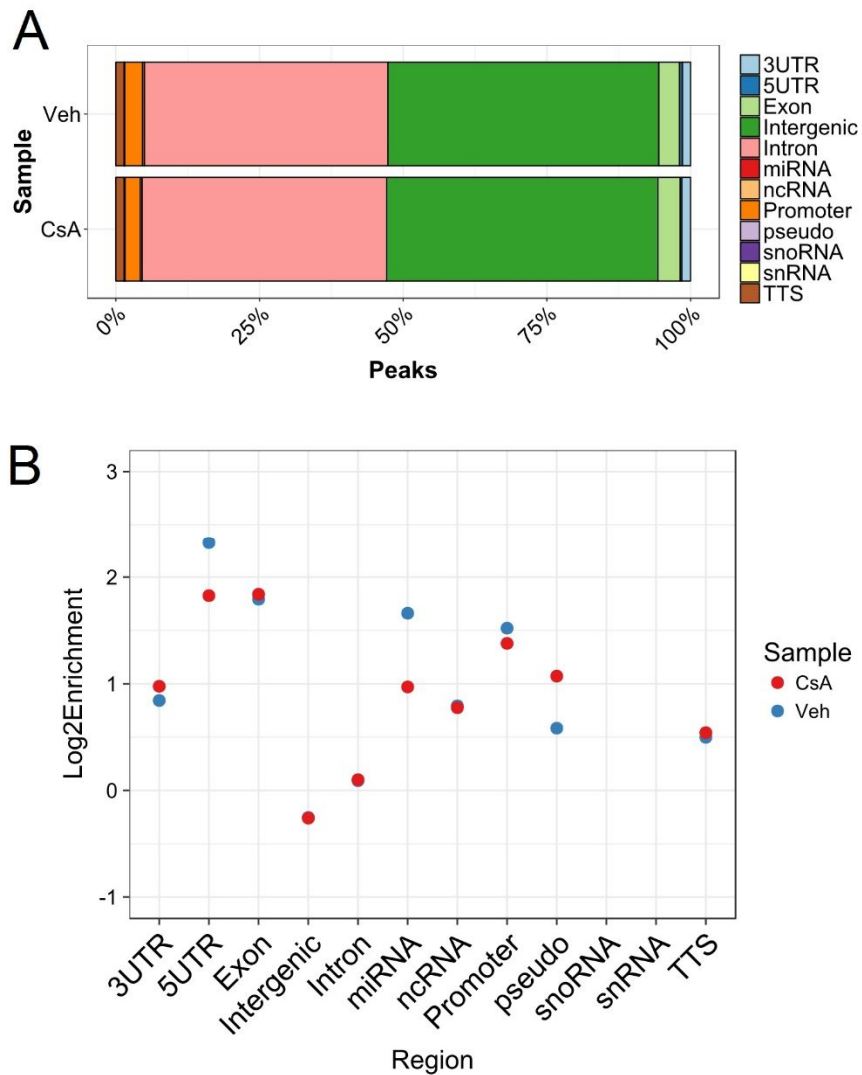


Figure 4-10. AGO2-PAR-CLIP target sites are enriched in transcripts. (A) Genomic distribution of crosslinking sites identified by Ago2-PAR-CLIP in vehicle and CsA-treated HK-2 cells. (B) Log2 enrichment of Ago2 crosslinking sites in genomic regions based on normalization to relative region sizes in the reference genome. snoRNA and snRNA features were not detected.

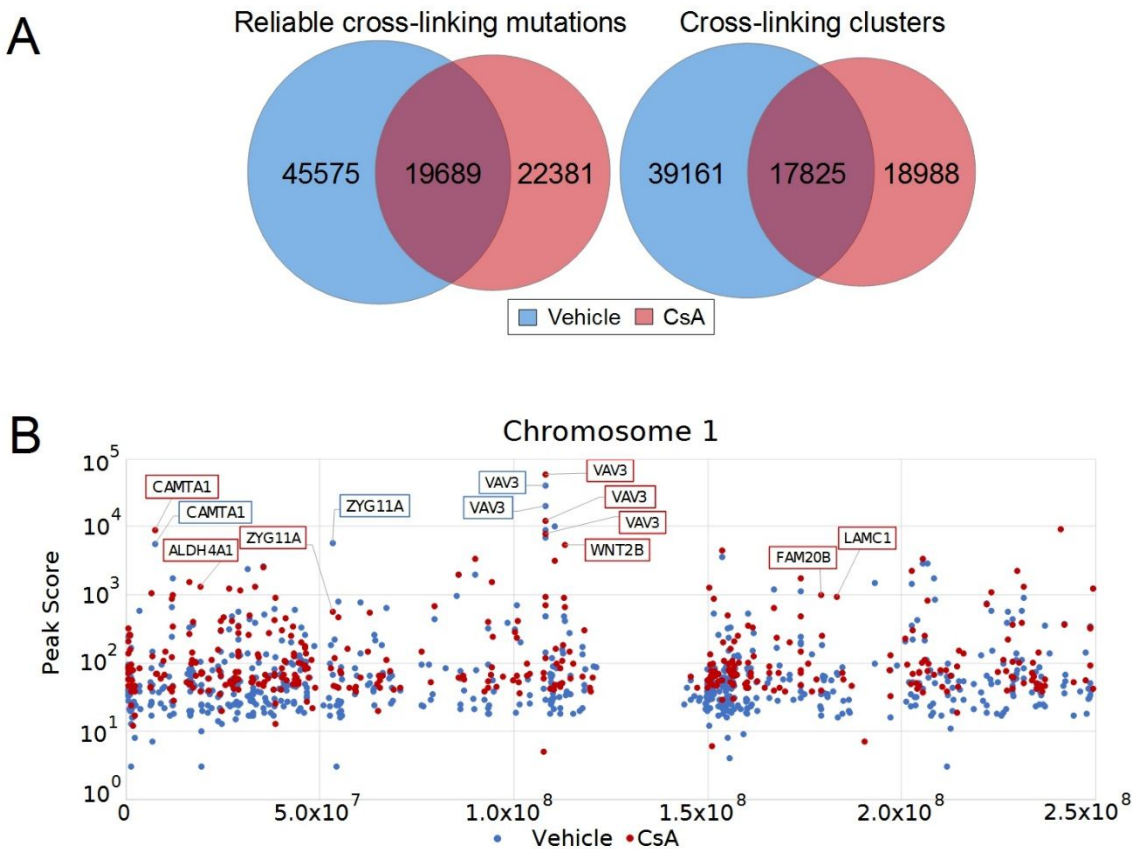


Figure 4-11. AGO2-PAR-CLIP identifies CsA-induced miRNA target sites. (A) Venn diagrams demonstrating the number of unique and shared Ago2 crosslinking mutations and sequence clusters in vehicle versus CsA-treated HK-2 cells. Reliable crosslinking mutations are determined by fitting a binomial distribution to assess the significance of T>C mutations. Mutations with an FDR (Benjamini-Hochberg method) less than 0.05 are considered ‘reliable.’ For crosslinking sequence clusters, a zero-truncated negative binomial regression is first used to identify enriched clusters of overlapping sequences. The enriched clusters (with FDR < 0.05) that also contain a reliable mutation are considered ‘crosslinking clusters.’ (B) PIPE-CLIP peak scores of AGO2 crosslinking sites in vehicle and CsA-treated HK-2 cells mapping to chromosome 1 (excluding intergenic and intronic regions). 3UTR: 3' untranslated region, 5UTR: 5' untranslated region, ncRNA: non-coding RNA, snoRNA: small nucleolar RNA, snRNA: small nuclear RNA, TTS: transcription termination site.

mutations were present in 39,161 sequence clusters from vehicle control, 17,825 from both vehicle controls, and CsA treated samples, and 18,988 from CsA treated samples (**Figure 4-11A**). PIPE-CLIP peak scores were computed for all clusters based on read counts of sequences containing mutations. Strength and location of binding based on depth of read coverage and number of mutations varied between CsA and vehicle-treated samples (**Figure 4-11B**). Many crosslinking sites were identified that were present in both vehicle and control samples; however, many exhibited significant increases or decreases in peak signal strength after CsA treatment. Together, these data suggest that CsA treatment of human proximal tubule cells induces genome-wide differential RISC binding by AGO2.

4.4. mRNAs in the AGO2 complex contain seed sequences of miRNAs identified by PAR-CLIP

Analysis of crosslinking sites based on mutations located within mRNAs accounted for 3,264 and 2,157 of total sites in vehicle and CsA-treated samples respectively. This represents an approximately 3-fold enrichment of mRNA crosslinking sites when normalized to genomic region size. We assigned crosslinked miRNAs to target mRNA clusters by mapping them to the transcript crosslinking sites based on complementarity to the seed sequences from miRNA clusters we identified for each condition. Seed sequences that matched canonical 8-mer, 7-mer, and 6-mer seed sequences corresponding to miRNA positions 1-8, 1-7, 2-8, 1-6, 2-7, and 3-8 were analyzed. The canonical and best studied mechanism by which miRNAs achieve regulation of transcripts involves

miRNA guided RISC binding to the 3'UTR of mRNAs (Grimson et al. 2007). Sixty-eight percent (514/748) of 3'UTR clusters in vehicle controls and forty-eight percent (257/530) of 3'UTR clusters in CsA treated samples contained a canonical seed match for at least one of the miRNAs we identified by PAR-CLIP.

Mapping of genome-wide interactions for canonical 7-mer seed matches indicated that apparent miRNA-mRNA interactions in vehicle and CsA-treated samples occur throughout the genome (**Figure 4-12**). miRNA-mRNA interactions unique to either vehicle or CsA-treated samples are also apparent, as unique miRNA-mRNA interactions are observed in both vehicle and CsA-treated groups (**Figure 4-12**). The ten miRNAs with most the frequent seed matches in vehicle and CsA-treated samples are shown in **Table 4-6**. Five out of the top ten miRNAs were present in both vehicle and CsA treated samples, while five seed matches were present only in either vehicle or CsA treated samples (**Table 4-6**). However, only 21.29 (23/108) and 31.08% (23/74) of the mRNAs predicted to be targeted by miRNAs in vehicle and CsA treated samples respectively were present in both samples. Thus, although several mRNAs containing complementary miRNA seed sequences were abundant in both conditions, relatively few targeting interactions were shared.

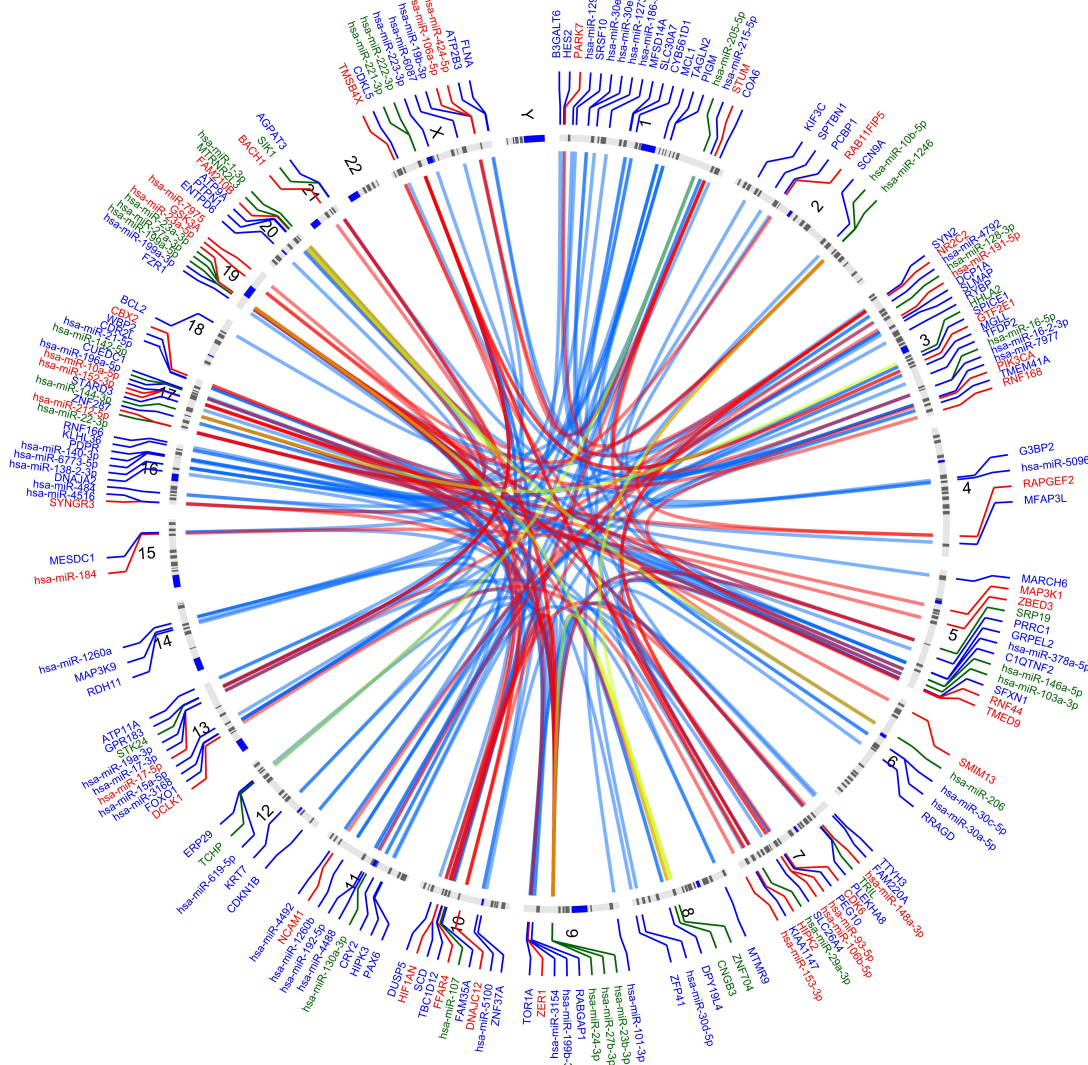


Figure 4-12. Differential miRNA targetome induced by CsA treatment of HK-2 cells. Genome-wide differential targeting of mRNAs by miRNAs in CsA (red) treated HK-2 cells compared to vehicle control (blue). Arcs link target genes containing seed complementarity in the 3'UTR to immunoprecipitated miRNAs (positions 2-8) with their putative miRNA regulator, as determined by AGO2-PAR-CLIP. Green arcs represent common miRNA-mRNA interactions between sample groups. Genes and miRNA genes in green text were observed in both CsA and vehicle control but may reflect sample-specific targeting interactions.

Table 4-6. Top miRNA seed matches in 3'UTR

Sample	miRNA	Targets	Genes
Veh	hsa-miR-1260a/b	28	CBFA2T3, CCBE1, CCL22, CCNB1, CRY2, CUX2, CYB561D1, DCX, FUT11, HSPA12A, IRX6, KCNE3, KIF5A, LUC7L, MGLL, NFATC2, NRXN1, PAX8, PCBP1, PRKN, RAB34, SESN2, SMARCD1, TLX3, TMEM119, WBP2, ZNF37A, ZNF426
Veh	hsa-miR-7977	27	ADAR, ATP9A, C2CD4B, C8orf33, CCNI2, CDKL5, DHRS7B, FAM127B, FUT11, G3BP2, GATAD2A, GNE, IFI44L, MARCH1, NRXN1, PCBP1, PTPN18, RAB34, SESN3, SLC16A3, TCN2, TLE3, TMED9, TNF, WSB1, ZNF37A, ZNF704,
Veh	hsa-miR-5100	24	AGTR2, C14orf180, CD164, CLDN10, CUEDC1, DSG1, EXPH5, GUCY1A2, KCNN3, PAG1, PLCG2, QDPR, RBFOX2, RIMKLA, SCD, SLC22A18AS, SMIM12, SPICE1, SZT2, TALDO1, TBC1D16, TSC1, TUFT1
Veh	hsa-miR-103a-3p/107	23	AGRN, ANXA8L1, BRWD1, C12orf73, CAMK2A, CHMP1B, DCP1A, FLYWCH1, G3BP2, KLF13, KLHL36, LDOC1, NDUFB4, PCBP1, PDE6A, PPARD, PXDN, SAT2, STAT5B, TOR1A, TRIAP1, USP22, XRN1
Veh	hsa-miR-140-3p	23	BACE1, CLDND1, DCAF7, DDAH1, DIP2C, DYRK2, FFAR4, KDSR, KIAA1147, METRNL, PDK3, PHACTR2, PXDN, RAB34, RXRA, SLMAP, SMIM12, TAGLN2, TBC1D12, TUSC2, ZC3H12D, ZFP41, ZRANB1
Veh	hsa-miR-199a-5p	22	AAK1, C2CD4B, CMPK2, COL2A1, DNAL4, FRRS1L, GATAD2B, GOPC, HES2, KIF3C, PTPN18, SAT2, SESN2, SESN3, SIRPG, SLC35B4, SLC7A1, STARD3, TMED9, TMOD2, TRIL, WSB1
Veh	hsa-miR-30e-3p	21	AASS, ABCB5, BAHCC1, C12orf73, CD164, CDKN2B, CLDN10, CSPG4, DESI1, DNAJC8, FRRS1L, GATAD2B, GRIK4, NR2F1, PLEKHA8, PPP1R12B, RBFOX2, SLC7A11, SNX9, TTC8, ZNF655
Veh	hsa-miR-23a/b-3p	20	AASS, CCDC50, DNAJC8, EAF1, EHD2, FOXO1, HNRNPR, KDM3B, LAMC1, PACSIN1, PEG10, PLCG2, PPP1CB, SH3BP2, SRP19, STX1B, TMEM74B, TRIM66, ZNF544, ZNF704
Veh	hsa-miR-27a/b-3p	20	AASS, DHX33, DPY19L4, FOXO1, GRAMD3, MAU2, MCL1, MESDC1, PHACTR2, PRDM10, RABGAP1, RAX, SCN9A, SRP19, STARD7, STX1B, TECRL, TLCD2, TRAF3IP1, TUFT1
Veh	hsa-miR-5096	20	AASS, ABCB5, AGPAT3, CHIC1, DESI1, DPY19L4, EXPH5, MCL1, PROX2, PXDN, RORA, RYBP, SMIM7, SMU1, SNX9, TMPO, TMSB4X, TTC8, TUFT1, ZBTB47
CsA	hsa-miR-27a/b-3p	18	AMOTL2, ATP6V1A, CBX2, CCNJ, CELF1, DNAJC12, FFAR4, MAP3K1, MAU2, PHACTR2, PKIA, PRDM10, RUNX1, SIK1, SPEN, SRP19, TSC22D3, ZBTB34
CsA	hsa-miR-140-3p	17	ARPC4, ARSB, C15orf53, CCNJ, COX10, DDAH1, FFAR4, HES7, KIAA1147, L2HGDH, PHACTR2, PPP1R15B, RAB34, RXRA, TSC22D3, ZFAND5, ZRANB1
CsA	hsa-miR-144-3p	16	ANGPT1, CYSTM1, DNAJC12, FAM127A, HHLA2, KPNA2, MAP3K1, POLR3K, PTGFRN, RAB34, SESN3, SLC4A8, SRP19, TMEM117, TMSB4X, TSC22D3
CsA	hsa-miR-199a-5p	15	CMPK2, CNGA3, DNAL4, FRRS1L, GATAD2B, GPR26, HSPA5, MYO1D, SEC61A1, SESN3, SH2B3, SLC7A1, TBC1D13, THBD, TRIL
CsA	hsa-miR-128-3p	15	AMOTL2, CCNJ, CXCL3, DNAJC12, FFAR4, GAD1, MAP3K1, MAU2, MYO1D, PHACTR2, RUNX1, SIK1, SPEN, TSC22D3, ZBTB34
CsA	hsa-miR-205-5p	14	BRWD1, CHIC1, FOXE3, GALNT13, HDX, KIAA1147, NCOA2, PKD1L2, SLC30A9, SMU1, TCHP, TMED9, WDR17, ZNF544
CsA	hsa-miR-101-3p	13	ANGPT1, CYSTM1, DNAJC12, HHLA2, KPNA2, LCN10, MAP3K1, PTGFRN, SLC4A8, SRP19, TMEM117, TMSB4X, TSC22D3
CsA	hsa-miR-103a-3p/107	12	BRWD1, LOC101928841, NDUFB4, PPARD, RDH10, RHOQ, RUNX1, SLC7A5, STUM, TSC22D3, ZBTB34, ZFAND5
CsA	hsa-miR-23a/b-3p	11	BTBD10, CBX2, DNAJC12, EHD2, LAMC1, NPAP1, SRP19, SYNGR3, TMED10, ZNF585B, ZNF704
CsA	hsa-miR-125b-5p	10	ABCC5, CD81, CYP26B1, NR3C2, PEG10, PHLDB1, RAB11FIP5, RNF44, TMEM201, YRDC

4.5. Comparing PAR-CLIP and RNA-seq reveals that a relatively small number of miRNAs and mRNAs are involved in active targeting

We next sought to examine the extent to which sequence clusters identified by PAR-CLIP reflect total RNA abundance. We therefore examined the miRNA expression profiles using our miRNA-seq data on total RNA from HK-2 cells after treatment with CsA or vehicle control. To summarize, of the possible 2,586 mature miRNAs in miRbase v21, 1,575 were detected at any level. The top 100 expressed miRNAs accounted for 98.8% of reads across all samples. Differential expression analysis identified that 72 miRNAs were differentially regulated after CsA treatment (Benjamini-Hochberg adjusted P value < 0.1), of which 35 were up-regulated and 37 were down-regulated when compared with control samples. We next compared sequencing data obtained from miRNA-seq and PAR-CLIP. miRNA-seq identified 1542 mature miRNAs in vehicle samples and 1525 in CsA-treated samples. Of these miRNAs, 177 in vehicle and 124 in CsA treated samples were also identified by PAR-CLIP (**Figure 4-13**). In addition, 26 mature miRNAs in vehicle and 13 in CsA treated samples were uniquely identified by PAR-CLIP. Due to the technical nature of PAR-CLIP these miRNAs discovered only after immunoprecipitation may represent false positives. Within the protocol, RNase treatment of AGO2-bound RNAs may trim miRNAs as well as mRNAs. As the sequencing and bioinformatics protocol allows many short reads to be retained, these reads may map more promiscuously due to lack of sequence complexity. Further, as mismatches are allowed in the mapping pipeline to account for experimentally induced T>C transitions, reads may misalign to miRNA reference sequences that contain the altered sequence as we have demonstrated in the case of hsa-miR-1290. However, reads

detected only in PAR-CLIP libraries may indeed represent bona fide miRNAs that were bound to the RISC complex by undetectable by total miRNA-seq. As we observed in the miRNA-seq experiment, high abundance reads such as hsa-miR-21 dominate the pool of reads so greatly that power of detection at standard sequencing depths may be compromised. Thus, AGO2-enrichment by PAR-CLIP may actually improve the detection of low-abundance miRNAs.

We next set out to examine what fraction of cellular mRNAs undergo active targeting following CsA treatment. We compared the mRNAs detected previously by RNA-seq to the mRNA targets identified by AGO2-PAR-CLIP. Comparing RNA-seq and PAR-CLIP sequencing data revealed that 868 mRNA clusters in CsA treated samples and 1503 in vehicle controls identified by PAR-CLIP were also observed by RNA-seq, while 775 were shared in all data sets (**Figure 4-13B**). PAR-CLIP identified 68 and 286 mRNA clusters that were uniquely present in CsA or vehicle samples (**Figure 4-13B**). Fifty-nine clusters identified by PAR-CLIP were present in both CsA and vehicle controls (**Figure 4-13B**). Together, our data suggest that CsA induces specific post-transcriptional regulation of gene expression through differential expression of mRNAs and recruitment of unique mRNA pools to the RISC complex.

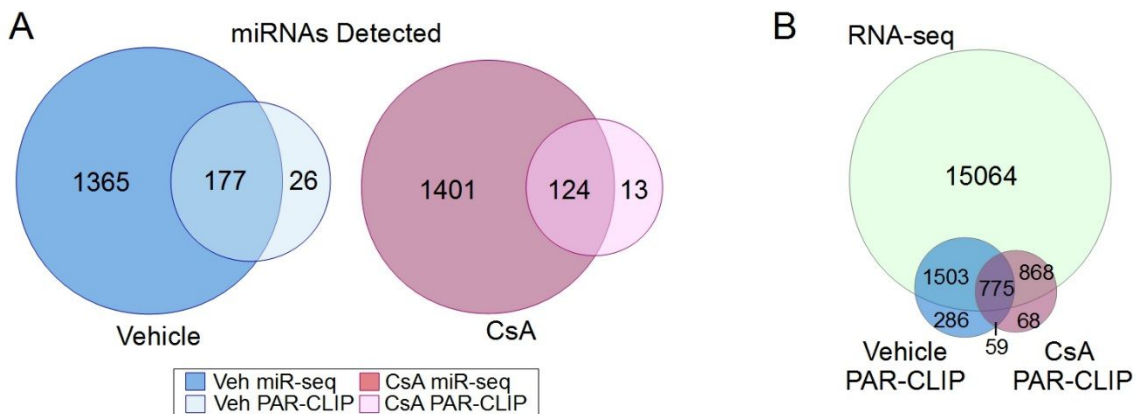


Figure 4-13. miRNAs and mRNAs detected by AGO2-PAR-CLIP represent a small proportion of the total RNA pool in HK-2 cells. (A) By comparing the miRNAs detected by immunoprecipitation of the AGO2 complex to the total pool of miRNAs detected previously by miRNA-seq, we observed only a fraction (8-12%) of mature miRNAs were observed by both methods in treated and control HK-2 cells. Further, some miRNAs were detected by PAR-CLIP that were not detected by conventional miRNA-seq. (B) Similarly, comparison of PAR-CLIP mRNA targets to total RNA-seq data revealed that in both CsA-treated and vehicle-treated control HK-2 cells, only a fraction of the transcriptome is regulated by miRNAs in the RISC complex.

4.6. Gene pathways regulated by miRNAs following CsA treatment

To determine the cellular processes regulated by miRNAs in CsA-induced nephrotoxicity, we performed Ingenuity Pathway Analysis (IPA) on the sets of transcripts identified by AGO2-PAR-CLIP. First, we identified the canonical pathways enriched in gene sets composed of all mRNA targets in either vehicle ($n= 3,264$) or CsA ($n= 2,157$) treated samples. In vehicle-treated proximal tubule cells, the top canonical pathways enriched in the AGO2-PAR-CLIP target gene set were Cellular Effects of Sildenafil (Viagra), Calcium Signaling, Actin Cytoskeleton Signaling, Protein Kinase A Signaling, and Tight Junction Signaling (**Figure 4-14A**). In CsA treated cells, the top pathways enriched were Integrin Linked Kinase Signaling, Actin Cytoskeleton Signaling, Cellular Effects of Sildenafil (Viagra), Epithelial Adherens Junction Signaling, and Glucocorticoid Receptor Signaling (**Figure 4-14B**). Of the top 20 canonical pathways enriched in each group, 11 were enriched in both (**Figure 4-15**). Thus, despite only modest overlap in the transcripts that are targeted by miRNAs in both conditions, several critical pathways are found to be regulated by the RISC complex in CsA-treated and vehicle control HK-2 cells related to cell-cell adhesion, integrin-cytoskeleton signaling, and calcium signaling.

To assess which pathways were most negatively regulated by miRNAs after CsA treatment, we identified the pathways enriched only in the set of genes identified by PAR-CLIP that were also down-regulated after CsA treatment as determined by RNA-seq. In this analysis, the most enriched pathways were Hepatic Fibrosis/Hepatic Stellate Cell Activation, Calcium Signaling, Epithelial Adherens Junction Signaling, Tight Junction Signaling, Cellular Effects of Sildenafil (Viagra), and ILK Signaling (**Figure 4-**

14C). In the Hepatic Fibrosis/Hepatic Stellate Cell Activation pathway, this analysis indicates targeting and down-regulation of several collagen (*COL11A1*, *COL11A2*, *COL1A1*, *COL22A1*, *COL4A1*, *COL4A2*, *COL4A5*, *COL6A6*, *COL9A2*) and myosin (*MYH1*, *MYH2*, *MYH3*, *MYH4*, *MYH7*, *MYH8*, *MYH10*, *MYH13*, *MYH7*) isoforms. These myosin isoforms are also contained within the other top enriched pathways (**Figure 4-15**).

To determine the function of the most active miRNAs targeting high confidence binding sites, we analyzed the transcripts which were previously matched in the 3'UTR with the most frequently occurring miRNA seeds by IPA. In vehicle treated HK-2 cells the top enriched canonical pathways were PPAR Signaling and PXR/RXR activation. In CsA-treated cells the top enriched canonical pathways were VDR/RXR Activation and Glucocorticoid Receptor Signaling. Notably, the Glucocorticoid Receptor Signaling pathway was also identified as one of the top canonical pathway enriched in CsA-treated PAR-CLIP transcripts and exhibited the highest enrichment in transcripts that were exclusively regulated by miRNAs in CsA-treated cells (**Figure 4-14D**). The miRNA-targeted transcripts in CsA-treated proximal tubule cells involved in Glucocorticoid Receptor Signaling are C-X-C motif chemokine ligand 3 (*CXCL3*), heat shock protein family A (Hsp70) member 5 (*HSPA5*), mitogen-activated protein kinase kinase kinase 1 (*MAP3K1*), nuclear receptor coactivator 2 (*NCOA2*), nuclear receptor subfamily 3 group C member 2 (*NR3C2*), and TSC22 domain family member 2 (*TSC22D2*).

To determine the putative roles these miRNA-mRNA targeting relationships play in Glucocorticoid Receptor Signaling we integrated RNA-seq expression data of the target genes and related pathway members and implemented the Ingenuity Molecule

Activity Predictor to model downstream effects (**Figure 4-16**). In Glucocorticoid Receptor Signaling there is crosstalk between the active glucocorticoid receptor complex and MAPK signaling, including direct binding to JNK which mediates inhibition of the JNK pathway and trans-repression of AP-1 (Bruna et al. 2003). 3'UTR targeting of *MAP3K1/MEKK1* and *TSC22D3/GILZ* was identified by PAR-CLIP in CsA-treated HK-2 cells. In RNA-seq, a corresponding decrease in expression was found in both genes (*MAP3K1/MEKK1* = -1.12 log2FC, adj P-value = 1.80×10^{-23} ; *TSC22D3/GILZ* = -0.61 log2FC, adj P-value = 7.65×10^{-35}). Further, in both genes, the PAR-CLIP target clusters contained seed sequences complementary to miR-27a-3p and miR-101-3p, miRNAs which were up-regulated after CsA treatment (+0.384 log2FC, FDR = 0.007; +0.259 log2FC, FDR = 0.25, respectively). Down-regulation of these transcripts is predicted to inhibit JNK and p38 signaling and allow activation of ERK1/2 (**Figure 4-16**).

CsA has previously been demonstrated to inhibit JNK and p38, but not ERK pathways in Jurkat T lymphocytes (Matsuda et al. 2000). In RNA-seq we observed down-regulation of the tissue specific *MAPK10/JNK3* isoform (-1.69 log2FC, adj P-value = 2.24×10^{-12}). *HSPA5* and *NR3C2*, the mineralcorticoid receptor, were both detected by PAR-CLIP in CsA-treated HK-2 cells and both transcripts are significantly up-regulated compared to vehicle control (+1.48 log2FC, adj P-value = 6.21×10^{-157} and +1.29 log2FC, adj P-value = 1.23×10^{-21} ; **Figure 4-16**). Increased expression of both genes contributes to reduced signaling by the glucocorticoid-GCR dimer complex, thus suggesting that JNK/p38 inhibition may occur upstream (Derfoul et al. 2000; Kirschke et al. 2014).

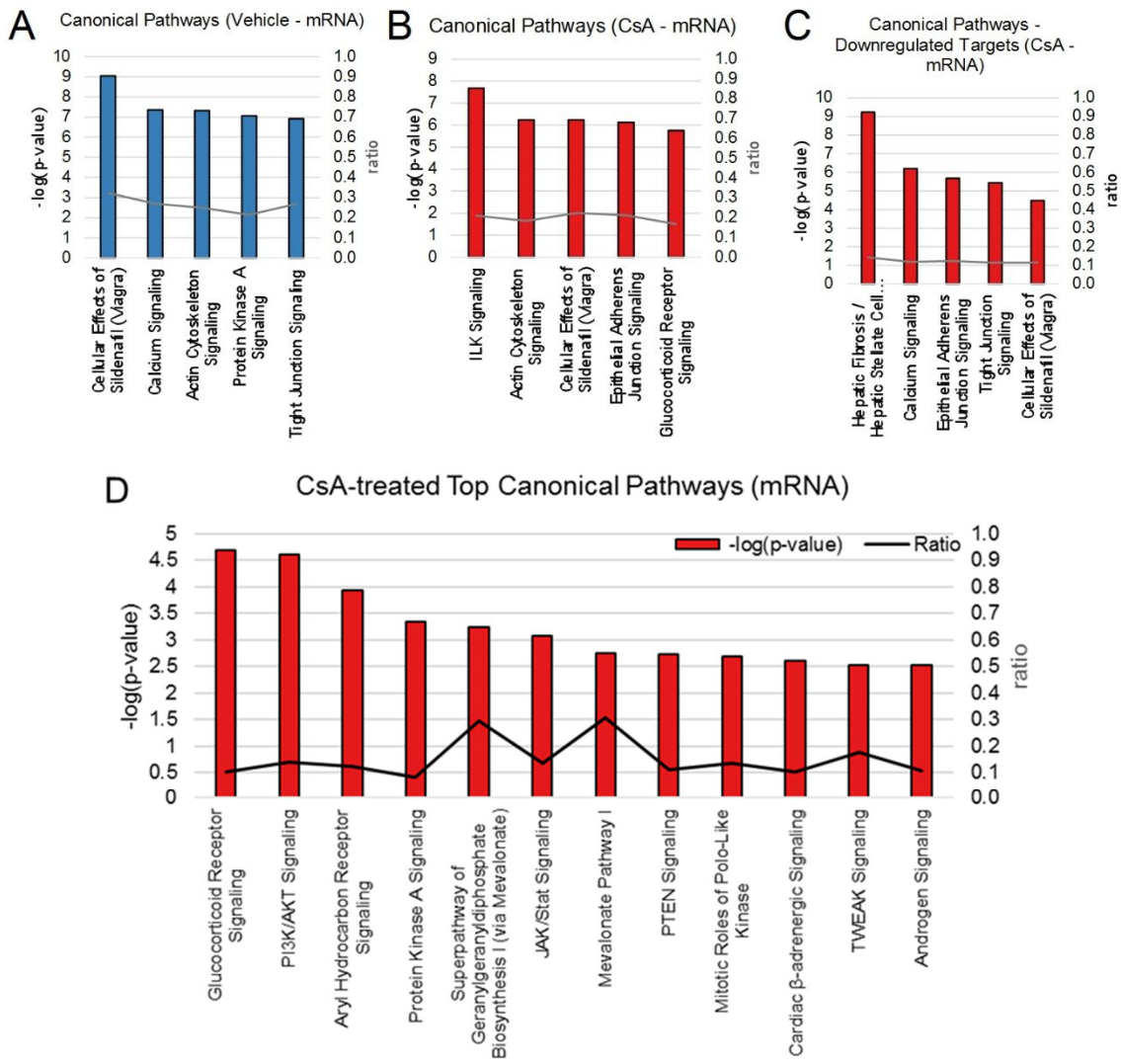


Figure 4-14. Canonical pathways regulated by miRNAs in CsA-treated HK-2 cells. Bar graphs indicate the top five canonical pathways enriched in the mRNA targets of miRNAs as identified by AGO2-PAR-CLIP in (A) vehicle and (B) CsA-treated HK-2 cells as determined by Ingenuity Pathway Analysis (IPA). Bars represent the negative log of p-value and lines represent the total fraction of the canonical gene set matched. (C) Bar graph indicates the top five canonical pathways enriched in CsA-treated AGO2-PAR-CLIP mRNA targets that were also down-regulated in RNA-seq after CsA treatment. (D) Top canonical pathways enriched for genes specifically regulated by miRNAs in CsA-treated HK-2 cells. IPA analysis of the genes containing specific CsA-induced AGO2-PAR-CLIP sequence clusters in the 3'UTR identified the top enriched canonical pathways. Bars represent the -log(p-value) of enrichment compared to a reference gene set. The line indicates the proportion, ratio, of total genes making up the canonical pathway gene set which were identified specifically in the CsA-treated PAR-CLIP mRNA dataset.

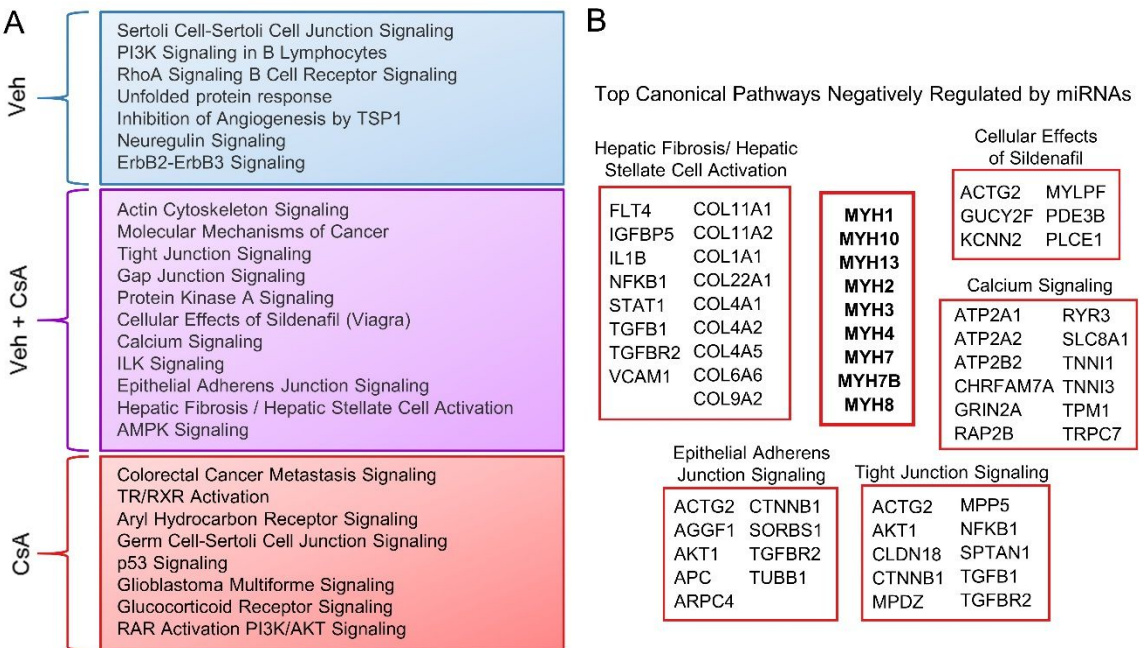


Figure 4-15. Canonical pathways regulated by miRNAs in CsA-treated versus vehicle-treated HK-2 cells. (A) We compared the top 20 canonical pathways enriched in mRNA targets in vehicle (blue box) and CsA-treated (red box) HK-2 cells by Ingenuity Pathway Analysis. 11 pathways were enriched in both treatments (purple box). (B) The target genes identified in each of the top pathways from Figure 4-8C which were down-regulated in RNA-seq. All five pathways include the set of nine myosin transcripts, middle.

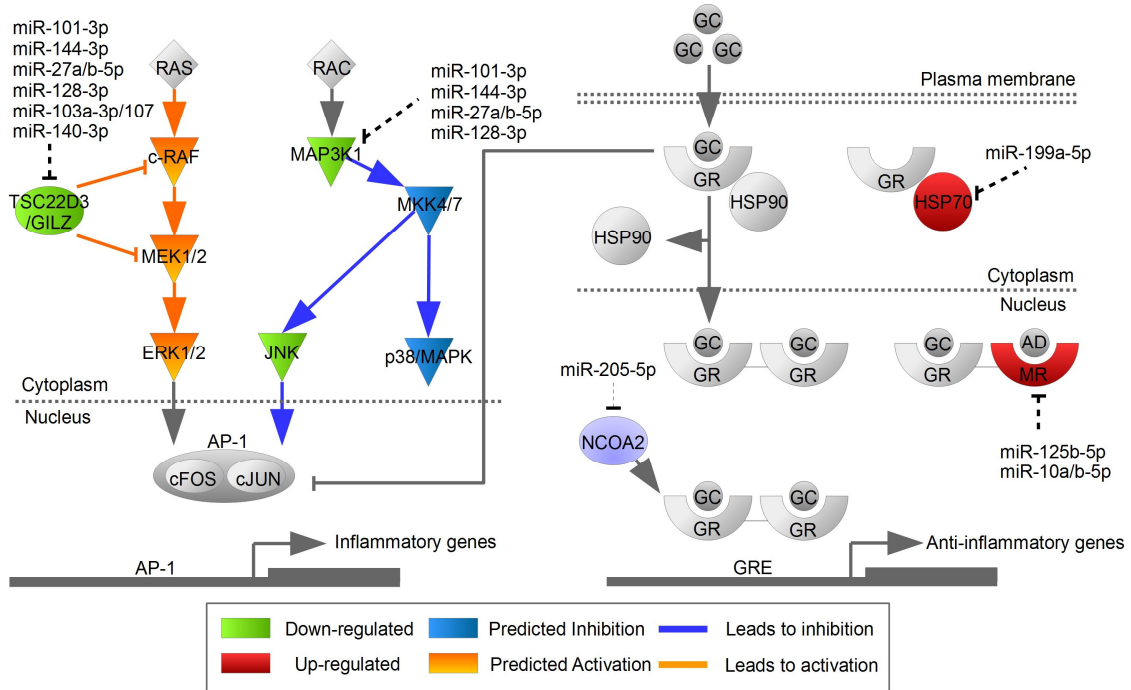


Figure 4-16. Glucocorticoid receptor signaling pathway genes specifically regulated by miRNAs in CsA-treated HK-2 cells. Diagram of the glucocorticoid receptor signaling pathway which crosstalks with MAPK-ERK, MAPK-JNK, and MAPK-p38 signaling. The pathway is integrated with RNA-seq differential expression data from CsA-treated HK-2 cells and predictive downstream analysis conducted with Ingenuity Pathway Analysis. Left, putative RISC target sites were identified by AGO2-PAR-CLIP in the 3'UTRs of *TSC22D3/GILZ* and *MAP3K1*, which inhibit MAPK-ERK and activate MAPK-JNK and MAPK-p38 signaling, respectively. The putative miRNA regulators shown share seed sequence homology. Genes that are shaded green (*TSC22D3/GILZ*, *MAP3K1/MEKK1*, *JNK3*) were down-regulated in CsA-treated HK-2 cells in the RNA-seq experiment. Genes that are shaded orange (c-RAF, MEK1/2, ERK1/2) are predicted to be activated as a result of *TSC22D3/GILZ* down-regulation. Genes that are shaded in blue (MKK4/7, p38/MAPK) are predicted to be inhibited as a result of *MAP3K1* down-regulation. Right, putative RISC target sites were identified by AGO2-PAR-CLIP in the 3'UTRs of *HSPA5/HSP70* and *NR3C2/MR* that can both reduce signaling by the glucocorticoid-GCR dimer complex, as well as the transcriptional activator *NCOA2*. Genes that are shaded red (*HSPA5/HSP70* and *NR3C2/MR*) were up-regulated in CsA-treated HK-2 cells in the RNA-seq experiment. Expression of *NCOA2* was unchanged.

4.7. miR-101-3p targets MAP3K1 expression in vitro

Previous experiments have demonstrated that CsA and tacrolimus inhibit p38 and JNK activation in Jurkat T cells in a calcineurin-independent manner (Matsuda et al. 2000). Further, the authors demonstrated that inhibition of these MAPKs is dependent on *MAP3K1*, as the inhibitory effect of CsA and tacrolimus was abrogated by expression of a constitutively active *MAP3K1*. Based on the identification of a RISC binding site in the 3'UTR of *MAP3K1* exclusively in CsA-treated HK-2 cells, we hypothesized that miRNA targeting of *MAP3K1* contributes to CsA-dependent down-regulation of *MAP3K1* and thus inhibition of p38 and JNK signaling. The cluster sequence identified by AGO2-PAR-CLIP in the 3'UTR of *MAP3K1* contains seed complementarity to several miRNAs which were also identified in CsA AGO2-PAR-CLIP samples. Hsa-miR-144-3p matched the cluster with 7mer canonical seed complementarity, whereas hsa-miR-101-3p and hsa-miR-27a-3p matched the cluster with canonical 6mer and offset-6mer seed complementarity, respectively (**Figure 4-17A**). Seed complementarity was also found for hsa-miR-128-3p, hsa-miR-199b-3p, and hsa-miR-223-3p (not shown). As previously mentioned, hsa-miR-101-3p and hsa-miR-27a-3p were up-regulated in CsA treated HK-2 cells. Further, in our analysis of the RISC-bound miRNAs, hsa-miR-101-3p exhibited 7.64-fold increased binding to AGO2 after CsA treatment (**Table 4-3**). In CsA-treated HK-2 cells we detected decreased expression of *MAP3K1* after 48 hours by RNA-seq (-1.12 log₂ fold change, adjusted P-value = 1.76 × 10⁻⁴⁶, **Figure 4-17B**). We confirmed the CsA-induced down-regulation of *MAP3K1* mRNA by qPCR (**Figure 4-17C**).

Based on the above evidence that miR-101-3p may target the 3'UTR of *MAP3K1*, we sought to determine whether miR-101-3p could regulate *MAP3K1* expression *in vitro*.

We utilized the lentiviral backbone expression vector (pLL3.7) to express the pre-miR-101 stem-loop hairpin. Transfection of HK-2 cells with this vector or an empty vector control was monitored by GFP expression. Transfection of HK-2 cells routinely achieved rates between 20-30% transfected cells (data not shown). Compared to empty vector control, expression of the pre-miR-101 hairpin in HK-2 cells reduced expression of MAP3K1 protein as determined by western blot (**Figure 4-17D and E**). In HK-2 cells, we detected two MAP3K1 bands at apparent molecular weight ~140 kDa and ~55kDa. Full length MAP3K1 has been found to regulate cell migration and pro-survival signaling whereas the caspase-3-generated cleavage product promotes apoptosis (Pham et al. 2013). Both MAP3K1 fragments were decreased in cells transfected with the pre-miR-101 expression vector. In order to determine whether *MAP3K1* down-regulation in HK-2 cells was related to calcineurin inhibitor nephrotoxicity *in vivo* we examined expression of transcripts in whole kidney samples of mice administered CsA (30 mg/kg/day) or olive oil control. In this model, treatment of mice with CsA induces arteriopathy, tubular injury, increased serum creatinine, and increased expression of α -SMA and FSP-1, which are markers of EMT and indicators of fibrosis (Yuan et al. 2015). Compared to control mice, CsA-treated mice exhibited decreased levels of *MAP3K1* mRNA after two and three weeks of daily injections (**Figure 4-17F**).

To determine whether miR-101-3p mediated down-regulation of *MAP3K1* could affect downstream transcriptional targets of p38-MAPK and JNK, we analyzed the mRNA expression of select transcripts after transfection of HK-2 cells with the miR-101 pre-miRNA expression vector or control vector in the presence or absence of CsA. *PAX6*, *STAT1*, *SLC2A2* (GLUT2), *CXCL2*, *CXCL14*, and *GBPI* genes were identified by

Ingenuity databases to be regulated downstream of p38 or JNK. Neither miR-101-3p expression nor CsA treatment affected expression of *PAX6* or *CXCL2* (**Figure 4-18A and B**). Although CsA treatment greatly down-regulated expression of *STAT1*, *CXCL14*, *SLC2A2* (GLUT2), and *GBP1*, miR-101-3p overexpression had no effect on CsA-treated or vehicle-treated cells (**Figure 4-18B-E**). Therefore, we do not see evidence of miR-101-3p-mediated effects on these downstream targets of p38-MAPK and JNK signaling.

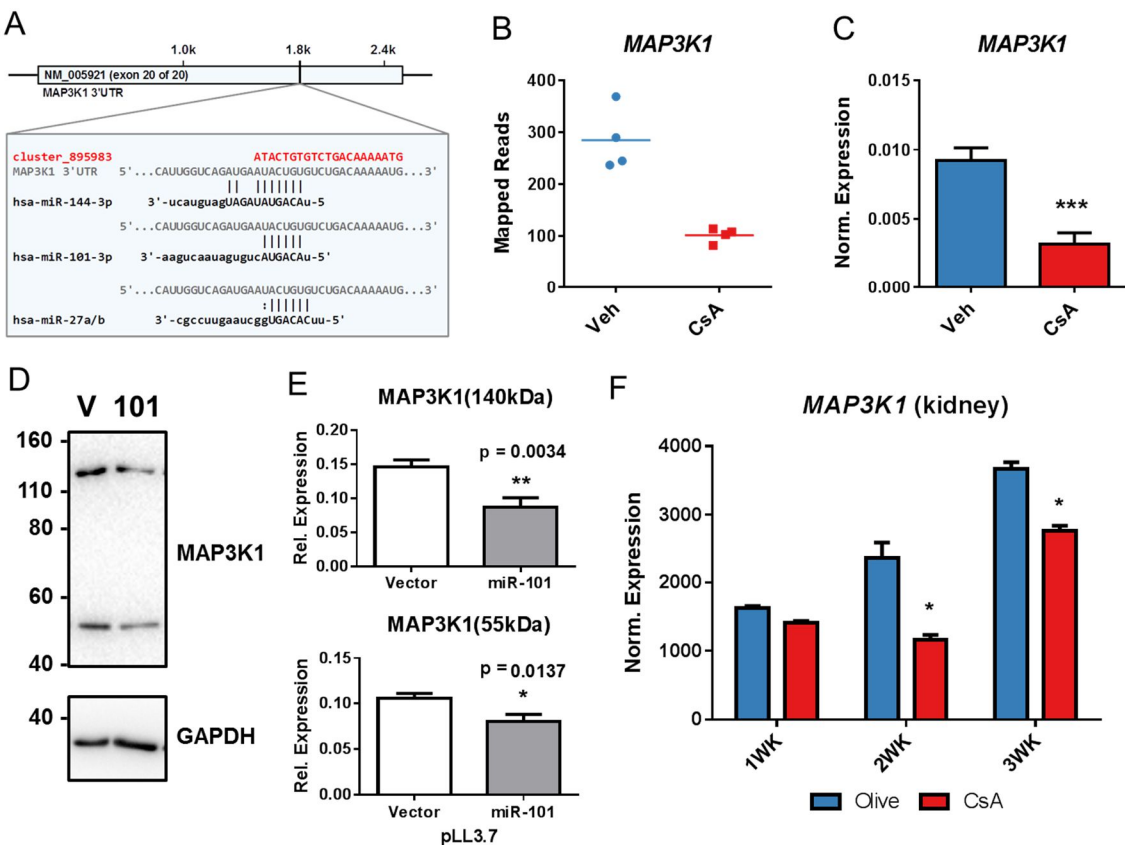


Figure 4-17. miR-101-3p targets MAP3K1 expression in HK-2 cells. (A) AGO2-PAR-CLIP identified CsA-induced putative RISC binding in the 3'UTR of MAP3K1. Within the identified sequence cluster, 7mer and 6mer seed complementarity for miRNAs also immunoprecipitated by AGO2-PAR-CLIP are shown. (B) Raw mapped read counts in vehicle (Veh) and CsA-treated HK-2 cells mapping to the MAP3K1 gene from the RNA-seq experiment. (C) qPCR of MAP3K1 transcripts in HK-2 cells treated with CsA for 48 hours. *** p < 0.001 by unpaired t-test, n = 3 (D) Immunoblot for MAP3K1 protein expression in HK-2 cells transfected with pLL3.7 lentiviral backbone expressing hsa-miR-101 or empty vector control, compared to GAPDH loading control. Representative of six replicate experiments. MAP3K1 immunoblot detects two bands at ~140kDa and ~55 kDa. (E) Quantification of MAP3K1 immunoblots normalized to GAPDH; ** p < 0.01, * p < 0.05 by one-tailed unpaired t-test. (F) qPCR of MAP3K1 mRNA in whole kidney tissue from mice injected daily with CsA (30 mg/kg/day) or olive oil after 1, 2, and 3 weeks. Four mice were examined in each group at each time point. * p < 0.01 by unpaired t-test.

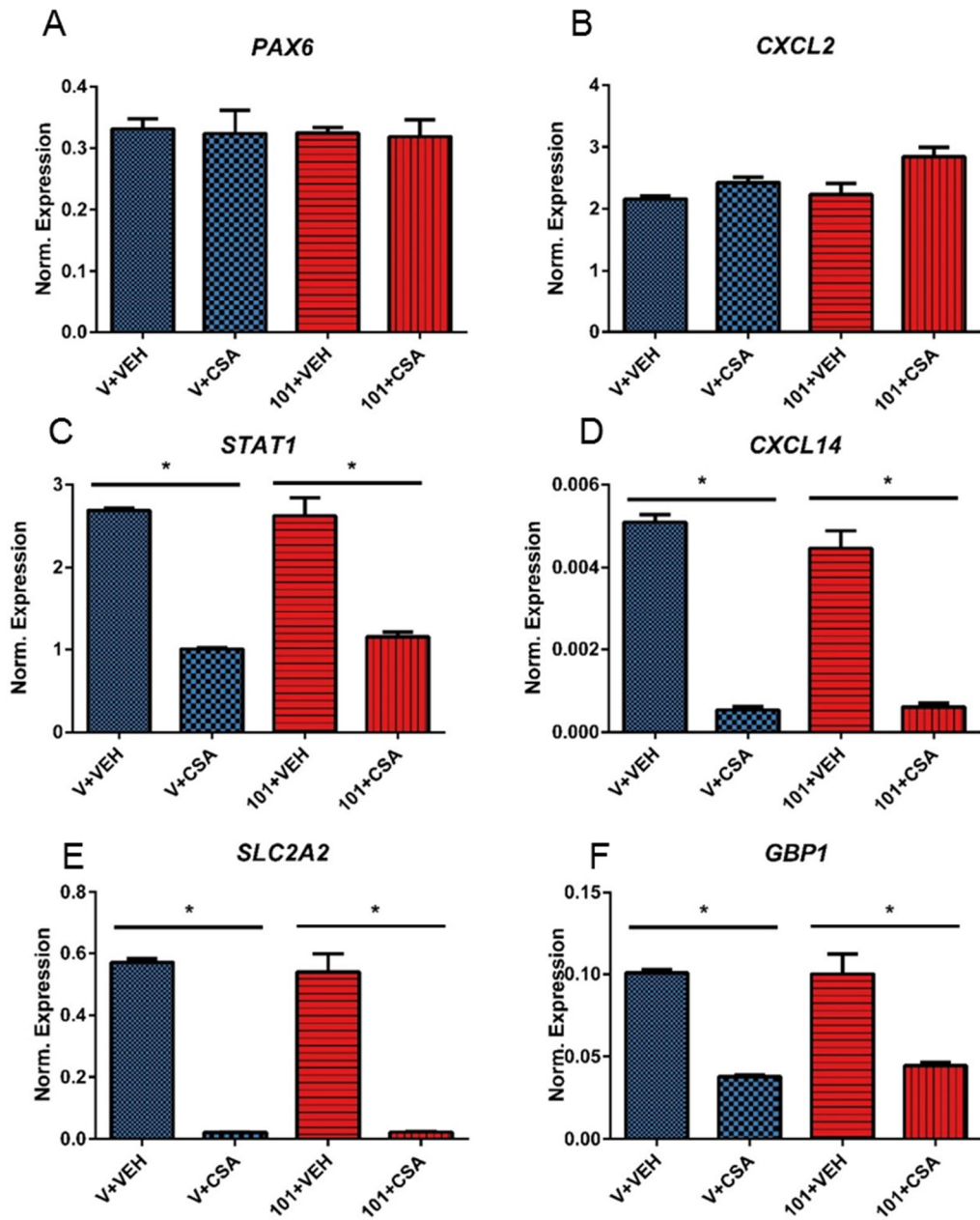


Figure 4-18. miR-101-3p overexpression is not sufficient to affect downstream p38/JNK MAPK transcriptional targets. Selected targets of downstream p38 and JNK MAPK signaling were evaluated by qPCR after transfection with pLL3.7-miR-101 or control vector and treatment with CsA [5 ug/mL] or vehicle control for 48 h. *PAX6* and *CXCL2* were unaffected by CsA treatment or miR-101-3p overexpression. *STAT1*, *CXCL14*, *SLC2A2* (GLUT2), and *GBP1* were all significantly down-regulated by CsA treatment in both miR-101-3p overexpression and control samples. miR-101-3p expression alone or in combination with CsA treatment had no effect on expression of the target genes. * p < 0.05 by unpaired t-test.

4.8 Conclusions

In this section, we describe two AGO-PAR-CLIP experiments designed to analyze the miRNA-mRNA targetome in HK-2 proximal tubule epithelial cells under normal conditions and in a model of CIN. Using this approach, we identified 8,059 AGO1-4 crosslinking target sites, 56,985 AGO2 vehicle-treated target sites and 36,812 AGO2 CsA treated-target sites. Mapping and annotation of the target sites to genomic features revealed that binding sites were enriched to mature transcript features (5'UTR, exon, and 3'UTR) compared to intronic and intergenic regions. Compared to previous studies and conventional targeting models, we observed an abundance of ‘non-canonical’ binding locations in the 5'UTR and exons of genes. This was especially evident in the AGO2 data, in which both exon and 5'UTR binding sites were more enriched than 3'UTR sites. We further observed enrichment for binding sites in the promoter region of genes (defined as the region -1 kb and +100 bp from the transcription start site).

Using luciferase reporter constructs and seed-sequence mutational analysis we were able to confirm the functional targeting of these relatively small regions (~20 bp) in cell based assays. Using these methods we identified a new functional miR-21-5p target site in the 3'UTR of *DDAH1* and a new dually regulated miR-27a/miR-33 targeting site in the 3'UTR of *ECT2*. From the RNA-seq and miRNA-seq data we observed that miR-27a is up-regulated and *ECT2* is down-regulated. Further functional analysis of this relationship to elucidate the roles of both miR-27a and *ECT2* in CsA-induced EMT is warranted. A role for *ECT2* in tight junction function and maintenance of cell polarity has been identified in focal segmental glomerulosclerosis (Izu et al. 2012).

To define the CsA-induced miRNA-mRNA targetome in proximal tubule cells we performed AGO2-PAR-CLIP on HK-2 cells. Our analysis identified the differential binding of both miRNAs and mRNAs to the RISC complex, thus enriching for the most physiologically relevant RNA regulators and targets in this model of CIN. Based on these findings we were able to pair miRNAs present in the RISC complex with mRNA targets to generate high confidence putative target relationships, which we previously demonstrated are reliable and functional. Our results indicate that not only is expression of miRNAs and mRNAs largely regulated by CsA-treatment (Chapter 3), but also the functional pairing of these RNA species is dramatically altered. The two processes are likely dependent upon one another as increased or decreased miRNA expression drives regulation of mRNA abundances and the availability of both miRNAs and mRNAs as substrates governs their incorporation into the RISC complex.

By comparing the pathways enriched by target genes in CsA and vehicle-treated samples, we determined that CsA-induced miRNA targeting regulates Integrin Linked Kinase Signaling, Actin Cytoskeleton Signaling, Cellular Effects of Sildenafil (Viagra), Epithelial Adherens Junction Signaling, and Glucocorticoid Receptor Signaling. Further, several critical pathways were found to be regulated by the RISC complex in both conditions: cell-cell adhesion, integrin-cytoskeleton signaling, and calcium signaling. Evidence of putative miRNA targeting of the glucocorticoid receptor signaling pathway led us to hypothesize that miRNAs may play an integral role in regulating MAPK signaling in proximal tubule cells. We demonstrated that overexpression of miR-101-3p repressed expression of *MAP3K1*, an upstream regulator of MAPK signaling. However, we were unable to determine the downstream effects of this targeting.

Chapter 5: Discussion

In this study, we describe a comprehensive and integrative miRNA-mRNA interaction map of calcineurin inhibitor nephrotoxicity in human kidney proximal tubule cells. To our knowledge, a robust transcriptome-wide study of gene and miRNA expression in calcineurin inhibitor nephrotoxicity has not been conducted. Previous studies of gene expression in this field have relied on microarray technology and imprecise targeting algorithms to define the role of miRNAs in the functional changes that are observed in proximal tubule cells treated with CsA. We previously identified a role for miRNAs regulating renal injury resulting from CsA treatment (Yuan et al. 2015). In a similar manner, it was demonstrated that induction of miR-21 could also repress PTEN in the PT-2 human proximal tubule cell line, leading to activation of AKT signaling and expression of EMT markers (Chen et al. 2015). However, these studies relied on methods with associated limitations have been discussed in-depth previously (Git et al. 2010; Pritchard et al. 2012). Our primary goals were to define the physiologically relevant miRNA targeting interactions that may contribute to the molecular pathology of calcineurin inhibitor nephrotoxicity and more completely define the effect of CsA on proximal tubule gene expression. We therefore sought to define the transcriptome-wide miRNA targetome in proximal tubule cells to understand how miRNAs regulate renal injury resulting from CsA treatment. To accomplish this, we used PAR-CLIP, a technique that achieves high resolution mapping of RBPs, and active miRNA-mRNA targeting interactions by defining RNAs intimately associated with RISC complex protein AGO2.

Our analysis of miRNA and mRNA gene expression in CsA-treated HK-2 cells provides an updated and more in-depth profiling of RNA expression in this model of CIN. Slattery et al. originally probed 7,070 genes by microarray to assess differential regulation in HK-2 cells by CsA treatment (Slattery et al. 2005). 128 genes were identified as significantly up or down-regulated. Analysis of these genes and subsequent cellular and functional assays led the authors to conclude that CsA-induced EMT of PTECs was a key event in the progression of CIN leading ultimately to fibrosis. Further, from their analysis they identified *TGFB1* (one of the up-regulated genes) as a key mediator of this pathophysiology. Their analysis did not include analysis of non-coding RNAs or miRNAs.

In our study, we used the same cell line, drug concentration and length of treatment. By using mRNA-seq to determine digital gene expression in treated vs control cells we were able to achieve complete transcriptome coverage. Also, this method allowed us to use ample replicates to assign significance to differential expression calculations. We therefore were able to identify a much larger number of differentially expressed genes with a high level of confidence. We used GSEA to systematically identify the most enriched pathways and biological processes in treatment and control cells. Our results did indeed support the standing model that CsA induces EMT which contributes to CIN pathology. Further, we identified several signaling pathways which are associated with EMT that were activated (Erbb/RTK, KRAS, TGF- β , ERK, WNT, PI3K/AKT, NOTCH1). GSEA also confirmed at the transcriptional level some of the key events in CsA-induced EMT which have been demonstrated at the cellular level: down-regulation and disruption of cell-cell junction organization, ECM organization, and loss

of apical-basal polarity. By focusing on families of genes we observed widespread down-regulation of important tight junction and adherens junction genes, the claudins and cadherins. In addition to the gene sets which maintain the structural integrity of the epithelium we also observed direct dysregulation of the enzymes which impart some of the PTECs' specialized functions. Namely, a vast number of solute carrier family genes were dysregulated (the majority were down-regulated). Thus, by transcriptional re-programming, both structural and functional elements of the proximal tubule epithelium are compromised by CsA.

In our mRNA-seq analysis we also identified discrepancies with the conventional model of CsA-induced EMT in PTECs. Namely, although we identified evidence of TGF- β signaling in GSEA we did not observe induction of the *TGFB1* gene itself nor the *TGFB1* inducible gene. Further, two conventional markers of EMT and fibrosis progression, *ACTA2* and *S100A4*, were down-regulated rather than up-regulated. In accordance with previous data, we observed up-regulation of *VIM*, *SNAII*, and *SNAI2*. These discrepancies bear further validation by methods such as immunoblotting, ELISA, and intracellular staining. The role and expression of TGF- β has been controversial in studies examining CsA action on immune cells as well. At this point, we can only speculate why we observed contrary results. One possibility is that factors related to the culture of HK-2 cells are confounding results obtained by different labs. Although guidelines for the culture of keratinocytes are prescribed by ATCC, there is great variability in adherence to protocols within the literature. For instance, DMEM rather than specified keratinocyte medium is often used. Typical DMEM formulations contain far higher concentrations of glucose than base keratinocyte media. The effects of high

glucose on TGF- β and PKC signaling have previously been reported (Ha, Yu, and Lee 2001). Often FBS is used when serum-free preparations are recommended, which may confound signaling responses. Passage number and confluence of cells may also contribute to the differences in reported results. Thus, it will be essential to perform controlled experiments to determine the individual effects of each media component in CsA treatment of proximal tubule epithelial cells.

Our mRNA-seq analysis uncovered several interesting connections to other diseases and tissue-specific cellular processes. It is important to note that systemic treatment with CsA in patients does not only impart direct toxicity to the kidneys, but also may result in hypertension, neurotoxicity, metabolic abnormalities, gastrointestinal side effects, infections, and risk of malignancies (Hardinger and Magee 2017). These comorbidities may be directly related to nephrotoxicity, as, for instance, hypertension may be caused by CsA-induced renal vasoconstriction and increased sodium transport (Esteva-Font et al. 2007; Takeda et al. 1995). However, the pathophysiology of the majority of CsA-induced comorbidities is poorly understood.

Our GSEA analysis of the gene expression re-programming that takes place in HK-2 cells revealed a number of pathways and genes which were altered that have documented roles in neuron development and function as well as several types of cancer and metastases. For instance, we identified by GSEA that CsA down-regulated a number of genes which are expressed on the apical membrane surface of PTECs. This was also the gene set with the largest absolute enrichment score in our analysis of the MiSigDB Hallmark gene sets. A particularly interesting finding within this gene set was that CsA reduced expression of the gene encoding amyloid beta precursor protein, *APP*, by over

50%. Although this protein is expressed in many tissues its functions are best understood in the synapses of neurons where it has been implicated in regulating synapse function, neural plasticity, and iron export (Priller et al. 2006; Turner et al. 2003; Duce et al. 2010). As indicated by the name of this gene, the encoded protein is infamously cleaved to produce beta amyloid ($A\beta$), the major component of amyloid plaques associated with Alzheimer's disease. Although CsA transport may be restricted by the blood-brain barrier, studies have already demonstrated positive effects of CNIs on dementia in organ transplant recipients (Taglialatela, Rastellini, and Cicalese 2015). Further, studies are ongoing to evaluate the neuroprotective capacity of CsA in treatment of traumatic brain injury (Dixon et al. 2016). Apical surface genes *MAL* and *NTNG1* also have critical roles in cells of the nervous system and in axonal growth. Further experiments are necessary to determine the role of these apical genes in either the neurotoxic side effects observed in CsA-treated patients or the potential therapeutic effects in Alzheimer's disease and traumatic brain injury.

Our gene expression analysis and GSEA also revealed unmistakable connections to cancer and metastasis, especially breast cancer. First, as the gene expression profiling corroborates the working model that CsA induces EMT progression of target PTECs, long-term CsA treatment may promote cancer invasiveness and metastasis of renal and non-renal tissues insofar as EMT is a key mediator of these pathological events. Further work needs to be done to determine whether CsA induces EMT in other tissues and identify what role CsA may have in cancer tumorigenesis and metastasis. Currently, the link between transplant-related immunosuppression and malignancy is well-established (Durnian et al. 2007). Notably, skin cancers (mostly squamous cell carcinomas) and

lymphoproliferative disease are common malignancies associated with immunosuppressive regiments including CNIs. In mice, CsA induces renal cancer cells to acquire an invasive phenotype and promotes tumour growth *in vivo* (Hojo et al. 1999). Initially, cancer progression and invasiveness induced by CsA was attributed to TGF- β synthesis (Hojo et al. 1999). Subsequent studies have also implicated CsA-induced *VEGF* expression as tumorigenic due to angiogenesis (Durnian et al. 2007). Our data in PTECs supports the induction of *VEGFA* and *VEGFB* genes but not *TGFB1*. Lastly, DNA repair mechanisms have been reported to be inhibited experimentally by CsA in keratinocytes which may contribute to tumorigenesis (Durnian et al. 2007; Herman et al. 2001). Our GSEA analysis of CsA-treated PTECs confirmed down-regulation of major DNA repair gene sets and pathways.

The gene expression changes we observed in PTECs due to CsA-treatment may have consequences for breast cancer in particular. In breast cancer, EMT, albeit debated for years, is understood to play roles in progression, invasion, and metastasis (Tomaskovic-Crook, Thompson, and Thiery 2009). Further, mutations which affect the expression of DNA repair genes *BRCA1* and *BRCA2* are associated with increased breast cancer risk (Fackenthal and Olopade 2007; Wilson et al. 1999; Miki et al. 1994; Wooster et al. 1995). Low claudin expression in breast cancer has been shown to define a subtype and may affect prognosis (Kwon 2013; Dias et al. 2017). Together, our data demonstrate that CsA is capable of altering gene expression programs in human cells that may contribute to processes related to tumorigenesis and metastasis such as EMT, DNA repair, cell junction, and apical polarity. Further work must be done to determine the

consequences of this expression re-programming in renal and non-renal cells in the context of cancer.

Non-coding RNAs have emerged as major sources of both transcriptional and post-transcriptional regulation in virtually every critical cell process. Understanding the roles of non-coding RNAs in normal biology and disease states is as crucial to our broader understanding of eukaryotic gene expression. Perhaps one of the most challenging aspects to this endeavor is identifying the networks of RNAs which regulate one another physiologically. For instance, our understanding of miRNA biology was formed and shaped by the early findings that seed complementarity to the 3'UTR could repress target gene expression. Only until recently, with the development of more sophisticated methods of analyzing miRNA-mRNA interactions globally, has the field adopted more “non-canonical” mechanisms by which miRNAs (and the miRISC complex) regulate target genes. Thus, in order to more fully define the miRNA-mRNA targetome in the model of CIN previously described and expand upon the understanding of global miRNA regulation, we employed PAR-CLIP on control and CsA-treated PTECs.

Using PAR-CLIP, we found that a unique set of miRNAs was enriched in the RISC complex of HK-2 cells. This RISC-enriched profile was altered after treatment with CsA, suggesting that differential targeting is a fundamental mechanism for regulating the CsA-induced gene program in these cells. Surprisingly, overall changes in total miRNA abundance after CsA treatment defined by RNA-seq of total cellular RNA did not correlate with increased or decreased miRNA RISC binding. This suggests that miRNAs in the RISC complex represent a subset of total cellular miRNAs and that only a fraction

of expressed miRNAs actively target mRNAs. This phenomenon has been observed previously in an AGO-PAR-CLIP study of TP53-dependent miRNA-AGO2 association where most miRNAs differentially associated to AGO2 did not correspond to altered abundance in total RNA samples (Krell et al. 2016). Comparing RNA-seq and PAR-CLIP data revealed that while 868 mRNA clusters in CsA treated samples and 1503 in vehicle controls identified by PAR-CLIP were also observed by RNA-seq, PAR-CLIP identified 68 and 286 mRNA clusters that were uniquely present in CsA or vehicle samples. Together, these data suggest that changes in total cellular miRNA abundance alone cannot predict functional targeting of mRNAs.

While control and CsA-treated cells exhibited expression of unique sets of miRNAs that were enriched in the targeting complex we did observe a relatively small degree of overlap. 21.29 (23/108) and 31.08% (23/74) of the mRNAs predicted to be targeted by the top ten miRNAs in vehicle and CsA treated samples respectively were present in both samples. This suggests that although we could identify miRNAs in our PAR-CLIP data present in CsA-treated samples and vehicle controls, it appears that under each condition each miRNA targets different genes. It is possible that this overlap may be related to the amount of time cells were exposed to CsA and that with a longer exposure this overlap will shrink. Nevertheless, it seems apparent that functional consequences of targeting are the result of a balance between differential expression of both miRNAs and mRNAs.

Analysis of the AGO-bound miRNA sequences by miRdeep2 indicated that three miRs (hsa-miR-1246, hsa-miR-1290, and hsa-miR-7641) were the most enriched in the RISC-complex and therefore the most active in targeting. While experiments have

demonstrated various roles for hsa-miR-1246 and hsa-miR-1290 in cancer cells, close analysis of our PAR-CLIP reads suggests that these miRNAs have been incorrectly assigned based on the miRDeep2 analysis parameters. Hsa-miR-1246 and hsa-miR-1290 share perfect or near-perfect sequence homology with a processed fragment of the RNU2 gene. In the PAR-CLIP reads assigned to hsa-miR-1290, 99.9% (26,158/26,185) contained an alignment mismatch. The majority of these reads align perfectly to the RNU2 gene. Further, no sequence reads aligning to hsa-miR-1290 were detected by miRNA-seq. Because mature hsa-miR-1246 shares perfect homology with the RNU2 gene we cannot exclude the possibility that it is in fact present in the cells and in the RISC complex at some level. However, most reads assigned to hsa-miR-1246 also contain a mismatch that aligns perfectly to the RNU2 gene. Hsa-miR-7641 shares perfect homology with 5S ribosomal RNAs and it has been suggested that this miRNA is in fact derived from rRNA repeats. One study has provided evidence for miR-7641 targeting of the cytokine CXCL1 in HUVEC cells (Yoo et al. 2013). However, in our study, there was no supporting evidence of the mature hsa-miR-7641 in miRNA-seq despite the apparent enrichment in the RISC complex.

To identify the genome-wide target sites of the miRNAs we identified in the RISC complex we performed PIPE-CLIP analysis on AGO-PAR-CLIP libraries, which identifies enriched clusters using sequence read counts and locates reliable binding sites using cross-linking-induced mutations. Statistically significant target sites were identified across all annotated genomic regions. After normalization to relative region size, we found that sites were enriched in the mature transcript regions of genes (5'UTR, exons, and 3'UTR). Within the gene body, we observed that the enrichment for sites in the

5'UTR and exon regions were both almost 2-fold greater than the canonical 3'UTR region. We also found enrichment in promoters regions (-1Kb to +100bp) and to a lesser degree transcription termination sites (-100bp to 1Kb). This is somewhat surprising since canonical miRNA-mRNA targeting is thought to largely occur in the 3'UTR. Analysis of other PAR-CLIP studies has revealed that genomic location distributions vary widely by study and method of analysis used to determine clusters (Bottini et al. 2017). In the original PAR-CLIP study, Hafner et al. observed crosslink-centered regions predominantly in the 3'UTR and coding sequence (CDS) regions (Hafner et al. 2010). Although the authors acknowledged that widespread miRNA binding to the CDS had been previously reported and that miRNA-binding to individual 5'UTRs and CDS sites were experimentally functional, they re-iterated the standing belief that miRNAs predominantly regulate target mRNAs by acting on the 3'UTR (Bartel 2009; Easow, Teleman, and Cohen 2007; Lewis, Burge, and Bartel 2005; Forman, Legesse-Miller, and Coller 2008; Lytle, Yario, and Steitz 2007; Tay et al. 2008). Using their PAR-CLIP data as a reference, Hafner et al experimentally tested this by inhibiting the 25 most abundant miRNAs in HEK293 cells and examining mRNA stability by microarray. They concluded that destabilization was dependent on length of seed-complementary region (imperfect pairs did not destabilize), multiple binding sites within a crosslink region were more destabilizing, and CDS-localized sites only marginally reduced mRNA stability compared to 3'UTR sites (Hafner et al. 2010). Although there were differences in mRNA destabilization effects, the authors conceded that CDS sites were associated with an increased incidence of rare codon usage, which could in principle reduce translational rate (Hafner et al. 2010). As previously mentioned, the PAR-CLIP studies that followed

demonstrated varying degrees of enrichment in the three transcript regions. An alternate method of CLIP which also ligates mRNAs to miRNAs in the RISC complex, CLASH, identified widespread ‘non-canonical’ sites which did not require canonical seed pairing and were often located in the 5’UTR and CDS. Even compared to these studies our enrichment for 5’UTR is quite high. In the subsequent analyses of functional sites we included all mRNA-located sites as well as focused on 3’UTR sites, since the tools to validate them are well established.

Future work must be done to more completely evaluate the functionality of these miRNA-mRNA sites *in vitro* and *in vivo*. For instance, inhibition and overexpression of miRNA oligos (i.e. miR-101-3p) followed by RNA-seq would define the global destabilizing effects of the miRNA. Similarly, stable isotope labeling with amino acids in cell culture (SILAC) or proteomic assays would evaluate the degree translational repression that occurs in these putative target genes. Further, the development of assays to validate individual functions of non-canonical sites within the CDS and 5’UTR must be developed to properly evaluate the extent of regulation which may occur by these mechanisms.

PIPE-CLIP annotation of PAR-CLIP clusters allowed us to identify AGO2 crosslinking regions within 3’UTRs with a high degree of confidence. We coupled this information with Ingenuity Pathway Analysis (IPA) to identify pathways in which genes in the RISC complex play a role. In vehicle-treated proximal tubule cells, the top canonical pathways enriched in the AGO2-PAR-CLIP target gene set were Cellular Effects of Sildenafil (Viagra), Calcium Signaling, Actin Cytoskeleton Signaling, Protein Kinase A Signaling, and Tight Junction Signaling. In CsA treated cells, the top pathways

enriched were Integrin Linked Kinase Signaling, Actin Cytoskeleton Signaling, Cellular Effects of Sildenafil (Viagra), Epithelial Adherens Junction Signaling, and Glucocorticoid Receptor Signaling. Interestingly, 11 of the top 20 canonical pathways were enriched in CsA treated samples and vehicle controls. While this may be related to the relatively short exposure to CsA in vitro, these data nevertheless suggest that miRNAs play a central role in controlling several complex signaling pathways in control samples. CsA appears to influence tubular epithelial cells by affecting additional pathways such as the Intergrin Linked Kinase Signaling pathway which has been known to play a major role in TGF β induced EMT (Lee et al. 2004). It also appears to affect Epithelial Adherens Junction Signaling which is critical for maintenance of E-cadherin junctions, which when disrupted drive EMT through effects on cytoskeleton reorganization, stress fiber formation, and cell adhesion (Böttinger and Bitzer 2002). Identification of these pathways that are central to EMT strongly suggests that our data reflect physiologically relevant regulation of processes occurring because of CIN that are regulated by the RISC complex.

CsA inhibits T cell activation by inhibiting calcineurin, thereby affecting NFAT localization to the nucleus that is required for IL-2 transcription. However, CsA has also been suggested to suppress activation of JNK and p38 upstream of mitogen activated protein kinase kinases (MAPKKs), MAP3K, independently of its effect of calcineurin (Matsuda et al. 2000). We noted that targeting of the 3'UTR of MAP3K1/MEKK1 was identified by PAR-CLIP in CsA-treated cells. Moreover, our RNA-seq data showed a corresponding decrease in expression. The cluster sequence we identified in the 3'UTR of MAP3K1 contained seed complementarity to several miRNAs identified in the RISC

complex. Among these miRNAs, hsa-miR-101-3p and hsa-miR-27a-3p were up-regulated in CsA treated HK-2 cells suggesting a possible targeting interaction. Indeed, expression of the pre-miR-101 hairpin in HK-2 cells resulted in reduced expression of MAP3K1 protein as determined by western blot, suggesting that miR-101 functionally targets MAP3K. We suggest that CsA suppresses JNK and p38 by inducing targeting of MAP3K1 by miR-101-3p. Future work must be done to validate the downstream effects of MAP3K1 repression by miR-101-3p. It must also be determined whether blockade of miR-101-3p prevents CsA-induced inhibition of JNK and p38 signaling. Further, other putative miRNAs must also be evaluated, as multiple miRNAs may regulate this gene target for maximal effect.

Our results define a microRNA-mRNA targetome for calcineurin inhibitor induced nephrotoxicity. By identifying active targeting interactions that occur because of CsA treatment, we define pathways that are likely to be affected and contribute to CIN. This analysis also provided novel insight to a poorly understood mechanism by which CsA affects calcineurin independent processes that could contribute to side effects by affecting cellular activation and or cell death. While the physiological role of the pathways, miRNAs and mRNAs we identified that are specifically associated with CsA treatment remain to be elucidated, these data serve as a resource for the community and could lead to the identification of new druggable targets that could reduce toxicity associated with CsA.

Chapter 6: Bibliography

- 't Hoen, Peter A C, Yavuz Ariyurek, Helene H. Thygesen, Erno Vreugdenhil, Rolf H A M Vossen, Renée X. de Menezes, Judith M. Boer, Gert-Jan B. van Ommen, and Johan T. den Dunnen. 2008. "Deep Sequencing-Based Expression Analysis Shows Major Advances in Robustness, Resolution and Inter-Lab Portability over Five Microarray Platforms." *Nucleic Acids Research* 36 (21): e141. doi:10.1093/nar/gkn705.
- Abba, Mohammed, Nitin Patil, Jörg Leupold, and Heike Allgayer. 2016. "MicroRNA Regulation of Epithelial to Mesenchymal Transition." *Journal of Clinical Medicine* 5 (1): 8. doi:10.3390/jcm5010008.
- Agarwal, Vikram, George W. Bell, Jin Wu Nam, and David P. Bartel. 2015. "Predicting Effective microRNA Target Sites in Mammalian mRNAs." *eLife* 4 (AUGUST2015): 1–38. doi:10.7554/eLife.05005.
- Aguado-Fraile, Elia, Edurne Ramos, Elisa Conde, Macarena Rodríguez, Fernando Liaño, and M Laura García-Bermejo. 2013. "MicroRNAs in the Kidney: Novel Biomarkers of Acute Kidney Injury." *Nefrología : Publicación Oficial de La Sociedad Española Nefrologia* 33 (6): 826–34. doi:10.3265/Nefrologia.pre2013.Aug.12198.
- Aherne, Sinead T, Paul Smyth, Michael Freeley, Leila Smith, Cathy Spillane, John O'Leary, and Orla Sheils. 2016. "Altered Expression of Mir-222 and Mir-25 Influences Diverse Gene Expression Changes in Transformed Normal and Anaplastic Thyroid Cells, and Impacts on MEK and TRAIL Protein Expression." *International Journal of Molecular Medicine* 38 (2). Greece: 433–45. doi:10.3892/ijmm.2016.2653.
- Anders, S., P. T. Pyl, and W. Huber. 2015. "HTSeq--a Python Framework to Work with High-Throughput Sequencing Data." *Bioinformatics* 31 (2): 166–69. doi:10.1093/bioinformatics/btu638.
- Aplin, A E, B P Hogan, J Tomeu, and R L Juliano. 2002. "Cell Adhesion Differentially Regulates the Nucleocytoplasmic Distribution of Active MAP Kinases." *J Cell Sci* 115 (Pt 13): 2781–90. <http://www.ncbi.nlm.nih.gov/pubmed/12077368>.
- Balen, Daniela, Marija Ljubojevic, Davorka Breljak, Hrvoje Brzica, Vilim Zlender, Hermann Koepsell, and Ivan Sabolic. 2008. "Revised Immunolocalization of the Na+-D-Glucose Cotransporter SGLT1 in Rat Organs with an Improved Antibody." *American Journal of Physiology. Cell Physiology* 295: C475–89. doi:10.1152/ajpcell.00180.2008.
- Barbarino, Julia M, Christine E Staatz, Raman Venkataraman, Teri E Klein, and Russ B Altman. 2013. "PharmGKB Summary: Cyclosporine and Tacrolimus Pathways." *Pharmacogenetics and Genomics* 23 (10): 563–85. doi:10.1097/FPC.0b013e328364db84.
- Barr, Meaghan L, Lucia B Jilaveanu, Robert L Camp, Adebawale J Adeniran, Harriet M Kluger, and Brian Shuch. 2015. "PAX-8 Expression in Renal Tumours and Distant Sites: A Useful Marker of Primary and Metastatic Renal Cell Carcinoma?" *Journal of Clinical Pathology* 68 (1). England: 12–17. doi:10.1136/jclinpath-2014-202259.
- Bartel, David P. 2009. "Review MicroRNAs : Target Recognition and Regulatory Functions," 215–33. doi:10.1016/j.cell.2009.01.002.
- Basile, David P., Melissa D. Anderson, and Timothy A. Sutton. 2012. "Pathophysiology

- of Acute Kidney Injury.” *Comprehensive Physiology* 2 (2): 1303–53. doi:10.1002/cphy.c110041.
- Bastani, Bahar. 2015. “The Worsening Transplant Organ Shortage in USA; Desperate Times Demand Innovative Solutions.” *Journal of Nephropathology* 4 (4): 105–9. doi:10.12860/jnp.2015.20.
- Bastos, A. P., and L. F. Onuchic. 2011. “Molecular and Cellular Pathogenesis of Autosomal Dominant Polycystic Kidney Disease.” *Brazilian Journal of Medical and Biological Research* 44 (7): 606–17. doi:10.1590/S0100-879X2011000700001.
- Bellomo, Rinaldo, John A. Kellum, and Claudio Ronco. 2012. “Acute Kidney Injury.” *The Lancet* 380 (9843): 756–66. doi:10.1016/S0140-6736(11)61454-2.
- Bellomo, Rinaldo, Claudio Ronco, John A Kellum, Ravindra L Mehta, and Paul Palevsky. 2004. “Acute Renal Failure - Definition, Outcome Measures, Animal Models, Fluid Therapy and Information Technology Needs: The Second International Consensus Conference of the Acute Dialysis Quality Initiative (ADQI) Group.” *Critical Care (London, England)* 8 (4): R204-12. doi:10.1186/cc2872.
- Bennett, Jason, Hilary Cassidy, Craig Slattery, Michael P Ryan, and Tara McMorrow. 2016. “Tacrolimus Modulates TGF- β Signaling to Induce Epithelial-Mesenchymal Transition in Human Renal Proximal Tubule Epithelial Cells” 5 (5): 1–25. doi:10.3390/jcm5050050.
- Bennett, William M. 2014. “Cyclosporine and Tacrolimus Nephrotoxicity.” In *UpToDate*, edited by TW Post. Waltham, MA: UpToDate.
- Bernstein, E, A A Caudy, S M Hammond, and G J Hannon. 2001. “Role for a Bidentate Ribonuclease in the Initiation Step of RNA Interference.” *Nature* 409 (6818): 363–66. doi:10.1038/35053110.
- Bertorello, A, and A Aperia. 1989. “Na⁺-K⁺-ATPase Is an Effector Protein for Protein Kinase C in Renal Proximal Tubule Cells.” *Am J Physiol* 256 (2 Pt 2): F370-3.
- Bobulescu, I. Alexandru, and Orson W. Moe. 2009. “Luminal Na⁺/H⁺ Exchange in the Proximal Tubule.” *Pflugers Archiv European Journal of Physiology* 458 (1): 5–21. doi:10.1007/s00424-008-0595-1.
- Bohle, A, J Jahnecke, D Meyer, and G E Schubert. 1976. “Morphology of Acute Renal Failure: Comparative Data from Biopsy and Autopsy.” *Kidney International. Supplement* 6 (October). United States: S9-16.
- Bohnsack, Markus T, Kevin Czaplinski, and Dirk Gorlich. 2004. “Exportin 5 Is a RanGTP-Dependent dsRNA-Binding Protein That Mediates Nuclear Export of Pre-miRNAs.” *RNA (New York, N.Y.)* 10 (2): 185–91. doi:10.1261/rna.5167604.
- Bolarin, D M, and E C Azinge. 2007. “Biochemical Markers, Extracellular Components in Liver Fibrosis and Cirrhosis.” *Nigerian Quarterly Journal of Hospital Medicine* 17 (1). Nigeria: 42–52.
- Borchert, Glen M, William Lanier, and Beverly L Davidson. 2006. “RNA Polymerase III Transcribes Human microRNAs.” *Nature Structural & Molecular Biology* 13 (12): 1097–1101. doi:10.1038/nsmb1167.
- Boron, Walter F, and Emile L T A - T T - Boulpaep. 2017. “Medical Physiology.” Philadelphia, PA : Elsevier,.
- Bottini, Silvia, Nedra Hamouda-Tekaya, Bogdan Tanasa, Laure-Emmanuelle Zaragozi, Valerie Grandjean, Emanuela Repetto, and Michele Trabucchi. 2017. “From

- Benchmarking HITS-CLIP Peak Detection Programs to a New Method for Identification of miRNA-Binding Sites from Ago2-CLIP Data." *Nucleic Acids Research*, gkx007. doi:10.1093/nar/gkx007.
- Boymen, Onur, and Jonathan Sprent. 2012. "The Role of Interleukin-2 during Homeostasis and Activation of the Immune System." *Nature Reviews Immunology* 12 (3): 180–90. doi:10.1038/nri3156.
- Bracht, Thilo, Vincent Schweinsberg, Martin Trippler, Michael Kohl, Maike Ahrens, Juliet Padden, Wael Naboulsi, et al. 2015. "Analysis of Disease-Associated Protein Expression Using Quantitative Proteomics-Fibulin-5 Is Expressed in Association with Hepatic Fibrosis." *Journal of Proteome Research* 14 (5). United States: 2278–86. doi:10.1021/acs.jproteome.5b00053.
- Braun, Joerg E., Eric Huntzinger, Maria Fauser, and Elisa Izaurralde. 2011. "GW182 Proteins Directly Recruit Cytoplasmic Deadenylase Complexes to miRNA Targets." *Molecular Cell* 44 (1): 120–33. doi:10.1016/j.molcel.2011.09.007.
- Buffart, T E, R M Overmeer, R D M Steenbergen, M Tijsen, N C T van Grieken, P J F Snijders, H I Grabsch, et al. 2008. "MAL Promoter Hypermethylation as a Novel Prognostic Marker in Gastric Cancer." *British Journal of Cancer* 99 (11): 1802–7. doi:10.1038/sj.bjc.6604777.
- Busby, Michele A., Chip Stewart, Chase A. Miller, Krzysztof R. Grzeda, and Gabor T. Marth. 2013. "Scotty: A Web Tool for Designing RNA-Seq Experiments to Measure Differential Gene Expression." *Bioinformatics* 29 (5): 656–57. doi:10.1093/bioinformatics/btt015.
- Calne, R.Y., K. Rolles, S. Thiru, P. McMaster, G.N. Craddock, S. Aziz, D.J.G. White, et al. 1979. "CYCLOSPORIN A INITIALLY AS THE ONLY IMMUNOSUPPRESSANT IN 34 RECIPIENTS OF CADAVERIC ORGANS: 32 KIDNEYS, 2 PANCREASES, AND 2 LIVERS." *The Lancet* 314 (8151): 1033–36. doi:10.1016/S0140-6736(79)92440-1.
- Calne, R.Y., S. Thiru, P. McMaster, G.N. Craddock, D.J.G. White, D.B. Evans, D.C. Dunn, B.D. Pentlow, and Keith Rolles. 1978. "CYCLOSPORIN A IN PATIENTS RECEIVING RENAL ALLOGRAFTS FROM CADAVER DONORS." *The Lancet* 312 (8104): 1323–27. doi:10.1016/S0140-6736(78)91970-0.
- Canzanello, V J, S C Textor, S J Taler, L L Schwartz, M K Porayko, R H Wiesner, and R A Krom. 1998. "Late Hypertension after Liver Transplantation: A Comparison of Cyclosporine and Tacrolimus (FK 506)." *Liver Transplantation and Surgery: Official Publication of the American Association for the Study of Liver Diseases and the International Liver Transplantation Society* 4 (4): 328–34. doi:S1527646598000604 [pii].
- Carew, Rosemarie M, Bo Wang, and Phillip Kantharidis. 2012. "The Role of EMT in Renal Fibrosis." *Cell and Tissue Research* 347 (1): 103–16. doi:10.1007/s00441-011-1227-1.
- Chantry, D, M Turner, E Abney, and M Feldmann. 1989. "Modulation of Cytokine Production by Transforming Growth Factor-Beta." *J Immunol* 142 (12): 4295–4300.
- Chapman, J R. 2011. "Chronic Calcineurin Inhibitor Nephrotoxicity-Lest We Forget." *American Journal of Transplantation* 11 (4): 693–97. doi:10.1111/j.1600-6143.2011.03504.x.

- Chen, Beibei, Jonghyun Yun, Min Soo Kim, Joshua T Mendell, and Yang Xie. 2014. "PIPE-CLIP: A Comprehensive Online Tool for CLIP-Seq Data Analysis." *Genome Biology* 15 (1): R18. doi:10.1186/gb-2014-15-1-r18.
- Chen, Jianguo, Anna Zmijewska, Degui Zhi, and Roslyn B. Mannon. 2015. "Cyclosporine-Mediated Allograft Fibrosis Is Associated with Micro-RNA-21 through AKT Signaling." *Transplant International* 28 (2): 232–45. doi:10.1111/tri.12471.
- Chen, Xiu, Shan Liang Zhong, Peng Lu, Dan Dan Wang, Si Ying Zhou, Su Jin Yang, Hong Yu Shen, et al. 2016. "miR-4443 Participates in the Malignancy of Breast Cancer." *PLoS ONE* 11 (8). doi:10.1371/journal.pone.0160780.
- Chendrimada, Thimmaiah P., Richard I. Gregory, Easwari Kumaraswamy, Jessica Norman, Neil Cooch, Kazuko Nishikura, and Ramin Shiekhattar. 2005. "TRBP Recruits the Dicer Complex to Ago2 for microRNA Processing and Gene Silencing." *Nature* 436 (7051): 740–44. doi:10.1038/nature03868.
- Chi, Sung Wook, Julie B Zang, Aldo Mele, and Robert B Darnell. 2009. "Argonaute HITS-CLIP Decodes microRNA-mRNA Interaction Maps." *Nature* 460 (7254). Nature Publishing Group: 479–86. doi:10.1038/nature08170.
- Chia, Joanne, Germaine Goh, and Frederic Bard. 2016. "Short O-GalNAc Glycans: Regulation and Role in Tumor Development and Clinical Perspectives." *Biochimica et Biophysica Acta* 1860 (8): 1623–39. doi:10.1016/j.bbagen.2016.03.008.
- Chu, Yanfang, Patricia A. Solski, Roya Khosravi-Far, Channing J. Der, and Kathleen Kelly. 1996. "The Mitogen-Activated Protein Kinase Phosphatases PAC1, MKP-1, and MKP-2 Have Unique Substrate Specificities and Reduced Activity in Vivo toward the ERK2 Sevenmaker Mutation." *Journal of Biological Chemistry* 271 (11): 6497–6501. doi:10.1074/jbc.271.11.6497.
- Chugh, Pauline, and Dirk P. Dittmer. 2012. "Potential Pitfalls in microRNA Profiling." *Wiley Interdisciplinary Reviews: RNA*. doi:10.1002/wrna.1120.
- Clement, Lionel C, Carmen Avila-Casado, Camille Macé, Elizabeth Soria, Winston W Bakker, Sander Kersten, and Sumant S Chugh. 2011. "Podocyte-Secreted Angiopoietin-like-4 Mediates Proteinuria in Glucocorticoid-Sensitive Nephrotic Syndrome." *Nature Medicine* 17 (1): 117–22. doi:10.1038/nm.2261.
- Cloonan, Nicole. 2015. "Re-Thinking miRNA-mRNA Interactions: Intertwining Issues Confound Target Discovery." *BioEssays* 37 (4): 379–88. doi:10.1002/bies.201400191.
- Comoglio, Federico, Cem Sievers, and Renato Paro. 2015. "Sensitive and Highly Resolved Identification of RNA-Protein Interaction Sites in PAR-CLIP Data." *BMC Bioinformatics* 16 (1): 32. doi:10.1186/s12859-015-0470-y.
- Corcoran, David L, Stoyan Georgiev, Neelanjan Mukherjee, Eva Gottwein, Rebecca L Skalsky, Jack D Keene, and Uwe Ohler. 2011. "PARalyzer: Definition of RNA Binding Sites from PAR-CLIP Short-Read Sequence Data." *Genome Biology* 12 (8). BioMed Central Ltd: R79. doi:10.1186/gb-2011-12-8-r79.
- Coroneos, E, M Assouad, B Krishnan, and L D Truong. 1997. "Urinary Obstruction Causes Irreversible Renal Failure by Inducing Chronic Tubulointerstitial Nephritis." *Clinical Nephrology* 48 (2): 125–28.
<http://www.ncbi.nlm.nih.gov/pubmed/9285152>.

- Crompton, Tessa, Kimberly C. Gilmour, and Michael J. Owen. 1996. "The Map Kinase Pathway Controls Differentiation from Double-Negative to Double-Positive Thymocyte." *Cell* 86 (2): 243–51. doi:10.1016/S0092-8674(00)80096-3.
- Daley, William P., Elise M Gervais, Samuel W Centanni, Kathryn M. Gulfo, Deirdre A Nelson, and Melinda Larsen. 2012. "ROCK1-Directed Basement Membrane Positioning Coordinates Epithelial Tissue Polarity." *Development (Cambridge, England)* 139 (2): 411–22. doi:10.1242/dev.075366.
- Denli, Ahmet M, Bastiaan B J Tops, Ronald H a Plasterk, René F Ketting, and Gregory J Hannon. 2004. "Processing of Primary microRNAs by the Microprocessor Complex." *Nature* 432 (7014): 231–35. doi:10.1038/nature03049.
- Dias, Kay, Anna Dvorkin-Gheva, Robin M. Hallett, Ying Wu, John Hassell, Gregory R. Pond, Mark Levine, Tim Whelan, and Anita L. Bane. 2017. "Claudin-Low Breast Cancer; Clinical & Pathological Characteristics." *PLOS ONE* 12 (1): e0168669. doi:10.1371/journal.pone.0168669.
- Dixon, C. Edward, Helen M. Bramlett, W. Dalton Dietrich, Deborah A. Shear, Hong Q. Yan, Ying Deng-Bryant, Stefania Mondello, et al. 2016. "Cyclosporine Treatment in Traumatic Brain Injury: Operation Brain Trauma Therapy." *Journal of Neurotrauma* 33 (6): 553–66. doi:10.1089/neu.2015.4122.
- Doench, John G, and Phillip A Sharp. 2004. "Specificity of microRNA Target Selection in Translational Repression." *Genes & Development* 18 (5): 504–11. doi:10.1101/gad.1184404.
- Dong, Chen, Roger J Davis, and Richard a Flavell. 2002. "MAP Kinases in the Immune Response." *Annual Review of Immunology* 20: 55–72. doi:10.1146/annurev.immunol.20.091301.131133.
- Dreyfuss, M., E. Harri, H. Hofmann, H. Kobel, W. Pache, and H. Tscherter. 1976. "Cyclosporin A and C." *European Journal Of Applied Microbiology* 3 (2): 125–33. doi:10.1007/BF00928431.
- Du, Bin, Li Ming Ma, Mian Bo Huang, Hui Zhou, Hui Lin Huang, Peng Shao, Yue Qin Chen, and Liang Hu Qu. 2010. "High Glucose down-Regulates miR-29a to Increase Collagen IV Production in HK-2 Cells." *FEBS Letters* 584 (4): 811–16. doi:10.1016/j.febslet.2009.12.053.
- Du, S., N. Hiramatsu, K. Hayakawa, A. Kasai, M. Okamura, T. Huang, J. Yao, et al. 2009. "Suppression of NF- B by Cyclosporin A and Tacrolimus (FK506) via Induction of the C/EBP Family: Implication for Unfolded Protein Response." *The Journal of Immunology* 182 (11): 7201–11. doi:10.4049/jimmunol.0801772.
- Duce, James A., Andrew Tsatsanis, Michael A. Cater, Simon A. James, Elysia Robb, Krutika Wikhe, Su Ling Leong, et al. 2010. "Iron-Export Ferroxidase Activity of β -Amyloid Precursor Protein Is Inhibited by Zinc in Alzheimer's Disease." *Cell* 142 (6): 857–67. doi:10.1016/j.cell.2010.08.014.
- Durnian, Jonathan M, Rosalind M K Stewart, Richard Tatham, Mark Batterbury, and Stephen B Kaye. 2007. "Cyclosporin-A Associated Malignancy." *Clinical Ophthalmology (Auckland, N.Z.)* 1 (4): 421–30. <http://www.ncbi.nlm.nih.gov/pmc/articles/PMC2704538/>
- Easow, George, Aurelio A Teleman, and Stephen M Cohen. 2007. "Isolation of

- microRNA Targets by miRNP Immunopurification.” *RNA (New York, N.Y.)* 13 (8): 1198–1204. doi:10.1261/rna.563707.
- Esteva-Font, Cristina, Elisabet Ars, Elena Guillen-Gomez, Josep Maria Campistol, Laia Sanz, Wladimiro Jiménez, Mark Alan Knepper, et al. 2007. “Ciclosporin-Induced Hypertension Is Associated with Increased Sodium Transporter of the Loop of Henle (NKCC2).” *Nephrology Dialysis Transplantation* 22 (10): 2810–16. doi:10.1093/ndt/gfm390.
- Eulalio, Ana, Eric Huntzinger, and Elisa Izaurralde. 2008. “GW182 Interaction with Argonaute Is Essential for miRNA-Mediated Translational Repression and mRNA Decay.” *Nature Structural & Molecular Biology* 15 (4): 346–53. doi:10.1038/nsmb.1405.
- Eulalio, Ana, Felix Tritschler, and Elisa Izaurralde. 2009. “The GW182 Protein Family in Animal Cells: New Insights into Domains Required for miRNA-Mediated Gene Silencing.” *RNA (New York, N.Y.)* 15 (8): 1433–42. doi:10.1261/rna.1703809.
- Fabregat, Antonio, Konstantinos Sidiropoulos, Phani Garapati, Marc Gillespie, Kerstin Hausmann, Robin Haw, Bijay Jassal, et al. 2016. “The Reactome Pathway Knowledgebase.” *Nucleic Acids Research* 44 (D1): D481–87. doi:10.1093/nar/gkv1351.
- Fackenthal, James D., and Olufunmilayo I. Olopade. 2007. “Breast Cancer Risk Associated with BRCA1 and BRCA2 in Diverse Populations.” *Nature Reviews Cancer* 7 (12): 937–48. doi:10.1038/nrc2054.
- Faraoni, Isabella, Francesca Romana Antonetti, John Cardone, and Enzo Bonmassar. 2009. “miR-155 Gene: A Typical Multifunctional microRNA.” *Biochimica et Biophysica Acta - Molecular Basis of Disease*. doi:10.1016/j.bbadi.2009.02.013.
- Farazi, Thalia a, Jelle J Ten Hoeve, Miguel Brown, Aleksandra Mihailovic, Hugo M Horlings, Marc J van de Vijver, Thomas Tuschl, and Lodewyk Fa Wessels. 2014. “Identification of Distinct miRNA Target Regulation between Breast Cancer Molecular Subtypes Using AGO2-PAR-CLIP and Patient Datasets.” *Genome Biology* 15 (1): R9. doi:10.1186/gb-2014-15-1-r9.
- Felicetti, Federica, Alessandra De Feo, Carolina Coscia, Rossella Puglisi, Francesca Pedini, Luca Pasquini, Maria Bellenghi, Maria Cristina Errico, Elena Pagani, and Alessandra Care. 2016. “Exosome-Mediated Transfer of miR-222 Is Sufficient to Increase Tumor Malignancy in Melanoma.” *Journal of Translational Medicine* 14 (February). England: 56. doi:10.1186/s12967-016-0811-2.
- Forman, J. J., A. Legesse-Miller, and H. A. Coller. 2008. “A Search for Conserved Sequences in Coding Regions Reveals That the Let-7 microRNA Targets Dicer within Its Coding Sequence.” *Proceedings of the National Academy of Sciences* 105 (39): 14879–84. doi:10.1073/pnas.0803230105.
- Fragiadaki, Maria, and Roger M. Mason. 2011. “Epithelial-Mesenchymal Transition in Renal Fibrosis - Evidence for and against.” *International Journal of Experimental Pathology* 92 (3): 143–50. doi:10.1111/j.1365-2613.2011.00775.x.
- Frantz, B, E C Nordby, G Bren, N Steffan, C V Paya, R L Kincaid, M J Tocci, S J O’Keefe, and E a O’Neill. 1994. “Calcineurin Acts in Synergy with PMA to Inactivate I Kappa B/MAD3, an Inhibitor of NF-Kappa B.” *The EMBO Journal* 13 (4): 861–70.

- Friedersdorf, Matthew B, and Jack D Keene. 2014. "Advancing the Functional Utility of PAR-CLIP by Quantifying Background Binding to mRNAs and lncRNAs." *Genome Biology* 15 (1): R2. doi:10.1186/gb-2014-15-1-r2.
- Galardi, Silvia, Neri Mercatelli, Ezio Giorda, Simone Massalini, Giovanni Vanni Frajese, Silvia Anna Ciafrè, and Maria Giulia Farace. 2007. "miR-221 and miR-222 Expression Affects the Proliferation Potential of Human Prostate Carcinoma Cell Lines by Targeting p27kip1." *Journal of Biological Chemistry* 282 (32): 23716–24. doi:10.1074/jbc.M701805200.
- Gaziel-Sovran, Avital, Miguel F. Segura, Raffaella Di Micco, Mary K. Collins, Douglas Hanniford, Eleazar Vega-Saenz de Miera, John F. Rakus, et al. 2011. "MiR-30b/30d Regulation of GalNAc Transferases Enhances Invasion and Immunosuppression during Metastasis." *Cancer Cell* 20 (1): 104–18. doi:10.1016/j.ccr.2011.05.027.
- Gerondakis, Steve, Thomas S Fulford, Nicole L Messina, and Raelene J Grumont. 2014. "NF-κB Control of T Cell Development." *Nature Immunology* 15 (1): 15–25. doi:10.1038/ni.2785.
- Git, A, H Dvinge, M Salmon-Divon, M Osborne, C Kutter, J Hadfield, P Bertone, and C Caldas. 2010. "Systematic Comparison of Microarray Profiling, Real-Time PCR, and next-Generation Sequencing Technologies for Measuring Differential microRNA Expression." *Rna* 16 (5): 991–1006. doi:10.1261/rna.1947110.
- Godwin, Jonathan G, Xupeng Ge, Kristin Stephan, Anke Jurisch, Stefan G Tullius, and John Iacomini. 2010. "Identification of a microRNA Signature of Renal Ischemia Reperfusion Injury." *Proceedings of the National Academy of Sciences of the United States of America* 107 (32): 14339–44. doi:10.1073/pnas.0912701107.
- Gooch, Jennifer L, Clayton King, Cynthia E Francis, Paul S Garcia, and Yun Bai. 2017. "Cyclosporine A Alters Expression of Renal microRNAs : New Insights into Calcineurin Inhibitor Nephrotoxicity," 1–15.
- Goppelt-Strübe, Margarete, Birgit Esslinger, and Ulrich Kunzendorf. 2003. "Failure of Cyclosporin A to Induce Transforming Growth Factor Beta (TGF-Beta) Synthesis in Activated Peripheral Blood Lymphocytes." *Clinical Transplantation* 17 (1). Denmark: 20–25.
- Gravdal, Karsten, Ole J. Halvorsen, Svein A. Haukaas, and Lars A. Akslen. 2007. "A Switch from E-Cadherin to N-Cadherin Expression Indicates Epithelial to Mesenchymal Transition and Is of Strong and Independent Importance for the Progress of Prostate Cancer." *Clinical Cancer Research* 13 (23): 7003–11. doi:10.1158/1078-0432.CCR-07-1263.
- Gregory, Richard I, Kai-Ping Yan, Govindasamy Amuthan, Thimmaiah Chendrimada, Behzad Doratotaj, Neil Cooch, and Ramin Shiekhattar. 2004. "The Microprocessor Complex Mediates the Genesis of microRNAs." *Nature* 432 (7014): 235–40. doi:10.1038/nature03120.
- Griffiths-Jones, Sam, Russell J Grocock, Stijn van Dongen, Alex Bateman, and Anton J Enright. 2006. "miRBase: microRNA Sequences, Targets and Gene Nomenclature." *Nucleic Acids Research* 34 (Database issue): D140-4. doi:10.1093/nar/gkj112.
- Griffiths-Jones, Sam, Harpreet Kaur Saini, Stijn Van Dongen, and Anton J. Enright. 2008. "miRBase: Tools for microRNA Genomics." *Nucleic Acids Research* 36 (SUPPL. 1). doi:10.1093/nar/gkm952.

- Gruber, Andreas R, Georges Martin, Walter Keller, and Mihaela Zavolan. 2014. "Means to an End: Mechanisms of Alternative Polyadenylation of Messenger RNA Precursors." *Wiley Interdisciplinary Reviews. RNA* 5 (2). United States: 183–96. doi:10.1002/wrna.1206.
- Guo, Ge, Jian Yang, Jennifer Nichols, John Simon Hall, Isobel Eyres, William Mansfield, and Austin Smith. 2009. "Klf4 Reverts Developmentally Programmed Restriction of Ground State Pluripotency." *Development (Cambridge, England)* 136 (7): 1063–69. doi:10.1242/dev.030957.
- Guo, Shui Long, Zheng Peng, Xue Yang, Kai Ji Fan, Hui Ye, Zhen Hua Li, Yan Wang, et al. 2011. "Mir-148a Promoted Cell Proliferation by Targeting p27 in Gastric Cancer Cells." *International Journal of Biological Sciences* 7 (5): 567–74.
- Ha, H, M R Yu, and H B Lee. 2001. "High Glucose-Induced PKC Activation Mediates TGF-Beta 1 and Fibronectin Synthesis by Peritoneal Mesothelial Cells." *Kidney International* 59 (2): 463–70. doi:10.1046/j.1523-1755.2001.059002463.x.
- Habuka, Masato, Linn Fagerberg, Björn M. Hallström, Caroline Kampf, Karolina Edlund, Åsa Sivertsson, Tadashi Yamamoto, Fredrik Pontén, Mathias Uhlén, and Jacob Odeberg. 2014. "The Kidney Transcriptome and Proteome Defined by Transcriptomics and Antibody-Based Profiling." *PloS One* 9 (12): e116125. doi:10.1371/journal.pone.0116125.
- Haecker, Irina, Lauren A. Gay, Yajie Yang, Jianhong Hu, Alison M. Morse, Lauren M. McIntyre, and Rolf Renne. 2012. "Ago HITS-CLIP Expands Understanding of Kaposi's Sarcoma-Associated Herpesvirus miRNA Function in Primary Effusion Lymphomas." *PLoS Pathogens* 8 (8). doi:10.1371/journal.ppat.1002884.
- Hafner, Markus, Markus Landthaler, Lukas Burger, Mohsen Khorshid, Jean Hausser, Philipp Berninger, Andrea Rothballer, et al. 2010. "Transcriptome-Wide Identification of RNA-Binding Protein and microRNA Target Sites by PAR-CLIP." *Cell* 141 (1). Elsevier Ltd: 129–41. doi:10.1016/j.cell.2010.03.009.
- Hafner, Markus, Steve Lianoglou, Thomas Tuschl, and Doron Belenky. 2012. "Genome-Wide Identification of miRNA Targets by PAR-CLIP." *Methods (San Diego, Calif.)* 58 (2). Elsevier Inc.: 94–105. doi:10.1016/jymeth.2012.08.006.
- Hall, B M, D J Tiller, G G Duggin, J S Horvath, a Farnsworth, J May, J R Johnson, and a G Sheil. 1985. "Post-Transplant Acute Renal Failure in Cadaver Renal Recipients Treated with Cyclosporine." *Kidney International* 28: 178–86. doi:10.1038/ki.1985.138.
- Hamilton, Mark P, Kimal I Rajapakshe, David A Bader, Jasmina Z Cerne, Eric A Smith, Cristian Coarfa, Sean M Hartig, and Sean E McGuire. 2016. "The Landscape of microRNA Targeting in Prostate Cancer Defined by AGO-PAR-CLIP." *Neoplasia (New York, N.Y.)* 18 (6). The Authors: 356–70. doi:10.1016/j.neo.2016.04.008.
- HannonLab. 2014. "FASTX Toolkit." *Cold Spring Harbor Laboratory, Cold Spring Harbor, NY.*
- Hardinger, Karen, and Colm C. Magee. 2017. "Pharmacology of Cyclosporine and Tacrolimus." In *UpToDate*, edited by Ted W. Post. UpToDate.
- Hart, A., J. M. Smith, M. A. Skeans, S. K. Gustafson, D. E. Stewart, W. S. Cherikh, J. L. Wainright, et al. 2017. "OPTN/SRTR 2015 Annual Data Report: Kidney." *American Journal of Transplantation* 17 (S1): 21–116. doi:10.1111/ajt.14124.

- Heher, Eliot, and James F. Markmann. 2016. "The Clearer BENEFITS of Belatacept." *New England Journal of Medicine* 374 (4): 388–89. doi:10.1056/NEJMMe1515765.
- Helwak, Aleksandra, Grzegorz Kudla, Tatiana Dudnakova, and David Tollervey. 2013. "Mapping the Human miRNA Interactome by CLASH Reveals Frequent Noncanonical Binding." *Cell* 153 (3). Elsevier Inc.: 654–65. doi:10.1016/j.cell.2013.03.043.
- Herman, M, T Weinstein, A Korzets, A Chagnac, Y Ori, D Zevin, T Malachi, and U Gaster. 2001. "Effect of Cyclosporin A on DNA Repair and Cancer Incidence in Kidney Transplant Recipients." *The Journal of Laboratory and Clinical Medicine* 137 (1): 14–20. doi:10.1067/mlc.2001.111469.
- Hermann-Kleiter, Natascha, and Gottfried Baier. 2010. "NFAT Pulls the Strings during CD4+ T Helper Cell Effector Functions." *Blood*. doi:10.1182/blood-2009-10-233585.
- Hojo, Minoru, Takashi Morimoto, Mary Maluccio, Tomohiko Asano, Kengo Morimoto, Milagros Lagman, Toshikazu Shimbo, and Manikkam Suthanthiran. 1999. "Cyclosporine Induces Cancer Progression by a Cell-Autonomous Mechanism." *Nature* 397 (6719): 530–34. doi:10.1038/17401.
- Holz, Carmen, Franziska Niehr, Mariya Boyko, Tsvetana Hristozova, Luitpold Distel, Volker Budach, and Ingeborg Tinhofer. 2011. "Epithelial-Mesenchymal-Transition Induced by EGFR Activation Interferes with Cell Migration and Response to Irradiation and Cetuximab in Head and Neck Cancer Cells." *Radiotherapy and Oncology* 101 (1): 158–64. doi:10.1016/j.radonc.2011.05.042.
- Hoover, David M, and Jacek Lubkowski. 2002. "DNAWorks: An Automated Method for Designing Oligonucleotides for PCR-Based Gene Synthesis." *Nucleic Acids Research* 30 (10). England: e43.
- Horowitz, Jeffrey C., and Victor J. Thannickal. 2006. "Epithelial-Mesenchymal Interactions in Pulmonary Fibrosis." *Seminars in Respiratory and Critical Care Medicine* 27 (6): 600–612. doi:10.1055/s-2006-957332.
- Hoyos, B, D W Ballard, E Bohnlein, M Siekevitz, and W C Greene. 1989. "Kappa B-Specific DNA Binding Proteins: Role in the Regulation of Human Interleukin-2 Gene Expression." *Science* 244 (4903): 457–60.
- Huang, Han Chang, and Zhao Feng Jiang. 2011. "Amyloid-?? Protein Precursor Family Members: A Review from Homology to Biological Function." *Journal of Alzheimer's Disease*. doi:10.3233/JAD-2011-110335.
- Huang, Shuan S., and Jung S. Huang. 2005. "TGF-Beta Control of Cell Proliferation." *Journal of Cellular Biochemistry* 96 (3): 447–62. doi:10.1002/jcb.20558.
- Hunt, D., R. S. Coffin, and P. N. Anderson. 2002. "The Nogo Receptor, Its Ligands and Axonal Regeneration in the Spinal Cord; a Review." *Journal of Neurocytology*. doi:10.1023/A:1023941421781.
- Iman, Maryam, Seyede Samaneh Mostafavi, Seyed Shahriar Arab, Sadegh Azimzadeh, and Mansour Poorebrahim. 2016. "HOXB7 and Hsa-miR-222 as the Potential Therapeutic Candidates for Metastatic Colorectal Cancer." *Recent Patents on Anti-Cancer Drug Discovery* 11 (4). United Arab Emirates: 434–43.
- Iozzo, Renato V., and Ralph D. Sanderson. 2011. "Proteoglycans in Cancer Biology, Tumour Microenvironment and Angiogenesis." *Journal of Cellular and Molecular*

- Medicine*. doi:10.1111/j.1582-4934.2010.01236.x.
- Islam, M., J F Burke, T. A. McGowan, Y. Zhu, S. R. Dunn, P. McCue, J. Kanalas, and K. Sharma. 2001. "Effect of Anti-Transforming Growth Factor-Beta Antibodies in Cyclosporine-Induced Renal Dysfunction." *Kidney International* 59 (2): 498–506. doi:10.1046/j.1523-1755.2001.059002498.x.
- Jain, Jugnu, Christine Loh, and Anjana Rao. 1995. "Transcriptional Regulation of the IL-2 Gene." *Current Opinion in Immunology*. doi:10.1016/0952-7915(95)80107-3.
- Jeffrey, Kate L, Montserrat Camps, Christian Rommel, and Charles R Mackay. 2007. "Targeting Dual-Specificity Phosphatases: Manipulating MAP Kinase Signalling and Immune Responses." *Nature Reviews. Drug Discovery* 6 (5): 391–403. doi:10.1038/nrd2289.
- Justo, P., C Lorz, A Sanz, J Egido, and A Ortiz. 2003. "Intracellular Mechanisms of Cyclosporin A-Induced Tubular Cell Apoptosis." *Journal of the American Society of Nephrology* 14 (12): 3072–80. doi:10.1097/01.ASN.0000099383.57934.0E.
- Kalaji, Ruba, Ann P. Wheeler, Jennifer C. Erasmus, Sang Y. Lee, Robert G. Endres, Louise P. Cramer, and Vania M M Braga. 2012. "ROCK1 and ROCK2 Regulate Epithelial Polarisation and Geometric Cell Shape." *Biology of the Cell* 104 (8): 435–51. doi:10.1111/boc.201100093.
- Kalluri, Raghu, and Robert A. Weinberg. 2009. "The Basics of Epithelial-Mesenchymal Transition." *The Journal of Clinical Investigation* 119 (6): 1420–28. doi:10.1172/JCI39104.
- Kalmár, Alexandra, Bálint Péterfia, Péter Hollósi, Orsolya Galamb, Sándor Spisák, Barnabás Wichmann, András Bodor, et al. 2015. "DNA Hypermethylation and Decreased mRNA Expression of MAL, PRIMA1, PTGDR and SFRP1 in Colorectal Adenoma and Cancer." *BMC Cancer* 15 (1): 736. doi:10.1186/s12885-015-1687-x.
- Kang, Minkyung, Suyong Choi, Soo-Jin Jeong, Sin-Ae Lee, Tae Kyoung Kwak, Hyeonjung Kim, Oisun Jung, et al. 2012. "Cross-Talk between TGF β 1 and EGFR Signalling Pathways Induces TM4SF5 Expression and Epithelial-mesenchymal Transition." *Biochemical Journal* 443 (3): 691–700. doi:10.1042/BJ20111584.
- Kao, S-H, W-L Wang, C-Y Chen, Y-L Chang, Y-Y Wu, Y-T Wang, S-P Wang, et al. 2014. "GSK3 β Controls Epithelial-Mesenchymal Transition and Tumor Metastasis by CHIP-Mediated Degradation of Slug." *Oncogene* 33 (24): 3172–82. doi:10.1038/onc.2013.279.
- Ke, Ben, Chuqiao Fan, Liping Yang, and Xiangdong Fang. 2017. "Matrix Metalloproteinases-7 and Kidney Fibrosis." *Frontiers in Physiology* 8 (February): 1–7. doi:10.3389/fphys.2017.00021.
- Kemper, Jonna, and Kara Kniska. 2014. "Pathophysiology and Treatment of Calcineurin Inhibitor Nephrotoxicity." *Kidneycentric at Digital Commons@Becker All: Paper 2*.
- Khanna, A, V Cairns, and J D Hosenpud. 1999. "Tacrolimus Induces Increased Expression of Transforming Growth Factor-beta1 in Mammalian Lymphoid as Well as Nonlymphoid Cells." *Transplantation* 67 (4). United States: 614–19.
- Khanna, Ashwani, Matthew Plummer, Cathy Bromberek, Barbara Bresnahan, and Sundaram Hariharan. 2002. "Expression of TGF-Beta and Fibrogenic Genes in Transplant Recipients with Tacrolimus and Cyclosporine Nephrotoxicity." *Kidney International* 62 (6): 2257–63. doi:10.1046/j.1523-1755.2002.00668.x.

- Khorshid, Mohsen, Christoph Rodak, and Mihaela Zavolan. 2011. "CLIPZ: A Database and Analysis Environment for Experimentally Determined Binding Sites of RNA-Binding Proteins." *Nucleic Acids Research* 39 (SUPPL. 1): 245–52. doi:10.1093/nar/gkq940.
- Kim, Sun-Hee, Yun-Yong Park, Sang-Wook Kim, Ju-Seog Lee, Dingzhi Wang, and Raymond N DuBois. 2011. "ANGPTL4 Induction by Prostaglandin E2 under Hypoxic Conditions Promotes Colorectal Cancer Progression." *Cancer Research* 71 (22): 7010–20. doi:10.1158/0008-5472.CAN-11-1262.
- Kim, Young-Kook, Boseon Kim, and V Narry Kim. 2016. "Re-Evaluation of the Roles of DROSHA, Exportin 5, and DICER in microRNA Biogenesis." *Proceedings of the National Academy of Sciences of the United States of America* 113 (13): E1881–1889. doi:10.1073/pnas.1602532113.
- Kino, T, H Hatanaka, M Hashimoto, M Nishiyama, T Goto, M Okuhara, M Kohsaka, H Aoki, and H Imanaka. 1987. "FK-506, a Novel Immunosuppressant Isolated from a Streptomyces. I. Fermentation, Isolation, and Physico-Chemical and Biological Characteristics." *The Journal of Antibiotics* 40 (9): 1249–55. doi:<http://doi.org/10.7164/antibiotics.40.1249>.
- Kiuchi-Saishin, Yumiko, Shimpei Gotoh, Mikio Furuse, Akiko Takasuga, Yasuo Tano, and Shoichiro Tsukita. 2002. "Differential Expression Patterns of Claudins, Tight Junction Membrane Proteins, in Mouse Nephron Segments." *Journal of the American Society of Nephrology : JASN* 13 (4): 875–86.
- Kopp, Jeffrey B., and Paul E. Klotman. 1990. "Cellular and Molecular Mechanisms of Cyclosporin Nephrotoxicity." *Journal of the American Society of Nephrology* 1 (2): 162–79.
- Koshiol, Jill, Ena Wang, Yingdong Zhao, Francesco Marincola, and Maria Teresa Landi. 2010. "Strengths and Limitations of Laboratory Procedures for microRNA Detection." *Cancer Epidemiology Biomarkers and Prevention*. doi:10.1158/1055-9965.EPI-10-0071.
- Koskensalo, Selja, Johanna Louhimo, Stig Nordling, Jaana Hagström, and Caj Haglund. 2011. "MMP-7 as a Prognostic Marker in Colorectal Cancer." *Tumor Biology* 32 (2): 259–64. doi:10.1007/s13277-010-0080-2.
- Kozomara, Ana, and Sam Griffiths-Jones. 2011. "MiRBase: Integrating microRNA Annotation and Deep-Sequencing Data." *Nucleic Acids Research* 39 (SUPPL. 1). doi:10.1093/nar/gkq1027.
- . 2014. "miRBase: Annotating High Confidence microRNAs Using Deep Sequencing Data." *Nucleic Acids Research* 42 (1): D68–73. doi:10.1093/nar/gkt1181.
- Krell, Jonathan, Justin Stebbing, Claudia Carissimi, Aleksandra F. Dabrowska, Alexander De Giorgio, Adam E. Frampton, Victoria Harding, et al. 2016. "TP53 Regulates miRNA Association with AGO2 to Remodel the miRNA-mRNA Interaction Network." *Genome Research* 26 (3): 331–41. doi:10.1101/gr.191759.115.
- Kurashige, Junji, Genta Sawada, Yusuke Takahashi, Hidetoshi Eguchi, Tomoya Sudo, Toru Ikegami, Tomoharu Yoshizumi, et al. 2013. "Suppression of MAL Gene Expression in Gastric Cancer Correlates with Metastasis and Mortality." *Fukuoka*

- Igaku Zasshi = Hukuoka Acta Medica* 104 (10): 344–49.
- Kwon, Mi Jeong. 2013. “Emerging Roles of Claudins in Human Cancer.” *International Journal of Molecular Sciences*. doi:10.3390/ijms140918148.
- Lagos-Quintana, M, R Rauhut, W Lendeckel, and T Tuschl. 2001. “Identification of Novel Genes Coding for Small Expressed RNAs.” *Science (New York, N.Y.)* 294 (5543): 853–58. doi:10.1126/science.1064921.
- Lagos-Quintana, Mariana, Reinhard Rauhut, Abdullah Yalcin, Jutta Meyer, Winfried Lendeckel, and Thomas Tuschl. 2002. “Identification of Tissue-Specific MicroRNAs from Mouse.” *Current Biology* 12 (9): 735–39. doi:10.1016/S0960-9822(02)00809-6.
- Laiho, M, J a DeCaprio, J W Ludlow, D M Livingston, and J Massagué. 1990. “Growth Inhibition by TGF-Beta Linked to Suppression of Retinoblastoma Protein Phosphorylation.” *Cell* 62 (1): 175–85. doi:0092-8674(90)90251-9 [pii].
- Lamouille, Samy, Jian Xu, and Rik Deryck. 2014. “Molecular Mechanisms of Epithelial–mesenchymal Transition.” *Nature Reviews Molecular Cell Biology* 15 (3). Nature Publishing Group: 178–96. doi:10.1038/nrm3758.
- Lanese, D. M., and J. D. Conger. 1993. “Effects of Endothelin Receptor Antagonist on Cyclosporine-Induced Vasoconstriction in Isolated Rat Renal Arterioles.” *Journal of Clinical Investigation* 91 (5): 2144–49. doi:10.1172/JCI116440.
- Langmead, Ben, Cole Trapnell, Mihai Pop, and Steven L Salzberg. 2009. “Ultrafast and Memory-Efficient Alignment of Short DNA Sequences to the Human Genome.” *Genome Biology* 10 (3): R25. doi:10.1186/gb-2009-10-3-r25.
- Larue, Lionel, and Alfonso Bellacosa. 2005. “Epithelial-Mesenchymal Transition in Development and Cancer: Role of Phosphatidylinositol 3’ kinase/AKT Pathways.” *Oncogene* 24 (50): 7443–54. doi:10.1038/sj.onc.1209091.
- Laurén, Juha, Matti S. Airaksinen, Mart Saarma, and Tõnis Timmusk. 2003. “Two Novel Mammalian Nogo Receptor Homologs Differentially Expressed in the Central and Peripheral Nervous Systems.” *Molecular and Cellular Neuroscience* 24 (3): 581–94. doi:10.1016/S1044-7431(03)00199-4.
- le Sage, Carlos, Remco Nagel, David a Egan, Mariette Schrier, Elly Mesman, Annunziato Mangiola, Corrado Anile, et al. 2007. “Regulation of the p27(Kip1) Tumor Suppressor by miR-221 and miR-222 Promotes Cancer Cell Proliferation.” *The EMBO Journal* 26 (15): 3699–3708. doi:10.1038/sj.emboj.7601790.
- Lee, Ho Young, and Jennifer A Doudna. 2012. “TRBP Alters Human Precursor microRNA Processing in Vitro.” *RNA (New York, N.Y.)* 18 (11): 2012–19. doi:10.1261/rna.035501.112.
- Lee, Jae Wook, Chung-Lin Chou, and Mark a. Knepper. 2015. “Deep Sequencing in Microdissected Renal Tubules Identifies Nephron Segment-Specific Transcriptomes.” *Journal of the American Society of Nephrology : JASN* 26 (11): 2669–77. doi:10.1681/ASN.2014111067.
- Lee, R. C., and V Ambros. 2001. “An Extensive Class of Small RNAs in *Caenorhabditis Elegans*.” *Science (New York, N.Y.)* 294 (5543): 862–64. doi:10.1126/science.1065329.
- Lee, Rosalind C., Rhonda L. Feinbaum, and Victor Ambros. 1993. “The *C. Elegans* Heterochronic Gene Lin-4 Encodes Small RNAs with Antisense Complementarity

- to Lin-14.” *Cell* 75 (5): 843–54. doi:10.1016/0092-8674(93)90529-Y.
- Lee, Yoontae, Chiyoung Ahn, Jinju Han, Hyounjeong Choi, Jaekwang Kim, Jeongbin Yim, Junho Lee, et al. 2003. “The Nuclear RNase III Drosha Initiates microRNA Processing.” *Nature* 425 (6956): 415–19. doi:10.1038/nature01957.
- Lee, Yoontae, Kipyong Jeon, Jun Tae Lee, Sunyoung Kim, and V. Narry Kim. 2002. “MicroRNA Maturation: Stepwise Processing and Subcellular Localization.” *EMBO Journal* 21 (17): 4663–70. doi:10.1093/emboj/cdf476.
- Lee, Yoontae, Minju Kim, Jinju Han, Kyu-Hyun Yeom, Sanghyuk Lee, Sung Hee Baek, and V Narry Kim. 2004. “MicroRNA Genes Are Transcribed by RNA Polymerase II.” *The EMBO Journal* 23 (20): 4051–60. doi:10.1038/sj.emboj.7600385.
- Levey, Andrew S., and Josef Coresh. 2012. “Chronic Kidney Disease.” *The Lancet* 379 (9811). Elsevier Ltd: 165–80. doi:10.1016/S0140-6736(11)60178-5.
- Lewis, Benjamin P., Christopher B. Burge, and David P. Bartel. 2005. “Conserved Seed Pairing, Often Flanked by Adenosines, Indicates That Thousands of Human Genes Are microRNA Targets.” *Cell* 120 (1): 15–20. doi:10.1016/j.cell.2004.12.035.
- Li, Bailong, Ying Lu, Honghai Wang, Xiaocui Han, Jun Mao, Jiazhi Li, Lihui Yu, et al. 2016. “miR-221/222 Enhance the Tumorigenicity of Human Breast Cancer Stem Cells via Modulation of PTEN/Akt Pathway.” *Biomedicine & Pharmacotherapy = Biomedecine & Pharmacotherapie* 79 (April). France: 93–101. doi:10.1016/j.biopha.2016.01.045.
- Li, B, H Yu, W Zheng, R Voll, S Na, a W Roberts, D a Williams, R J Davis, S Ghosh, and R a Flavell. 2000. “Role of the Guanosine Triphosphatase Rac2 in T Helper 1 Cell Differentiation.” *Science (New York, N.Y.)* 288 (5474): 2219–22. doi:10.1126/science.288.5474.2219.
- Li, Hang, Xiong Z. Ruan, Stephen H. Powis, Ray Fernando, Wint Y. Mon, David C. Wheeler, John F. Moorhead, and Zac Varghese. 2005. “EPA and DHA Reduce LPS-Induced Inflammation Responses in HK-2 Cells: Evidence for a PPAR-??-Dependent Mechanism.” *Kidney International* 67 (3): 867–74. doi:10.1111/j.1523-1755.2005.00151.x.
- Li, Jipeng, Yulan Song, Yiping Wang, Jianping Luo, and Wanjun Yu. 2013. “MicroRNA-148a Suppresses Epithelial-to-Mesenchymal Transition by Targeting ROCK1 in Non-Small Cell Lung Cancer Cells.” *Molecular and Cellular Biochemistry* 380 (1–2): 277–82. doi:10.1007/s11010-013-1682-y.
- Li, Jun, Shanhui Liang, Hailin Yu, Jin Zhang, Duan Ma, and Xin Lu. 2010. “An Inhibitory Effect of miR-22 on Cell Migration and Invasion in Ovarian Cancer.” *Gynecologic Oncology* 119 (3): 543–48. doi:10.1016/j.ygyno.2010.08.034.
- Li, Ming O, Yisong Y Wan, Shomyseh Sanjabi, Anna-Karin L Robertson, and Richard a Flavell. 2006. “Transforming Growth Factor-Beta Regulation of Immune Responses.” *Annual Review of Immunology* 24: 99–146. doi:10.1146/annurev.immunol.24.021605.090737.
- Liang, Y, D Ridzon, L Wong, and C Chen. 2007. “Characterization of microRNA Expression Profiles in Normal Human Tissues.” *BMC Genomics* 8: 166. doi:10.1186/1471-2164-8-166.
- Liberzon, Arthur, Chet Birger, Helga Thorvaldsd??ttir, Mahmoud Ghandi, Jill P. Mesirov, and Pablo Tamayo. 2015. “The Molecular Signatures Database Hallmark

- Gene Set Collection.” *Cell Systems* 1 (6): 417–25. doi:10.1016/j.cels.2015.12.004.
- Licatalosi, Donny D, Aldo Mele, John J Fak, Jernej Ule, Melis Kayikci, Sung Wook Chi, Tyson a Clark, et al. 2008. “HITS-CLIP Yields Genome-Wide Insights into Brain Alternative RNA Processing.” *Nature* 456 (November): 464–69. doi:10.1038/nature07488.
- Lin, Shuibin, and Richard I Gregory. 2015. “MicroRNA Biogenesis Pathways in Cancer.” *Nature Review Cancer* 15 (6): 321–33. doi:10.1038/nrc3932.
- Lipchina, Inna, Yechiel Elkabetz, Markus Hafner, Robert Sheridan, Aleksandra Mihailovic, Thomas Tuschl, Chris Sander, Lorenz Studer, and Doron Betel. 2011. “Genome-Wide Identification of microRNA Targets in Human ES Cells Reveals a Role for miR-302 in Modulating BMP Response.” *Genes and Development* 25 (20): 2173–86. doi:10.1101/gad.17221311.
- Liptak, Peter, and Bela Ivanyi. 2006. “Primer: Histopathology of Calcineurin-Inhibitor Toxicity in Renal Allografts.” *Nature Clinical Practice. Nephrology* 2 (7): 398–404. doi:10.1038/ncpneph0225.
- Liu, Bi Cheng, Jian Dong Zhang, Xiao Liang Zhang, Guo Qiu Wu, and Min Xia Li. 2006. “Role of Connective Tissue Growth Factor (CTGF) Module 4 in Regulating Epithelial Mesenchymal Transition (EMT) in HK-2 Cells.” *Clinica Chimica Acta* 373 (1–2): 144–50. doi:10.1016/j.cca.2006.05.029.
- Liu, J, M A Valencia-Sanchez, G J Hannon, and R Parker. 2005. “MicroRNA-Dependent Localization of Targeted mRNAs to Mammalian P-Bodies.” *Nat Cell Biol* 7 (7): 719–23. doi:10.1038/ncb1274.
- Liu, Jun, Jesse D. Farmer, William S. Lane, Jeff Friedman, Irving Weissman, and Stuart L. Schreiber. 1991. “Calcineurin Is a Common Target of Cyclophilin-Cyclosporin A and FKBP-FK506 Complexes.” *Cell* 66 (4): 807–15. doi:10.1016/0092-8674(91)90124-H.
- Liu, Xiaojun, Yunhui Cheng, Shuo Zhang, Ying Lin, Jian Yang, and Chunxiang Zhang. 2009. “A Necessary Role of miR-221 and miR-222 in Vascular Smooth Muscle Cell Proliferation and Neointimal Hyperplasia.” *Circulation Research* 104 (4): 476–86. doi:10.1161/CIRCRESAHA.108.185363.
- Liu, Y-N, J J Yin, W Abou-Kheir, P G Hynes, O M Casey, L Fang, M Yi, et al. 2013. “MiR-1 and miR-200 Inhibit EMT via Slug-Dependent and Tumorigenesis via Slug-Independent Mechanisms.” *Oncogene* 32 (3): 296–306. doi:10.1038/onc.2012.58.
- López-Gómez, Juan M, and Francisco Rivera. 2008. “Renal Biopsy Findings in Acute Renal Failure in the Cohort of Patients in the Spanish Registry of Glomerulonephritis.” *Clinical Journal of the American Society of Nephrology : CJASN* 3 (3): 674–81. doi:10.2215/CJN.04441007.
- Love, M. I., Simon Anders, and Wolfgang Huber. 2014. *Differential Analysis of Count Data - the DESeq2 Package*. *Genome Biology*. Vol. 15. doi:10.1186/s13059-014-0550-8.
- Love, Michael I, Wolfgang Huber, and Simon Anders. 2014. “Moderated Estimation of Fold Change and Dispersion for RNA-Seq Data with DESeq2.” *Genome Biology* 15 (12): 550. doi:10.1186/s13059-014-0550-8.
- Lu, Yi Chien, Sung Hee Chang, Markus Hafner, Xi Li, Thomas Tuschl, Olivier Elemento, and Timothy Hla. 2014. “ELAVL1 Modulates Transcriptome-Wide

- miRNA Binding in Murine Macrophages." *Cell Reports* 9 (6): 2330–43. doi:10.1016/j.celrep.2014.11.030.
- Ludwig, Nicole, Petra Leidinger, Kurt Becker, Christina Backes, Tobias Fehlmann, Christian Pallasch, Steffi Rheinheimer, et al. 2016. "Distribution of miRNA Expression across Human Tissues." *Nucleic Acids Research* 44 (8): 3865–77. doi:10.1093/nar/gkw116.
- Lund, Elsebet, Stephan Güttinger, Angelo Calado, James E Dahlberg, and Ulrike Kutay. 2004. "Nuclear Export of microRNA Precursors." *Science* 303 (5654): 95–98. doi:10.1126/science.1090599.
- Lv, Zhi-Mei, Qun Wang, Qiang Wan, Jian-Gong Lin, Meng-Si Hu, You-Xia Liu, and Rong Wang. 2011. "The Role of the p38 MAPK Signaling Pathway in High Glucose-Induced Epithelial-Mesenchymal Transition of Cultured Human Renal Tubular Epithelial Cells." *PloS One* 6 (7): e22806. doi:10.1371/journal.pone.0022806.
- Lytle, J. R., T. A. Yario, and J. A. Steitz. 2007. "Target mRNAs Are Repressed as Efficiently by microRNA-Binding Sites in the 5' UTR as in the 3' UTR." *Proceedings of the National Academy of Sciences* 104 (23): 9667–72. doi:10.1073/pnas.0703820104.
- Macian, Fernando. 2005. "NFAT Proteins: Key Regulators of T-Cell Development and Function." *Nature Reviews. Immunology* 5 (6): 472–84. doi:10.1038/nri1632.
- Mahajan, Muktar A, and Herbert H Samuels. 2008. "Nuclear Receptor Coactivator/coregulator NCoA6(NRC) Is a Pleiotropic Coregulator Involved in Transcription, Cell Survival, Growth and Development." *Nuclear Receptor Signaling* 6: e002. doi:10.1621/nrs.06002.
- Mandl, M., D. N. Slack, and S. M. Keyse. 2005. "Specific Inactivation and Nuclear Anchoring of Extracellular Signal-Regulated Kinase 2 by the Inducible Dual-Specificity Protein Phosphatase DUSP5." *Molecular and Cellular Biology* 25 (5): 1830–45. doi:10.1128/MCB.25.5.1830-1845.2005.
- Masson, Philip, Lorna Henderson, Jeremy R. Chapman, Jonathan C. Craig, and Angela C. Webster. 2014. "Belatacept for Kidney Transplant Recipients." *The Cochrane Database of Systematic Reviews* 11. doi:10.1002/14651858.CD010699.pub2.
- Matsuda, Satoshi, Tetsuo Moriguchi, Shigeo Koyasu, and Eisuke Nishida. 1998. "T Lymphocyte Activation Signals for Interleukin-2 Production Involve Activation of MKK6-p38 and MKK7-SAPK/JNK Signaling Pathways Sensitive to Cyclosporin A." *Journal of Biological Chemistry* 273 (20): 12378–82. doi:10.1074/jbc.273.20.12378.
- Matsuda, Satoshi, Futoshi Shibasaki, Kenji Takehana, Hiroaki Mori, Eisuke Nishida, and Shigeo Koyasu. 2000. "Two Distinct Action Mechanisms of Immunophilin-Ligand Complexes for the Blockade of T-Cell Activation." *EMBO Reports* 1 (5): 428–34. doi:10.1093/embo-reports/kvd090.
- Mazières, Julien, Caroline Catherinne, Olivier Delfour, Sandrine Gouin, Isabelle Rouquette, Marie Bernadette Delisle, Grégoire Prévot, et al. 2013. "Alternative Processing of the U2 Small Nuclear RNA Produces a 19-22nt Fragment with Relevance for the Detection of Non-Small Cell Lung Cancer in Human Serum." *PLoS ONE* 8 (3). doi:10.1371/journal.pone.0060134.

- McMorrow, Tara, Michelle M. Gaffney, Craig Slattery, Eric Campbell, and Michael P. Ryan. 2005. "Cyclosporine A Induced Epithelial-Mesenchymal Transition in Human Renal Proximal Tubular Epithelial Cells." *Nephrology, Dialysis, Transplantation : Official Publication of the European Dialysis and Transplant Association - European Renal Association* 20 (10): 2215–25. doi:10.1093/ndt/gfh967.
- Meerson, Ari, and Hila Yehuda. 2016. "Leptin and Insulin up-Regulate miR-4443 to Suppress NCOA1 and TRAF4, and Decrease the Invasiveness of Human Colon Cancer Cells." *BMC Cancer* 16 (1): 882. doi:10.1186/s12885-016-2938-1.
- Meng, Xiao-ming, David J. Nikolic-Paterson, and Hui Yao Lan. 2016. "TGF- β : The Master Regulator of Fibrosis." *Nature Reviews Nephrology* 12 (6). Nature Publishing Group: 325–38. doi:10.1038/nrneph.2016.48.
- Merritt, C, H Enslen, N Diehl, D Conze, R J Davis, and M Rincon. 2000. "Activation of p38 Mitogen-Activated Protein Kinase in Vivo Selectively Induces Apoptosis of CD8(+) but Not CD4(+) T Cells." *Mol Cell Biol* 20 (3): 936–46. doi:10.1128/MCB.20.3.936-946.2000.
- Meyer, Stephanie, N. Gail Kohler, and Alison Joly. 1997. "Cyclosporine A Is an Uncompetitive Inhibitor of Proteasome Activity and Prevents NF-??B Activation." *FEBS Letters* 413 (2). Federation of European Biochemical Societies: 354–58. doi:10.1016/S0014-5793(97)00930-7.
- Miki, Y, J Swensen, D Shattuck-Eidens, P A Futreal, K Harshman, S Tavtigian, Q Liu, C Cochran, L M Bennett, and W Ding. 1994. "A Strong Candidate for the Breast and Ovarian Cancer Susceptibility Gene BRCA1." *Science* 266 (5182): 66–71. doi:10.1126/science.7545954.
- Minguillon, Jordi, Beatriz Morancho, Seong-Jin Kim, Miguel Lopez-Botet, and Jose Aramburu. 2005. "Concentrations of Cyclosporin A and FK506 That Inhibit IL-2 Induction in Human T Cells Do Not Affect TGF-beta1 Biosynthesis, Whereas Higher Doses of Cyclosporin A Trigger Apoptosis and Release of Preformed TGF-beta1." *Journal of Leukocyte Biology* 77 (5). United States: 748–58. doi:10.1189/jlb.0904503.
- Moses, H L, E Y Yang, and J A Pietenpol. 1990. "TGF-Beta Stimulation and Inhibition of Cell Proliferation: New Mechanistic Insights." *Cell* 63 (2). United States: 245–47.
- Mulholland, David J., Naoko Kobayashi, Marcus Ruscetti, Allen Zhi, Linh M. Tran, Jiaoti Huang, Martin Gleave, and Hong Wu. 2012. "Pten Loss and RAS/MAPK Activation Cooperate to Promote EMT and Metastasis Initiated from Prostate Cancer Stem/progenitor Cells." *Cancer Research* 72 (7): 1878–89. doi:10.1158/0008-5472.CAN-11-3132.
- Murer, Heini, Nati Hernando, Ian Forster, and Jürg Biber. 2003. "Regulation of Na/Pi Transporter in the Proximal Tubule." *Annual Review of Physiology* 65 (1): 531–42. doi:10.1146/annurev.physiol.65.042902.092424.
- Muto, Shigeaki, Mikio Furuse, and Eiji Kusano. 2012. "Claudins and Renal Salt Transport." *Clinical and Experimental Nephrology*. doi:10.1007/s10157-011-0491-4.
- Muto, Shigeaki, Masaki Hata, Junichi Taniguchi, Shuichi Tsuruoka, Kazumasa Moriwaki, Mitinori Saitou, Kyoko Furuse, et al. 2010. "Claudin-2-Deficient Mice Are Defective in the Leaky and Cation-Selective Paracellular Permeability

- Properties of Renal Proximal Tubules.” *Proceedings of the National Academy of Sciences of the United States of America* 107 (17): 8011–16. doi:10.1073/pnas.0912901107.
- Naesens, Maarten, Dirk R J Kuypers, and Minnie Sarwal. 2009. “Calcineurin Inhibitor Nephrotoxicity.” *Clinical Journal of the American Society of Nephrology* 4 (2): 481–508. doi:10.2215/CJN.04800908.
- Nagamoto, T, G Eguchi, and D C Beebe. 2000. “Alpha-Smooth Muscle Actin Expression in Cultured Lens Epithelial Cells.” *Investigative Ophthalmology & Visual Science* 41 (5). United States: 1122–29.
- Narlis, Melina, David Grote, Yaned Gaitan, Sami K Boualia, and Maxime Bouchard. 2007. “Pax2 and pax8 Regulate Branching Morphogenesis and Nephron Differentiation in the Developing Kidney.” *Journal of the American Society of Nephrology : JASN* 18 (4): 1121–29. doi:10.1681/ASN.2006070739.
- Neria, Fernando, Maria A. Castilla, Ruth Fernandez Sanchez, Francisco R. Gonzalez Pacheco, Juan J.P. P Deudero, Olalla Calabia, Alberto Tejedor, et al. 2009. “Inhibition of JAK2 Protects Renal Endothelial and Epithelial Cells from Oxidative Stress and Cyclosporin A Toxicity.” *Kidney International* 75 (2). Elsevier Masson SAS: 227–34. doi:10.1038/ki.2008.487.
- Newman, Martin a., Vidya Mani, and Scott M. Hammond. 2011. “Deep Sequencing of microRNA Precursors Reveals Extensive 3’ End Modification.” *RNA (New York, N.Y.)* 17 (10): 1795–1803. doi:10.1261/rna.2713611.
- Noormohammad, Mina, Samira Sadeghi, Hossein Tabatabaeian, Kamran Ghaedi, Ardesir Talebi, Mansoureh Azadeh, Mehri Khatami, and Mohammad Mehdi Heidari. 2016. “Upregulation of miR-222 in Both Helicobacter Pylori- Infected and Noninfected Gastric Cancer Patients.” *Journal of Genetics* 95 (4). India: 991–95.
- Novick, A C, H H Hwei, D Steinmuller, S B Streem, R J Cunningham, D Steinhilber, M Goormastic, and C Buszta. 1986. “Detimental Effect of Cyclosporine on Initial Function of Cadaver Renal Allografts Following Extended Preservation. Results of a Randomized Prospective Study.” *Transplantation* 42 (2): 154–58. <http://www.ncbi.nlm.nih.gov/pubmed/3526655>.
- O’Leary, Dennis Dm, and David G. Wilkinson. 1999. “Eph Receptors and Ephrins in Neural Development.” *Current Opinion in Neurobiology*. doi:10.1016/S0959-4388(99)80008-7.
- O’Neill, Luke A J. 2002. “Toll-like Receptor Signal Transduction and the Tailoring of Innate Immunity: A Role for Mal?” *Trends in Immunology*. doi:10.1016/S1471-4906(02)02222-6.
- Ogata, Hiroyuki, Susumu Goto, Kazushige Sato, Wataru Fujibuchi, Hidemasa Bono, and Minoru Kanehisa. 1999. “KEGG: Kyoto Encyclopedia of Genes and Genomes.” *Nucleic Acids Research*. doi:10.1093/nar/27.1.29.
- Ogawa, T., M. Enomoto, H. Fujii, Y. Sekiya, K. Yoshizato, K. Ikeda, and N. Kawada. 2012. “MicroRNA-221/222 Upregulation Indicates the Activation of Stellate Cells and the Progression of Liver Fibrosis.” *Gut* 61: 1600–1609. doi:10.1136/gutjnl-2011-300717.
- Okuda, Hiroshi, Fei Xing, Puspa R. Pandey, Sambad Sharma, Misako Watabe, Sudha K. Pai, Yin Yuan Mo, et al. 2013. “MiR-7 Suppresses Brain Metastasis of Breast

- Cancer Stem-like Cells by Modulating KLF4.” *Cancer Research* 73 (4): 1434–44. doi:10.1158/0008-5472.CAN-12-2037.
- Osanto, Susanne, Yongjun Qin, Henk Buermans, Johannes Berkers, Evelyne Lerut, Jelle Goeman, and Hendrik van Poppel. 2012. “Genome-Wide MicroRNA Expression Analysis of Clear Cell Renal Cell Carcinoma by Next Generation Deep Sequencing.” *PLoS ONE* 7 (6): e38298. doi:doi: 10.1371/journal.pone.0038298.
- Padua, David, Xiang H F Zhang, Qiongqing Wang, Cristina Nadal, William L. Gerald, Roger R. Gomis, and Joan Massagué. 2008. “TGF β Primes Breast Tumors for Lung Metastasis Seeding through Angiopoietin-like 4.” *Cell* 133 (1): 66–77. doi:10.1016/j.cell.2008.01.046.
- Palkowitsch, Lysann, Uta Marienfeld, Cornelia Brunner, Andrea Eitelhuber, Daniel Krappmann, and Ralf B. Marienfeld. 2011. “The Ca $^{2+}$ -Dependent Phosphatase Calcineurin Controls the Formation of the Carma1-Bcl10-Malt1 Complex during T Cell Receptor-Induced NF-??B Activation.” *Journal of Biological Chemistry* 286 (9): 7522–34. doi:10.1074/jbc.M110.155895.
- Panchapakesan, U, C a Pollock, and X M Chen. 2004. “The Effect of High Glucose and PPAR-Gamma Agonists on PPAR-Gamma Expression and Function in HK-2 Cells.” *American Journal of Physiology. Renal Physiology* 287: F528–34. doi:10.1152/ajprenal.00445.2003.
- Panwar, Bharat, Gilbert S. Omenn, and Yuanfang Guan. 2017. “miRmine: A Database of Human miRNA Expression Profiles.” *Bioinformatics*, no. June 2014 (January): btx019. doi:10.1093/bioinformatics/btx019.
- Paraskevopoulou, Maria D., Georgios Georgakilas, Nikos Kostoulas, Ioannis S. Vlachos, Thanasis Vergoulis, Martin Reczko, Christos Filippidis, Theodore Dalamagas, and A. G. Hatzigeorgiou. 2013. “DIANA-microT Web Server v5.0: Service Integration into miRNA Functional Analysis Workflows.” *Nucleic Acids Research* 41 (Web Server issue). doi:10.1093/nar/gkt393.
- Park, Jong-Eun, Inha Heo, Yuan Tian, Dhirendra K Simanshu, Hyeshik Chang, David Jee, Dirshaw J Patel, and V Narry Kim. 2011. “Dicer Recognizes the 5’ End of RNA for Efficient and Accurate Processing.” *Nature* 475 (7355): 201–5. doi:10.1038/nature10198.
- Park, S. H., H. J. Choi, J. H. Lee, C. H. Woo, J. H. Kim, and H. J. Han. 2001. “High Glucose Inhibits Renal Proximal Tubule Cell Proliferation and Involves PKC, Oxidative Stress, and TGF-Beta 1.” *Kidney International* 59 (5). United States: 1695–1705. doi:10.1046/j.1523-1755.2001.0590051695.x.
- Pasquinelli, a E, B J Reinhart, F Slack, M Q Martindale, M I Kuroda, B Maller, D C Hayward, et al. 2000. “Conservation of the Sequence and Temporal Expression of Let-7 Heterochronic Regulatory RNA.” *Nature* 408 (6808): 86–89. doi:10.1038/35040556.
- Patel, J B, H N Appaiah, R M Burnett, P Bhat-Nakshatri, G Wang, R Mehta, S Badve, et al. 2011. “Control of EVI-1 Oncogene Expression in Metastatic Breast Cancer Cells through microRNA miR-22.” *Oncogene* 30 (11): 1290–1301. doi:10.1038/onc.2010.510.
- Peng, S L, a J Gerth, a M Ranger, and L H Glimcher. 2001. “NFATc1 and NFATc2 Together Control Both T and B Cell Activation and Differentiation.” *Immunity* 14

- (1): 13–20. doi:S1074-7613(01)00085-1 [pii].
- Prashar, Y, a Khanna, P Sehajpal, V K Sharma, and M Suthanthiran. 1995. “Stimulation of Transforming Growth Factor-Beta 1 Transcription by Cyclosporine.” *FEBS Letters* 358 (2): 109–12. doi:10.1016/0014-5793(94)01382-B.
- Priller, Christina, Thomas Bauer, Gerda Mittelregger, Bjarne Krebs, Hans a Kretzschmar, and Jochen Herms. 2006. “Synapse Formation and Function Is Modulated by the Amyloid Precursor Protein.” *The Journal of Neuroscience : The Official Journal of the Society for Neuroscience* 26 (27): 7212–21. doi:10.1523/JNEUROSCI.1450-06.2006.
- Pritchard, Colin C., Heather H. Cheng, and Muneesh Tewari. 2012. “MicroRNA Profiling: Approaches and Considerations.” *Nature Reviews Genetics* 13 (5). Nature Publishing Group: 358–69. doi:10.1038/nrg3198.
- Radisky, Derek C., and Mark A. LaBarge. 2008. “Epithelial-Mesenchymal Transition and the Stem Cell Phenotype.” *Cell Stem Cell* 2 (6): 511–12. doi:10.1016/j.stem.2008.05.007.
- Rangel, L B a, C Caruso-Neves, L S Lara, and a G Lopes. 2002. “Angiotensin II Stimulates Renal Proximal Tubule Na(+) -ATPase Activity through the Activation of Protein Kinase C.” *Biochimica et Biophysica Acta* 1564 (2): 310–16. <http://www.ncbi.nlm.nih.gov/pubmed/12175912>.
- Rao, A, C Luo, and P G Hogan. 1997. “Transcription Factors of the NFAT Family: Regulation and Function.” *Annu Rev Immunol* 15: 707–47. doi:10.1146/annurev.immunol.15.1.707.
- Rastaldi, Maria Pia. 2006. “Epithelial-Mesenchymal Transition and Its Implications for the Development of Renal Tubulointerstitial Fibrosis.” *Journal of Nephrology* 19 (4). Italy: 407–12.
- Ray, M E, G Wistow, Y A Su, P S Meltzer, and J M Trent. 1997. “AIM1, a Novel Non-Lens Member of the Betagamma-Crystallin Superfamily, Is Associated with the Control of Tumorigenicity in Human Malignant Melanoma.” *Proc Natl Acad Sci U S A* 94 (7): 3229–34. doi:10.1073/pnas.94.7.3229.
- Reczko, Martin, Manolis Maragkakis, Panagiotis Alexiou, Ivo Grosse, and Artemis G Hatzigeorgiou. 2012. “Functional microRNA Targets in Protein Coding Sequences.” *Bioinformatics (Oxford, England)* 28 (6): 771–76. doi:10.1093/bioinformatics/bts043.
- Reinhart, B J, F J Slack, M Basson, a E Pasquinelli, J C Bettinger, a E Rougvie, H R Horvitz, and G Ruvkun. 2000. “The 21-Nucleotide Let-7 RNA Regulates Developmental Timing in *Caenorhabditis Elegans*.” *Nature* 403 (6772): 901–6. doi:10.1038/35002607.
- Rincón, M. 2001. “MAP-Kinase Signaling Pathways in T Cells.” *Current Opinion in Immunology* 13 (3): 339–45. doi:10.1016/S0952-7915(00)00224-7.
- Rosenthal, R., S. Milatz, S. M. Krug, B. Oelrich, J.-D. Schulzke, S. Amasheh, D. Gunzel, and M. Fromm. 2010. “Claudin-2, a Component of the Tight Junction, Forms a Paracellular Water Channel.” *Journal of Cell Science* 123 (11): 1913–21. doi:10.1242/jcs.060665.
- Roush, Sarah, and Frank J. Slack. 2008. “The Let-7 Family of microRNAs.” *Trends in Cell Biology*. doi:10.1016/j.tcb.2008.07.007.

- Roy, Rohini, Jarin Chun, and Simon N. Powell. 2011. "BRCA1 and BRCA2: Different Roles in a Common Pathway of Genome Protection." *Nature Reviews Cancer* 12 (1): 68–78. doi:10.1038/nrc3181.
- Robinson, Douglas a, Christopher P Dillon, Adam V Kwiatkowski, Claudia Sievers, Lili Yang, Johnny Kopinja, Dina L Rooney, et al. 2003. "A Lentivirus-Based System to Functionally Silence Genes in Primary Mammalian Cells, Stem Cells and Transgenic Mice by RNA Interference." *Nature Genetics* 33 (3): 401–6. doi:10.1038/ng1117.
- Ruff, Valerie A., and Karen L. Leach. 1995. "Direct Demonstration of NFATp Dephosphorylation and Nuclear Localization in Activated HT-2 Cells Using a Specific NFATp Polyclonal Antibody." *Journal of Biological Chemistry* 270 (38): 22602–7. doi:10.1074/jbc.270.38.22602.
- Ruggenenti, P, N Perico, L Mosconi, F Gaspari, a Benigni, C S Amuchastegui, I Bruzzi, and G Remuzzi. 1993. "Calcium Channel Blockers Protect Transplant Patients from Cyclosporine-Induced Daily Renal Hypoperfusion." *Kidney International* 43 (3): 706–11. doi:10.1038/ki.1993.101.
- Rusnak, Frank, and Pamela Mertz. 2000. "Calcineurin: Form and Function." *Physiological Reviews* 80 (4): 1483–1521. doi:10.1172/JCI57909.date.
- Ryan, Michael J, Gretchen Johnson, Judy Kirk, Sally M Fuerstenberg, Richard A Zager, and Beverly Torok-Storb. 1994. "HK-2: An Immortalized Proximal Tubule Epithelial Cell Line from Normal Adult Human Kidney." *Kidney International* 45 (1): 48–57. doi:<http://dx.doi.org/10.1038/ki.1994.6>.
- Saladin, Kenneth S. 2008. *Human Anatomy*. New York; London: McGraw-Hill Higher Education ; McGraw-Hill [distributor].
- Salyer, Sarah a, Jason Parks, Michelle T Barati, Eleanor D Lederer, Barbara J Clark, Janet D Klein, and Syed J Khundmiri. 2013. "Aldosterone Regulates Na(+), K(+) ATPase Activity in Human Renal Proximal Tubule Cells through Mineralocorticoid Receptor." *Biochimica et Biophysica Acta* 1833 (10): 2143–52. doi:10.1016/j.bbamcr.2013.05.009.
- Sanford, Jeremy R., Xin Wang, Matthew Mort, Natalia Vanduyn, David N. Cooper, Sean D. Mooney, Howard J. Edenberg, and Yunlong Liu. 2009. "Splicing Factor SFRS1 Recognizes a Functionally Diverse Landscape of RNA Transcripts." *Genome Research* 19 (3): 381–94. doi:10.1101/gr.082503.108.
- Schreiber, S L, and G R Crabtree. 1992. "The Mechanism of Action of Cyclosporin A and FK506." *Immunology Today* 13 (4). England: 136–42. doi:10.1016/0167-5699(92)90111-J.
- Schroeder, Andreas, Odilo Mueller, Susanne Stocker, Ruediger Salowsky, Michael Leiber, Marcus Gassmann, Samar Lightfoot, Wolfram Menzel, Martin Granzow, and Thomas Ragg. 2006. "The RIN: An RNA Integrity Number for Assigning Integrity Values to RNA Measurements." *BMC Molecular Biology* 7 (1): 3. doi:10.1186/1471-2199-7-3.
- Shan, Sze Wan, Ling Fang, Tatiana Shatseva, Zina Jeyapalan Rutnam, Xiangling Yang, William Du, Wei-Yang Lu, Jim W Xuan, Zhaoqun Deng, and Burton B Yang. 2013. "Mature miR-17-5p and Passenger miR-17-3p Induce Hepatocellular Carcinoma by Targeting PTEN, GalNT7 and Vimentin in Different Signal Pathways." *Journal of*

- Cell Science* 126 (Pt 6): 1517–30. doi:10.1242/jcs.122895.
- Sharfuddin, Asif a, and Bruce a Molitoris. 2011. “Pathophysiology of Ischemic Acute Kidney Injury.” *Nature Reviews. Nephrology* 7 (4). Nature Publishing Group: 189–200. doi:10.1038/nrneph.2011.16.
- Shaw, J P, P J Utz, D B Durand, J J Toole, E a Emmel, and G R Crabtree. 1988. “Identification of a Putative Regulator of Early T Cell Activation Genes.” *Science (New York, N.Y.)* 241 (4862): 202–5. doi:10.1126/science.3260404.
- Shaw, K T, A M Ho, A Raghavan, J Kim, J Jain, J Park, S Sharma, A Rao, and P G Hogan. 1995. “Immunosuppressive Drugs Prevent a Rapid Dephosphorylation of Transcription Factor NFAT1 in Stimulated Immune Cells.” *Proc Natl Acad Sci U S A* 92 (24): 11205–9. doi:10.1073/pnas.92.24.11205.
- Shen, Hongyu, Dandan Wang, Liangpeng Li, Sujin Yang, Xiu Chen, Siying Zhou, Shanliang Zhong, Jianhua Zhao, and Jinhai Tang. 2017. “MiR-222 Promotes Drug-Resistance of Breast Cancer Cells to Adriamycin via Modulation of PTEN/Akt/FOXO1 Pathway.” *Gene* 596 (January). Netherlands: 110–18. doi:10.1016/j.gene.2016.10.016.
- Shibasaki, F, E R Price, D Milan, and F McKeon. 1996. “Role of Kinases and the Phosphatase Calcineurin in the Nuclear Shuttling of Transcription Factor NF-AT4.” *Nature* 382 (6589): 370–73. doi:10.1038/382370a0.
- Shin, G T, A Khanna, R Ding, V K Sharma, M Lagman, B Li, and M Suthanthiran. 1998. “In Vivo Expression of Transforming Growth Factor-beta1 in Humans: Stimulation by Cyclosporine.” *Transplantation* 65 (3). United States: 313–18.
- Sievers, Cem, Tommy Schlumpf, Ritwick Sawarkar, Federico Comoglio, and Renato Paro. 2012. “Mixture Models and Wavelet Transforms Reveal High Confidence RNA-Protein Interaction Sites in MOV10 PAR-CLIP Data.” *Nucleic Acids Research* 40 (20). doi:10.1093/nar/gks697.
- Slack, Frank J, Michael Basson, Zhongchi Liu, Victor Ambros, H. Robert Horvitz, and Gary Ruvkun. 2000. “The Lin-41 RBCC Gene Acts in the C. Elegans Heterochronic Pathway between the Let-7 Regulatory RNA and the LIN-29 Transcription Factor.” *Molecular Cell* 5 (4): 659–69. doi:10.1016/S1097-2765(00)80245-2.
- Slattery, Craig, Eric Campbell, Tara McMorrow, and Michael P. Ryan. 2005. “Cyclosporine A-Induced Renal Fibrosis - A Role for Epithelial-Mesenchymal Transition.” *American Journal of Pathology* 167 (2). American Society for Investigative Pathology: 395–407. doi:10.1016/S0002-9440(10)62984-7.
- Slattery, Craig, Tara McMorrow, and Michael P Ryan. 2006. “Overexpression of E2A Proteins Induces Epithelial-Mesenchymal Transition in Human Renal Proximal Tubular Epithelial Cells Suggesting a Potential Role in Renal Fibrosis.” *FEBS Letters* 580 (17). England: 4021–30. doi:10.1016/j.febslet.2006.06.039.
- Smith-Garvin, Jennifer E, Gary a Koretzky, Martha S Jordan, and 1 Gary A Koretzky. 2009. “T Cell Activation.” *Annual Review of Immunology* 27 (1): 591–619. doi:10.1146/annurev.immunol.021908.132706.
- Smith, a N, J Skaug, K a Choate, A Nayir, A Bakkaloglu, S Ozen, S a Hulton, et al. 2000. “Mutations in ATP6N1B, Encoding a New Kidney Vacuolar Proton Pump 116-kD Subunit, Cause Recessive Distal Renal Tubular Acidosis with Preserved Hearing.” *Nature Genetics* 26 (1): 71–75. doi:10.1038/79208.

- Solez, K, L Morel-Maroger, and J D Sraer. 1979. "The Morphology Of 'acute Tubular Necrosis' in Man: Analysis of 57 Renal Biopsies and a Comparison with the Glycerol Model." *Medicine* 58 (5). United States: 362–76.
- Song, Su Jung, Keisuke Ito, Ugo Ala, Lev Kats, Kaitlyn Webster, Su Ming Sun, Mojca Jongen-Lavrencic, et al. 2013. "The Oncogenic MicroRNA miR-22 Targets the TET2 Tumor Suppressor to Promote Hematopoietic Stem Cell Self-Renewal and Transformation." *Cell Stem Cell* 13 (1): 87–101. doi:10.1016/j.stem.2013.06.003.
- Spitzer, Jessica, Markus Hafner, Markus Landthaler, Manuel Ascano, Thalia Farazi, Greg Wardle, Jeff Nusbaum, et al. 2014. "PAR-CLIP (Photoactivatable Ribonucleoside-Enhanced Crosslinking and Immunoprecipitation): A Step-By-Step Protocol to the Transcriptome-Wide Identification of Binding Sites of RNA-Binding Proteins." *Methods in Enzymology* 539: 113–61. doi:10.1016/B978-0-12-420120-0.00008-6.
- Sripada, Lakshmi, Kritarth Singh, Anastasiya V Lipatova, Aru Singh, Paresh Prajapati, Dhanendra Tomar, Khyati Bhatelia, et al. 2017. "Hsa-miR-4485 Regulates Mitochondrial Functions and Inhibits the Tumorigenicity of Breast Cancer Cells." *Journal of Molecular Medicine (Berlin, Germany)*, February. Germany. doi:10.1007/s00109-017-1517-5.
- Stone, Rivka C, Irena Pastar, Nkemcho Ojeh, Vivien Chen, Sophia Liu, Karen I Garzon, and Marjana Tomic-Canic. 2016. "Epithelial-Mesenchymal Transition in Tissue Repair and Fibrosis." *Cell and Tissue Research* 365 (3). Germany: 495–506. doi:10.1007/s00441-016-2464-0.
- Subramanian, Aravind, Pablo Tamayo, Vamsi K Mootha, Sayan Mukherjee, Benjamin L Ebert, Michael a Gillette, Amanda Paulovich, et al. 2005. "Gene Set Enrichment Analysis: A Knowledge-Based Approach for Interpreting Genome-Wide Expression Profiles." *Proceedings of the National Academy of Sciences of the United States of America* 102 (43): 15545–50. doi:10.1073/pnas.0506580102.
- Tagliafata, Giulio, Cristiana Rastellini, and Luca Cicalese. 2015. "Reduced Incidence of Dementia in Solid Organ Transplant Patients Treated with Calcineurin Inhibitors." *Journal of Alzheimer's Disease* 47 (2): 329–33. doi:10.3233/JAD-150065.
- Takahashi, Kazutoshi, and Shinya Yamanaka. 2006. "Induction of Pluripotent Stem Cells from Mouse Embryonic and Adult Fibroblast Cultures by Defined Factors." *Cell* 126 (4): 663–76. doi:10.1016/j.cell.2006.07.024.
- Takeda, Y., I. Miyamori, P. Wu, T. Yoneda, K. Furukawa, and R. Takeda. 1995. "Effects of an Endothelin Receptor Antagonist in Rats With Cyclosporine-Induced Hypertension." *Hypertension* 26 (6): 932–36. doi:10.1161/01.HYP.26.6.932.
- Tay, Yvonne, Jinqiu Zhang, Andrew M. Thomson, Bing Lim, and Isidore Rigoutsos. 2008. "MicroRNAs to Nanog, Oct4 and Sox2 Coding Regions Modulate Embryonic Stem Cell Differentiation." *Nature* 455 (7216): 1124–28. doi:10.1038/nature07299.
- The U.S. Multicenter FK506 Liver Study Group. 1994. "A Comparison of Tacrolimus (FK 506) and Cyclosporine for Immunosuppression in Liver Transplantation." *New England Journal of Medicine* 331 (17): 1110–15. doi:10.1056/NEJM199410273311702.
- Tomaskovic-Crook, Eva, Erik W Thompson, and Jean Paul Thiery. 2009. "Epithelial to Mesenchymal Transition and Breast Cancer." *Breast Cancer Research : BCR* 11 (6): 213. doi:10.1186/bcr2416.

- Tong, Guo-Xia, Woojin M Yu, Nike T Beaubier, Erin M Weeden, Diane Hamele-Bena, Mahesh M Mansukhani, and Kathleen M O'Toole. 2009. "Expression of PAX8 in Normal and Neoplastic Renal Tissues: An Immunohistochemical Study." *Modern Pathology : An Official Journal of the United States and Canadian Academy of Pathology, Inc* 22 (9). United States: 1218–27. doi:10.1038/modpathol.2009.88.
- Tran, Duy T., and Kelly G. Ten Hagen. 2013. "Mucin-Type O-Glycosylation during Development." *Journal of Biological Chemistry*. doi:10.1074/jbc.R112.418558.
- Trapnell, Cole, Adam Roberts, Loyal Goff, Geo Pertea, Daehwan Kim, David R Kelley, Harold Pimentel, Steven L Salzberg, John L Rinn, and Lior Pachter. 2012. "Differential Gene and Transcript Expression Analysis of RNA-Seq Experiments with TopHat and Cufflinks." *Nature Protocols* 7 (3). Nature Publishing Group: 562–78. doi:10.1038/nprot.2012.016.
- Tsuchiya, K, W Wang, G Giebisch, and P A Welling. 1992. "Atp Is a Coupling Modulator of Parallel Na,K-Atpase K-Channel Activity in the Renal Proximal Tubule." *Proceedings of the National Academy of Sciences of the United States of America* 89 (14): 6418–22. doi:10.1073/pnas.89.14.6418.
- Turner, Paul R., Kate O'Connor, Warren P. Tate, and Wickliffe C. Abraham. 2003. "Roles of Amyloid Precursor Protein and Its Fragments in Regulating Neural Activity, Plasticity and Memory." *Progress in Neurobiology*. doi:10.1016/S0301-0082(03)00089-3.
- Tzortzaki, Eleni G, Jay A Tischfield, Amrik Sahota, Nikolaos M Siafakas, Marion K Gordon, and Donald R Gerecke. 2003. "Expression of FACIT Collagens XII and XIV during Bleomycin-Induced Pulmonary Fibrosis in Mice." *The Anatomical Record. Part A, Discoveries in Molecular, Cellular, and Evolutionary Biology* 275 (2). United States: 1073–80. doi:10.1002/ar.a.10120.
- Ule, Jernej, Kirk B Jensen, Matteo Ruggiu, Aldo Mele, Aljaz Ule, and Robert B Darnell. 2003. "CLIP Identifies Nova-Regulated RNA Networks in the Brain." *Science (New York, N.Y.)* 302 (5648): 1212–15. doi:10.1126/science.1090095.
- Ule, Jernej, Kirk Jensen, Aldo Mele, and Robert B Darnell. 2005. "CLIP: A Method for Identifying Protein-RNA Interaction Sites in Living Cells." *Methods (San Diego, Calif.)* 37 (4): 376–86. doi:10.1016/jymeth.2005.07.018.
- Uranishi, H, T Tetsuka, M Yamashita, K Asamitsu, M Shimizu, M Itoh, and T Okamoto. 2001. "Involvement of the pro-Oncoprotein TLS (Translocated in Liposarcoma) in Nuclear Factor-Kappa B p65-Mediated Transcription as a Coactivator." *The Journal of Biological Chemistry* 276 (16). United States: 13395–401. doi:10.1074/jbc.M011176200.
- Vallon, Volker, Kenneth A Platt, Robyn Cunard, Jana Schroth, Jean Whaley, Scott C Thomson, Hermann Koepsell, and Timo Rieg. 2011. "SGLT2 Mediates Glucose Reabsorption in the Early Proximal Tubule." *Journal of the American Society of Nephrology : JASN* 22 (1): 104–12. doi:10.1681/ASN.2010030246.
- Vaught, David, Dana M Brantley-Sieders, and Jin Chen. 2008. "Eph Receptors in Breast Cancer: Roles in Tumor Promotion and Tumor Suppression." *Breast Cancer Research : BCR* 10 (6): 217. doi:10.1186/bcr2207.
- Velthut-Meikas, Agne, Jaak Simm, Timo Tuuri, Juha S Tapanainen, Madis Metsis, and Andres Salumets. 2013. "Research Resource: Small RNA-Seq of Human Granulosa

- Cells Reveals miRNAs in FSHR and Aromatase Genes.” *Molecular Endocrinology (Baltimore, Md.)* 27 (February): 1128–41. doi:10.1210/me.2013-1058.
- Verine, Jérôme, Jacqueline Lehmann-Che, Hany Soliman, Jean Paul Feugeas, Jean Sébastien Vidal, Pierre Mongiat-Artus, Stéphanie Belhadj, et al. 2010. “Determination of angptl4 mRNA as a Diagnostic Marker of Primary and Metastatic Clear Cell Renal-Cell Carcinoma.” *PLoS ONE* 5 (4). doi:10.1371/journal.pone.0010421.
- Vincenti, Flavio, Gilles Blancho, Antoine Durrbach, Peter Friend, Josep Grinyo, Philip F Halloran, Jurgen Klempnauer, et al. 2010. “Five-Year Safety and Efficacy of Belatacept in Renal Transplantation.” *Journal of the American Society of Nephrology : JASN* 21: 1587–96. doi:10.1681/ASN.2009111109.
- Vlachos, Ioannis S., Konstantinos Zagganas, Maria D. Paraskevopoulou, Georgios Georgakilas, Dimitra Karagkouni, Thanasis Vergoulis, Theodore Dalamagas, and Artemis G. Hatzigeorgiou. 2015. “DIANA-miRPath v3.0: Deciphering microRNA Function with Experimental Support.” *Nucleic Acids Research* 43 (W1): W460–66. doi:10.1093/nar/gkv403.
- Vos, S, F Vesuna, V Raman, P J van Diest, and P van der Groep. 2015. “miRNA Expression Patterns in Normal Breast Tissue and Invasive Breast Cancers of BRCA1 and BRCA2 Germ-Line Mutation Carriers.” *Oncotarget* 6 (31): 32115–37. doi:10.18632/oncotarget.5617.
- Voulgari, Angeliki, and Alexander Pintzas. 2009. “Epithelial-Mesenchymal Transition in Cancer Metastasis: Mechanisms, Markers and Strategies to Overcome Drug Resistance in the Clinic.” *Biochimica et Biophysica Acta - Reviews on Cancer*. doi:10.1016/j.bbcan.2009.03.002.
- Wang, Feng Qiang, John So, Scott Reierstad, and David A. Fishman. 2005. “Matrilysin (MMP-7) Promotes Invasion of Ovarian Cancer Cells by Activation of Progelatinase.” *International Journal of Cancer* 114 (1): 19–31. doi:10.1002/ijc.20697.
- Wang, Qi, Ye Lu, Min Yuan, Inger M. Darling, Elizabeth A. Repasky, and Marilyn E. Morris. 2006. “Characterization of Monocarboxylate Transport in Human Kidney HK-2 Cells.” *Molecular Pharmaceutics* 3 (6): 675–85. doi:10.1021/mp060037b.
- Wang, Shuang, Zhu-Xu Z.-X. Zhang, Ziqin Yin, Weihua Liu, Bertha Garcia, Xuyan Huang, Philip Acott, and Anthony M Jevnikar. 2011. “Anti-IL-2 Receptor Antibody Decreases Cytokine-Induced Apoptosis of Human Renal Tubular Epithelial Cells (TEC).” *Nephrology, Dialysis, Transplantation : Official Publication of the European Dialysis and Transplant Association - European Renal Association* 26 (7): 2144–53. doi:10.1093/ndt/gfq714.
- Wang, Sui Han, Xu Li, Li Sheng Zhou, Zhong Wei Cao, Chao Shi, Chong Zhi Zhou, Yu Gang Wen, Yang Shen, and Ji Kun Li. 2013. “MicroRNA-148a Suppresses Human Gastric Cancer Cell Metastasis by Reversing Epithelial-to-Mesenchymal Transition.” *Tumor Biology* 34 (6): 3705–12. doi:10.1007/s13277-013-0954-1.
- Wee, Liang Meng, C. Fabián Flores-Jasso, William E. Salomon, and Phillip D. Zamore. 2012. “Argonaute Divides Its RNA Guide into Domains with Distinct Functions and RNA-Binding Properties.” *Cell* 151 (5): 1055–67. doi:10.1016/j.cell.2012.10.036.
- Weisz, O. A., and E. Rodriguez-Boulan. 2009. “Apical Trafficking in Epithelial Cells:

- Signals, Clusters and Motors.” *Journal of Cell Science* 122 (23): 4253–66. doi:10.1242/jcs.032615.
- Wesselborg, S., D. A. Fruman, J. K. Sagoo, B. E. Bierer, and S. J. Burakoff. 1996. “Identification of a Physical Interaction between Calcineurin and Nuclear Factor of Activated T Cells (NFATp).” *Journal of Biological Chemistry* 271 (3): 1274–77. doi:10.1074/jbc.271.3.1274.
- Wiederkehr, M R, H Zhao, and O W Moe. 1999. “Acute Regulation of Na/H Exchanger NHE3 Activity by Protein Kinase C: Role of NHE3 Phosphorylation.” *The American Journal of Physiology* 276 (5 Pt 1). United States: C1205-17.
- Wiederrecht, G, E Lam, S Hung, M Martin, and N Sigal. 1993. “The Mechanism of Action of FK-506 and Cyclosporin A.” *Annals of the New York Academy of Sciences* 696: 9–19. doi:10.1111/j.1749-6632.1993.tb17137.x.
- Wightman, Bruce, Ilho Ha, and Gary Ruvkun. 1993. “Posttranscriptional Regulation of the Heterochronic Gene Lin-14 by Lin-4 Mediates Temporal Pattern Formation in *C. Elegans*.” *Cell* 75 (5): 855–62. doi:10.1016/0092-8674(93)90530-4.
- Wilkinson DG. 2001. “Multiple Roles of EPH Receptors and Ephrins in Neural Development.” *Nature Reviews. Neuroscience* 2 (March): 155–64. doi:10.1038/35058515.
- Willenbrock, H, J Salomon, R Sokilde, K B Barken, T N Hansen, F C Nielsen, S Moller, and T Litman. 2009. “Quantitative miRNA Expression Analysis: Comparing Microarrays with next-Generation Sequencing.” *RNA* 15 (11): 2028–34. doi:10.1261/rna.1699809.
- Wilson, C a, L Ramos, M R Villaseñor, K H Anders, M F Press, K Clarke, B Karlan, et al. 1999. “Localization of Human BRCA1 and Its Loss in High-Grade, Non-Inherited Breast Carcinomas.” *Nature Genetics* 21 (2): 236–40. doi:10.1038/6029.
- Wooster, R, G Bignell, J Lancaster, S Swift, S Seal, J Mangion, N Collins, S Gregory, C Gumbs, and G Micklem. 1995. “Identification of the Breast Cancer Susceptibility Gene BRCA2.” *Nature* 378 (6559): 789–92. doi:10.1038/378789a0.
- Wu, Yang, David Connors, Lauren Barber, Sukhanya Jayachandra, Umesh M. Hanumegowda, and Stephen P. Adams. 2009. “Multiplexed Assay Panel of Cytotoxicity in HK-2 Cells for Detection of Renal Proximal Tubule Injury Potential of Compounds.” *Toxicology in Vitro* 23 (6): 1170–78. doi:10.1016/j.tiv.2009.06.003.
- Xia, Jiazeng, Xiaoqiang Guo, Jiang Yan, and Kaiyuan Deng. 2014. “The Role of miR-148a in Gastric Cancer.” *Journal of Cancer Research and Clinical Oncology*. doi:10.1007/s00432-014-1649-8.
- Xu, Dan, Fumitaka Takeshita, Yumiko Hino, Saori Fukunaga, Yasusei Kudo, Aya Tamaki, Junko Matsunaga, et al. 2011. “miR-22 Represses Cancer Progression by Inducing Cellular Senescence.” *Journal of Cell Biology* 193 (2): 409–24. doi:10.1083/jcb.201010100.
- Xu, Jian, Samy Lamouille, and Rik Derynck. 2009. “TGF-β-Induced Epithelial to Mesenchymal Transition.” *Cell Research* 19 (2): 156–72. doi:10.1038/cr.2009.5.
- Xu, Lijun, Yue Zhang, Hui Wang, Guanhua Zhang, Yanqing Ding, and Liang Zhao. 2014. “Tumor Suppressor miR-1 Restraints Epithelial-Mesenchymal Transition and Metastasis of Colorectal Carcinoma via the MAPK and PI3K/AKT Pathway.” *Journal of Translational Medicine* 12: 244. doi:10.1186/s12967-014-0244-8.

- Xue, Liang, Yi Wang, Shuyuan Yue, and Jianning Zhang. 2017. "The Expression of miRNA-221 and miRNA-222 in Gliomas Patients and Their Prognosis." *Neurological Sciences : Official Journal of the Italian Neurological Society and of the Italian Society of Clinical Neurophysiology* 38 (1). Italy: 67–73. doi:10.1007/s10072-016-2710-y.
- Xue, Yuanchao, Yu Zhou, Tongbin Wu, Tuo Zhu, Xiong Ji, Young Soo Kwon, Chao Zhang, et al. 2009. "Genome-Wide Analysis of PTB-RNA Interactions Reveals a Strategy Used by the General Splicing Repressor to Modulate Exon Inclusion or Skipping." *Molecular Cell* 36 (6): 996–1006. doi:10.1016/j.molcel.2009.12.003.
- Yamashita, M, M Katsumata, M Iwashima, M Kimura, C Shimizu, T Kamata, T Shin, et al. 2000. "T Cell Receptor-Induced Calcineurin Activation Regulates T Helper Type 2 Cell Development by Modifying the Interleukin 4 Receptor Signaling Complex." *The Journal of Experimental Medicine* 191 (11): 1869–79.
- Yamashita, M, M Kimura, M Kubo, C Shimizu, T Tada, R M Perlmutter, and T Nakayama. 1999. "T Cell Antigen Receptor-Mediated Activation of the Ras/mitogen-Activated Protein Kinase Pathway Controls Interleukin 4 Receptor Function and Type-2 Helper T Cell Differentiation." *Proceedings of the National Academy of Sciences of the United States of America* 96 (3): 1024–29. doi:10.1073/pnas.96.3.1024.
- Yan, Ji-Dong, Shuang Yang, Jie Zhang, and Tian-Hui Zhu. 2009. "BMP6 Reverses TGF-beta1-Induced Changes in HK-2 Cells: Implications for the Treatment of Renal Fibrosis." *Acta Pharmacologica Sinica* 30 (7): 994–1000. doi:10.1038/aps.2009.56.
- Yanagishita, M. 1993. "Function of Proteoglycans in the Extracellular Matrix." *Acta Pathologica Japonica* 43 (6): 283–93. doi:10.5357/kouyou.64.193.
- Yang, Jiajia, Yixuan Hou, Mingli Zhou, Siyang Wen, Jian Zhou, Liyun Xu, Xi Tang, Yan E. Du, Ping Hu, and Manran Liu. 2016. "Twist Induces Epithelial-Mesenchymal Transition and Cell Motility in Breast Cancer via ITGB1-FAK/ILK Signaling Axis and Its Associated Downstream Network." *International Journal of Biochemistry and Cell Biology* 71: 62–71. doi:10.1016/j.biocel.2015.12.004.
- Yang, Jr-Shiuan, Thomas Maurin, Nicolas Robine, Kasper D Rasmussen, Kate L Jeffrey, Rohit Chandwani, Eirini P Papapetrou, Michel Sadelain, Dónal O'Carroll, and Eric C Lai. 2010. "Conserved Vertebrate Mir-451 Provides a Platform for Dicer-Independent, Ago2-Mediated microRNA Biogenesis." *Proceedings of the National Academy of Sciences of the United States of America* 107 (34): 15163–68. doi:10.1073/pnas.1006432107.
- Yang, Li, Tatiana Y Besschetnova, Craig R Brooks, Jagesh V Shah, and Joseph V Bonventre. 2010. "Epithelial Cell Cycle Arrest in G2/M Mediates Kidney Fibrosis after Injury." *Nature Medicine* 16 (5): 535-U27. doi:10.1038/nm.2144.
- Yeo, Gene W, Nicole G Coufal, Tiffany Y Liang, Grace E Peng, Xiang-Dong Fu, and Fred H Gage. 2009. "An RNA Code for the FOX2 Splicing Regulator Revealed by Mapping RNA-Protein Interactions in Stem Cells." *Nature Structural & Molecular Biology* 16 (2): 130–37. doi:10.1038/nsmb.1545.
- Yi, Rui, Yi Qin, Ian G. Macara, and Bryan R. Cullen. 2003. "Exportin-5 Mediates the Nuclear Export of Pre-microRNAs and Short Hairpin RNAs." *Genes and Development* 17 (24): 3011–16. doi:10.1101/gad.1158803.

- Yuan, J., C. J. Benway, J. Bagley, and J. Iacomini. 2015. "MicroRNA-494 Promotes Cyclosporine-Induced Nephrotoxicity and Epithelial to Mesenchymal Transition by Inhibiting PTEN." *American Journal of Transplantation* 15 (6): 1682–91. doi:10.1111/ajt.13161.
- Zeisberg, Michael, and Raghu Kalluri. 2004. "The Role of Epithelial-to-Mesenchymal Transition in Renal Fibrosis." *Journal of Molecular Medicine (Berlin, Germany)* 82 (3): 175–81. doi:10.1007/s00109-003-0517-9.
- Zekri, Latifa, Eric Huntzinger, Susanne Heimstädt, and Elisa Izaurralde. 2009. "The Silencing Domain of GW182 Interacts with PABPC1 to Promote Translational Repression and Degradation of microRNA Targets and Is Required for Target Release." *Molecular and Cellular Biology* 29 (23): 6220–31. doi:10.1128/MCB.01081-09.
- Zhang, Haidi, Fabrice A. Kolb, Vincent Brondani, Eric Billy, and Witold Filipowicz. 2002. "Human Dicer Preferentially Cleaves dsRNAs at Their Termini without a Requirement for ATP." *EMBO Journal* 21 (21): 5875–85. doi:10.1093/emboj/cdf582.
- Zhang, H, Y Li, Q Huang, X Ren, H Hu, H Sheng, and M Lai. 2011. "MiR-148a Promotes Apoptosis by Targeting Bcl-2 in Colorectal Cancer." *Cell Death and Differentiation* 18 (11): 1702–10. doi:10.1038/cdd.2011.28.
- Zhang, J-P, C Zeng, L Xu, J Gong, J-H Fang, and S-M Zhuang. 2014. "MicroRNA-148a Suppresses the Epithelial-Mesenchymal Transition and Metastasis of Hepatoma Cells by Targeting Met/Snail Signaling." *Oncogene* 33 (31): 4069–76. doi:10.1038/onc.2013.369.
- Zhang, J, J X Gao, K Salojin, Q Shao, M Grattan, C Meagher, D W Laird, and T L Delovitch. 2000. "Regulation of Fas Ligand Expression during Activation-Induced Cell Death in T Cells by p38 Mitogen-Activated Protein Kinase and c-Jun NH₂-Terminal Kinase." *The Journal of Experimental Medicine* 191 (6): 1017–30. doi:10.1084/jem.191.6.1017.
- Zhang, Liping, Duy T. Tran, and Kelly G. Ten Hagen. 2010. "An O-Glycosyltransferase Promotes Cell Adhesion during Development by Influencing Secretion of an Extracellular Matrix Integrin Ligand." *Journal of Biological Chemistry* 285 (25): 19491–501. doi:10.1074/jbc.M109.098145.
- Zhang, Long, Fangfang Zhou, Amaya GarcíadeVinuesa, EstherM deKruijf, WilmaE Mesker, Li Hui, Yvette Drabsch, et al. 2013. "TRAF4 Promotes TGF-β Receptor Signaling and Drives Breast Cancer Metastasis." *Molecular Cell* 51 (5): 559–72. doi:10.1016/j.molcel.2013.07.014.
- Zhang, Wei, Hui Tu Liu, and Hui Tu LIU. 2002. "MAPK Signal Pathways in the Regulation of Cell Proliferation in Mammalian Cells." *Cell Research* 12 (1): 9–18. doi:10.1038/sj.cr.7290105.
- Zhao, Qun, Xianxi Wang, Leif D. Nelin, Yongxue Yao, Ranyia Matta, Mary E. Manson, Reshma S. Baliga, et al. 2006. "MAP Kinase Phosphatase 1 Controls Innate Immune Responses and Suppresses Endotoxic Shock." *The Journal of Experimental Medicine* 203 (1): 131–40. doi:10.1084/jem.20051794.
- Zheng, Binqiang, Linhui Liang, Chunmeng Wang, Shenglin Huang, Xi Cao, Ruopeng Zha, Li Liu, et al. 2011. "MicroRNA-148a Suppresses Tumor Cell Invasion and

- Metastasis by Downregulating ROCK1 in Gastric Cancer.” *Clinical Cancer Research : An Official Journal of the American Association for Cancer Research* 17 (24): 7574–83. doi:10.1158/1078-0432.CCR-11-1714.
- Zhong, Shanliang, Xiu Chen, Dandan Wang, Xiaohui Zhang, Hongyu Shen, Sujin Yang, Mengmeng Lv, Jinhai Tang, and Jianhua Zhao. 2016. “MicroRNA Expression Profiles of Drug-Resistance Breast Cancer Cells and Their Exosomes.” *Oncotarget* 7 (15): 19601–9. doi:10.18632/oncotarget.7481.
- Zhong, Zhi, Gavin E. Arteel, Henry D. Connor, Ming Yin, Moritz V. Frankenberg, Robert F. Stachlewitz, James A. Raleigh, Ronald P. Mason, and Ronald G. Thurman. 1998. “Cyclosporin A Increases Hypoxia and Free Radical Production in Rat Kidneys: Prevention by Dietary Glycine.” *Am J Physiol Renal Physiol*. <http://ajprenal.physiology.org/content/275/4/F595.full-text.pdf+html>.
- Zhou, Ziliang, Lijie Zhou, Fangfang Jiang, Binghui Zeng, Changbo Wei, Wei Zhao, and Dongsheng Yu. 2017. “Downregulation of miR-222 Induces Apoptosis and Cellular Migration in Adenoid Cystic Carcinoma Cells.” *Oncology Research* 25 (2). United States: 207–14. doi:10.3727/096504016X14732772150460.
- Zisoulis, Dimitrios G, Michael T Lovci, Melissa L Wilbert, Kasey R Hutt, Tiffany Y Liang, Amy E Pasquinelli, and Gene W Yeo. 2010. “Comprehensive Discovery of Endogenous Argonaute Binding Sites in *Caenorhabditis Elegans*.” *Nature Structural & Molecular Biology* 17 (2). Nature Publishing Group: 173–79. doi:10.1038/nsmb.1745.